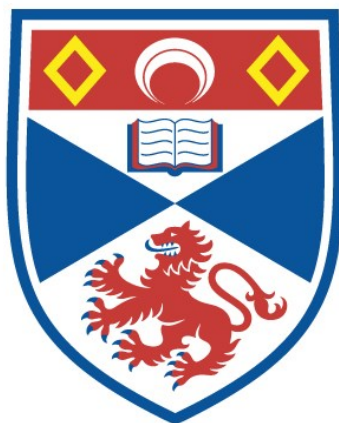


**N-HETEROCYCLIC CARBENE RHODIUM(I) AND
IRIDIUM(I) HYDROXIDE COMPLEXES**

Byron John Truscott

**A Thesis Submitted for the Degree of PhD
at the
University of St Andrews**



2014

**Full metadata for this item is available in
St Andrews Research Repository
at:**

<http://research-repository.st-andrews.ac.uk/>

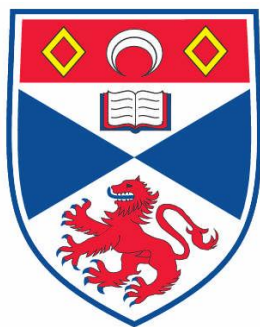
Please use this identifier to cite or link to this item:

<http://hdl.handle.net/10023/7049>

This item is protected by original copyright

***N-HETEROCYCLIC CARBENE RHODIUM(I) AND
IRIDIUM(I) HYDROXIDE COMPLEXES***

Byron John Truscott



This thesis is submitted in partial fulfilment for the degree of

PhD

at the

University of St Andrews

25 September 2014

DECLARATION

1. Candidate's declarations:

I, Byron Truscott, hereby certify that this thesis, which is approximately 50,000 words in length, has been written by me, and that it is the record of work carried out by me, or principally by myself in collaboration with others as acknowledged, and that it has not been submitted in any previous application for a higher degree. I was admitted as a research student in August, 2010 and as a candidate for the degree of PhD in August, 2011; the higher study for which this is a record was carried out in the University of St Andrews between 2010 and 2014.

Date 14-10-2014 signature of candidate

2. Supervisor's declaration:

I hereby certify that the candidate has fulfilled the conditions of the Resolution and Regulations appropriate for the degree of PhD in the University of St Andrews and that the candidate is qualified to submit this thesis in application for that degree.

Date signature of supervisor

3. Permission for publication:

In submitting this thesis to the University of St Andrews I understand that I am giving permission for it to be made available for use in accordance with the regulations of the University Library for the time being in force, subject to any copyright vested in the work not being affected thereby. I also understand that the title and the abstract will be published, and that a copy of the work may be made and supplied to any bona fide library or research worker, that my thesis will be electronically accessible for personal or research use unless exempt by award of an embargo as requested below, and that the library has the right to migrate my thesis into new electronic forms as required to ensure continued access to the thesis. I have obtained any third-party copyright permissions that may be required in order to allow such access and migration, or have requested the appropriate embargo below.

The following is an agreed request by candidate and supervisor regarding the publication of this thesis:

PRINTED COPY

- a) No embargo on print copy

Supporting statement for printed embargo request:

ELECTRONIC COPY

- a) Embargo on all of electronic copy for a period of two years on the following ground(s):
 - Publication would preclude future publication

Date 14-10-2014 signature of candidate signature of supervisor

This thesis is dedicated to my parents

ACKNOWLEDGEMENTS

There are many people that have provided invaluable support for me during this PhD. Firstly I would like to thank Professor Steven Nolan for the opportunity to study under his guidance at the University of St. Andrews and for all his support and advice during this time. Thank you to Dr George Fortman whose guidance and friendship was invaluable during the first year of my PhD.

Thank you to Dr Cristina Luján Barroso, Dr David Nelson, Dr Paul Webb, Professor Michael Buehl and Hedi Kruger for their collaborative contributions towards the work described in this thesis.

Gratitude to the technical advisors, without whom, none of this work would have been completed, particularly Professor Alexandra Slawin and Dr David Cordes for X-ray crystal analysis and to Dr Tomas Lebl and Melanja Smith for their assistance with NMR studies. Thank you to Dr Andrew Smith and his group for the use of their FTIR machine.

To the people who read and re-read this thesis and guided me through it, particularly Dr Alba Collado-Martinez and Dr David Nelson, as well as Dr Fady Nahra, Dr Martin Corpet, Dr Jose Fernández-Salas and Dr Marcel Brill, thank you for your invaluable time.

Thank you to Adrian, Scott, Simone and Stephanie, the other PhD students, we were all in this together.

Sasol Technologies Ltd. has funded my studies for the last eight years, without their financial support I would not be here today. Thank you to the EPSRC, ERC and St Andrews University of for financial support during my PhD. Thank you to Umicore AG for the generous gift of iridium and rhodium starting materials.

Lastly thank you to my family: Jason and Katie, Mum and Dad. Your love and support has always pushed me further and higher.

ABSTRACT

The unique reactivity that hard/soft-acid/base mismatched metal hydroxide complexes are capable of makes this elusive class of highly reactive organometallic complexes very interesting. The stabilisation of rhodium and iridium hydroxide bonds using electron rich *N*-heterocyclic carbene (NHC) ligands has enabled us to examine their rich chemistry and proved to be very rewarding. A general method was established for the preparation of a family of Rh(I)-NHC hydroxide complexes (four members), which proved to be highly active promoters of the conjugate addition of arylboronic acids to α,β -unsaturated ketones, achieving TONs and TOFs of 100,000 and 6,600 h⁻¹ respectively. In addition, we have studied the activity of Rh(I)-NHC hydroxides in catalysing the hydrosilylation and dehydrogenative silylation of terminal alkenes. The two competing reactions were studied under the same conditions and a scope for each transformation with good selectivity is presented.

The scope of metal hydroxides was extended to include Ir(I)-NHC hydroxides (six members). Reactivity of this motif towards a wide range of organic substrates has been explored, undergoing reaction with arylboronic acids to form Ir(I)-aryl complexes and reacting with silanes to form Ir(I)-siloxides. The Ir(I)-hydroxide is able to deprotonate an array of O-H and N-H bonds to give new Ir(I)-alkoxides and Ir(I)-amides. In addition, C-H activation of a range of *sp*-, *sp*²- and *sp*³-hybridised carbon centres has been explored, delivering Ir(I)-alkyl complexes under very mild conditions, with the generation of H₂O as the sole by-product. Subsequently, we have examined the insertion of CO₂ into a number of Ir(I)-O and Ir(I)-N bonds, leading to Ir(I)-carbonates and Ir(I)-carbamates, respectively. In the case of reaction between CO₂ and Ir(I)-hydroxide, a fascinating [$\{\text{Ir(I)}\}_2-(\mu-\kappa^1\text{O}:\kappa^2\text{O},\text{O}-\text{CO}_3)$] complex was obtained under extremely mild conditions. This reaction has been studied in detail using kinetic and theoretical methods to calculate activation parameters and elucidate the insertion and concomitant dimerisation mechanism.

In addition, we have utilised a series of methods for the preparation of a range of interesting fluorinated Rh(I)-NHC and Ir(I)-NHC complexes; bearing fluoride, bifluoride and trifluoromethyl groups. We disclose the first iridium bifluoride complexes and briefly discuss the relationship between these and the fluoride species in solution. We also report the first Ir(I)-NHC and Rh(I)-NHC trifluoromethyl complexes.

PUBLISHED WORK

The majority of the work reported in this thesis has been published as peer-reviewed journal articles as described below. Unless stated otherwise, the work reported is all my own work and I was the primary researcher on all projects and prepared all published manuscripts:

Chapter 2: Large parts of this chapter are reported in:

1. [Well-defined \[Rh\(NHC\)\(OH\)\] Complexes Enabling the Conjugate Addition of Arylboronic Acids to \$\alpha,\beta\$ -unsaturated Ketones](#), B. J. Truscott, G. C. Fortman, A. M. Z. Slawin and S. P. Nolan, *Org. Biomol. Chem.*, 2011, **9**, 7038-7041. *Adapted with permission from The Royal Society of Chemistry*

Chapter 3: Material from this chapter has been published as:

2. [Well-defined \(NHC\)-Rhodium Hydroxide Complexes as Alkene Hydrosilylation and Dehydrogenative Silylation Catalysts](#), B. J. Truscott, A. M. Z. Slawin and S. P. Nolan, *Dalton Trans.*, 2013, **42**, 270-276. *Adapted with permission from The Royal Society of Chemistry*

Chapter 4: The work in this chapter has been published as a more concise report in:

3. [Iridium\(I\) Hydroxides: Powerful Synthons for Bond Activation](#), B. J. Truscott, D. J. Nelson, C. Lujan, A. M. Z. Slawin and S. P. Nolan, *Chem. Eur. J.*, 2013, **19**, 7904-7916. *Adapted with permission from John Wiley and Sons Inc.*

In this chapter Dr David Nelson performed all DFT calculations.

Chapter 5: The reactivity studies described in this chapter have been published:

4. [CO₂ Fixation Employing an Iridium\(I\) Hydroxide Complex](#), B. J. Truscott, D. J. Nelson, A. M. Z. Slawin and S. P. Nolan, *Chem. Commun.*, 2014, **50**, 286-288. *Reproduced by permission of The Royal Society of Chemistry*

DFT calculations in this chapter were performed by Michael Bühl and Hedi Kruger as a collaborative effort and their results have been submitted as a dissertation at the University of St Andrews by Hedi Kruger. This discussion makes up a manuscript under submission at the time of examination entitled:

5. [Shedding light on CO₂ insertion into Ir\(I\)-alkoxide and Ir\(I\)-amide bonds: a kinetic and computational study](#), B. J. Truscott, H. Kruger, P. B. Webb, M. Bühl and S. P. Nolan.

Chapter 6: The work presented in this chapter has been submitted for publication as:

6. [Fluoride, Bifluoride and Trifluoromethyl Complexes of Iridium\(I\) and Rhodium\(I\)](#), B. J. Truscott, F. Nahra, A. M. Z. Slawin, D. B. Cordes and Nolan S. P., *submitted manuscript*

Several articles were also published during the course of my PhD as a result of collaborative efforts but have not been included in this thesis:

7. [Iridium\(I\) hydroxide-catalysed rearrangement of allylic alcohols to ketones](#), D. J. Nelson, J. A. Fernández-Salas, B. J. Truscott and S. P. Nolan, *Org. Biomol. Chem.*, *accepted*.
8. [Exploring the Limits of Catalytic Ammonia-Borane Dehydrogenation Using a Bis\(N-Heterocyclic Carbene\) Iridium\(III\) Complex](#), D. J. Nelson, B. J. Truscott, J. D. Egbert, S. P. Nolan, *Organometallics* **2013**, *32*, 3769.
9. [Synthesis and Reactivity of New Bis\(N-Heterocyclic Carbene\) Iridium\(I\) Complexes](#), D. J. Nelson, B. J. Truscott, A. M. Z. Slawin, S. P. Nolan, *Inorg. Chem.*, **2013**, *52*, 12674.

LIST OF ABBREVIATIONS

acac	acetylacetonato
Ad	adamantyl
anal. calcd	analytically calculated
Ar	aryl
atm	atmosphere
aq.	aqueous
BARF	tetrakis[3,5-bis(trifluoromethyl)phenyl]borate
Bn	benzyl
^t Bu	tert-butyl
cod	cyclooctadiene
coe	<i>cis</i> -cyclooctene
Cp	cyclopentadiene
Cp*	pentamethylcyclopentadiene
d	doublet
dipp	di(<i>isopropyl</i>)phenyl
DFT	density functional theory
DMF	dimethylformamide
DMSO	dimethylsulfoxide
dppe	bis(diphenylphosphino)ethane
DRIFTS	Diffuse reflectance fourier transform
ee	enantiomeric excess
eq	equation
equiv	equivalent
Et	ethyl
h	hours
hex	hexyl
HSAB	hard/soft-acid/base
IAd	1,3-diadamantylimidazol-2-ylidene
ICy	1,3-dicyclohexylimidazol-2-ylidene
ⁱ Pr	1,3-diisopropylimidazol-2-ylidene
ⁱ Pr ^{Me}	1,3-di <i>isopropyl</i> -4,5-dimethylimidazol-2-ylidene
IMe	1,3-dimethylimidazol-2-ylidene
IMes	1,3-bis(2,4,6-trimethylphenyl)imidazol-2-ylidene
IPr	1,3-bis(2,6-diisopropylphenyl)imidazol-2-ylidene
^t Bu	1,3-di- <i>tert</i> -butylimidazol-2-ylidene
LTM	late-transition metal

<i>m</i>	<i>meta</i>
Me	methyl
Mes	mesityl [1,3,5-trimethylphenyl]
min	minutes
mol	moles
mol%	molar percentage
mmol	millimoles
mw	microwave
NMR	nuclear magnetic resonance
NHC	nitrogen-containing heterocyclic carbene
<i>o</i>	<i>ortho</i>
ORTEP	Oak Ridge Thermal Ellipsoid Plot
<i>p</i>	<i>para</i>
PCy ₃	tricyclohexyl phosphine
PPh ₃	triphenylphosphine
Ph	phenyl
PhMe	toluene
PPh ₃	triphenyl phosphine
ppm	parts per million
ⁱ Pr	<i>isopropyl</i>
py	pyridine
q	quartet
R	alkyl group
rt	room temperature
s	singlet
satd.	saturated
SICy	1,3-dicyclohexylimidazolin-2-ylidene
SIMes	1,3-bis(2,4,6-trimethylphenyl)imidazolin-2-ylidene
SIPr	1,3-bis(2,6-diisopropylphenyl)imidazolin-2-ylidene
<i>t</i>	<i>tert</i>
t	triplet
^t be	<i>tert</i> -butyl ethylene
TFA	trifluoroacetic acid
THF	tetrahydrofuran
TOF	turn over frequency
TON	turn over number
TM	transition metal

TABLE OF CONTENTS

1.	General introduction.....	1
1.1.	Transition metal organometallic chemistry	1
1.1.1.	Transition metal hydroxides	2
1.2.	<i>N</i> -heterocyclic carbenes (NHCs)	14
1.2.1.	NHC complexation	19
1.2.2.	Rhodium and iridium NHC complexes	23
2.	Well-defined rhodium(I) hydroxides and their activity in the conjugate addition of arylboronic acids to activated alkenes.....	39
2.1.	Introduction.....	39
2.2.	Complex synthesis	45
2.3.	Catalysis.....	46
2.4.	Mechanistic studies.....	50
2.5.	Conclusions	53
2.6.	Experimental details	55
2.6.1.	General considerations	55
2.6.2.	Synthesis and Characterisation data	55
2.6.3.	Catalysis	58
2.6.4.	Characterisation data	59
3.	Alkene hydrosilylation and dehydrogenative silylation catalysed by Rh(I)-hydroxides	67
3.1.	Introduction.....	67
3.2.	Results and discussion	71
3.3.	Conclusions	80
3.4.	Experimental details	81
3.4.1.	General considerations	81
3.4.2.	Synthesis and Characterisation.....	81
3.4.3.	Catalysis	82
3.4.4.	General method for catalytic hydrosilylation	82
3.4.5.	Optimisation studies	82
3.4.6.	Characterisation data	84
4.	Well-defined iridium(I) hydroxides and their activity in bond activation	89
4.1.	Introduction.....	89
4.2.	Results and Discussion	90

4.2.1.	Iridium(I) hydroxide synthesis	90
4.2.2.	Reactivity.....	97
4.3.	Conclusions	105
4.4.	Experimental details	107
4.4.1.	General considerations	107
4.4.2.	Synthesis and characterisation data	107
5.	CO ₂ fixation by iridium(I) alkoxide and amide complexes	123
5.1.	Introduction.....	123
5.2.	Results and Discussion	127
5.2.1.	Reactivity.....	127
5.2.2.	Mechanistic studies	133
5.3.	Conclusions	138
5.4.	Experimental Details	140
5.4.1.	General considerations	140
5.4.2.	Synthesis and characterisation data	140
5.4.1.	Kinetic Experiments	145
5.4.2.	Calculation of activation parameters	150
5.4.3.	DFT Calculations.....	151
6.	Fluoride, bifluoride and trifluoromethyl complexes of iridium(I) and rhodium(I)	153
6.1.	Introduction.....	153
6.2.	Discussion.....	158
6.3.	Conclusions	167
6.4.	Experimental details	168
6.4.1.	General considerations	168
6.4.2.	Synthesis and Characterisation data	168
7.	Conclusions	179
8.	References	181

1. GENERAL INTRODUCTION

1.1. TRANSITION METAL ORGANOMETALLIC CHEMISTRY

The development of new transition metal catalysed processes continues to drive advances in the important fields of organic synthesis, materials chemistry and small-molecule activation. Many crucial technologies, such as olefin metathesis¹ and palladium-catalysed cross couplings,² have relied on the exploration of new structural motifs. For example, the use of *N*-heterocyclic carbene (NHC) ligands led to a remarkable change in the reactivity of olefin metathesis catalysts,³ while ligand choice in Pd-mediated processes influenced reaction outcomes such as regio-, chemo- and stereoselectivity.⁴ Catalysis is of growing importance in industry, where highly efficient processes are necessary in order to perform cost-effective chemical procedures on a large scale. In the past, catalyst research and development focused on activity and optimisation of turnover rates. However, the focus is shifting towards the development of reactions with greater selectivity and the elimination of by-products in order to enable cleaner transformations, eliminate the need for waste disposal and ultimately deliver green chemistry.^{5,6} The underlying principle of green chemistry is the design of environmentally benign processes and products. Catalysis plays a vital role, being identified as one of the twelve green chemistry principles,⁷ which can be summarised into a working definition as the efficient utilisation of raw materials (preferably renewable), the elimination of waste and the avoidance of toxic reagents and solvents in the manufacture and utilisation of chemical products.⁸

Advancements in combinatorial chemistry, molecular modelling, high-performance analytical techniques and more efficient data collection and correlation are all driving catalyst development, while the replacement of fossil fuels by alternative energy sources calls for crucial scientific breakthroughs.⁹ In the fine chemicals sector, enantioselective catalysis by supported metals is a major challenge,¹⁰ while soluble transition metal catalysts have important applications in the manufacture of bulk commodities and specialty products. Industrial competition and the demand for selective, efficient and environmentally friendly processes continue to drive catalyst research.¹¹

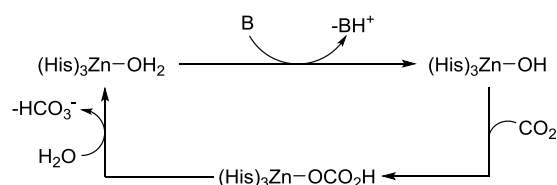
It is therefore of paramount importance to fully explore new structural motifs in order to understand and implement them in the development of next generation catalytic systems. While efficient chemistry can often be performed by active catalyst species made *in situ*, the careful preparation and study of well-defined complexes provides a solid foundation from which to study reactivity and fundamental steps in organometallic chemistry.

1.1.1. Transition metal hydroxides

Organometallic complexes are most often prepared in organic solvents and the presence of adventitious water in reaction media containing sensitive organometallic compounds can result in the (detrimental) formation of oxide, hydroxide, (oxo)hydroxide and aqua complexes, which may also precede organometallic decomposition. The demand for ‘green’ processes has meant that more environmentally friendly reaction media are sought after, particularly with respect to solvents. Most organic processes are not compatible with aqueous solvents due to poor solubility and in the case of organometallic compounds, instability in water. However, the development of organometallic complexes that are insensitive to water and the exploration of their potential as catalysts may lead to more environmentally friendly processes that can be carried out in aqueous media.¹²

Hydroxide complexes of the transition metals (TMs), and in particular, the late-transition metals (LTMs) are rare due primarily to the inherent weakness of metal hydroxide (M-OH) bonds.¹² Metal ions of LTMs usually adopt low oxidation states and their large size and loosely held (easily excited) outer d-orbital electrons make them highly polarisable. By the Pearson system,¹³ LTMs in low-oxidation states are classified as soft Lewis acids, with ‘hardness’ increasing with increasing oxidation state. Hydroxide ions are classified by hard/soft-acid/base (HSAB) theory as hard Lewis bases, and by Pearson’s acid-base concept,¹³ soft acids will form more stable complexes in solution with soft bases. Therefore, the interaction of a hard base (OH)⁻ with a soft acid (LTM) is disfavoured, and is predicted to result in a weak metal-hydroxide bond.¹²¹⁴ By the same logic, the HSAB mismatch should lead to very reactive complexes, with labile OH groups and this is the fundamental reason for our interest in LTM hydroxides.¹²

Another reason for our interest in LTM hydroxides is due to numerous reports where metal hydroxides are implicated as important intermediates in catalytic transformations, particularly where water is involved as a substrate. Examples include the 1,4-addition of aryl boronic acids to α,β -unsaturated ketones,¹⁵ nitrile¹⁶ and olefin hydrations,¹⁷ hydrogen – deuterium exchange¹⁸ and water oxidation.^{11, 21} Interactions between transition metals and hydroxide moieties are also considered to be critical in reactions such as the Wacker oxidation,¹⁹ water-gas shift reaction,²⁰ olefin hydrocarbonylation,³⁶ methoxycarbonylation,²¹ carbonyl hydrogenation,¹⁹ and alcohol dehydrogenation.¹⁹ In addition, hydroxide and aqua complexes have been studied due to their biological significance. Several metalloenzymes, such as carbonic anhydrase consist of a Zn-H₂O active site. The major activation step in the catalytic cycle of carbonic anhydrase involves a base assisted deprotonation of the Zn-H₂O to generate a Zn-OH moiety. Nucleophilic attack by the Zn-OH at CO₂ forms a zinc hydrogen carbonate and subsequent hydrolysis releases the hydrogen carbonate anion and regenerates the Zn-H₂O (Scheme 1.1).²²



Scheme 1.1. Simplified mechanism of carbonic anhydrase (B = base, His = histidine)²²

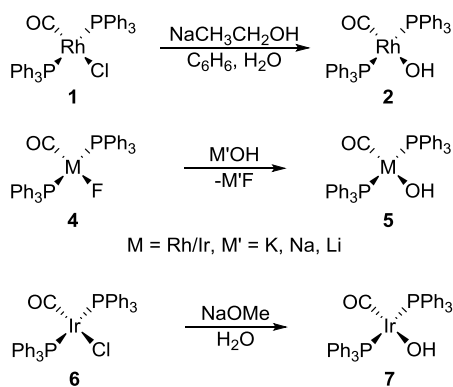
Hydroxide complexes of most of the d-block metals of the periodic table have been prepared, ranging from hydroxide complexes of yttrium²³ to those of zinc,²⁴ cadmium²⁵ and mercury,²⁶ either serendipitously in the presence of adventitious moisture,¹² or by synthetic methods involving processes such as ligand or salt metathesis, oxidative addition or protonation reactions.¹⁹ The various preparative methods for LTM hydroxides will be discussed briefly in the next section. Most of the procedures described are general for metal alkoxides and amides but for the sake of this study, discussions will be focussed on metal hydroxides.

1.1.1.1. Metal hydroxide synthesis

1.1.1.1.1. Ligand metathesis

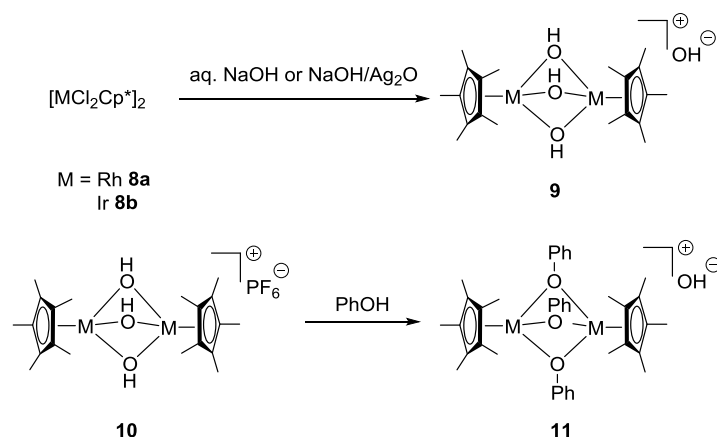
TM hydroxide (and alkoxide) complexes have been prepared mostly by metal exchange or ligand (salt) metathesis reactions. The earliest reports of synthetic routes to

Rh and Ir hydroxides were reported in the late 1960s and early 1970s *via* metathesis reactions. For example, in 1969 Ugo prepared Rh(I) hydroxide **2** from $[\text{RhCl}(\text{CO})(\text{PPh}_3)_2]$ (**1**) and sodium methoxyethoxide in the presence of H_2O (Scheme 1.2).²⁷ Roper reported the Ir(I) analogue from *trans*- $[\text{Ir}(\text{CO})(\text{MeCN})(\text{PR}_3)_2]\text{ClO}_4$ (**3**) and NaOH ²⁸ and Vaska prepared hydroxides of both Ir (**5a**) and Rh (**5b**) *via* metathesis with corresponding fluoride complexes **4**.²⁹ Vaska's complex *trans*- $[\text{IrCl}(\text{CO})(\text{PPh}_3)_2]$ (**6**) also reacts with NaOMe , followed by hydrolysis to give the Ir(I) hydroxide **7**.³⁰



Scheme 1.2. Preparation of Rh and Ir hydroxides by metathesis reactions^{27, 29}

Several bridged hydroxide complexes of Rh and Ir have been prepared by salt metathesis. For example, $[\text{MCp}^*(\mu\text{-Cl})_2]_2$ ($\text{M} = \text{Rh}$ **8a**, Ir **8b**, $\text{Cp}^* =$ pentamethylcyclopentadiene) complexes react with NaOH and Ag_2O in the presence of moisture to give $[(\text{MCp}^*)_2(\mu\text{-OH})_3]\text{OH}$ ($\text{M} = \text{Rh}$ **9a**, Ir **9b**).³¹ **9a** can easily be converted to $[(\text{RhCp}^*)_2(\mu\text{-OH})_3]\text{PF}_6$ (**10**), which reacts with PhOH to give the corresponding phenoxide-bridged dimer **11** (Scheme 1.3),^{31b}



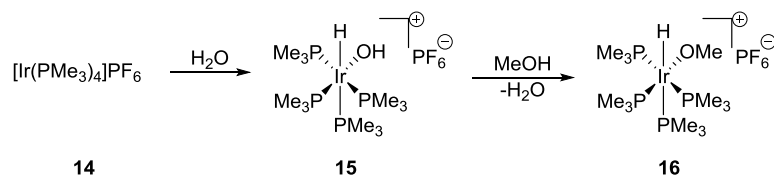
Scheme 1.3. Preparation of Rh and Ir bridged hydroxide complexes by salt metathesis.³¹

$[\text{M}(\text{cod})(\text{OH})]_2$ ($\text{M} = \text{Rh}$ **13a**, Ir **13b**) can be prepared easily from the commercially available chloride complexes $[\text{M}(\text{cod})\text{Cl}]_2$ (**12**) and KOH , providing valuable synthons.

For example, reaction of $[\text{Ir}(\text{cod})(\text{OH})]_2$ (**13b**) with chelating phosphines leads to cleavage of the dimer to give four co-ordinate Ir-hydroxide complexes.³² Complex **13b** can also react with aqueous HF to give $[\text{Ir}(\text{cod})(\text{F})]_n$, which in turn can be isolated as monomeric $[\text{Ir}(\text{cod})(\text{F})(\text{PPh}_3)]$ upon treatment with triphenyl phosphine (PPh_3).³³ $[\text{M}(\text{cod})(\text{OH})]_2$ (**13**) has found application as a catalyst in a large number of transformations. For example, Mori and co-workers have shown the superior activity of the hydroxide complex **13a** over the chloride complex **12a** in 1,4-hydrosilylation³⁴ and Mizoroki-Heck type coupling³⁵ with α,β -unsaturated carbonyls. The same group have also reported **13a** as an efficient promoter of hydroarylation and alkenylation of alkynes³⁶ and aldehydes³⁷ using silanediols. The catalytic efficiency of **13a** has also been shown in combination with phosphine ligands, particularly chiral biphosphines to enable asymmetric transformations. A particular case in point was reported by Hayashi and co-workers who showed that **13a/L** (L = chiral biphosphine) provided more active catalysts for the conjugate addition of arylboronic acids to α,β -unsaturated ketones, than the corresponding chloride systems generated from **12a/L**.^{38, 39}

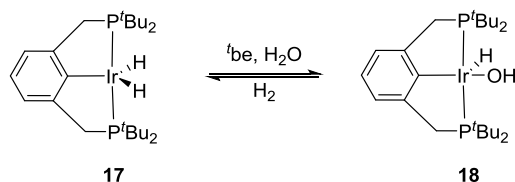
1.1.1.1.2. Oxidative syntheses

The second method for preparing metal hydroxides is through oxidative addition, particularly of H_2O , to give hydrido-hydroxo complexes. For example, Milstein and co-workers have described oxidative addition of water across several Ir complexes⁴⁰ such as $[\text{Ir}(\text{PMe}_3)_4]\text{PF}_6$ (**14**) to give $[\text{Ir}(\text{H})(\text{OH})(\text{PMe}_3)_4]\text{PF}_6$ (**15**) (Scheme 1.4).^{40b} The Ir(III)-hydroxide **15** is stable to air and will not reductively eliminate water, even at high temperatures, but is able to deprotonate methanol to give an Ir(III)-methoxide complex **16**.



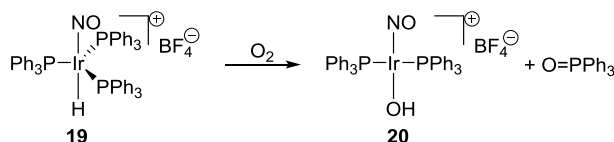
Scheme 1.4. Oxidative addition of H_2O to give an Ir(III) hydroxide^{40b}

Jensen⁴¹ reported that the 16-electron Ir-dihydride complex **17** reacts under dehydrogenation with *tert*-butyl ethylene (*t*be) to form the hydrido-hydroxide complex **18**, presumably *via* the oxidative addition of adventitious H_2O . This was confirmed by adding excess H_2O to the reaction mixture to deliver **18** in high yield (Scheme 1.5), and the transformation can be reversed by addition of H_2 .



Scheme 1.5 Oxidative addition of H₂O to an Ir pincer complex⁴¹

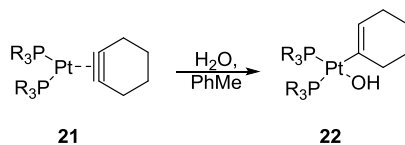
Less common is the addition of molecular oxygen to form metal hydroxide bonds such as the conversion of a five-coordinate Ir hydride **19** to an Ir hydroxide **20** as shown in Scheme 1.6. The exact mechanism has not been described but was postulated to involve the formation of a di-oxygen adduct, which is unstable and consequently releases O=PPh₃ to give complex **20**.⁴²



Scheme 1.6. O₂ addition to an Ir hydride to give an Ir hydroxide⁴²

1.1.1.1.3. Protonation and σ -ligand metathesis

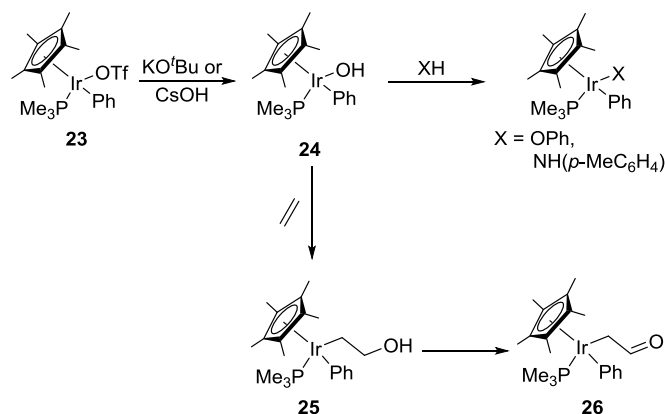
σ -Ligand metathesis differs from the salt metathesis described above in that only hydrogen atoms are transferred between σ -ligands. The transformation is normally preceded by oxidative addition and can either be reversible or irreversible, with reversible σ -ligand metathesis being driven to completion by excess reagent.¹⁹ Bennet and co-workers developed an irreversible σ -ligand metathesis route to access platinum cyclohexenyl hydroxides **22** as shown in Scheme 1.7. The oxidative addition of H₂O is followed by hydrogen transfer to the coordinated cyclohexyne. Reactions are thermodynamically favourable, and the products are stable towards β -hydride elimination and the reformation of metal hydrides.^{16a, 43} Similar results have been reported by Keim upon heating [Rh(PMe₃)₃Me] in the presence of PhOH to give [Rh(PMe₃)₃(OPh)] and methane.⁴⁴



Scheme 1.7. σ -Ligand metathesis on Platinum^{16a, 43}

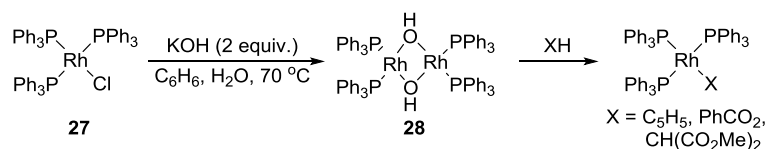
1.1.1.2. Metal hydroxides and reactivity

Several terminal Ir(I) and Ir(III)-hydroxide complexes have been reported. Of note, Woerpel and Bergman reported the synthesis of $[\text{Ir}(\text{Cp}^*)(\text{OH})(\text{Ph})(\text{PMe}_3)]$ (**24**) from the corresponding iridium trifluoromethanesulfonate (OTf) complex **23** and CsOH or KO^tBu (Scheme 1.8).⁴⁵ In their report, the authors studied the activation of a number of nucleophilic and electrophilic reagents. Reactivity was restricted to the hydroxyl moiety, for example **24** is able to activate X-H bonds ($X = \text{PhO}, \text{NH}(p\text{-MeC}_6\text{H}_4)$) by deprotonation with complete conversion to the corresponding Ir-X complex.⁴⁵ The authors also reported the unprecedented insertion of alkenes and alkynes into the Ir-OH bond, for example ethylene reacts with **24** to give complex **25**, which rearranges over time to give the formylmethyl complex **26**. In a later communication, Ritter and Bergman reported that the apparent insertion of an inactivated alkene into the Ir-OH bond is catalysed by trace amounts of **23** present in the reaction mixture, which effects the initial alkene activation, followed by attack of the Ir-hydroxide to form a bimetallic intermediate.⁴⁶



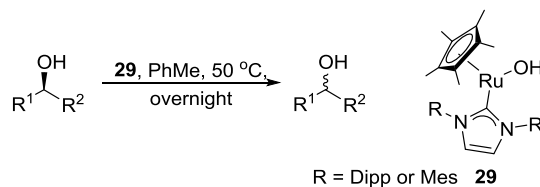
Scheme 1.8. Preparation of Ir(III)-hydroxide and its reactivity towards organic substrates.⁴⁵

In a similar study to that conducted by Woerpel and Bergman, Alper and Grushin⁴⁷ reported the preparation of $[\text{Rh}(\text{PPh}_3)_2(\mu\text{-OH})_2]$ (**28**) from Wilkinson's catalyst (**27**) and aqueous KOH in biphasic media (Scheme 1.9). Complex **28** performed C-H or O-H activation on a number of substrates including cyclopentadiene, methylmalonate and benzoic acid to give the corresponding monomeric Rh complexes and H₂O. Complex **28** also reacts with $[\text{M}(\text{CO})_3\text{CpH}]$ ($\text{M} = \text{Cr}, \text{Mo}, \text{W}$) to generate heterobimetallic complexes.



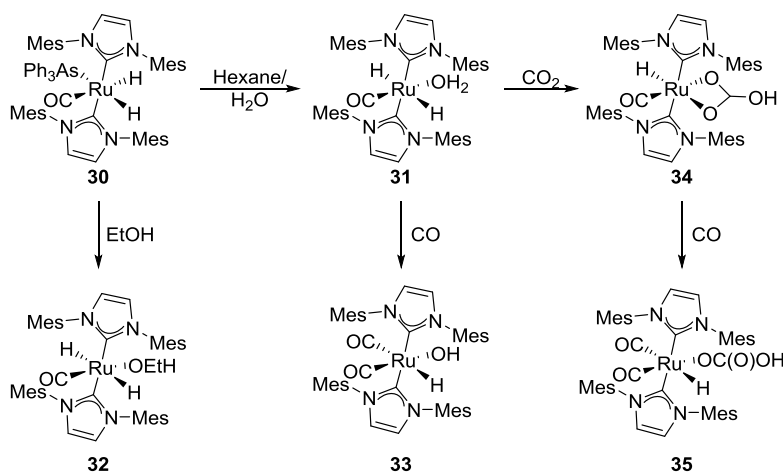
Scheme 1.9. Preparation of $[\text{Rh}(\text{PPh}_3)_2(\mu\text{-OH})]_2$ from Wilkinson's catalyst (**27**)⁴⁷

Several interesting hydroxide complexes of ruthenium have been prepared, a number of them *via* the oxidative addition of H_2O to form hydrido-hydroxo complexes such as $[\text{Ru}(\text{OH})(\text{PMe}_3)_4(\text{R})]$ ($\text{R} = \text{H}$ or Ph).⁴⁸ $[\text{Ru}(\text{Cp}^*)(\text{NHC})(\text{OH})]$ (**29**, Scheme 1.10) was prepared by our group from the corresponding chloride complex and CsOH and proved to be an effective catalyst for the racemisation of aliphatic and aromatic secondary alcohols. Although the parent chloride complex was more active, the inclusion of an on-board base on **29** meant that reactions could be performed without the need to add a stoichiometric amount of base.⁴⁹



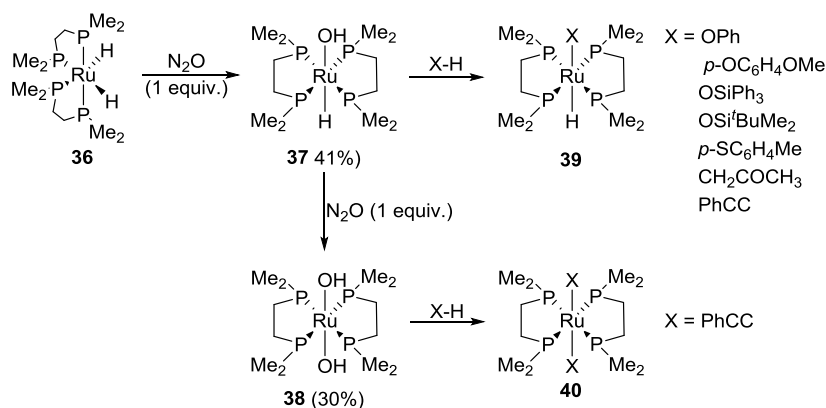
Scheme 1.10 Ru-NHC hydroxide and its use in base free alcohol racemisation⁴⁹

Whittlesey *et al.*⁵⁰ have reported the preparation of a monomeric ruthenium aqua complex **31** somewhat serendipitously *via* adventitious water during the attempted recrystallisation of a Ru-dihydride complex **30** in hexane (Scheme 1.11). The corresponding ethanol complex **32** was isolated in the same way in ethanol and both **31** and **32** reacted with CO . Complex **32** inserts CO into the Ru-O bond to give $\text{Ru}(\text{C}(\text{O})\text{OEt})$, while the aqua complex **31** eliminates H_2 in the presence of CO , leading to the hydrido-hydroxide adduct **33**. Furthermore, CO_2 can be inserted into the $\text{Ru}(\text{H}_2\text{O})$ bond on **31** to give a monomeric Ru bicarbonate complex **34**. When placed under CO , the $\text{Ru}(\kappa^2\text{O},\text{O}-\text{CO}_2\text{H})$ **34** rearranges to give $\text{Ru}(\eta^1\text{-OCO}_2\text{H})$ **35**. The authors described the presence of the two bulky 1,3-dimethylimidazol-2-ylidene (IMes) ligands to play a vital role in stabilising bonds between Ru and oxygen and enabling isolation of these interesting compounds.



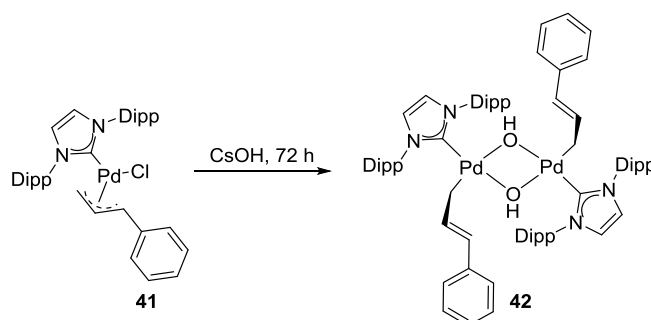
Scheme 1.11. Studies on Ru-IMes₂ complexes by Whittlesey⁵⁰

Kaplan and Bergman described the interesting preparation of a ruthenium hydrido-hydroxide complex **37** via oxygen atom insertion into the metal-hydride bond, mediated by N₂O (1 equiv., Scheme 1.12).⁵¹ Reaction with a second equivalent of N₂O leads to isolation of the dihydroxide complex **38**, albeit in low yields. The Ru-hydroxide moiety of **37** was reactive to a number of substrates, generating Ru thiolates, siloxides and alkoxides as shown, in yields between 25% and 40% (**39**). Complex **37** could also be reacted with silica to provide a silica supported system in the same way as Bergman has previously reported for the Ir-complex **24**.⁵² Both Ru-hydroxides **37** and **38** reacted with phenylacetylene to form either the Ru-acetylide or Ru-di(acetylide) **40** respectively. The authors indicate that the first step in the mechanism of bond activation is likely the reversible dissociation of the hydroxide to give a metal⁺/OH⁻ ion pair. In the case of addition of a weak acid (X-H), the initial ion pair formation is followed by oxidative addition of X-H and concomitant removal of a hydride by the (OH)⁻ to give M-X.⁵³



Scheme 1.12. Preparation of Ru-hydroxides by O-insertion of N₂O⁵³

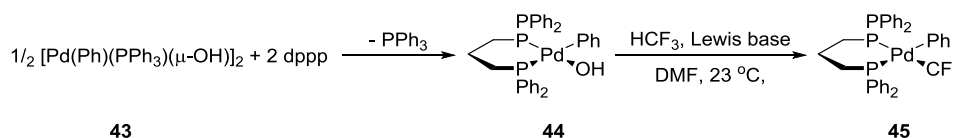
Group 10 metal hydroxides have been proposed as intermediates in several catalytic cycles and a number of these have been prepared synthetically. Nickel tends to form bridged complexes very easily and hence, most of the hydroxide complexes of Ni tend to be multi-metallic in nature.¹² Pd(II) complexes have been isolated as bridged dimers, such as $[\text{Pd}(\text{Ar})(\text{L})(\mu\text{-OH})]_2$ (L = tertiary phosphine)⁵⁴ and the NHC-bearing $[\text{Pd}(\eta^3\text{-allyl})(\text{NHC})(\mu\text{-OH})]_2$ **42** reported by our group (Scheme 1.13).⁵⁵ Complex **42** was used as a precatalyst in Buchwald-Hartwig aryl amination and Suzuki-Miyaura coupling, providing evidence that Pd-OH complexes may act as intermediates in the generation of catalytically active Pd(0) species from Pd(II)-Cl precatalysts.⁵⁵ This report supported the mechanistic study by Carrow and Hartwig,⁵⁶ on the transmetalation step of the Suzuki-Miyaura reaction which identified Pd-OH as the active species that undergoes transmetalation with arylboronic acids and not the Pd-halide precatalyst. In contrast to the lighter members of the group, platinum is able to form monomeric hydroxides of Pt(II) or Pt(IV) by oxidative addition reactions with H_2O .⁵⁷



Scheme 1.13 Preparation of Pd(II)(NHC) hydroxide by salt metathesis⁵⁵

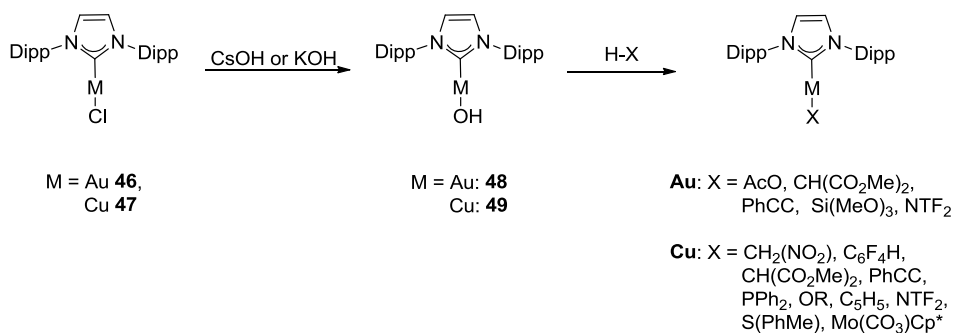
Takemoto and Grushin⁵⁸ have isolated a monomeric Pd(II)-hydroxide in the form of $[\text{Pd}(\text{dppp})(\text{OH})(\text{Ph})]$ **44** by reaction of the Pd dimer **43** with 2 equivalents of the bisphosphine ligand (bis(diphenylphosphino)propane, dppp, Scheme 1.14). Using complex **44**, the authors reported the first palladation of fluoroform (HCF_3) to give Pd- CF_3 complex **45**. The reaction is driven by Lewis base assisted H-bonding between the HCF_3 and the hydroxyl moiety, with the most effective Lewis base being $^t\text{Bu}_3\text{P}$. Fluoroform is a side product of the fluoropolymer industry, which generates more than 20 ktonnes annually.⁵⁹ Although it is non-toxic, the large scale release of HCF_3 into the atmosphere has raised environmental concerns due to its green-house effect. HCF_3 has a long atmospheric lifetime (>250 years)⁶⁰ and it has a global warming potential calculated at >10,000 times higher than that of CO_2 .⁵⁹ As a result, waste streams cannot be released into the atmosphere and must be destroyed. The incineration of HCF_3 is very

energy inefficient since it acts as a flame retardant and hence, the use of HCF_3 as a feedstock is a much more desirable approach than its destruction.⁵⁸ Palladium complexes dominate the field of trifluoromethylation catalysis⁶¹ and therefore, the activation of HCF_3 by Pd(II)-OH was a very important break-through for the field. The preparation of CF_3 complexes will be dealt with in more detail in Chapter 6.



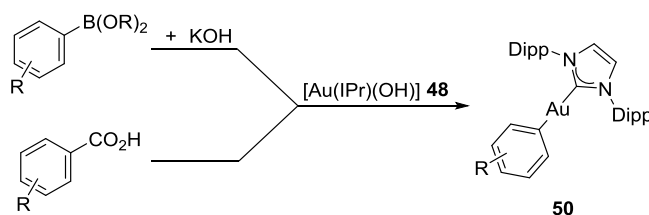
Scheme 1.14. C-H activation of HCF_3 by Pd(II)-hydroxide⁵⁸

Monomeric linear hydroxide complexes of the coinage metals were the first metal hydroxides to be developed in our group.⁶² Mechanistic investigations into gold-mediated transformations in the presence of water implicated $[\text{Au}(\text{IPr})(\text{OH})]$ **48** (IPr = 1,3-bis(2,6-diisopropylphenyl)imidazol-2-ylidene) as an important intermediate and furthermore, described **48** as being very stable. Treatment of $[\text{Au}(\text{IPr})\text{Cl}]$ (**46**) with KOH led to the isolation of $[\text{Au}(\text{IPr})(\text{OH})]$ (**48**) as a stable complex (Scheme 1.15) and $[\text{Cu}(\text{IPr})(\text{OH})]$ (**49**) was later prepared in the same way from the corresponding Cu-chloride **47**. Both **48** and **49** proved to be valuable synthons for selective X-H bond activation *via* deprotonation of a wide range of organic substrates, including *sp*, *sp*² and *sp*³-hybridised C-H bonds to give a plethora of new Au(I) and Cu(I) species (Scheme 1.15).^{34a, 34d, 35} The Cu(I)-hydroxide **49** was also able to cleave Si-N and Si-C bonds to give cyano- and silyl-copper complexes. Complex **49** is able to deprotonate a Mo complex in the form of $[\text{Mo}(\text{CO})_3\text{Cp}(\text{H})]$ to give a heterobimetallic Cu-Mo complex. A number of alcohols, HNTf_2 , *p*-thiocresol, fluorinated arenes and even HPPH_2 were all activated by Cu(I)-hydroxide **49** (Scheme 1.15). These reports demonstrated the breadth of appreciable reactivity that can be achieved by metal hydroxides, stabilised by suitable supporting ligands.⁶³



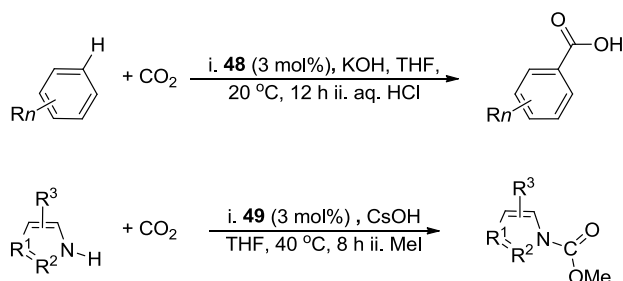
Scheme 1.15. Preparation of Cu(I) and Au(I)-hydroxides and representative examples of bond activation (deprotonation) reactions by these complexes.^{62a, 62d}

The gold hydroxide **48** reacts with a wide range of acetylene compounds, both terminal and internal to give Au(I)-acetylide complexes and in the case of triethynylbenzene, a (Au)₃-acetylide species was generated.⁶⁴ The hydroxide moiety on **48** was found to facilitate transmetalation with boronic acids, giving swift access to an array of Au(I)-aryl complexes **50** (Scheme 1.16).⁶⁵ The Au(I)-aryl complexes **50** can also be accessed *via* the decarboxylation of carboxylic acids in the presence of **48**.⁶⁶



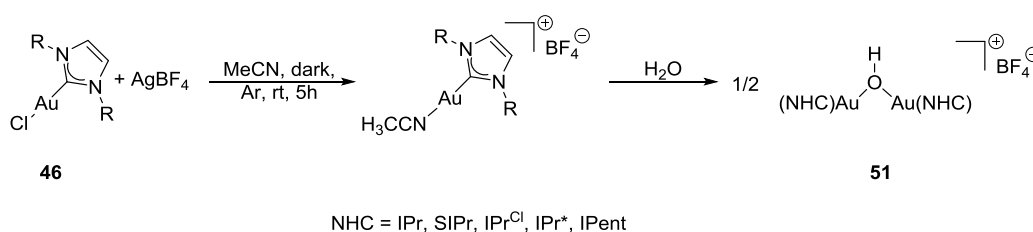
Scheme 1.16. Preparation of Au(I)-aryl complexes from Au(I)-hydroxide⁶⁵⁻⁶⁶

[Au(IPr)(OH)] (**48**) has been used as a catalyst for the solvent-free polymerisation of *rac*- β -butyrolactone to biodegradable polymers,⁶⁷ and in 2010 Boogaerts and Nolan reported that **48** promoted the regioselective carboxylation of aromatic C-H bonds under CO₂ (1.5 bar).^{62b} [Cu(IPr)(OH)] (**49**) was later shown to catalyse the same reaction, as well as the N-H carboxylation of various nitrogen heterocycles (Scheme 1.17).^{62e}



Scheme 1.17. Regioselective carboxylation of C-H and N-H bonds using Au(I) and Cu(I) hydroxides^{62b, 62e}

The Nolan group has also reported the synthesis of a di-gold complex bearing a bridging hydroxide [$\{\text{Au}(\text{IPr})\}_2(\mu\text{-OH})\text{BF}_4$ (**51**) *via* several routes from either the Au chloride **46** and AgBF_4 or the Au hydroxide **48** in the presence of HBF_4 .⁶⁸ For example, an aqueous based methodology allowed preparation of a number of the diaurated species, bearing different NHCs (scheme 1.18).⁶⁹ These interesting complexes have provided rich chemistry and proven to be highly active as catalysts in a number of water-inclusive transformations, including alkyne and nitrile hydration and Meyer-Schuster rearrangement⁶⁹ and have even provided access to aryl vinyl ethers by hydrophenoxylation of alkynes under very mild conditions.⁷⁰



Scheme 1.18. Preparation of digold hydroxides from the Au chloride⁶⁹

There is a common theme to all of the work described on LTM hydroxides by the Nolan group. In all of these reports, the metal hydroxides have been isolated with the assistance of NHC groups as ancillary ligands. As mentioned, the stabilisation of the HSAB mismatching metal hydroxide pair by attachment of an NHC is counter intuitive, yet the enhanced stability of metal NHC complexes has provided access to a number of stable LTM-hydroxides and allowed our group to pursue some very fascinating chemistry.

1.2. N-HETEROCYCLIC CARBENES (NHCs)

The supporting or ancillary ligands bound to an organometallic complex have a direct effect on the stability and reactivity of the complex. Therefore, it is important that the ancillary ligands can be tailored to some extent to suit the function of a particular organometallic complex. Three classes of ligands exist that can be tailored both sterically and electronically for broad use on late transition-metals. The traditional phosphines (PR_3) and cyclopentadienyls (C_5R_5) have been used extensively in organometallic chemistry and modification of their substituents allows for adjustment of both steric and electronic characteristics. However, in most cases the two characteristics cannot be altered independently.⁷¹

The third class of ‘tuneable’ spectator ligands are the carbenes, compounds containing a 6-electron divalent carbon centre.⁷² More specifically, *N*-heterocyclic carbenes (NHCs) are cyclic carbenes containing at least one α -amino substituent.⁷²⁻⁷³ The α -amino substituents play an important role in stabilising the ground state multiplicity of the carbene *via* cooperative inductive and mesomeric roles. Their σ -withdrawing character stabilises the formally sp^2 -hybridised non-bonding lone pair, while π -donation of the α -amino lone pairs into the vacant p-orbitals destabilises them. The result is a polarised four-electron three-centre π -system with some multiple bond character at the carbene carbon and hence the existence of a zwitterionic type structure with the negative charge localised at the carbon. This ensures that electroneutrality at the carbene centre is maintained and renders the singlet state dominant.⁷⁴ Although NHCs are very different to phosphines in terms of electronics and spatial arrangement (and hence steric impact), they both contain a non-bonding singlet lone pair and act as two electron donors.⁷⁴ As a result, the two ligand classes are comparable as supporting ligands and in the early years of NHC explorations, they were often termed as phosphine mimics.

NHCs may consist of three-, four-, five- or even seven-membered heterocycles. The most commonly utilised NHCs are the five-membered imidazol-2-ylidenes **NHC-1**, imidazolin-2-ylidines **NHC-2**, benzimidazol-2-ylidines **NHC-3** and triazol-2-ylidines **NHC-4** (Figure 1.1).

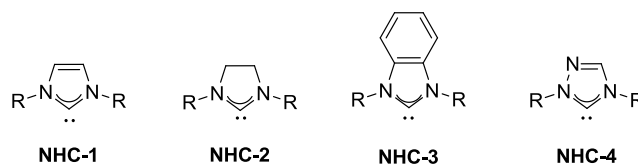
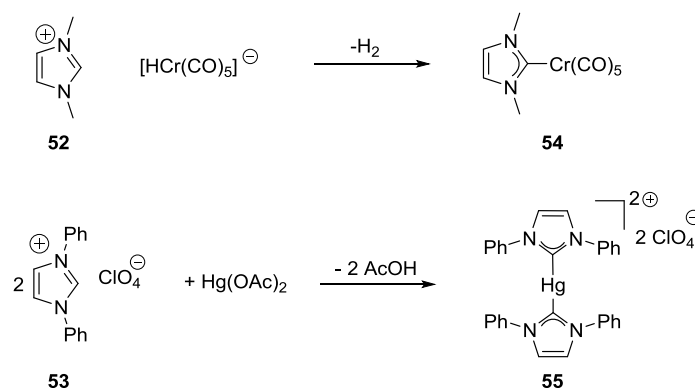


Figure 1.1. Common five-membered NHCs.⁷⁵

Early fundamental work on NHCs was reported by Wanzlick⁷⁶ and Öfele⁷⁷ in the 1960s, who independently isolated the first metal-NHC complexes. Both procedures involved the deprotonation of an imidazolium salt (**52** and **53**) to afford the imidazol-2-ylidene complexes of chromium **54** and mercury **55** as shown in Scheme 1.19. This methodology was later extended by Lappert to include complexes of the saturated imidazolin-2-ylidines (of the type **NHC-2**).⁷⁸



Scheme 1.19. Preparation of the first metal-NHC complexes by Öfele⁷⁷ and Wanzlick⁷⁶

Arguably the most important breakthrough in NHC investigations came in 1991, when Arduengo⁷⁹ isolated the first free carbene, 1,3-bisadamantylimidazol-2-ylidene (IAd) *via* deprotonation of the corresponding imidazolium chloride salt. This was later followed by isolation of the *p*-tolyl and mesityl analogues (ITol and IMes, Figure 1.2).⁸⁰ The isolation of ‘free’ carbenes and the discovery that they could be handled and stored under inert atmospheres enabled the direct preparation of metal-NHC complexes, and triggered explorations into NHC coordination chemistry and their utility as ancillary ligands.⁷³ The potential of NHC compounds as supporting ligands was realised by Herrmann,⁸¹ Enders,⁸² and Dixneuf,⁸³ who capitalised on their unique properties, transforming them from ‘mere laboratory curiosities’ into a class of highly versatile supporting ligands for homogeneous catalysis, with a range of applications, comparable to the established cyclopentadienyl and phosphine ligands.^{71, 73}

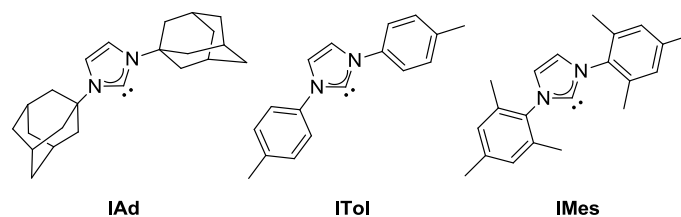


Figure 1.2. First reported free NHCs: Arduengo's imidazol-2-ylidenes.⁷⁹⁻⁸⁰

The application of NHCs as supporting ligands has led to improved reactivity in a wide range of reactions, with the impact being perhaps most prolific in the fields of ruthenium catalysed olefin metathesis¹ and palladium catalysed cross couplings.² More recently, gold chemistry has flourished; and its growth has a lot to do with the employment of NHC ligands in stabilising Au complexes and the elucidation of straight-forward synthetic routes to Au(I)-NHC complexes.⁸⁴ The success of NHCs as ligands in catalysis is often attributed to their powerful σ -electron donating ability, enabling the formation of strong metal-carbene bonds.⁸⁵ In comparisons between NHCs and phosphines, the superior σ -donation of NHCs is often noted.^{71, 81a, 81c, 86} NHCs are powerful σ -donor nucleophiles with comparatively low π -acidity, typically forming strong metal-carbon bonds with high dissociation energies that are chemically and thermodynamically more inert to cleavage than metal-phosphine bonds.⁸⁷ This concept was proven by Huang and Nolan, who performed calorimetric studies on a series of [RuClCp*(L)] complexes (L = PR₃ or NHC). The authors reported that, with the exception of IAd, ligand substitution reactions on the Ru complexes were more exothermic (higher bond dissociation enthalpies) for NHC ligands (5 entries) than for PCy₃ or P^{*i*}Pr₃.⁸⁸ It was originally thought that strong metal-NHC bonds were a result of essentially pure σ -bonds between the metal and the NHC,^{81a, 87} however, studies have provided evidence to the contrary. In particular, a study by Cavallo and co-workers on a series of NHC complexes showed that the M-carbene bond cannot be considered as purely σ in nature. Even in the case of d⁰ systems, there is a considerable amount of π -bonding (*ca.* 10%) that contributes to the overall orbital interaction. In systems with a low d-electron count, both π -bonding and π -back bonding have a significant contribution to the overall π -bond. However, as the d-electron count increases across a series, π -back bonding becomes more dominant, ranging from *ca.* 65% of the total π -bond in d⁰ systems to as high as 90% for d¹⁰ systems.⁸⁹

The difference in shape and connectivity of NHC ligands compared to phosphines and cyclopentadienyls has a direct impact on steric and electronic characteristics. For

example, in the latter two classes, the ligands can be thought of as ‘cone shaped,’ particularly the phosphines, with their substituents bonded directly to the donor atoms and generally pointing away from the metal (B and C, Figure 1.3). NHC ligands on the other hand are ‘fan shaped,’ with the *N*-substituents pointing towards the metal and separated from the donor atom by two bonds (C, Figure 1.3). This has the implication that substituent alterations on phosphines or cyclopentadienyls normally affects both the steric and electronic characteristics of the ligand, which often cannot be varied independently. Alterations to the *N*-substituents on NHCs, on the other hand have a much larger effect on the steric nature of the ligand than the electronic character. Significant electronic alterations are often effected by making structural changes within the azole ring itself, particularly on the carbon backbone.^{71, 90}

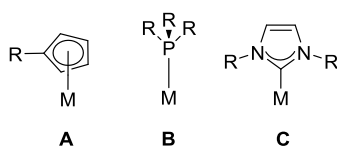


Figure 1.3. Spatial representation of typical cyclopentadienyl (A), phosphine (B) and NHC (C) ligands.⁷¹

The ability to alter the steric and electronic properties of NHC ligands independently makes them very versatile as supporting ligands and the ease with which specific properties can be tailored to fit particular catalytic applications has been documented in several articles.^{3b, 90b, 90c, 91} The electronic character of NHCs varies much less than for example, a series of phosphines; however, the establishment of a reliable method for the quantification of ligand electron-donation, *via* calculation of the Tolman electronic parameter (TEP)⁹² has enabled targeted ligand architecture, leading to an expansion of the NHC library with significantly divergent electronic characteristics.^{86a}

The TEP method was originally designed to quantify the electronic properties of tertiary phosphine ligands but is useful for most two electron donor ligands and has become a widely accepted method of electronic quantification.^{86a, 93} When a ligand (L) is coordinated to Ni in $[\text{Ni}(\text{CO})_3\text{L}]$, σ -electron donation from L increases electron density at the metal and hence strengthens the π -back donation from Ni into the π^*_{CO} anti-bonding orbital. The stronger the π -donation is from the metal, the weaker the triple bond between C and O will be in the carbonyl ligand. Hence, the electronic character of the ligand L can be inferred from the A_1 vibrational frequency of CO in an IR spectrum

of $[\text{Ni}(\text{CO})_3\text{L}]$. The TEP is the frequency of A_1 and is directly proportional to the σ -donating character of L, hence, the more σ -donating L is, the lower the TEP will be.^{93a}

Although this method was established using Ni, the precursor $[\text{Ni}(\text{CO})_4]$ is extremely toxic. Complexes of the type $[\text{MCl}(\text{CO})_2\text{L}]$ ($\text{M} = \text{Rh}/\text{Ir}$) are much easier and safer to access. The corresponding $[\text{MCl}(\text{cod})\text{L}]$ complexes are reacted with CO to give $[\text{MCl}(\text{CO})_2\text{L}]$, with the two CO ligands arranged *cis* to each other. Hence, the average of the two carbonyl stretching vibrations is used to calculate TEP and several researchers have worked to develop equations to correlate the values obtained from Rh or Ir systems to TEP values calculated for the parent $[\text{Ni}(\text{CO})_3\text{L}]$ system.^{86a, 93a, 94}

As previously mentioned, the steric bulk of the NHC can have a profound effect on the stability and activity of a metal complex to which it is bound. For example, Maj and co-workers reported that catalysts bearing various alkyl substituted NHCs were inactive in the polymerisation of cyclooctene, whereas those bearing aryl-substituted NHCs were active as long as the *ortho* positions were blocked by alkyl groups, avoiding *ortho*-metalation.⁹⁵ In order to compare the steric bulk of different NHCs, the well-established Tolman cone angle⁹² was inadequate since the NHC is not cone-shaped. In order to provide a method of quantifying steric demand within the metal sphere, Nolan, Cavallo and their co-workers developed the concept of buried volume ($\%V_{\text{Bur}}$) which is suitable for calculating the steric influence of a wide array of ligands. Buried volume relies on the ability to generate a well-defined sphere around the metal, either by obtaining a crystal structure of the complex or by theoretical calculations. The $\%V_{\text{Bur}}$ refers to the percentage of a sphere (with a radius r) that is occupied by atoms of a ligand of interest.⁹⁶ The $\%V_{\text{Bur}}$ is strongly dependent on the nature of the complex and the parameters used.⁹⁷ It also does not account for ligand flexibility in solution⁹⁸ and hence, it provides only a semi-quantitative comparison of the steric demand of the ligand. However, comparison of bond dissociation energies (BDE's) have clearly illustrated a correlation between M-L bond distances and $\%V_{\text{Bur}}$.⁹⁹ More recently, this concept has been elaborated to include a method of mapping the steric bulk within the coordination sphere in 3 dimensions, giving further insight into the spatial arrangement of a ligand.⁹⁸

There are a variety of synthetic routes for the preparation of NHCs and their precursors. The most commonly employed methods target the deprotonation of azolium

salts, while alternatives often involve reductive desulfurisation of thioureas or α -elimination of small molecules.¹⁰⁰ NHC precursors are made up of three distinct subunits: the backbone functionality, the pre-carbenic unit and the amino unit (Figure 1.4). Whichever route is used to access the NHC precursor, whether *via* an azolium salt or a thiourea, the critical step in the synthesis is most often the cyclisation event, either by introduction of the pre-carbenic unit, linkage of the backbone to the preassembled pre-carbenic and amino units, or ring closure by introduction of the amino moiety.¹⁰⁰ The high demand for NHC precursors has meant that many of the imidazolium salts have become commercially available and their syntheses are scalable to kilogram batches.

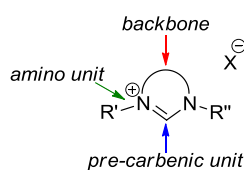


Figure 1.4. Simplified imidazolium unit

NHC complexes of almost every metal in the periodic table are now known. Most synthetic protocols can be divided into three main categories: (i) *in situ* deprotonation of ligand precursors; (ii) complexation of free carbenes; and (iii) cleavage of electron rich olefins. The main complexation methods will be discussed in the next section, with particular attention being paid to examples of rhodium and iridium wherever possible.

1.2.1. NHC complexation

1.2.1.1. *In situ* deprotonation of ligand precursors

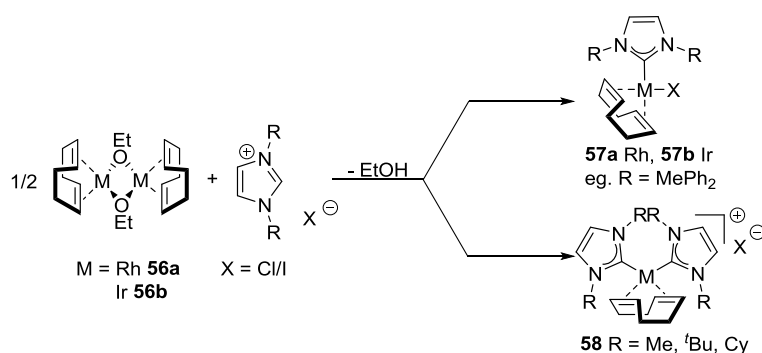
These routes are particularly useful when the corresponding carbenes are unstable or difficult to handle, since the free NHC does not need to be isolated.⁸⁷

1.2.1.1.1. Deprotonation by basic metalates

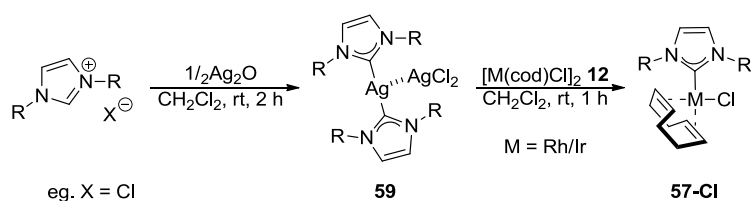
Although this route is limited by the nature and oxidation state of the metal, azolium cations can be deprotonated by Brønsted basic metalate anions upon heating, with the metal of the base acting as the ligand acceptor. This method was the first NHC coordination method described by Öfele⁷⁷ to prepare $[\text{Cr}(\text{CO})_5(\text{NHC})]$ **54** (Scheme 1.19).

1.2.1.1.2. Deprotonation by basic anions

Brønsted basic anions of the azolium salt or attached to the metal precursor can deprotonate the azolium salt *in situ* to give the desired NHC. Wanzlick used this strategy to prepare his mercury bis-NHC complex **55** (Scheme 1.19) and the method was utilised extensively before the isolation of free carbenes was first reported.⁷⁶ This method is still valuable in some cases, for example, Rh and Ir(μ -alkoxo) complexes **56** can be easily prepared by adding $[M(\text{cod})\text{Cl}]_2$ ($M = \text{Rh}$ **12a**, Ir **12b**) to an alcohol solution of a metal alkoxide. The μ -alkoxo ligand then acts as an internal base, deprotonating the imidazolium salt at room temperature to generate either monomeric metal-NHCs $[M(\text{cod})(\text{NHC})\text{X}]$ (**57**), or bis-NHC complexes $[M(\text{cod})(\text{NHC})_2]\text{X}$ (**58**) depending on the NHC and the conditions employed (Scheme 1.20).^{81d, 101}

Scheme 1.20. Deprotonation by basic anions^{81d, 101}

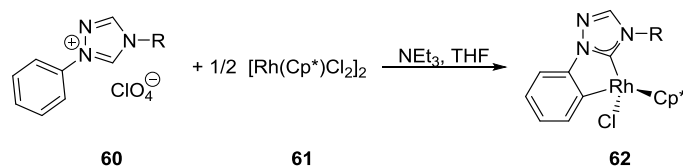
Silver(I) oxide is also a good precursor for this route, deprotonating imidazolium salts to give bis-NHC Ag(I) complexes which provide valuable transmetallation reagents, see section 1.2.1.4 (Scheme 1.21).¹⁰²

Scheme 1.21. Deprotonation of imidazolium salts using Ag_2O ¹⁰³

1.2.1.1.3. Deprotonation by an external base

External bases can be added to deprotonate azolium salts and will often lead to different products compared to the use of metal salts with basic anions. For example, lithium alkoxides or a combination of a potassium alkoxide and sodium hydride can deprotonate imidazolium salts *in situ*.¹⁰⁴ Triethylamine (NEt_3) in THF can also be used

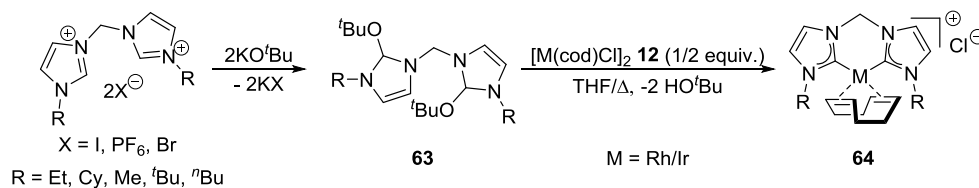
as an external base for *in situ* deprotonation of triazolium salts, as shown in Scheme 1.22. The perchlorate salt **60** is deprotonated to give the corresponding free carbene, coordination to Rh and concomitant *ortho*-metalation on the phenyl group leads to $[\text{RhCl}(\text{Cp}^*)(\text{NHC})]$ (**62**).¹⁰⁵



Scheme 1.22. Preparation of *ortho*-metalated Rh(III)-complexes via *in-situ* deprotonation¹⁰⁵

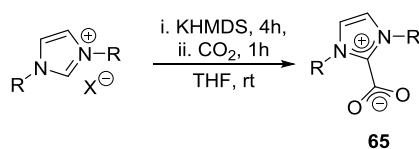
1.2.1.1.4. Small molecule elimination from neutral ligand precursors

Imidazolium salts, when reacted with a metal alcoholate such as KO^tBu will either be deprotonated or transformed into an alkoxy imidazolidine **63** as in Scheme 1.23.^{82a, 101b, 106} The alcoholate **63** is able to release the alcohol thermally to give the free NHC *in situ*.



Scheme 1.23. Small molecule activation route via alcoholate precursor^{101b, 106}

NHC- CO_2 adducts can be prepared by bubbling CO_2 through a solution of the imidazolium salt in the presence of a base such as potassium hexamethyldisilazane (KHMDs) or KO^tBu (Scheme 1.24). The resultant CO_2 adducts (**65**) are stable zwitterions that can be stored under air for long periods of time but will release CO_2 when heated with metal precursors such as $[\text{RuCl}_2(p\text{-cymene})]_2$ or $[\text{Rh}(\text{cod})\text{Cl}]_2$ **12a** to generate the corresponding metal-NHC complexes.¹⁰⁷



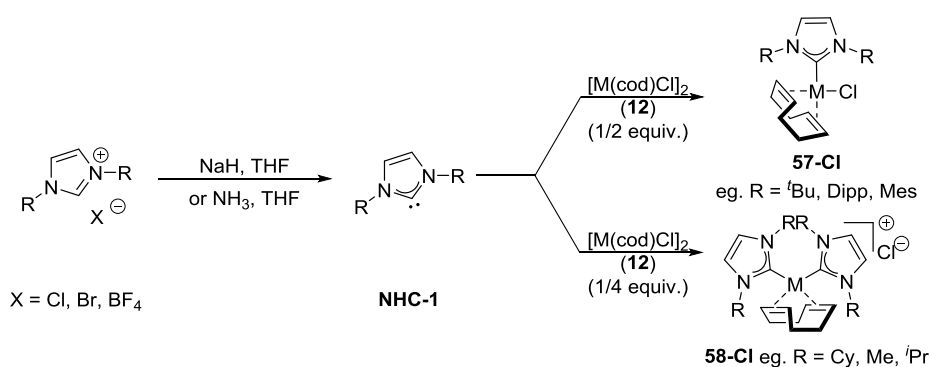
Scheme 1.24. Preparation of CO_2 -imidazolium adducts¹⁰⁷

1.2.1.2. The free NHC route

Isolation of stable free NHCs by Arduengo⁷⁹ (Figure 1.2) meant that they could be directly coordinated to metal complexes. The advantage of this approach is that metal precursors with varying oxidation states and ligand spheres can be utilised. Imidazolium salts can be deprotonated to form free NHCs by bases such as NaH or KO^tBu in THF⁷⁹⁻⁸⁰ or by NaH in liquid ammonia (Scheme 1.25).^{81d, 108} Methylene bridged bis-imidazolium salts can be deprotonated by KHMDS and coordination gives complexes such as **64**,¹⁰⁹ while cyclic thioureas such as 1,3,4,5-tetramethylimidazole-2(3*H*)-thione can be converted to free NHCs by elemental Na or K.¹¹⁰ The isolation of free NHCs has provided access to a wide range of metal-NHC complexes. The disadvantage of isolating free carbenes is that they are sensitive to air and moisture and need to be handled under an inert atmosphere and are often thermally unstable.⁸⁷

1.2.1.2.1. Dimer cleavage

Dimeric complexes with bridging halides, acetonitrile groups or CO ligands can be fragmented by nucleophilic NHCs. For example, Scheme 1.25 shows the dimer cleavage of [M(cod)Cl]₂ (**12**) to give monomeric metal-NHC complexes of the type (**57-Cl**).^{101b} NHCs with a small steric demand (for example when R = Me, Cy or ⁱPr) may form bis-NHC complexes (**66**).^{81d}

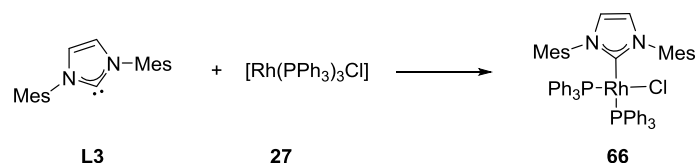


Scheme 1.25. Free NHC route with metal dimer cleavage^{81d, 87}

1.2.1.2.2. Ligand exchange

Phosphines have relatively low dissociation energies and can be exchanged easily on metal complexes. In many cases this route leads to mixed NHC-phosphine systems.⁸⁷ For example, a phosphine on Wilkinson's catalyst (**27**) can be replaced by reaction with a free NHC such as IMes to give [RhCl(IMes)(PPh₃)₂] **66** (Scheme 1.26).¹¹¹ Other ligands, such as CO or cod can be substituted by NHCs on homoleptic

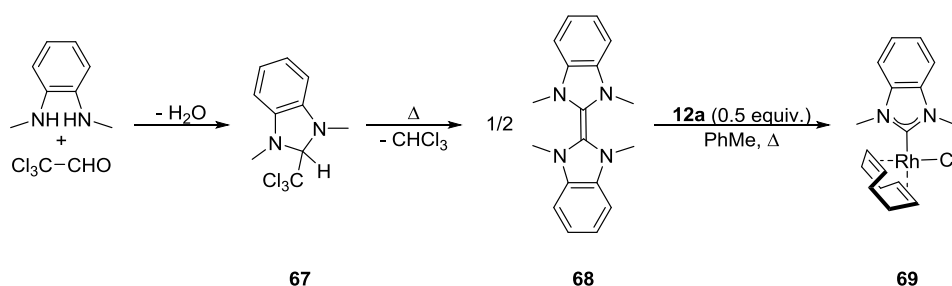
complexes such as $[\text{Cr}(\text{CO})_6]$, $[\text{W}(\text{CO})_6]$, $[\text{Fe}(\text{CO})_5]$, $[\text{Ni}(\text{CO})_4]$,^{87, 108} $[\text{Ni}(\text{cod})_2]$ or $[\text{Pt}(\text{cod})_2]$.¹¹²



Scheme 1.26. Phosphine substitution on Wilkinson's catalyst **27** to give a mixed NHC-phosphine system¹¹¹

1.2.1.3. Olefin Cleavage

Electron-rich olefins are nucleophilic and can be cleaved thermally by transition-metal complexes. There are various methods for the dimerisation of non-stable NHCs to form tetraaminoethylenes (or enetetramines).⁸⁷ For example, the benzimidazolin-2-ylidene complex **69** can be prepared from the corresponding enetetramine **68** and $[\text{Rh}(\text{cod})\text{Cl}]_2$ (**12a**) in refluxing toluene (Scheme 1.27).¹¹³



Scheme 1.27. Olefin cleavage of an enetetramine by $[\text{Rh}(\text{cod})(\text{Cl})_2]$ (**12a**)¹¹³

1.2.1.4. Ligand transfer reactions

NHC ligands can be transferred intermolecularly from one metal to another. For example, NHC complexes of Cr, Mo, and W have been reported to transfer NHCs to Rh(I), Pd(II), Pt(II), Cu(I), Ag(I) and Au(I).¹¹⁴ Ag(I)-NHC or Cu(I)-NHC complexes prepared from Ag(I) or Cu(I) *via* basic anion deprotonation act as excellent ligand transfer agents as they are prepared directly from the imidazolium salts. This method is useful for the transfer of NHCs to a number of metal complexes. For example, in the case of Ir, the unwanted dicoordination of small NHCs can be avoided by transmetalation with Ag (Scheme 1.21),¹⁰²⁻¹⁰³ while Cazin and co-workers have shown that $[\text{Cu}(\text{NHC})\text{Cl}]$ (**47**) efficiently transfers NHC ligands to Pd or Au.¹¹⁵

1.2.2. Rhodium and iridium NHC complexes

Rhodium and iridium are two of the rarest elements on earth. This combined with their widespread use makes them very expensive transition metals. However, the chemistry of these metals is unique and worthy of investigation. Rh- and Ir-NHC investigations have experienced an exponential growth over the last three decades and the complexes described in this section and their uses in catalysis and organometallic synthesis by no means constitute a thorough account. This section will merely provide representative examples of the rich and diverse chemistry that these motifs have grown to encompass.

1.2.2.1. Rhodium NHC complexes

Rhodium, along with palladium and nickel dominates the field of LTM-NHC catalysis in terms of the number of published reports. The number of isolated Rh-NHC complexes is large and continues to grow. Their uses outside of catalysis are numerous, and even include a limited number of biochemical applications.¹¹⁶ The coordination of NHC ligands to Rh has been documented extensively for the quantification of electronic ligand parameters by the TEP method.^{86a, 93a}

In addition to showing complementary reactivity to other metals, rhodium has delivered new reactivity and holds the potential for development of more environmentally friendly processes due to its insensitivity to water. This has enabled the utilisation of H₂O as either a proton source or as a solvent, for example, where hydrolysis is important in preparing new organic compounds.¹¹⁷ Rh typically adopts the +1 or +3 oxidation state within a catalytic cycle and there is unique chemistry associated with each oxidation state.¹¹⁷ For the purpose of this investigation, focus will be concentrated more heavily on Rh(I) complexes.

The first report of an LTM-NHC complex as an efficient catalyst was with rhodium in the form of [Rh(cod)(IMe)Cl] **70** (IMe = dimethyl(imidazolin-2-ylidene), which was used as an efficient hydrosilylation catalyst.¹¹⁸ Since the mid 1990's, Rh-NHC complexes have featured extensively as homogeneous catalysts, promoting several transformations including but not limited to arylation, hydrosilylation, conjugate addition, hydroformylation and a number of cyclisations.^{84, 119}

1.2.2.1.1. Arylation with organoboron reagents

The addition of organoboron reagents to carbonyl compounds or α,β -unsaturated ketones is typically catalysed by rhodium complexes bearing phosphine or diene based ligands. As such, these transformations, along with hydrosilylation and hydrogenation reactions have been some of the most heavily investigated transformations promoted by Rh-NHC catalysts.¹¹⁹ The Rh-catalysed addition of boronic acids to aldehydes to give diarylmethanol compounds was first discovered by Miyaura in 1998.¹²⁰ Fürstner improved the method by using monodentate imidazolium salts with Rh, the best results being obtained with IPr·HCl and RhCl₃·3H₂O (1.0 mol% each). This allowed for the arylation of a range of aryl and alkyl aldehydes, while vinyl boronic acids were used to give allylic alcohols.¹²¹ Following this report, a number of Rh-NHC complexes were reported in addition reactions. Particularly, complexes of the type [Rh(cod)(NHC)Cl] have proven to be active precatalysts in the addition of arylboronic acids to benzaldehydes (Eq. 1, Figure 1.5). These complexes (**71**) have varied from those bearing five membered imidazol-2-ylidenes (**NHC-1**) such as **57a-Cl**,¹²² imidazolin-2-ylidines (**NHC-2**),¹²³ benzimidazol-2-ylidenes¹²⁴ and the perhydrobenzimidazol-2-ylidenes¹²⁵ (Figure 1.5); one of the most active catalysts to date for this transformation is that bearing the 6-membered tetrahydropyrimidin-2-ylidene on **73**, Figure 1.5.¹²⁶

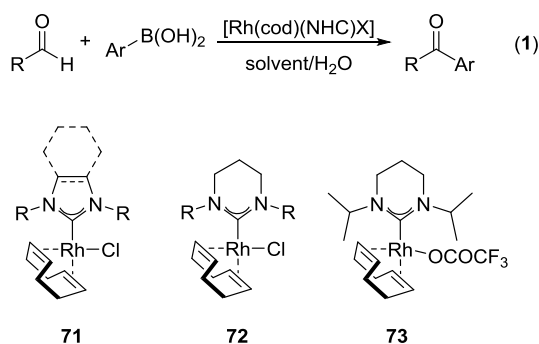


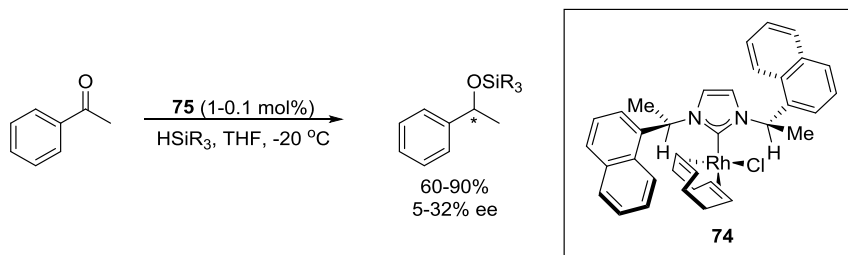
Figure 1.5. Arylation of aldehydes using [Rh(cod)(NHC)X] complexes

Although Rh complexes have been very successful in the conjugate addition of boronic acids to α,β -unsaturated ketones, there are relatively few reports of Rh-NHC complexes catalysing this reaction, which will be dealt with in detail in Chapter 2.

1.2.2.1.2. Hydrosilylation

Hydrosilylation reactions as a whole, constitute one of the most extensively studied transformations using Rh-NHC complexes.⁸⁴ The hydrosilylation of alkenes, alkynes, carbonyls and imines have all been catalysed by Rh-NHC complexes in both racemic and asymmetric fashions. The first report of an NHC complex performing

asymmetric catalysis was the hydrosilylation of acetophenone by diphenylsilane, in the presence of a naphthyl-derived NHC complex **74** (Scheme 1.28).¹²⁷

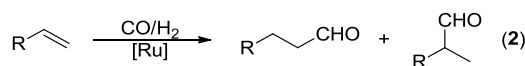


Scheme 1.28. Asymmetric hydrosilylation of acetophenone¹²⁷

Polydentate NHC ligands have been used extensively in the hydrosilylation of carbonyl compounds. In particular, Gade and co-workers have reported using oxazoline-based NHCs to reduce aryl and alkyl ketones.¹²⁸ There are many variations, particularly of the [Rh(cod)(NHC)Cl] scaffold reported in the literature that have been used in carbonyl hydrosilylation.⁸⁴ Alkene and alkyne hydrosilylation by comparison have been investigated much less using NHC complexes and these complexes will be discussed in Chapter 3. Recently, Oro *et al.*¹²⁹ developed a method for the preparation of dimeric [Rh(NHC)(coe)(μ -OH)]₂ (**75**, NHC = IPr or IMes, coe = *cis*-cyclooctene). The authors showed that the complexes were very efficient in the hydrothiolation of alkynes to give α -vinyl sulphides with high selectivity.

1.2.2.1.3. Hydroformylation

The hydroformylation of alkenes (Eq. 2) is one of the largest homogeneous industrial processes by volume.¹³⁰ Reactions have historically been dominated by phosphine based systems such as Wilkinson's catalyst (**27**) and therefore, a number of Rh-NHC complexes have been tested in hydroformylation, particularly variants of the [Rh(cod)(NHC)X] (**57a**) framework.^{119,1184} Crudden and co-workers reported the first Rh-NHC catalysed hydroformylation of various styrene derivatives in high yield and selectivity towards branched products using Wilkinson analogues [RhCl(IMes)(PPh₃)L] (**67**: L = PPh₃, **76**: L = CO, Figure 1.6).^{111a, 131}



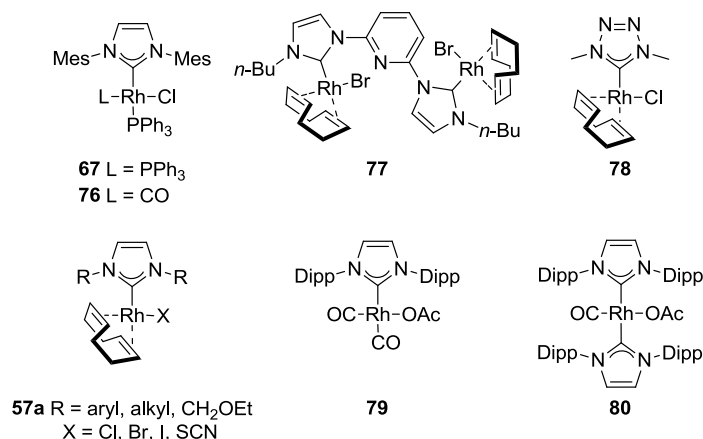


Figure 1.6. Rh(I)-NHC complexes tested in hydroformylation reactions¹¹⁹

Bimetallic complexes (**77**) were tested by Peris and Fernandez¹³² in the hydroformylation of alkyl and aryl alkenes, showing high selectivity for the branched products. Buchmeiser¹³³ has investigated the use of tetrahydropyrimidinylidene systems such as **73** and Weberskich has tested several tetrazole-based systems, with one of the most active catalysts to date being **78**, boasting TOFs of up to 3540 h⁻¹.¹³⁴ The halide- and cod-free complexes such as **79** and **80**, coordinated to the bulky IPr ligand, also showed high activity in hydroformylation reactions. The steric bulk of IPr was reported to hinder detrimental isomerisation reactions on the product.¹³⁵ Danopoulos and co-workers have also reported hydroformylation using NHC-indenyl chelate ligands which showed weak activity in both the hydroformylation of 1-octene and in the carbonylation of methanol.¹³⁶

1.2.2.1.4. Hydrogenation

Hydrogenation of unsaturated organic compounds is an important transformation, demonstrating ideal atom-economy. The first homogeneous catalyst to be developed for hydrogenation was Wilkinson's catalyst (**27**).¹³⁷ Wilkinson's catalyst is active at room temperature under 1 atm of H₂ and easily reduces monosubstituted and *cis*-disubstituted alkenes (e.g. cyclohexene).¹³⁸ Previously mentioned [RhCl(IMes)(PPh₃)₂] (**66**) was designed as an analogue of Wilkinson's catalyst (**27**) and hence, **66** and its analogues, with various phosphines have been tested extensively in hydrogenation reactions, particularly of olefins.^{111a} Although Nolan¹³⁹ and Lebel¹⁴⁰ have independently shown **66** to be active in a number of hydrogenation and methenylation reactions, **66** and analogous complexes are often found to be less active than **27**,¹⁴¹ requiring high temperatures and the addition of phosphine scavengers such as CuCl. The low activity

of **66** compared to Wilkinson's catalyst (**27**) has been rationalised by comparing the phosphine dissociation rates between **66** and **27**. For example, phosphine dissociation on **66** is 10 – 15 times slower than on Wilkinson's catalyst. Since phosphine dissociation constitutes the essential activation step, slow dissociation has a detrimental effect on catalyst activity.¹⁴¹⁻¹⁴²

A number of monodentate and bidentate NHC ligands have been successfully deployed as supporting ligands for hydrogenation catalysts. The monodentate NHC complexes, particularly of the [Rh(cod)(NHC)Cl] (**57a-Cl**) type, tend to be sensitive to decomposition in the presence of H₂ and phosphines can be added to avoid decomposition of the active species. For example, Herrmann and co-workers^{111b} have used 1,3-dicyclohexylimidazol-2-ylidene (ICy) derivatives (**57a**, **81** to **83**, Figure 1.7) in the hydrogenation of aliphatic alkenes (Eq. 3, Figure 1.7). In their study, the phosphine-free catalyst [Rh(cod)(ICy)Cl] **57a-Cl**^{ICy} was prone to decomposition and only showed activity comparable to Wilkinson's catalyst (**27**) when tertiary phosphines were added to the reaction mixture to provide a stabilising effect, presumably *via* formation of a 3-coordinate [Rh(Cl)(ICy)(PR₃)] species *in situ*. The best results were obtained using PPh₃ (2 equiv.) in EtOH at 60 °C, H₂ (20 bar). Phosphine dissociation plays an important role in this reaction and among the well-defined mixed NHC-phosphine systems, **82** was less active than **81** due to poor dissociation of the phosphite and further phosphine substitution by NHC as in **83** led to even lower catalytic activity.^{111b}

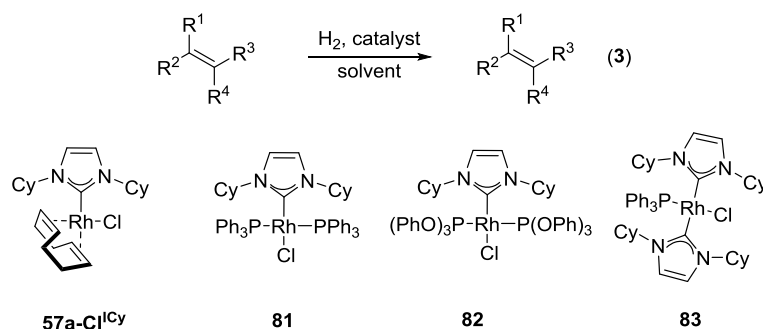


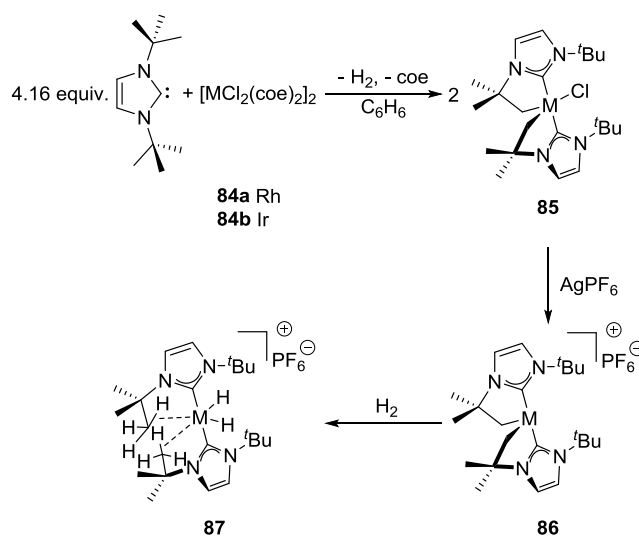
Figure 1.7. Rh-ICy complexes used in hydrogenation reactions^{111b}

1.2.2.2. Iridium NHC complexes

Ir-NHC complexes display reactivity comparable to the analogous Rh complexes, favouring the +1 and +3 oxidation states. A large amount of catalysis with Ir has focused on reduction reactions, with Ir-hydrides as key intermediates.⁸⁴ As with rhodium, many carbonyl-Ir-NHC complexes have been prepared in order to quantify

electronic characteristics of various NHCs¹⁰³ by the TEP method.⁹² The highly electron donating character of NHCs favours oxidative addition of C-H bonds involving the *N*-substituents. Since the *N*-substituents typically point towards the metal, coordination of NHCs to iridium and rhodium has produced interesting cyclometalated complexes.¹⁴³

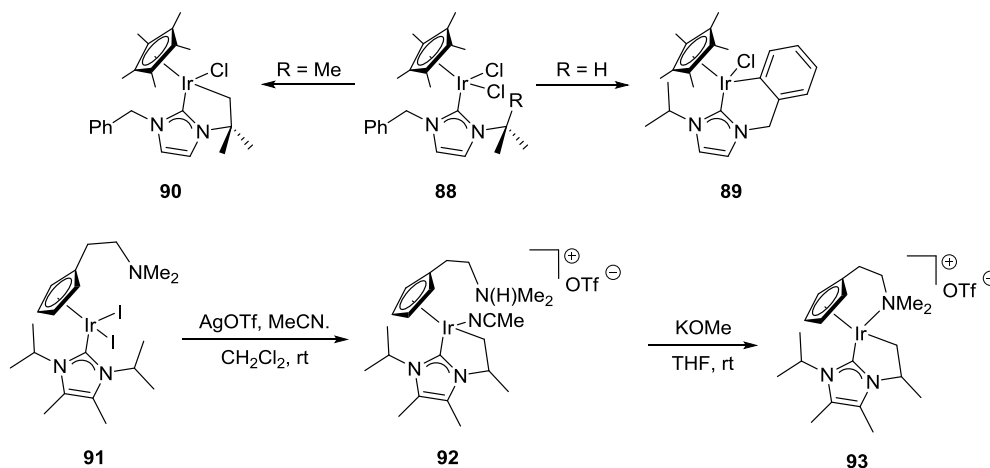
The most extensively studied process on iridium is C-H activation (both aromatic and aliphatic).⁸⁴ For example, our group has described the cyclometalation process by intramolecular C-H activation when *1,3*-di(*tert*-butyl)imidazol-2-ylidene (*t*Bu) is coordinated to $[M(\text{coe})_2(\mu\text{-Cl})_2]$ ($M = \text{Rh}$ **84a**, Ir **84b**, Scheme 1.29).¹⁴⁴ Halide abstraction using AgPF_6 afforded isolation of the unusual 14 electron complexes **86a-b** and the unusual stability of these electron deficient species was attributed to the high electron donor strength of the NHC. Furthermore, **86a** and **86b** could be reacted with H_2 to give the dihydride complexes **87a-b**, which are stabilised by agostic interactions with the metal centre.¹⁴⁵ Huang and Nolan have also shown that C-H activation of an *ortho* methyl group on IMes is possible on $[\text{RhCl}(\text{H})(\text{IMes})(\text{IMes}^*)]$.¹⁴⁶



Scheme 1.29. Cyclometalation processes resulting from bulky NHC ligands¹⁴⁴⁻¹⁴⁵

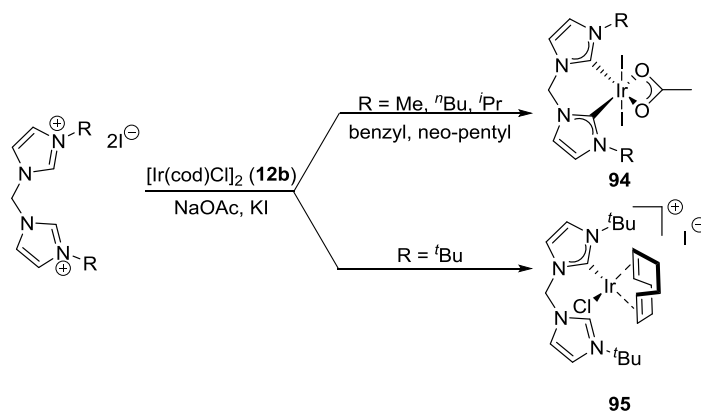
Several intramolecular C-H activation processes on Ir(III) have also been studied, such as the cyclometalation events that take place on $[\text{Ir}(\text{Cp}^*)(\text{NHC})]$ complexes reported by the groups of Peris and Yamaguchi (Scheme 1.30).¹⁴⁷ The C-H activations were found to be very facile in each case and the selectivity towards aromatic or aliphatic C-H activation was highly dependent on the steric nature of the NHC ligand. For example, in a report by Peris, on complexes of the type **88**, if R on the *N*-substituent (Scheme 1.30) is a proton then aromatic C-H activation occurs, leading to complex **89**. If R is an alkyl group such as a methyl, then the resultant *t*Bu group will be in closer

proximity to the metal centre and alkyl C-H activation will be favoured, giving **90**.^{147a} There are a number of different variations of intramolecular C-H activation involving these types of complexes and even examples where a basic functionality on the Cp ligand can act as a proton acceptor. For example, when **91** is reacted with AgOTf in acetonitrile, the cyclometalated carbene complex **92** is obtained. A proton on the ammonium moiety can be removed by reacting with KOMe to give the cationic tethered complex **93**.^{147d}



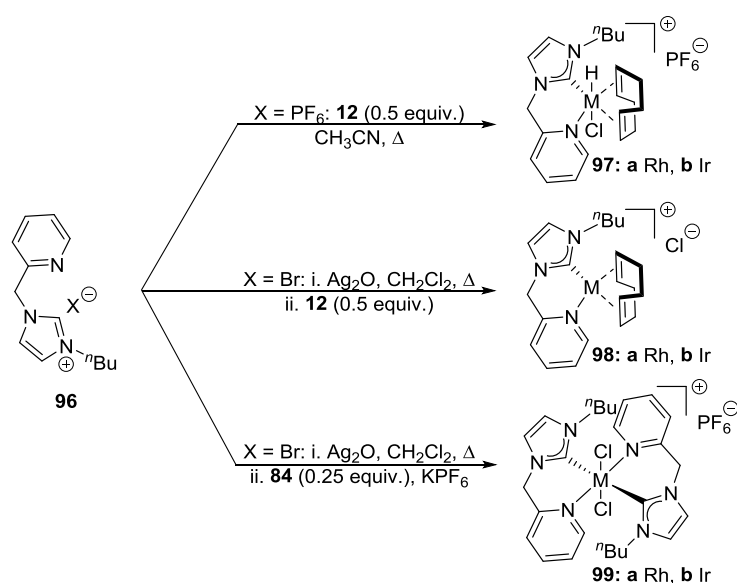
Scheme 1.30. C-H activation of Ir(III)(NHC) complexes

Polydentate NHC ligands have featured extensively on iridium, providing several different complexes where the topological properties of the ligand may be altered.¹⁴³ For example, chelate NHCs reported by Crabtree possess a methylene linker between the two imidazole units. The *N*-substituents in this case act as ‘wingtips’ and the steric bulk of the substituents may be tailored to switch the chelation on (**94**) or off (**95**, Scheme 1.31).¹⁴⁸



Scheme 1.31. Chelating NHCs and tailoring of steric bulk¹⁴⁸

The chelate effect can also favour oxidative addition, for example, in a report by Mas-Marzá *et al.*,¹⁴⁹ the authors showed how pyridine imidazolium salts (**96**) could be reacted with Rh or Ir dimers (**12**) and the chelate nature of the NHC lent itself towards C-H oxidative addition, leading in each case to a metal(III)-NHC hydride complex (**97**, Scheme 1.32). The C-H oxidative addition can be suppressed by transferring the NHC *via* Ag(I), leading instead to Rh(I) or Ir(I) complexes (**98**). If the metal precursor is changed for $[MCl(\text{coe})_2]_2$ (**84**) and reacted with the Ag-NHC in only 0.25 equiv. then metal(III)-*bis*NHC complexes are generated as shown (**99**).¹⁴⁹ The broad versatility shown by this chelating NHC compound is very interesting and complexes **97** - **99** were tested in benchmark catalytic transformations, with the complexes of **98** both showing decent activity in the hydrosilylation of phenylacetylene but with poor selectivity. The cyclisation of acetylenic carboxylic acids was successful and the authors reported the first cyclisation of 4-pentynoic acid by an Ir complex, **98b**.¹⁴⁹



Scheme 1.32. Coordination of pyridine imidazolium salts¹⁴⁹

1.2.2.3. Catalysis with Iridium NHC complexes

1.2.2.3.1. Hydrogenation

Following the development of Wilkinson's catalyst, Osborn and Schrock investigated the use of cationic Rh complexes, with the aim of eliminating the phosphine dissociation step involved in the activation of Wilkinson's catalyst (**27**). The cationic dihydride complexes proved to be very active in the reduction of alkynes to *cis* olefins and the reduction of dienes to monoenes.¹⁵⁰ Following thorough investigation of

cationic Rh complexes, Osborn and co-workers investigated cationic Ir complexes as hydrogenation catalysts but apparent low activity meant that they were disfavoured over their Rh analogues. However, in 1977, Crabtree and co-workers¹⁵¹ reported that the use of non-coordinating solvents with $[\text{Ir}(\text{cod})(\text{py})(\text{PR}_3)]\text{PF}_6$ complexes enabled the dehydrogenation of highly substituted alkenes. The most active catalyst in this series became known as Crabtree's catalyst, $[\text{Ir}(\text{cod})(\text{py})(\text{PCy}_3)]\text{PF}_6$ (**100**, Figure 1.8). Crabtree's catalyst soon became the benchmark in hydrogenation reactions, able to dehydrogenate a range of substrates with varying degrees of substitution and unchallenged in the hydrogenation of tri- and tetra-substituted olefins. However, the Achilles' heel of Crabtree's catalyst is its stability under catalytic conditions, **100** rapidly decomposes to irreversibly form inactive Ir-hydride clusters.¹⁵² In the hope of developing more thermally stable hydrogenation catalysts, Buriak¹⁵³ and Nolan¹⁵⁴ investigated the use of NHC ligands to stabilise Crabtree's catalyst. Lee and Nolan prepared the NHC (SIMes) analogue **101a** (Figure 1.8) of Crabtree's catalyst from $[\text{Ir}(\text{cod})\text{py}_2]\text{PF}_6$.

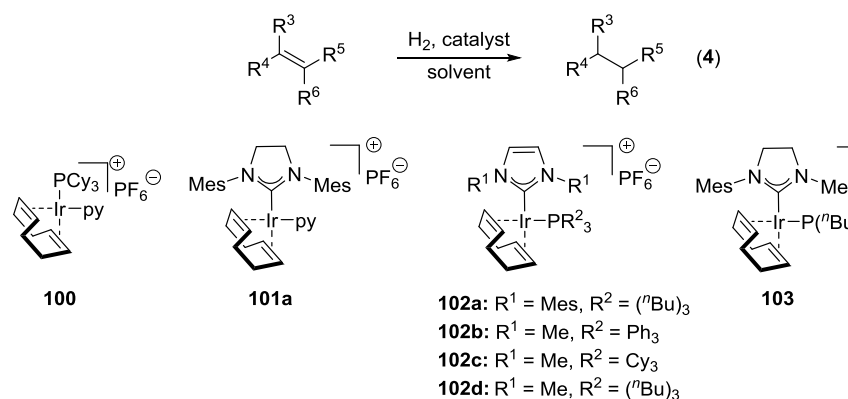


Figure 1.8. The development of Ir hydrogenation catalysts¹⁵³⁻¹⁵⁴

Although **101a** was less active than Crabtree's catalyst (**100**) in the hydrogenation of simple olefins at room temperature under H₂ (1 atm), **101a** proved to have higher thermal stability than **100** and was still catalytically active under mild H₂ pressure (60 psi) at 50 °C.¹⁵⁴ Buriak and co-workers investigated the effect of replacing the pyridine ligand with NHC ligands, rather than the phosphine (**102**, Figure 1.8). The authors reported that the mixed phosphine-NHC complexes showed comparable reactivity to **100** in the hydrogenation of primary (1-octene) and secondary (cyclohexene) olefins and that **102** showed enhanced stability compared to **100**. Hydrogenation reactions could be carried out in air, using reagent grade solvents.^{153a} Furthermore, the phosphine

complexes (**102**) out-performed the pyridine analogue **101** and the most active complex among them was that containing the IMe ligand and $P(t\text{Bu})_3$ (**102d**). The high steric bulk of IMes limited its coordination to complexes with smaller phosphine groups and **102a** showed high catalytic activity in the hydrogenation of unhindered alkenes but activity decreased with tertiary (1-methylcyclohexene) and quaternary (2,3-dimethyl-2-butene) alkenes. Overall, catalytic activity of **102** was comparable to **100** at 1 mol% catalyst loading but with enhanced stability towards air and un-purified reagents. These catalyst systems were further developed by Buriak's group, who in 2006 reported a highly active catalyst with reactivity surpassing even the state of the art, Crabtree's catalyst (**100**). By replacing the NHC with a saturated version (SIMes) as Nolan and Lee¹⁵⁴ had reported, and replacing the PF_6^- counter ion with the non-coordinating tetrakis[3,5-bis(trifluoromethyl)phenyl]borate (BARF), the resultant complex **103** showed high reactivity in hydrogenation reactions, even with tri- and tetra substituted alkenes and remarkable longevity under catalytic conditions.^{153b}

Nilsson and co-workers have further proven the utility of this scaffold and shown that analogues of complex **103**, bearing unsaturated NHCs are effective in a range of hydrogenation reactions, including the reduction of alkynes to alkenes.¹⁵⁵ In the same year as Lee and Nolan published their investigations of **101a**, Burgess and co-workers¹⁵⁶ reported the use of chiral chelating NHC ligands to prepare complexes of the type **104**, which were able to hydrogenate aryl alkenes (Eq. 5, Figure 1.9) giving enantioselectivities up to 98%.

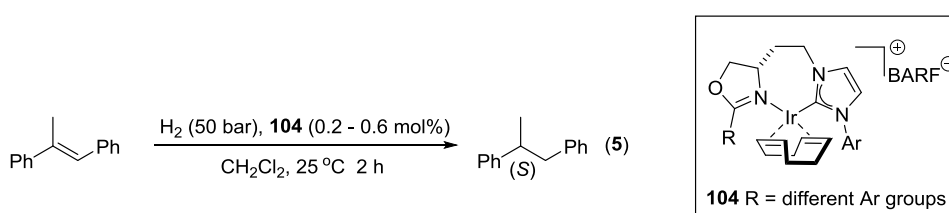


Figure 1.9. Enantioselective hydrogenation using chiral NHC ligands¹⁵⁶

Transfer hydrogenation refers to hydrogenation by a hydrogen source other than molecular H_2 and has typically been catalysed by Ru complexes,¹⁵⁷ by Wilkinson's catalyst (**27**) or by Crabtree's catalyst (**100**). More recently, there have been several reports using NHC complexes of Rh and Ir, particularly in the reduction of imides, carbonyls and alkenes with *isopropanol* as the hydrogen donor (Eq. 6, Figure 1.10).¹⁵⁸ Our group¹⁵⁸ reported the first active Ir-NHC catalysts in transfer hydrogenation. The

ICy analogue of Crabtree's catalyst (**101b**, Figure 1.10) was very reactive in the reduction of ketones, and showed moderate activity in the transfer hydrogenation of olefins but was inactive in the reduction of imines or nitriles.¹⁵⁸ The SIMes derivative **101a** (Figure 1.9) was also tested in transfer hydrogenation with simple olefins and was found to be comparable in activity to **100**.¹⁵⁴ The chelating Ir(III) complexes **94** (particularly the neo-pentyl analogue, Scheme 1.31) were also active promoters of transfer hydrogenation, especially on ketones and to a lesser extent, aldehydes and imines.¹⁵⁹

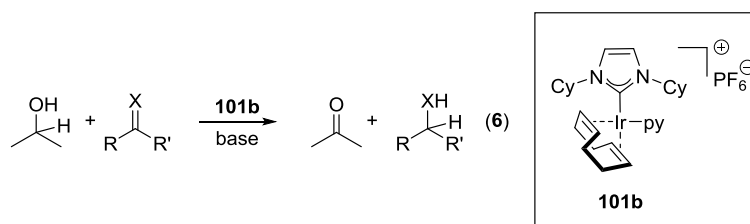


Figure 1.10. Transfer hydrogenation

1.2.2.3.2. C-H borylation

The selective functionalisation of un-activated aryl C-H bonds constitutes one of the greatest challenges in C-H activation and much attention has been devoted to this problem. Aryl boronic esters provide valuable substrates for a number of reactions such as Suzuki-Miyaura cross-coupling, 1-2 and 1,4-addition to carbonyl compounds and oxidative aminations.¹⁶⁰ Aryl boronates are widely available but their preparation is dependent on the availability of aryl halide starting materials. The direct borylation of arenes provides access to a wide array of aryl boronates *via* the reaction shown in Eq. 7, Figure 1.11. This reaction has been the subject of at least two decades of extensive research and there are several metals that are capable of catalysing the transformation, including Rh and Ir. The first Ir complexes to perform aryl borylation were Ir-Cp* complexes, but with low turn-over numbers. The introduction of phosphines and NHC ligands have led to successively higher activities and Herrmann and co-workers have studied various complexes of Ir(I) and Rh(I) for aryl borylation.^{101b,101b, 160a} For example, the authors prepared a large array of Rh and Ir complexes bearing different mono and *bis* NHC ligands, but in particular they tested variants of the three systems shown in Figure 1.11 in the C-H borylation of a number of arenes (including toluene and aryl halides). Under the conditions shown in Eq. 7, all five Ir catalysts gave between 92% and 100% conversion for each arene, showing high chemo-selectivity with C-X

bonds not being attacked and high regio-selectivity with only one product in each case, while the analogous Rh-catalysts showed no activity at all. Catalytic activity, particularly of the most active species, **58b-TFA^{Me}** was comparable to some of the most active catalysts previously reported such as the [Ir(cod)(μ-OMe)]₂-dtpy system reported by Hartwig and Miyaura (dtpy = 4,4'-di-*tert*-butyl-2,2'-bipyridine).¹⁶¹

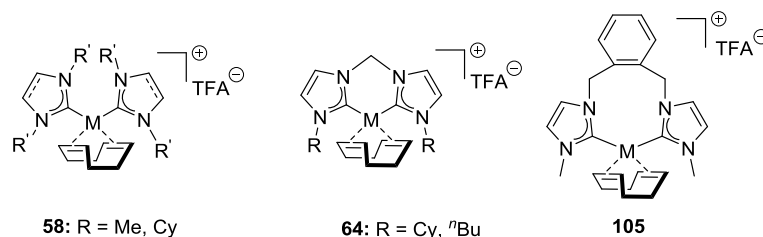
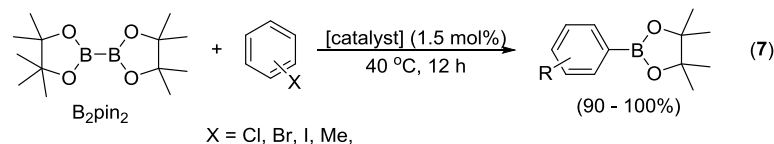


Figure 1.11. Aryl C-H borylation with metal-NHC complexes^{101b}

Following this report, Herrmann and co-workers published a more exhaustive scope, testing the complexes shown in Figure 1.12 in the C-H borylation of arenes under microwave irradiation and several trends in reactivity were established. The mono-NHC complexes **57b-Cl** showed lower stability under reaction conditions and as a result were much less active than the *bis*-NHC complexes (**58b**). The authors reported that catalytic activity increased with σ -donor strength and that the chelating NHCs delivered more active catalysts (**105** and **107**) than the non-chelating NHCs (**57**, **58** and **106**).^{160a} The length of the bridge between the two NHC fragments on **105** was important with the propylene bridge giving the best results, whereas a longer bridge led to steric hindrance at the coordination site and decreased catalytic activity. Furthermore, activity increased with growing basicity of the counter ion, with TFA giving the highest activity.^{160a}

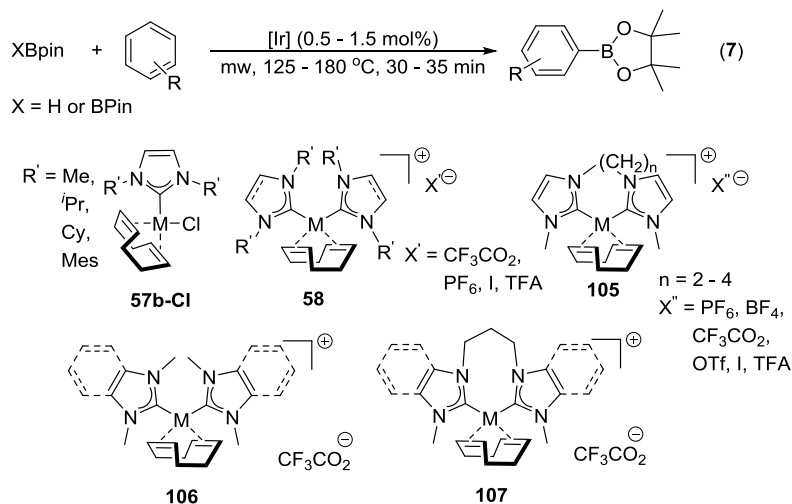


Figure 1.12. C-H borylation of arenes^{160a}

The catalytic application of Ir(III)(NHC) complexes has not been discussed here but is vast and in particular, complexes of the type $[\text{Ir}(\text{NHC})(\text{Cp}^*)\text{X}_2]$ have proven to be potent catalysts in several applications, including but not limited to deuteration of organic substrates,^{147b} dynamic kinetic resolution (DKR) of alcohols,¹⁶² and Oppenauer-type oxidation of alcohols, where acetone is used as the oxidant.¹⁶³

Success within our group in the preparation of LTM-hydroxides, particularly on gold and copper led us to examine whether the scope could be extended to include hydroxide complexes of rhodium and iridium. The use of NHCs as supporting ligands is a fundamental strategy in our group and their employment was essential in the isolation of Au- and Cu-hydroxides. Hence, the fundamental aim of this project was to develop general synthetic methods for the preparation of Rh(I)- and Ir(I)-NHC hydroxides. Once a general synthesis for Rh(I)-NHC hydroxides was established we intended to test the catalytic capabilities of these new complexes in established organic transformations, particularly where Rh-hydroxides have been identified as key intermediates such as the conjugate addition of boronic acids to activated alkenes.

Once the preparation of Rh(I)-hydroxides had been established, we endeavoured to extend the methodology to include Ir(I)-NHC hydroxides. Having accessed these complexes, our focus was to shift from catalysis to bond activation and small molecule activation. We aimed to explore the reactivity of Ir(I)-hydroxides towards a range of substrates in order to explore the benefit of using a metal-hydroxide motif. Furthermore, we aimed to explore reactivity with important molecules such as CO_2 .

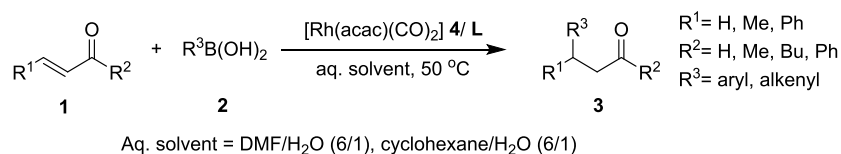
Finally we sought the development of general methods for the preparation of fluorinated Ir(I) and Rh(I)-NHC complexes. We aimed to prepare a range of complexes bearing fluoride, bifluoride and trifluoromethyl groups that may be useful in fluorination and trifluoromethylation chemistry.

2. WELL-DEFINED RHODIUM(I) HYDROXIDES AND THEIR ACTIVITY IN THE CONJUGATE ADDITION OF ARYLBORONIC ACIDS TO ACTIVATED ALKENES

2.1. INTRODUCTION

An organic transformation that has benefited largely from rhodium catalysis is the conjugate addition of organometallic compounds to activated alkenes. Various metals, including copper and nickel have been used in combination with organometallic reagents such as Grignard's, diorganozincs and organolithiums to prepare β -substituted carbonyls.¹¹⁷ However, these reagents are very sensitive to moisture and high temperatures and therefore require the employment of strictly anhydrous conditions at low temperatures.

In 1997, Miyaura and co-workers provided an alternative method for the preparation of β -substituted carbonyls **3** by the addition of alkyl- and arylboronic acids **2** to α,β -unsaturated ketones **1** in the presence of a rhodium catalyst (Scheme 2.1).¹⁶⁴ They reported that $[\text{Rh}(\text{acac})(\text{CO})_2]$ **4** with a variety of ligands, particularly biphosphines with large bite angles such as 1,3-Bis(diphenylphosphino)propane (dppp **L1**) could successfully catalyse conjugate addition in an aqueous medium.¹⁶⁴

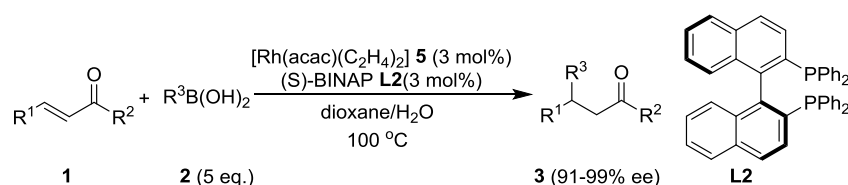


Scheme 2.1. 1,4-Addition of aryl and alkenyl boronic acids to activated alkenes.^{117, 164}

Miyaura's new method (Scheme 2.1) showed several advantages over previous techniques: (1) organoboronic acids are stable to oxygen and moisture as compared to other organometallic reagents employed, enabling the utilisation of protic and even aqueous solvent systems; (2) organoboronic acids are less reactive towards ketones in the absence of a catalyst than the organomagnesiums or organolithiums used thus far, eliminating unwanted 1,2-additions; (3) various alkenyl and aryl substituents can be introduced at the β -position. In contrast, there had not been any reports so far of

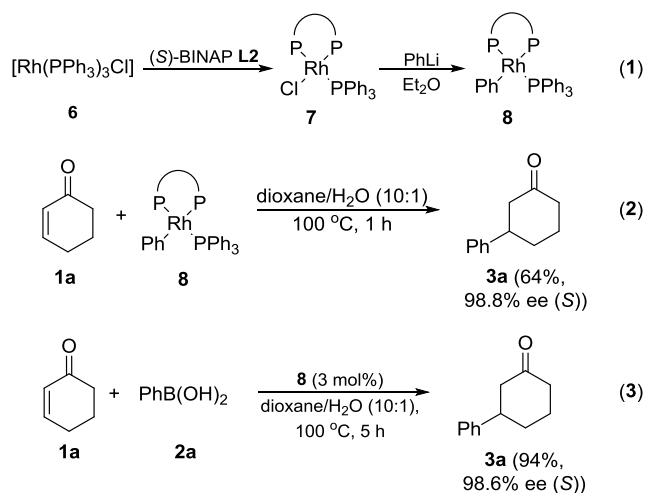
successful enantioselective introduction of sp^2 -hybridised carbons, using copper-catalysed methods.¹⁶⁵

In 1998, Hayashi reported the first asymmetric 1,4-addition of boronic acids **2** to activated alkenes **1** using $[\text{Rh}(\text{acac})(\text{C}_2\text{H}_4)_2]$ (**5**) and enantiopure (*S*)-BINAP ligand **L2** (Scheme 2.2).¹⁶⁶ Hydrolytic deboronation was found to be a problematic side reaction under these conditions, overcome by the addition of a large excess of boronic acid **2**. Hayashi's method enabled the coupling of arylboronic acids substituted with both electron-withdrawing and electron-donating groups to both linear and cyclic α,β -unsaturated ketones with very high ee (91-99%) .



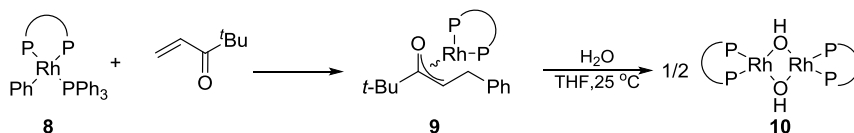
Scheme 2.2. Asymmetric 1,4-addition of aryl- and alkenylboronic acids to activated alkenes.¹⁶⁶

The development of catalytic methods for 1,4-addition was accelerated by the elucidation of the reaction mechanism by Hayashi and co-workers.¹⁵ By performing a series of stoichiometric reactions, they gained access to postulated reaction intermediates (Scheme 2.3).¹⁵ Hence, the square-planar Rh(I)-phenyl complex **8** was obtained by phenylation of the Rh-Cl bond in $[\text{RhCl}(\text{PPh}_3)((\text{S})\text{-BINAP})]$ (**7**) and characterised by ^{31}P NMR (Eq. 1, Scheme 2.3). Complex **8** was reacted with an excess of cyclohexen-2-one (**1a**) to give **3a** (Eq. 2, Scheme 2.3) and when used as a catalyst, in the reaction between **1a** and **2a**, led to **3a** in 94% yield and 98.6% ee (Eq. 3, Scheme 2.3). The reactivity of **8** was comparable to that of $[\text{Rh}(\text{acac})(\text{C}_2\text{H}_4)_2]/(\text{S})\text{-BINAP}$ (**5/L2**), implicating the Rh-phenyl complex **8** as a likely intermediate in the catalytic cycle.



Scheme 2.3. Reactions performed to elucidate the catalytic cycle by Hayashi.¹⁵

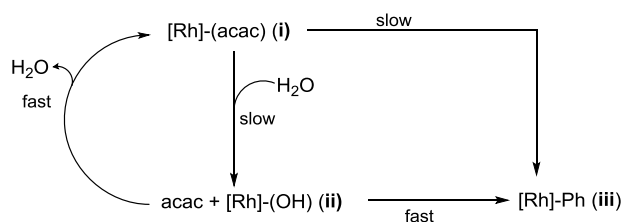
In a stoichiometric reaction, **8** was reacted with *tert*-butyl vinyl ketone, and the transformation was monitored by ³¹P NMR. A new complex was observed and assigned as the oxa- π -allylrhodium intermediate **9** (Scheme 2.4). This assignment was supported by comparison of the ³¹P NMR spectrum with that of an independent allyl complex prepared from [RhCl(BINAP)]₂ and a potassium enolate.¹⁶⁷ In the last step, H₂O was added to a solution containing the transient allyl species **9**. A new rhodium complex was observed upon hydrolysis and assigned as the Rh-hydroxide dimer **10** (Scheme 2.4).¹⁵



Scheme 2.4. Preparation of transient oxa- π -allyl complex and subsequent hydrolysis to the Rh-hydroxide.¹⁵

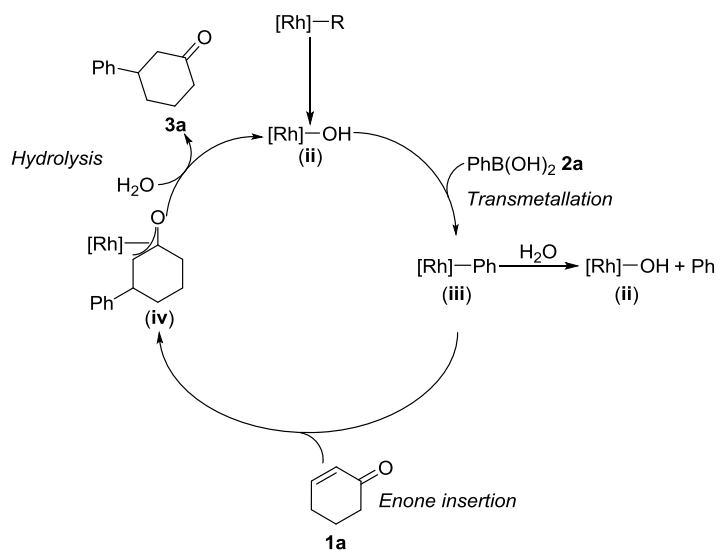
Upon addition of phenylboronic acid **2a** to **10**, a very fast transmetalation at room temperature afforded the Rh-phenyl compound **8**. This was an important observation and upon further investigation, the authors reported that transmetalation with **10** was faster than with the analogous [Rh(acac)(BINAP)]₂ (**11**). Furthermore, that reaction of **10** with acetylacetone quickly afforded **11**.

To explain these results, Hayashi reported that the Rh(acac) complex (**i**) (Scheme 2.5) in aqueous media would be converted to a Rh-hydroxide (**ii**) complex and that transmetalation with **ii** to give the Rh-phenyl complex (**iii**) is faster than with **i** (Scheme 2.5). However, formation of **ii** is reversible, with reformation of Rh(acac) (**i**) having a detrimental effect on catalyst activity.



Scheme 2.5. Reversible *in situ* conversion of Rh(acac) (**i**) to Rh(OH) (**ii**) and comparative transmetalation to Rh-Ph (**iii**).¹⁵

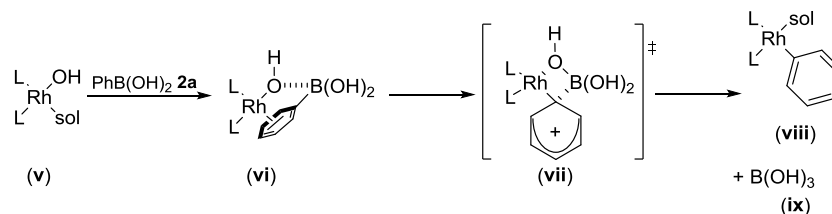
Based on these findings, the same group presented a new catalyst in the form of [Rh(BINAP)(OH)]₂ (**10**), which was more active than the previously reported catalysts.¹⁵ The catalytic cycle, with the three key intermediates and the processes that lead to them are shown in Scheme 2.6. Hence, transmetalation between a Rh-hydroxide (**ii**) and phenylboronic acid **2a** affords the Rh-phenyl intermediate (**iii**). Once **iii** has been formed, it may react with H₂O to reform the Rh-hydroxide (**ii**) and benzene. Alternatively, an enone insertion into the Rh-phenyl bond will afford an oxa- π -allyl-rhodium intermediate (**iv**). The cycle is completed by hydrolysis to give the conjugated product **3a** and regenerate the Rh-hydroxide (**ii**), propagating the cycle.¹⁵



Scheme 2.6. Catalytic cycle for 1,4-addition of arylboronic acids to α,β -unsaturated carbonyls.¹⁵

The rate enhancement in the transmetalation shown by Rh-hydroxide complexes has been explained by considering the high oxophilicity of boron.¹¹⁷ In analysing the transmetalation studies between organoboranes and palladium(II) or platinum(II) by Suzuki¹⁶⁸ and Venanzi¹⁶⁹ respectively, Lautens extrapolated their findings to propose a mechanism for an isoelectronic Rh(I) system (Scheme 2.7).¹¹⁷ Loss of a coordinated solvent moiety from the Rh-hydroxide (**v**) is followed by coordination of the phenylboronic acid (**2a**) to the hydroxyl moiety, potentially assisted by η^6 -binding to the

rhodium metal to give organoboronate intermediate (**vi**). Transmetalation then occurs *via* the transition state complex (**vii**) to give the phenylrhodium (**viii**) and the dissociated $B(OH)_3$ (**ix**).



Scheme 2.7. Mechanism of transmetalation between boronic acid **2a** and representative Rh-hydroxide (**v**)¹¹⁷

Much effort has been focused on tailoring rhodium complexes to improve both activity and selectivity for 1,4-addition, with particular attention being paid to ancillary ligands.^{39a, 39c-g} The recurring trend in the literature is that activity is enhanced by the use of electron-poor ligands.¹⁷⁰ Examples of electron-poor ligands employed on particularly active catalyst systems are shown in Figure 2.1 and include the chiral dienes **L3**,^{39d, 39f, 171} phosphoramidites **L4** and **L5**,^{39b, 39c, 170c} diphosphines **L6**, **L7** and **L8**,^{170, 172} and the BINAP-type ligands **L2** discussed *vide supra*.^{15, 166, 173} For example, a Rh-complex bearing an electron-poor chiral diphosphine, MeO-F₁₂-BIPHEP **L6** was reported by Sakai,^{170a} showing very high activity (TON and TOF of 320,000 and 53,000 h⁻¹ respectively at 2.5 x 10⁻⁴ mol% loading) in 1,4-addition. The extraordinary activity was attributed to the superior π -accepting capability of the ligand; inducing favourable conditions for transmetalation between boron and rhodium.^{170b}

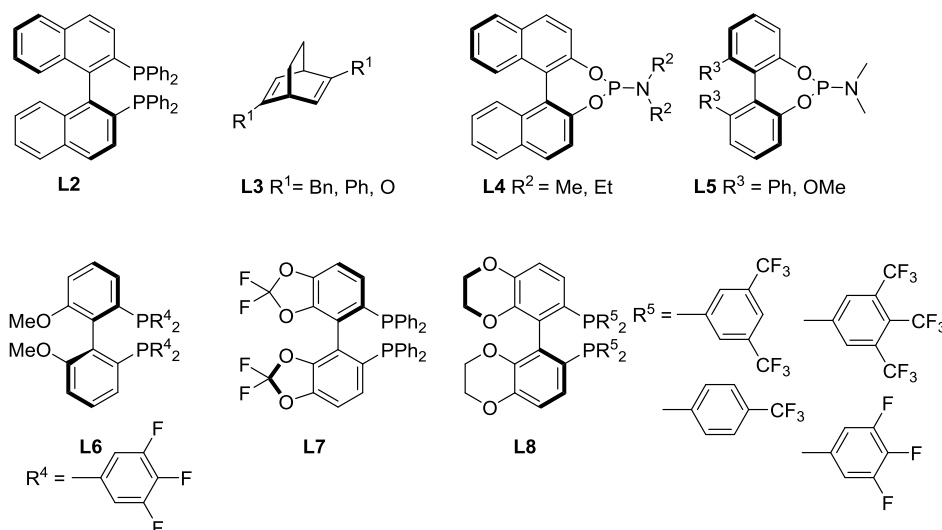


Figure 2.1. Commonly used electron-poor ligands in 1,4-addition.³⁹

Due to the success of electron-poor ligands, the use of NHCs as ligands for 1,4-addition is very underdeveloped. To our knowledge, there are only a handful of reports where NHCs have been used as supporting ligands in the conjugate addition of arylboronic acids to activated alkenes to date. Two reports make use of chiral NHC ligands to perform 1,4-addition reactions asymmetrically (Figure 2.2). Andrus *et al.*^{39g} described the use of dicyclophane imidazolium salts **L9** (3.0 mol%) with [Rh(acac)(C₂H₄)₂] (**5**, 2 mol%) to deliver a range of conjugate addition products in high yields (89-97%) with high ee (87-93%). Jeletic and co-workers¹⁷⁴ showed that a number of κ^2 -*bis*-NHCs on well-defined rhodium complexes **12** and **13** could catalyse the reaction between **1a** and **2a** in dioxane/MeOH to deliver the product in up to 98% isolated yield and up to 82% ee with a catalyst loading of 1.5 mol%.

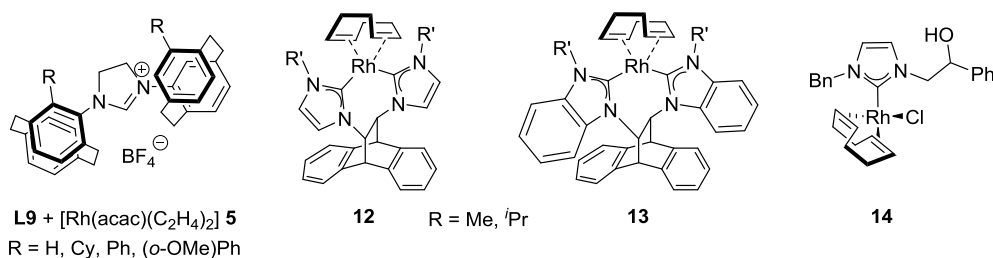


Figure 2.2. Rhodium NHC systems for catalytic conjugate addition of arylboronic acids to enones.^{39g, 174}

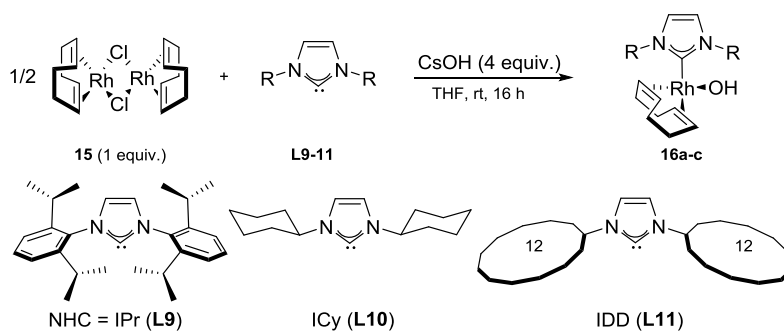
A third report, making use of Rh-NHC complexes in conjugate addition was reported after the work in this chapter was published. In the report by Esteruelas *et al.*¹⁷⁵ [Rh(cod)(NHC)Cl] (**14**, NHC = 3-benzyl-1-(2-hydroxy-2-phenylethyl)imidazol-2-ylidene, Figure 2.2) catalysed the conjugate addition of **2a** to **1a** at 1 mol% under anhydrous conditions. This is an interesting result since the authors showed that by attaching a hydroxide to the terminus of the alkyl *N*-substituent, the pendant alkoxide could perform the role of H₂O. In particular, the hydroxide is able to cleave the product from the Rh complex by nucleophilic substitution at the metal, negating the need for aqueous solvent.

Our main aim in this study was firstly to develop a synthesis for the preparation of Rh(I)-hydroxides since we were primarily interested in extending the chemistry of LTM-NHC hydroxides to include rhodium. Previous success in our group had indicated that NHC ligands were able to stabilise metal-hydroxide bonds on Au^{62a} and Cu^{62d} and we hoped to employ the same strategy to deliver Rh(I)-hydroxides. Due to the

implications of Rh-hydroxides as important intermediates in conjugate addition reactions, we hoped to test the Rh(I)-hydroxides in conjugate addition reactions.

2.2. COMPLEX SYNTHESIS

In order to prepare Rh(I)-NHC hydroxide complexes, we chose to utilise the commercially available $[\text{Rh}(\text{cod})\text{Cl}]_2$ (**15**) as starting material. As described in Chapter 1, the preparation of $[\text{Rh}(\text{cod})(\text{NHC})\text{Cl}]$ complexes has been well documented by reacting **15** with free NHCs **L10** – **L11**.^{81c, 87} Gratifyingly, we were able to modify the reported methods, and by adding an excess of CsOH to the reaction mixture, the chloride was replaced in a one pot procedure to give Rh(I)-NHC hydroxides **16a-c** (Scheme 2.8).



Scheme 2.8. Preparation of $[\text{Rh}(\text{cod})(\text{NHC})(\text{OH})]$ complexes **16a-c**.

Complexes **16a-c** were stable under inert conditions and were characterised by multinuclear NMR techniques and their purity was confirmed by elemental analysis. Single crystals of **16a** and **16b** were grown by slow evaporation of saturated hexane solutions. X-ray analysis unambiguously confirmed the identity of monomeric, 16-electron complexes, adopting square planar geometries around the metal centre (Figure 2.3).⁶⁸ Of note, the Rh-carbene bond on **16b** (2.022(3) Å) is considerably shorter than that on **16a** (2.046(6) Å). This may be due to the added steric bulk of IPr on **16a**, causing the Rh-carbene bond to lengthen. It could be a result of increased electron donation from ICy (TEP = 2049.6 cm⁻¹)¹⁷⁶ compared to IPr (TEP = 2051.5 cm⁻¹),^{94a} or a combination of decreased steric bulk and increased electron donation together. The Rh-OH bonds on **16a** and **16b** were very similar in length (2.030(4) Å, **16a** and 2.036(2) Å, **16b**) and considerably longer than the Ir-OH bond length reported for $[\text{Ir}(\text{cod})(\text{IMes})(\text{OH})]$ (2.007(5) Å), the closest reported relative of these complexes.¹⁷⁷

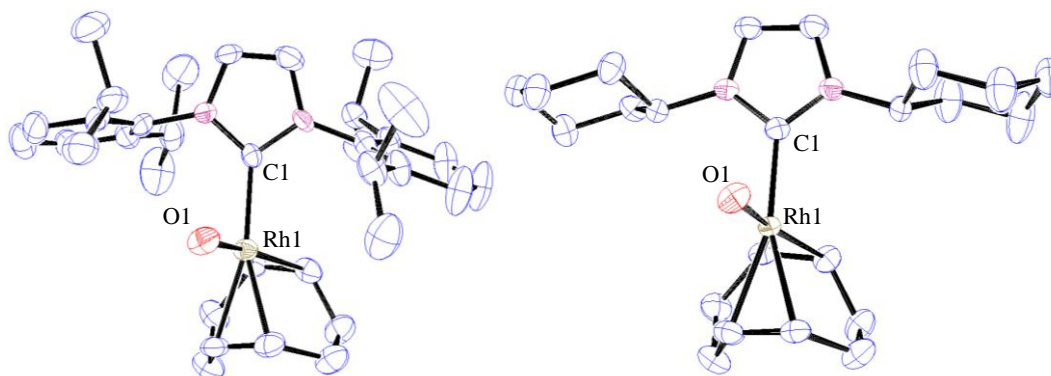
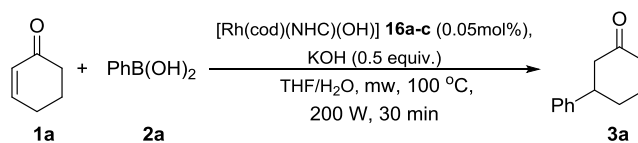


Figure 2.3. Thermal ellipsoid representations of [Rh(cod)(IPr)(OH)] **16a** and [Rh(cod)(ICy)(OH)] **16b**, showing 50% thermal ellipsoid probability. Selected distances (Å) for **16a**: Rh1-C1 2.046(6), Rh1-O1 2.030(4) and **16b**: Rh1-C1 2.022(3), Rh1-O1 2.036(2).

2.3. CATALYSIS

With complexes **16a-c** in hand, we turned our attention to the conjugate addition of arylboronic acids to α,β -unsaturated carbonyls. The addition of phenylboronic acid (**2a**) to cyclohexenone (**1a**) was selected as the benchmark reaction. In a trial reaction conducted at room temperature, the desired product **3a** was obtained in 54% isolated yield after 1 h with a catalyst loading of 0.2 mol% using [Rh(cod)(ICy)(OH)] (**16b**).

To rapidly afford optimised conditions and simultaneously test the thermal stability of our complexes under catalytic conditions, transformations were examined under microwave irradiation. Testing the well-defined complexes **16a-c** at 0.05 mol% in a THF/H₂O (10:1) solvent mixture at 100 °C for 30 min under the conditions illustrated in Scheme 2.9, the desired product, **3a** was obtained in 59% (using **16a**), 86% (using **16b**) and 74% (using **16c**) isolated yields (Table 2.1).



Scheme 2.9. Comparison between Rh-hydroxides in 1,4-addition under microwave irradiation.

Table 2.1. Comparison between catalysts **16a-c** in 1,4-addition of **2a** to **1a**^a.

Entry	Catalyst	Yield 3a (%) ^b
1	[Rh(cod)(IPr)(OH)] 16a	59
2	[Rh(cod)(ICy)(OH)] 16b	86
3	[Rh(cod)(IDD)(OH)] 16c	74
4	nil	0

^a Reaction conditions: [Rh(cod)(NHC)(OH)] (0.05 mol%), KOH (0.5 equiv.), mw, 100 °C, 200W, 30 min, THF/H₂O (10:1); ^b Isolated Yield.

The cycloalkyl-substituted NHC complexes **16b** and **16c** were found to outperform the aryl-substituted analogue **16a**. Among the cycloalkyl-NHCs, the complex containing the smaller ICy ligand **L10** resulted in the highest yields. Under these reaction conditions, the catalysts appeared to be tolerant of elevated reaction temperatures. Having identified [Rh(cod)(ICy)(OH)] (**16b**) as the most active catalyst, it was tested at homeopathic quantities, achieving full conversion after 12 h under conventional heating (100 °C) at 0.001 mol%, with a TON of 100,000 and TOF of 6,600 h⁻¹.

In the interest of performing rapid transformations, the reaction of phenylboronic acid (**2a**) and cyclohexenone (**1a**) was optimised under microwave irradiation after 30 min (Table 2.2). From the results obtained, we determined that the presence of an inorganic base (KOH) was essential for the reaction (Entry 5, Table 2.2) and that a catalyst loading of 0.2 mol% could be used to obtain almost complete conversions after only 30 min under microwave irradiation (Entry 2, Table 2.2).

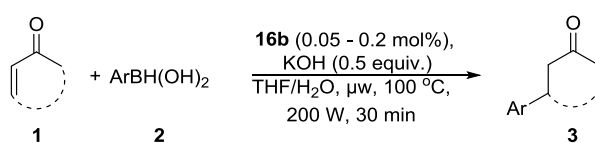
Table 2.2. Optimisation of reaction conditions for the 1,4-addition of **2a** to **1a**^a

Entry	16b (mol%)	Base	Yield (%) ^b
1	1.00	KOH	99
2	0.20	KOH	99
3	0.05	KOH	86
4	0.025	KOH	84
5	0.20	-	<10
6	0.20	KOH	85 ^b

^a Reaction conditions: mw, 100 °C, 200W, 30 min, THF/H₂O (10:1);

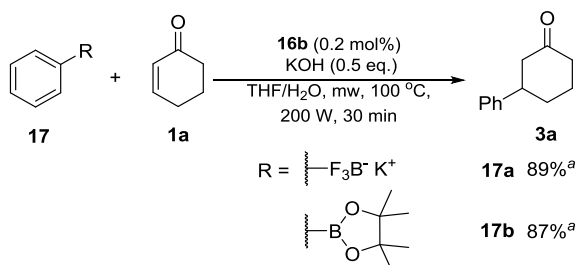
^b Isolated yields by column chromatography ; ^b Thermal, 100 °C, 1 h, PhMe/H₂O (10:1).

A scope for the transformation was next examined to demonstrate the versatility and the limitations of **16b**. We examined the coupling of four arylboronic acids: the parent system **2a**, two *para*-deactivated substrates (**2b** and **2c**) and the sterically demanding *ortho*-methylphenyl boronic acid (**2d**). The boronic acids were coupled to three cyclic enones **1a-c** of differing ring size under the optimised conditions (Scheme 2.10, Table 2.3). Cyclohexenone (**1a**) was very reactive towards the four arylboronic acids (**2a-d**), giving high yields in all cases (Entries 1-4, Table 2.3). Both cyclopentenone (**1b**) and cycloheptenone (**1c**) proved more difficult substrates, particularly when reacted with the deactivated 4-chlorophenylboronic acid (**2b**) and 4-(trifluoromethyl)phenylboronic acid (**2c**). These reactions were much slower under the conditions reported and reaction times had to be increased to 90 min in each case in order to achieve better yields (Entries 6, 7, 10 and 11, Table 2.3). Interestingly, the more sterically demanding, 2-methylphenylboronic acid (**2d**) was found to give high yields with the three enones examined (Entries 4, 8 and 12, Table 2.3).



Scheme 2.10 1,4-Addition of Arylboronic Acids to Cyclic Enones under optimised conditions.

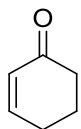
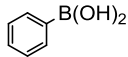
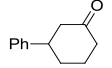
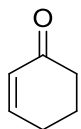
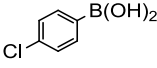
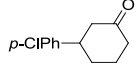
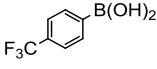
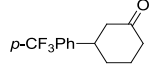
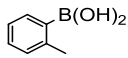
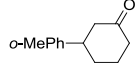
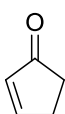
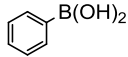
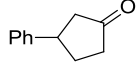
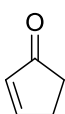
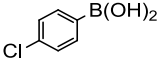
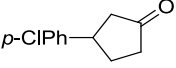
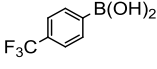
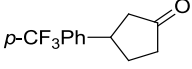
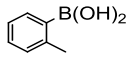
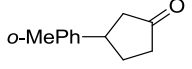
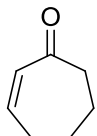
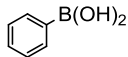
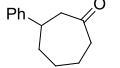
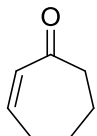
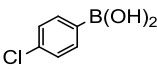
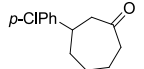
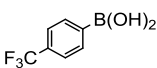
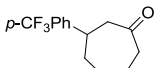
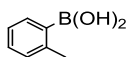
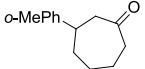
To further test the versatility and applicability of the Rh-ICy hydroxide motif, we explored alternative aryl delivery systems, successfully coupling potassium phenyltrifluoroborate (**17a**) and phenylboronic acid pinacol ester (**17b**) to cyclohexenone (**1a**) (Scheme 2.11), yielding phenylcyclohexanone (**3a**) in high conversions.



^aConversion by ¹H NMR and GC analysis

Scheme 2.11. Conjugate addition using alternative aryl delivery sources.

Table 2.3. Scope and limitations of 1,4-Addition of Arylboronic Acids **2** to Cyclic Enones **1**^a

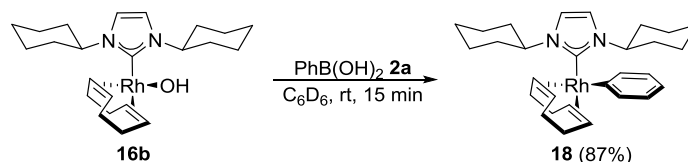
Entry	Enone 1	ArB(OH) ₂ 2	Product 3	Yield (%) ^b
1				99
2				93
3				94
4				96
5				
6				77 ^c
7				70 ^c
8				92
9				
10				68 ^c
11				53 ^c
12				92

^a Reaction conditions: [Rh(cod)(ICy)(OH)] (**16b**, 0.2 mol%), THF/H₂O (10:1), mw, 100 °C, 200 W, 30 min.^b Isolated yields are average of two runs and obtained after purification by flash chromatography. ^c

Irradiation time was 90 min.

2.4. MECHANISTIC STUDIES

Having demonstrated the high activity of **16b** in conjugate addition we conducted a series of stoichiometric reactions to shed light on the mechanism at play. [Rh(cod)(ICy)Ph] (**18**) was prepared from **16b** and phenylboronic acid (**2a**) in C₆D₆ in a very rapid transformation as shown in Scheme 2.12. ¹H NMR analysis confirmed complete conversion of **16b** into **18** after only 15 min at room temperature.



Scheme 2.12. Stoichiometric reaction to prepare phenyl rhodium intermediate **18**.

When the reaction was repeated with [Rh(cod)(IPr)(OH)] (**16a**) only 50% conversion (by ¹H NMR) was noted after 16 h. This difference in the rate of transmetalation between **16a** and **16b** may well account for the lower activity of **16a** observed during catalyst screening, the principal effect being a result of the steric bulk imposed by the NHC. The Rh(I)-phenyl complex **18** was isolated (87%) and fully characterised, with single crystal X-ray analysis unambiguously confirming the square planar geometry about the Rh centre (Figure 2.4). The phenyl ring is positioned orthogonal to the Rh-carbene plane, thereby minimising steric strain.

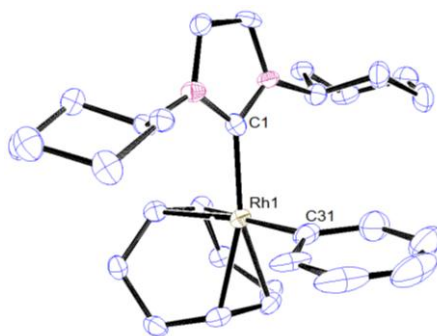
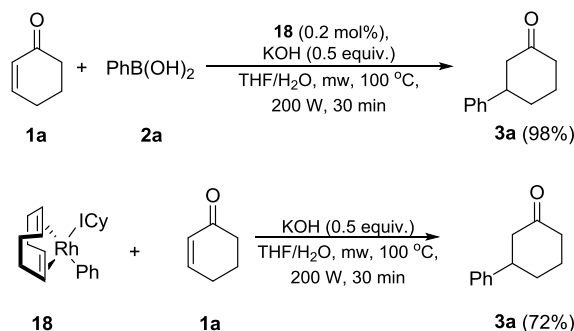


Figure 2.4. Thermal ellipsoid representation of [Rh(cod)(ICy)(Ph)] **18**, showing 50% thermal ellipsoid probability. Selected distances (Å): Rh1-C1 2.036(3), Rh1-C31 2.058(4).

Hartwig¹⁷⁸ has shown that transmetalation of an aryl moiety from boron to rhodium occurs *via* formation of a rhodium arylboronate (RhOB(OH)Ar) species, followed by β -aryl elimination to give the Rh-aryl complex. Complex **18** was used to catalyse the conjugate addition of phenylboronic acid **2a** to cyclohexenone **1a** under

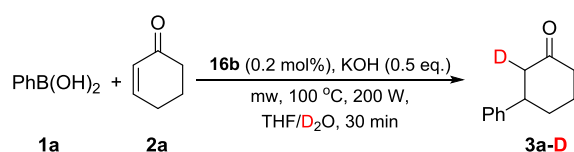
microwave irradiation and resulted in nearly identical activity to that of **16b** (98% isolated yield). Additionally, the reaction of **18** with 2 equivalents of cyclohexenone (**1a**) in THF/H₂O resulted in the formation of **3a** in a yield of 72% under catalytic conditions (Scheme 2.13). These experiments strongly suggest that **18** is an important intermediate along the catalytic pathway.



Scheme 2.13. Reactions performed in the presence of Rh(I)-Ph **18** to prepare (**3a**).

Our next step was to try to isolate the postulated oxa- π -allyl intermediate. Reaction between **18** and cyclohexenone (**1a**) in various solvents was very slow and unfortunately did not yield the desired product. Various reaction conditions were employed using different solvents, at temperatures ranging from -24 to 80 °C with reaction times up to 10 days, but to no avail (Table 2.4, experimental section). In a last effort, we attempted to react **18** with a pre-formed enolate Na⁺ salt of cyclohexanone as reported in a similar transformation by Slough.¹⁶⁷ Again this approach was unsuccessful and we can only postulate as to the exact structure of the allyl intermediate.

The last step to consider in the catalytic cycle is the hydrolytic cleavage of the conjugated product **3a** from the postulated allyl intermediate and simultaneous regeneration of the rhodium hydroxide **16b** to propagate the cycle. In order to understand the role of H₂O in the process, a reaction was performed under catalytic conditions with H₂O being replaced by D₂O (Scheme 2.14). ¹H NMR analysis of the final product showed deuterium incorporation (85%) into the conjugated product **3a-D**, α - to the carbonyl. This experiment confirmed hydrolytic cleavage of the addition product **3a** by H₂O from the rhodium centre.

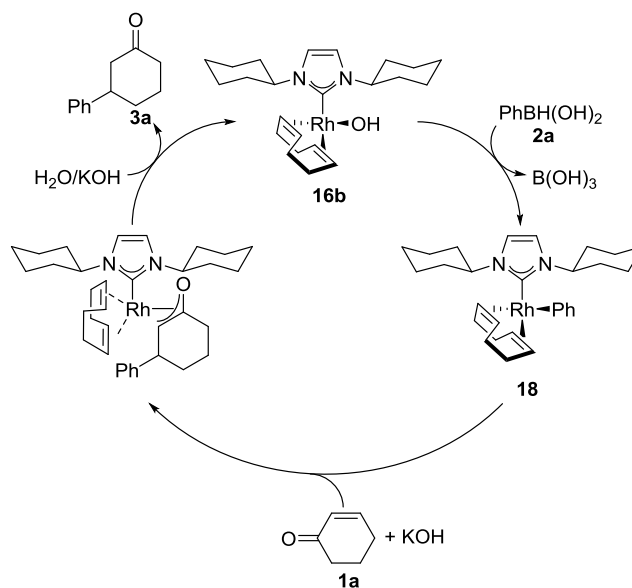


Scheme 2.14. Deuterium incorporation studies of the hydrolysis step.

The role played by the base in the reaction is still somewhat obscure. Several reports have indicated that base is essential for the *in situ* preparation of the hydroxorhodium species,^{39a, 170b, 179} where precatalysts such as [Rh(cod)Cl]₂ (**23**) or [Rh(acac)(C₂H₄)₂] (**6**) are used. Inorganic bases have been shown to accelerate transmetalation between organoborons and metal complexes,¹¹⁷ *via* quaternisation of the boronic acid to form an anionic organoboronate, which subsequently coordinates the metal centre. This concept has been explored by Suzuki¹⁶⁸ in Pd-catalysed cross-coupling and supported by DFT studies.¹⁸⁰ The theory has been extended to Rh-systems¹¹⁷ but has not yet been supported experimentally. Miyaura and co-workers^{39a} suggested that the base might play a further role in facilitating hydrolysis of the enolate intermediate.

There are several observations that we have highlighted, concerning the role of the base. Firstly, the Rh-hydroxide **16b** bears an internal base; secondly the transmetalation observed between **16b** and **2a** (Scheme 2.12) is so swift in the absence of a base that this kind of quaternisation would be unlikely to affect the reaction rate. However, catalysis in the absence of a base produces the conjugated product **3a** in less than 10% yield under optimised microwave conditions (Entry 5, Table 2.2). Studies on the allyl-formation step and subsequent hydrolytic cleavage of **3a** have drawn our attention to the possibility that KOH may play a role in facilitating enone insertion. A possible explanation is that a side reaction occurs with the enone to yield a potassium enolate, which reacts more favourably with the Rh-phenyl complex but our investigations into this hypothesis were inconclusive. A further role played by the base may be in the H₂O assisted regeneration of the catalyst, providing the hydroxyl group to reform the Rh(I)-hydroxide complex.

A proposed mechanism is presented in Scheme 2.15 which is consistent with the one proposed by Hayashi (*vide supra*).¹⁵ Activation of the arylboronic acid by the Rh-hydroxide **16b** forms the Rh-phenyl complex **18**, followed by enone insertion to most likely give the unobserved transient oxa- π -allyl Rh intermediate. Hydrolysis by H₂O, in the presence of KOH completes the cycle with release of the 1,4-addition product **3a** and reformation of the Rh(I)-hydroxide **16b**.



Scheme 2.15. Proposed catalytic cycle for Rh-catalysed 1,4-addition.

2.5. CONCLUSIONS

In summary, we have reported that Rh(I)-hydroxides may be prepared *via* a general one-pot procedure. Strongly electron-donating NHC ligands are able to stabilise the Rh-OH bond and we have isolated three complexes of the type [Rh(cod)(NHC)(OH)] (**16a-c**, NHC = IPr, ICy and IDD). Complexes **16a-c** were fully characterised by multinuclear NMR techniques and elemental analysis, with X-ray crystal structures being reported for **16a** and **16b**.

[Rh(cod)(ICy)(OH)] (**16b**) was found to be a very efficient catalyst in the conjugate addition of arylboronic acids (**2**) to cyclic enones (**1**), promoting full conversion at 0.001 mol% catalyst loading under thermal heating, with TON's and TOF's of 100,000 and 6,600 h⁻¹ respectively. This is in contrast to previous reports in which ancillary ligands with weaker electron donating properties were found to lead to optimal reactivity and catalytic conversions.¹⁷⁰ Furthermore, aryl molander salts **17a** and arylboronic esters **17b** were also found to serve as viable substrates in conjugate addition, leading to high conversions. Stoichiometric reactions were performed to isolate possible reaction intermediates and to discover the source of the high activity displayed by the Rh(I)-hydroxide **16b**. A very fast transmetalation between boronic acid **2a** and Rh(I)-hydroxide **16b** provided a plausible explanation for the high activity of **16b**, since transmetalation has been identified as the rate-limiting step in systems involving electron deficient ligands.¹⁸¹ Isolation and full characterisation, including X-

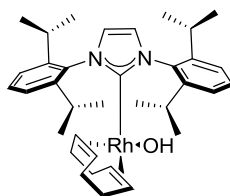
ray structural analysis of the Rh(I)-phenyl intermediate **18** was also achieved. Unfortunately, efforts towards the isolation of the second key intermediate, the proposed oxa- π -allyl species were unsuccessful and we suspect that insertion of the ketone may constitute the rate-limiting step. Deuterium labelling studies confirmed the role of H₂O in the hydrolysis of the rhodium enolate to release the conjugated product, with an 85% deuterium-incorporation on the α -carbon of product **3a-D**. The exact role that the base plays in the reaction is still somewhat obscure. We have shown experimentally that the base is not essential for transmetalation between Rh(I)-hydroxide and an arylboronic acid for this system. We propose two possible roles of the base, firstly that it may facilitate the enone insertion step and secondly, that the base is essential in regeneration of the active Rh(I)-hydroxide complex.

2.6. EXPERIMENTAL DETAILS

2.6.1. General considerations

Unless stated otherwise all reactions were carried out inside an MBraun Glovebox under inert conditions. All reagents were supplied by Aldrich and used without further purification and solvents were distilled and dried as required. Normal phase thin layer chromatography (TLC) was performed on Polygram 0.20 mm silica gel plates, Flash chromatography was performed using Silicycle Silia Flash silica gel 60 (particle size 0.040 – 0.063 mm). Visualisation on silica was achieved using either iodine vapour or UV light at 254 nm. NMR data was obtained using either a Bruker 400 MHz or 300 MHz spectrometer at 303 K in the specified deuterated solvent. All chemical shifts are given in ppm and coupling constants in Hz. Signals on the $^{13}\text{C}\{^1\text{H}\}$ spectra are singlets unless otherwise stated. Spectra were referenced to residual protonated solvent signals (for ^1H) or solvent signals (for ^{13}C): (CDCl_3 : ^1H δ 7.26 ppm, ^{13}C δ 77.00 ppm; C_6D_6 : ^1H δ 7.16 ppm, ^{13}C δ 128.06 ppm). Reactions under microwave irradiation were performed in a CEM Discover single-mode microwave apparatus, producing controlled irradiation at 2450 MHz. Reaction times refer to hold times at the indicated temperature and not total irradiation times with constant cooling *via* propelled air flow at a set power of 200 W. Elemental analyses were performed at the London Metropolitan University. CCDC-823666 (**16a**), CCDC-823667 (**16b**) and CCDC-823668 (**18**) contain the supplementary crystallographic data for these complexes. These data can be obtained free of charge from The Cambridge Crystallographic Data Centre via www.ccdc.cam.ac.uk/data_request/cif.

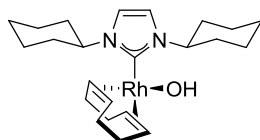
2.6.2. Synthesis and Characterisation data



[Rh(cod)(IPr)(OH)] **16a**

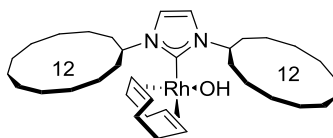
A 25 mL Schlenk tube was charged with $[\text{Rh}(\text{cod})\text{Cl}]_2$ **15** (100 mg, 0.2 mmol), IPr **L9** (158 mg, 0.4 mmol) and CsOH (122 mg, 0.8 mmol) in THF (5 mL). The resultant mixture was stirred overnight then filtered on celite and concentrated *in vacuo*. The resultant solid was washed with hexane (3 x 10 mL) and dried *in vacuo* to give

[Rh(cod)(IPr)(OH)] **16a** (190.0 mg, 75.8%) as a yellow solid; $^1\text{H NMR}$ (300 MHz, C_6D_6): δ 7.27 – 7.35 (m, 2H, ArH), 7.20 – 7.26 (m, 4H, ArH), 6.59 (s, 2H, NCH), 4.29 – 4.42 (m, 2H, cod-CH), 3.35 (m, 4H, $(\text{CH}(\text{CH}_3)_2)$), 2.99 (m, 2H, cod-CH), 1.83 – 2.02 (m, 4H, cod- CH_2), 1.59 – 1.72 (m, 2H, CH), 1.49 (d, 14H, $^3J_{\text{HH}} = 6.6$, CH_3 , m, 2H, cod- CH_2), 1.46 – 1.54 (m, 2H, CH), 1.06 (d, 12H, $^3J_{\text{HH}} = 6.9$, CH_3); $^{13}\text{C}\{^1\text{H}\}$ NMR (75 MHz, C_6D_6): δ 191.8 (d, $^1J_{\text{RhC}} = 56$, Rh-NHC), 147.0 (ArC), 137.3 (ArC), 129.9 (ArCH), 123.9 (NCH), 92.5 (d, $^1J_{\text{RhC}} = 9$, cod-CH), 63.5 (d, $^1J_{\text{RhC}} = 12$, cod-CH), 33.7 ($\text{CH}(\text{CH}_3)_2$), 29.0 (cod- CH_2), 28.9 (cod- CH_2), 26.5 (CH_3), 23.2 (CH_3); **Anal. Calcd** for $\text{C}_{35}\text{H}_{49}\text{N}_2\text{ORh}$ (MW 621.08): C, 68.17, H, 8.01, N, 4.54. Found: C, 68.26; H, 7.87; N, 4.38.

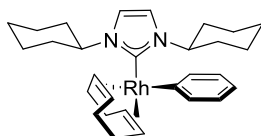


[Rh(cod)(ICy)(OH)] **16b**

A 25 mL Schlenk tube was charged with $[\text{Rh}(\text{cod})\text{Cl}]_2$ **15** (100 mg, 0.2 mmol), ICy **L10** (94 mg, 0.4 mmol) and CsOH (122 mg, 0.8 mmol) in THF (5 mL). The resultant mixture was stirred overnight then filtered on celite and concentrated *in vacuo*. The resultant solid was washed with hexane (3 x 10 mL) and dried *in vacuo* to give $[\text{Rh}(\text{cod})(\text{ICy})(\text{OH})]$ **16b** (163 mg, 84.4%) as a yellow solid; $^1\text{H NMR}$ (300 MHz, C_6D_6) δ 6.42 (s, 2H, $\text{N}(\text{CH}_2)_2\text{N}$), 5.73 (tt, 2H, $^3J_{\text{HH}} = 12.1$, 3.9, $\text{N}-\text{CH}(\text{CH}_2)_2$), 5.13 – 5.30 (m, 2H, cod-CH), 3.08 (m, 2H, cod-CH), 2.47 – 2.63 (m, 4H, cod- CH_2), 2.30 (d, 2H, $^3J_{\text{HH}} = 12.2$, CH_2), 2.12 (quint, 2H, $^3J_{\text{HH}} = 6.9$, CH_2), 1.84 – 2.00 (m, 4H, cod- CH_2), 1.34 – 1.73 (m, 10H, CH_2), 1.27 (qd, 2H, $^3J_{\text{HH}} = 12.5$, 3.6, CH_2), 1.10 (qd, 2H, $^3J_{\text{HH}} = 12.5$, 3.8, CH_2), 0.94 (qt, 2H, $^3J_{\text{HH}} = 12.8$, 3.7, CH_2); $^{13}\text{C}\{^1\text{H}\}$ NMR (75 MHz, C_6D_6) δ 186.3 (d, $^1J_{\text{RhC}} = 57$, Rh-NHC), 117.2 ($\text{N}(\text{CH}_2)_2\text{N}$), 97.4 (d, $^1J_{\text{RhC}} = 8$, cod-CH), 66.7 (d, $^1J_{\text{RhC}} = 13$, cod-CH), 60.5 ($\text{N}-\text{CH}(\text{CH}_2)_2$), 34.9, 34.5, 34.4, 29.5, 26.4, 26.0, 25.7 (ICy- CH_2). **Anal. Calcd** for $\text{C}_{23}\text{H}_{37}\text{N}_2\text{ORh}$ (MW 460.46): C, 59.99; H, 8.10; N, 6.08. Found: C, 59.90, H, 8.02; N, 5.97.

[Rh(cod)(IDD)(OH)] **16c**

A 25 mL Schlenk tube was charged with [Rh(cod)Cl]₂ **15** (100 mg, 0.2 mmol), IDD **L11** (162.5 mg, 0.4 mmol) and CsOH (123 mg, 0.8 mmol) in THF (5 mL). The resultant mixture was stirred overnight then filtered on celite and concentrated *in vacuo*. The resultant solid was washed with hexane (3 x 10 mL) and dried *in vacuo* to give [Rh(cod)(IDD)(OH)] **16c** (180.0 mg, 70.9%) as a yellow solid; ¹H NMR (300 MHz, C₆D₆) δ 6.45 (s, 2H, N(CH)₂N), 5.83 – 5.98 (m, 2H, N-CH(CH₂)₂), 5.20 (m, 2H, cod-CH), 3.04 – 3.15 (m, 2H, cod-CH), 2.53 – 2.72 (m, 4H, cod-CH₂), 2.01 – 2.13 (m, 4H, CH₂), 1.87 – 1.97 (m, 4H, cod-CH₂), 1.68 – 1.84 (m, 10H, CH₂), 1.15 – 1.54 (m, 30H, CH₂); ¹³C{¹H} NMR (75 MHz, C₆D₆): δ 187.1 (d, ¹J_{RhC} = 57, Rh-NHC), 117.2 (N(CH)₂N), 96.0 (d, ¹J_{RhC} = 8, cod-CH), 62.4 (d, ¹J_{RhC} = 13, cod-CH), 57.4 (N-CH(CH₂)₂), 34.4 (cod-CH₂), 32.2 (cod-CH₂), 31.7, 29.4, 25.0, 24.7, 24.3, 24.1, 24.0, 23.7, 23.2, 22.7, 22.5 (IDD-CH₂); **Anal. Calcd** for C₃₅H₆₁N₂ORh (MW 628.78): C, 66.86; H, 9.78; 4.46. Found: C, 66.88; H, 9.65; N, 4.46.

[Rh(cod)(ICy)Ph] **18**

A 25 mL Schlenk tube was charged with [Rh(cod)(ICy)(OH)] **16b** (500 mg, 1.08 mmol) and phenylboronic acid **2a** (130.0 mg, 1.08 mmol) in C₆H₆ (5 mL). The resultant solution was stirred for 1 h then filtered and reduced *in vacuo* to a yellow solid. The solid was dissolved in hexane (20 mL) and filtered before being reduced *in vacuo* to give [Rh(cod)(ICy)Ph] **18** (488.3 mg, 87.4%) as an orange solid; ¹H NMR (400 MHz, C₆D₆): δ 7.81 (d, 2H, ³J_{HH} = 7.7, *o*-ArH), 7.23 (t, 2H, ³J_{HH} = 7.4, *m*-ArH), 6.99 (t, 1H, ³J_{HH} = 7.3, *p*-ArH), 6.21 (s, 2H, NCH), 5.47 (tt, 2H, ³J_{HH} = 12.1, 3.5, (N-(CH)₂-N), 4.74 (m, 2H, cod-CH), 4.08 (m, 2H, cod-CH), 2.45 (m, 4H, cod-CH₂), 2.15 (d, 4H, ³J_{HH} = 8.9, ICy-CH₂), 1.99 – 1.92 (m, 4H, cod-CH₂), 1.66 (t, 4H, ³J_{HH} = 12.7, ICy-CH₂), 1.55 (d, 2H, ³J_{HH} = 13.5, ICy-CH₂), 1.41 – 1.52 (m, 4H, ICy-CH₂), 1.22 (qd, 2H, ³J_{HH} = 12.5, 3.6, ICy-CH₂), 1.06 (qd, 2H, ³J_{HH} = 12.5, 3.6, ICy-CH₂), 0.90 – 0.99 (m, 2H, ICy-CH₂); ¹³C{¹H} NMR (75 MHz, C₆D₆): δ 189.9 (d, ¹J_{RhC} = 60, Rh-NHC), 177.4 (d, ¹J_{RhC} = 36, Rh-Ph), 138.2 (ArC), 126.2 (ArCH), 121.0 (ArCH), 116.5 (N(CH)₂N), 87.5 (d, ¹J_{RhC} =

9, cod-CH), 81.7 (d, $^1J_{\text{RhC}} = 7$, cod-CH), 60.4 (N(CH)₂N), 35.2 (cod-CH₂), 34.7 (cod-CH₂), 32.0, 31.9, 26.4, 25.9, 25.7 (ICy-CH₂); **Anal. Calcd** for C₂₉H₄₁N₂Rh (MW 521.56): C, 66.91; H, 7.94; N, 5.38. Found: C, 66.81, H, 7.99 N, 5.31.

2.6.3. Catalysis

Method 1. 3-Phenylboronic acid **2a** (73.2 mg, 0.6 mmol), [Rh(cod)(ICy)(OH)] **16b** (0.46 mg, 1.0 μmol, 0.20 mol%) and KOH (14 mg, 0.25 mmol) were charged to a vial with THF (1 mL) inside a glove box. The vial was sealed and removed to air, where it was charged with cyclohexen-2-one **1a** (48.1 mg, 48.0 μL, 0.50 mmol) and degassed H₂O (100 μL) and allowed to stir at rt for 1 h. The product, 3-phenyl cyclohexanone **3a** was determined by ¹H NMR and GC analysis (54% conversion).

Method 2. A 10 mL Schlenk tube was charged with 3-phenylboronic acid **2a** (73.2 mg, 0.6 mmol), cyclohexen-2-one **1a** (48.1 mg, 48.0 μL, 0.50 mmol), [Rh(cod)(ICy)(OH)] **16b** (0.46 mg, 1.0 μmol, 0.20 mol%) and KOH (14 mg, 0.25 mmol) in THF (2 mL) and H₂O (200 μL) and refluxed under Ar for 1 h. The resultant mixture was chromatographed (flash chromatography, elution with hexane-ethyl acetate [4-1]) to give 3-phenyl cyclohexanone **3a** (75.6 mg, 86.8%) as a clear oil.

Method 3. General procedure for catalysis under microwave irradiation

Arylboronic acid **2a-d** (0.6 mmol), [Rh(cod)(ICy)(OH)] **16b** (0.46 mg, 1.0 μmol, 0.20 mol%) and KOH (14 mg, 0.25 mmol) were charged to a 10 mL microwave vial with THF (1 mL) inside a glove box. The vial was sealed and removed to air, where it was charged with cyclic enone **1a-c** (0.50 mmol) and H₂O (100 μL) before being irradiated in the microwave at 100 °C, 200 W for 30 min. The resultant mixture was chromatographed (flash chromatography, elution with hexane-ethyl acetate [4:1]) to afford the addition product **3a-l**.

TON reaction

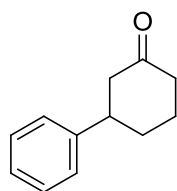
A 25 mL Schlenk flask was charged with phenylboronic acid **2a** (1.52 g, 12.4 mmol), cyclohexen-2-one **1a** (996 mg, 1.0 mL, 10.4 mmol), KOH (290 mg, 5.2 mmol) and [Rh(cod)(ICy)(OH)] **16b** (4.80 x 10⁻² mg, 1.04 x 10⁻¹ μmol, 0.001 mol%) in toluene (5 mL) and H₂O (500 μL). The resultant mixture was stirred at 100 °C for 12 h. 3-Phenyl cyclohexenone **3a** (1.8 g, 99.7%) was isolated as a clear oil by flash chromatography (elution with hexane-ethyl acetate [4:1]).

3-phenyl cyclohexanone 3a from phenylboronic acid pinacol ester

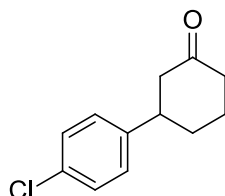
Catalytic preparation of 3-phenyl cyclohexenone **3a** under microwave irradiation was followed, using [Rh(cod)(ICy)(OH)] **16b** (0.46 mg, 1.0 μmol , 0.20%), phenylboronic acid pinacol ester (122.4 mg, 0.6 mmol), cyclohexen-2-one **1a** (48.1 mg, 48 μL , 0.50 mmol), KOH (14 mg, 0.25 mmol) in THF/D₂O (1/0.1 mL) to give 3-phenyl cyclohexenone **3a** (89% conversion by ¹H NMR and GC).

3-phenyl cyclohexanone 3a from potassium phenyltrifluoroborate

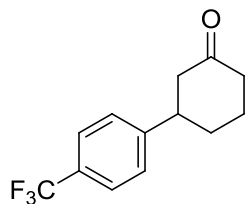
Catalytic preparation of 3-phenyl cyclohexenone **3a** under microwave irradiation was followed, using [Rh(cod)(ICy)(OH)] **16b** (0.46 mg, 1.0 μmol , 0.20 mol%), potassium phenyltrifluoroborate (110.4 mg, 0.6 mmol), cyclohexen-2-one **1a** (48.1 mg, 48 μL , 0.50 mmol), KOH (14 mg, 0.25 mmol) in THF/D₂O (1/0.1 mL) to give 3-phenyl cyclohexenone **3a** (87% conversion by ¹H NMR and GC).

2.6.4. Characterisation data3-Phenyl cyclohexanone **3a**¹⁸²

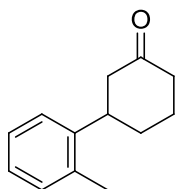
(86 mg, 99%) as a clear oil. ¹H NMR (300 MHz, CDCl₃) δ 7.32 - 7.39 (m, 2H), 7.21 - 7.30 (m, 3H), 2.97 - 3.10 (m, 1H), 2.33 - 2.68 (m, 4H), 2.06 - 2.23 (m, 2H), 1.76 - 1.96 (m, 2H); ¹³C{¹H} NMR (75MHz, CDCl₃): δ 211.0, 144.3, 128.6, 126.6, 126.5, 48.9, 44.7, 41.1, 32.7, 25.5.

3-(4-Chloro-phenyl)-cyclohexanone **3b**¹⁸³

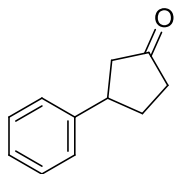
(97 mg, 93%) as a clear oil: ¹H NMR (400 MHz, CDCl₃) δ 7.28 (d, 2H, ³J_{HH} = 8.4), 7.15 (d, 2H, ³J_{HH} = 8.4), 2.09 - 3.05 (m, 1H), 2.29 - 2.60 (m, 4H), 2.00 - 2.19 (m, 2H), 1.71 - 1.89 (m, 2H); ¹³C{¹H} NMR (100 MHz, CDCl₃) δ 210.4, 142.7, 132.3, 128.7, 127.9, 48.7, 44.0, 41.0, 32.6, 25.3.

3-(4-Trifluoromethyl-phenyl)-cyclohexanone **3c**¹⁸²

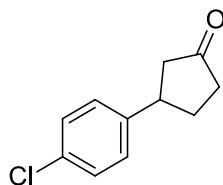
(112.6 mg, 93.5%) as a clear oil: **¹H NMR** (400 MHz, CDCl₃) δ 7.58 (d, 2H, ³J_{HH} = 8.4 Hz), 7.33 (d, 2H, ³J_{HH} = 8.4 Hz), 3.01 – 3.14 (m, 1H), 2.48 – 2.64 (m, 2H), 2.32 – 2.48 (m, 2H), 2.04 – 2.21 (m, 2H), 1.74 – 1.95 (m, 2H); **¹³C{¹H} NMR** (100 MHz, CDCl₃) δ 210.1, 148.2, 129.3 (q, ¹J_{FC} = 24.3), 127.0, 125.6 (q, ²J_{FC} = 2.5), 122.8, 48.8, 44.5, 41.1, 32.5, 25.4.

3-*o*-Tolyl-cyclohexanone **3d**¹⁸⁴

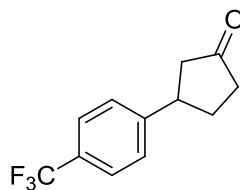
(90.2 mg, 95.8%) as a clear oil: **¹H NMR** (400 MHz, CDCl₃) δ 7.21 – 7.27 (m, 2H), 7.11 – 7.21 (m, 2H), 3.14 – 3.29 (m, 1H), 2.52 (d, 2H, ³J_{HH} = 8.9), 2.35 – 2.49 (m, 2H), 2.33 (s, 3H), 2.11 – 2.33 (m, 1H), 1.97 – 2.07 (m, 1H), 1.75 – 1.94 (m, 2H); **¹³C{¹H} NMR** (100 MHz, CDCl₃) δ 211.3, 142.3, 135.1, 130.7, 126.5, 126.4, 125.1, 48.4, 41.3, 40.3, 32.0, 25.8, 19.3.

3-Phenyl cyclopentanone **3e**¹⁸²

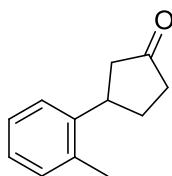
(72 mg, 90%) as a clear oil: **¹H NMR** (400 MHz, CDCl₃) δ 7.31 – 7.36 (m, 2H), 7.22 – 7.27 (m, 3H), 3.41 (tt, 1H, ³J_{HH} = 8.0, 3.2), 2.66 (dd, 1H, ³J_{HH} = 6.2), 2.39 – 2.51 (2H, m), 2.36 – 2.39 (2H, m), 1.92 – 2.05 (1H, m); **¹³C{¹H} NMR** (75 MHz, CDCl₃) δ 218.3, 143.0, 128.6, 126.6, 45.7, 42.1, 38.8, 31.1.

3-(4-Chloro-phenyl)-cyclopentanone **3f**^{39a}

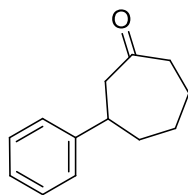
Irradiation time 90 min,(75 mg, 77%) as a clear oil: **¹H NMR** (400 MHz, CDCl₃) δ 7.31 – 7.36 (m, 2H), 7.22 – 7.27 (m, 2H), 3.41 (tt, 1H, ³J_{HH} = 10.8), 2.66 (dd, 1H, ³J_{HH} = 7.2), 2.39 – 2.51 (m, 2H), 2.24 – 2.38 (m, 2H), 1.92 – 2.05 (m, 1H); **¹³C{¹H}** NMR (100 MHz, CDCl₃) δ 218.3, 143.0, 132.0, 128.6, 126.7, 45.8, 42.2, 38.8, 31.1.

3-(4-Trifluoromethylphenyl)-cyclopentanone **3g**^{39a}

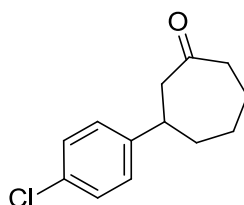
Irradiation time 90 min,(76.0 mg, 63%) as a clear oil: **¹H NMR** (400 MHz, CDCl₃) δ 7.60 (d, 2H, ³J_{HH} = 8.0), 7.37 (d, 2H, ³J_{HH} = 8.0), 3.48 (tt, 1H, ³J_{HH} = 7.1, 5.7), 2.70 (dd, 1H, ³J_{HH} = 7.6), 2.43 – 2.54 (m, 2H), 2.27 – 2.40 (m, 2H), 1.94 – 2.07 (m, 1H); **¹³C{¹H}** NMR (100 MHz, CDCl₃) δ 217.4, 147.0, 129.0 (q, ¹J_{FC} = 32.3), 127.1, 125.6 (q, ²J_{FC} = 3.7), 122.7, 45.4, 42.0, 38.7, 31.0.

3-*o*-Tolyl-cyclopentanone **3h**¹⁸⁴

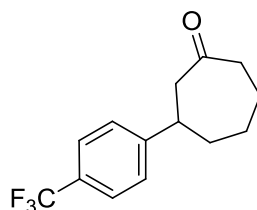
(79.9 mg, 91.7%) as a clear oil: **¹H NMR** (400 MHz, CDCl₃) δ 7.12 – 7.25 (m, 4H), 3.55 – 3.68 (m, 1H), 2.64 (dd, 1H ³J_{HH} = 7.6), 2.24 – 2.56 (m, 4H), 2.39 (s, 3H), 1.95 – 2.09 (m, 1H); **¹³C{¹H}** NMR (100 MHz, CDCl₃) δ 218.6, 140.9, 135.9, 130.6, 126.5, 126.4, 124.7, 45.3, 38.5, 38.3, 30.0, 19.6.

3-Phenyl cycloheptanone **3i**¹⁸²

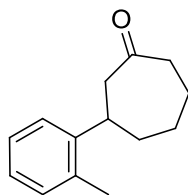
(75 mg, 80%) as a clear oil: $^1\text{H NMR}$ (400 MHz, CDCl_3) δ 7.30 (tt, 2H, $^3J_{\text{HH}} = 7.4, 1.5$), 7.16 – 7.23 (m, 3H), 2.86 – 2.98 (m, 2H), 2.64 (dd, 1H, $^3J_{\text{HH}} = 11.7, 1.6$), 2.56 – 2.62 (m, 2H), 1.93 – 2.13 (m, 3H), 1.65 – 1.80 (m, 2H), 1.43 – 1.56 (m, 1H); $^{13}\text{C}\{^1\text{H}\}$ NMR (75 MHz, CDCl_3) δ 213.4, 146.9, 128.6, 126.4, 126.3, 51.2, 43.9, 42.7, 39.2, 29.2, 24.1

3-(4-Chloro-phenyl)-cycloheptanone **3j**¹⁸⁵

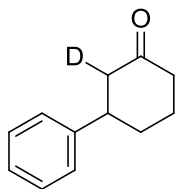
Irradiation time 90 min, (76 mg, 68.3%) as a clear oil: $^1\text{H NMR}$ (300 MHz, CDCl_3) δ 7.28 (dt, 2H, $^3J_{\text{HH}} = 8.6, 2.3$), 7.12 (dt, 2H, $^3J_{\text{HH}} = 8.5, 2.3$), 2.83 – 2.98 (m, 2H), 2.56 – 2.68 (m, 3H), 1.95 – 2.32 (m, 3H), 1.64 – 1.81 (m, 2H), 1.41 – 1.59 (m, 1H); $^{13}\text{C}\{^1\text{H}\}$ NMR (75 MHz, CDCl_3) δ 213.0, 145.3, 131.9, 128.7, 127.7, 51.0, 43.9, 42.1, 39.1, 29.1, 24.0.

3-(4-Trifluoromethylphenyl)-cycloheptanone **3k**

Irradiation time 90 min, (68 mg, 53%) as a clear oil: $^1\text{H NMR}$ (400 MHz, CDCl_3) δ 7.56 (d, 2H, $^3J_{\text{HH}} = 8.0$), 7.29 (d, 2H, $^3J_{\text{HH}} = 8.1$), 2.90 – 3.03 (m, 2H), 2.57 – 2.66 (m, 3H), 1.96 – 2.15 (m, 3H), 1.64 – 1.83 (m, 2H), 1.42 – 1.60 (m, 1H); $^{13}\text{C}\{^1\text{H}\}$ NMR (75 MHz, CDCl_3) δ 213.4, 146.9, 128.6 (q, $^1J_{\text{F-C}} = 32.5$), 126.4, 126.3, 125.9, 125.6 (q, $^2J_{\text{F-C}} = 3.5$), 122.3, 51.2, 43.9, 42.7, 39.2, 29.2, 24.1.

3-*o*-Tolyl-cycloheptanone **3l** ¹⁸⁴

(92.6 mg, 91.5%) as a clear oil: ¹H NMR (400 MHz, CDCl₃) δ 7.07 – 7.22 (m, 4H), 3.09 (tt, 1H, ³J_{HH} = 11.4, 2.0), 2.93 (t, 1H, ³J_{HH} = 12.8), 2.52 – 2.67 (m, 3H), 2.33 (s, 3H), 1.96 – 2.15 (m, 3H), 1.63 – 1.83 (m, 2H), 1.49 (q, 1H, ³J_{HH} = 11.9); ¹³C{¹H} NMR (100 MHz, CDCl₃) δ 213.7, 145.0, 134.4, 130.5, 126.4, 126.0, 125.0, 50.6, 43.9, 38.4, 37.8, 29.5, 24.2, 19.4.

²H-labelled 3-phenyl cyclohexanone **3a-d**

Catalytic preparation of 3-phenyl cyclohexenone **3a** under microwave irradiation was followed, using [Rh(cod)(ICy)(OH)] **16b** (0.46 mg, 1.0 μmol, 0.20 mol%), phenylboronic acid **2a** (73.2 mg, 0.6 mmol), cyclohexen-2-one (48.1 mg, 48 μL, 0.50 mmol), KOH (14 mg, 0.25 mmol) in THF/D₂O (1.0/0.1 mL) to give ²H-labeled 3-phenyl cyclohexenone **3a-d** (~ 85% ²H –incorporation by ¹H NMR) as a clear oil: ¹H NMR (300 MHz, CDCl₃) δ 7.31 - 7.41 (m, 2H), 7.21 – 7.32 (m, 3H), 2.97 - 3.10 (m, 1H), 2.33 – 2.63 (m, 3H), 2.06 – 2.23 (m, 2H), 1.76 – 1.96 (m, 2H); ¹³C{¹H} NMR (75MHz, CDCl₃): δ 211.0, 144.3, 128.6, 126.6, 126.5, 48.6 (m), 44.6, 41.1, 32.7, 25.5.

Catalysis using [Rh(cod)(ICy)Ph] **18**

Method 1. Catalytic preparation of 3-phenyl cyclohexenone **3a** under microwave irradiation was followed, using [Rh(cod)(ICy)Ph] **18** (0.5 mg, 1.0 μmol, 0.20mol%), phenylboronic acid **2a** (73.2 mg, 0.6 mmol), cyclohexen-2-one **1a** (48.1 mg, 48 μL, 0.50 mmol) and KOH (14 mg, 0.25 mmol) in THF/H₂O (1/0.1 mL) to give 3-phenyl cyclohexenone **3a** (85 mg, 98%).

Method 2. A microwave vial was charged with [Rh(cod)(ICy)Ph] **18** (40 mg, 7.7 x 10⁻²mmol), cyclohexen-2-one **1a** (15 mg, 15 μL, 1.5 x 10⁻¹ mmol) and KOH (4.3 mg, 7.7 x 10⁻²mmol) in THF/H₂O (600/60 μL) and irradiated at 100 °C, 200 W, 30 min

before being concentrated *in vacuo* and purified on silica with CH₂Cl₂ as eluent to give 3-phenyl cyclohexanone **3a** (72% by ¹H NMR and GC).

Attempted Synthesis of Rh(cod)(ICy)-oxa-π-allyl complex

Method 1. A round bottom flask/NMR tube was charged with [Rh(cod)(ICy)Ph] (**18**) (25 mg, 0.04 mmol), KOH (2.7 mg, 0.04 mmol) and cyclohexen-2-one (**1a**) (8.0 mg, 0.08 mmol) and mixed in the various solvents, under the conditions described in Entries 1 – 7, Table 2.4. Reactions were followed by ¹H NMR analysis, which did not reveal formation of the desired allyl complex.

Method 2. An NMR tube was charged with [Rh(cod)(ICy)Ph] (**18**) (25 mg, 0.04 mmol) and cyclohexen-2-one (**1a**) (8.0 mg, 0.08 mmol) in THF-*d*₈/D₂O (600/60 μL) and mixed for 3 days (Entry 8, Table 2.4). Reaction was followed by ¹H NMR analysis which did not reveal formation of the desired allyl complex.

Method 3. An NMR tube was charged with [Rh(cod)(ICy)Ph] (**18**) (25 mg, 0.04 mmol), KOH (4.3 mg, 0.08 mmol) and cyclohexen-2-one (**1a**) (8.0 mg, 0.08 mmol) in THF-*d*₈ (600 μL) and mixed for 3 days (Entry 9, Table 2.4). The reaction was followed by ¹H NMR analysis, which revealed the disappearance of ¹H NMR signals corresponding to cyclohexen-2-one (**1a**) after ~ 1 h. No further reaction was observed and the product could not be isolated.

Method 4. A 10 mL round bottom flask was charged with cyclohexen-2-one (**1a**) (9.2 mg, 0.1 mmol) and NaH (2.3 mg, 0.1 mmol) in THF-*d*₈ (1 mL). The suspension was allowed to stir for 1 h before being filtered and transferred to an nmr tube containing [Rh(cod)(ICy)Ph] (**18**) (25 mg, 0.04 mmol). The solution was mixed at rt for 3 days (Entry 10, Table 2.4). ¹H NMR analysis showed no change over 3 days, with only signals corresponding to [Rh(cod)(ICy)Ph] (**18**).

Method 5. A 10 mL round bottom flask was charged with 3-phenylcyclohexan-2-one (**3a**) (17.5 mg, 0.1 mmol) and NaH (2.3 mg, 0.1 mmol) in THF-*d*₈ (1 mL). The suspension was allowed to stir for 1 h before being filtered and transferred to a nmr tube containing [Rh(cod)(ICy)(OH)] (**16b**) (20 mg, 0.04 mmol). The solution was mixed at rt for 3 days (Entry 11, Table 2.4). ¹H NMR analysis showed no change over 3 days, with only signals corresponding to [Rh(cod)(ICy)(OH)] **16b**.

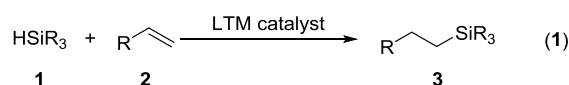
Table 2.4. Reaction conditions for the attempted preparation of oxa- π -allyl intermediate

Entry	Rh S.M.	Solvent	Temp (°C)	Time
1	18	C ₆ H ₆	rt	10 d
2	18	C ₆ H ₆	60	3 h
3	18	nil	rt	3 d
4	18	PhMe	80	3 h
5	18	THF	rt	1 d
6	18	THF	-24	1 d
7	18	THF	60	3 h
8	18	THF _{d8}	rt	3 d
9	18	THF _{d8}	rt	3 d
10	18	THF	rt	3 d
11	16b	THF	rt	3 d

3. ALKENE HYDROSILYLATION AND DEHYDROGENATIVE SILYLATION CATALYSED BY *RH(I)*-HYDROXIDES

3.1. INTRODUCTION

Silicon-carbon bond creation by the addition of silicon hydrides to multiple bonds (hydrosilylation or hydrosilation), particularly C=C or C≡C bonds is a key process in the preparation of organosilicons (Eq. 1).¹⁸⁶ Hydrosilylation reactions are typically employed in the preparation of industrially important organosilanes such as γ -substituted propylsilanes, silicon polymers (particularly silicon oils), functional siloxanes and silicon resins. Hydrosilylation is also an important process used in the cross-linking of silicon polymers to make elastomers and silicon-based release coatings, among other applications.^{186d} The hydrosilylation of multiple bonds represents an industrially relevant process that has seen much development, particularly with regard to the LTM complexes that drive the reaction.^{186d, 187}



Hydrosilylation of C=C bonds was conducted as early as 1947 by Sommer, who reported the hydrosilylation of 1-octene with trichlorosilane *via* a free-radical mechanism.¹⁸⁸ In the late 1950's, a LTM catalysed hydrosilylation process was developed by Speier, using hexachloroplatinic acid [Cl₆H₂Pt] (**4**).¹⁸⁹ This was an important milestone in the preparation of organosilicons, leading to wide industrial application, but suffered from long induction periods and poor selectivity. In 1973, Karstedt reported dramatic enhancements to Speier's catalyst. Karstedt's divinylsiloxane stabilised Pt(0) system (Pt₂[Me₂SiCH=CH₂)₂O]₃) (**5**) was to become the benchmark of hydrosilylation catalysts, still widely employed in industrial applications today.^{186d, 190} In spite of its high activity and wide application, Pt-catalysed hydrosilylation is plagued by competing side-reactions such as oligomerisation, polymerisation, hydrogenation, redistribution, dehydrogenation and dehydrogenative silylation.^{186d, 187} Regio- and stereoselectivity is a major concern, most notably in the hydrosilylation of alkynes. Hence, there is great interest in the development of highly selective hydrosilylation catalysts.^{186d}

Apart from advances made with Pt-catalysts,^{186d, 191} metal complexes of iridium, palladium, nickel, ruthenium^{186d, 187, 192} and more recently, non-noble metals¹⁹³ have been employed as efficient hydrosilylation catalysts. Rhodium complexes have been investigated extensively in the last half century. In particular, Wilkinson's catalyst and its analogues were the first Rh-complexes to be investigated ($[\text{Rh}(\text{PR}_3)_3\text{X}]$, $\text{X} = \text{Cl}$, $\text{R} = \text{Ph}$ for Wilkinson's catalyst)¹⁹⁴ or $[\text{Rh}(\text{CO})(\text{PR}_3)_2\text{X}]$ ^{192b} and were found to be very efficient in the hydrosilylation of ketones and aldehydes. Variations of these catalysts include the highly active dimethylglyoximate Rh(I-III) complexes, active at catalyst loadings as low as 0.004 mol%.¹⁹⁵ Rh-dimers containing π -acceptor ligands, e.g. $[\text{Rh}_2\text{X}_2\text{Y}_4]$ ($\text{X} = \text{Cl}$, alkyl groups, OSiOMe_3 , and $\text{Y} = \text{olefin}$, CO , cod , $\text{P}(\text{OR})_3$, Cp or Cp^*)^{187, 192b, 196} and $[\text{Rh}(\text{cod})\text{Cl}]_2/\text{L}$ ($\text{L} = \text{PR}_3$) have all been successfully employed as hydrosilylation promoters.¹⁸⁷ Of particular interest to us are carbene complexes, specifically those of the type $[\text{Rh}(\text{cod})(\text{NHC})\text{X}]$ ($\text{X} = \text{Cl}$, Br) which have shown promising results in the selective hydrosilylation of simple and functionalised alkenes.^{73, 84, 186b, 186c, 187, 197}

In comparison to other hydrosilylation reactions, particularly hydrosilylation of carbonyl compounds, the hydrosilylation of alkenes and alkynes, catalysed by Rh-NHC complexes is comparatively underdeveloped, with only limited examples in the literature. For example, Buchmeiser has reported the use of a tetrahydropyrimidine-based NHC complex, $[\text{Rh}(\text{cod})(\text{NHC})]\text{BF}_4$ (**6**) (Figure 3.1) which catalysed the hydrosilylation of ketones, alkenes and alkynes in only moderate yields but at low catalyst loading (0.05 mol%). Complex **6** was also active in the hydrosilylation of terminal and internal olefins, ketones and aldehydes.¹⁹⁸ Oro showed that $[\text{Rh}(\text{cod})(\text{NHC})\text{Cl}]$ complexes **7** and **8** could catalyse the hydrosilylation of terminal alkynes with good yields and decent selectivity, with the smaller Me-substituted ligand outperforming the bulkier Mes-substituted NHC ligand (Figure 3.1).¹⁹⁹

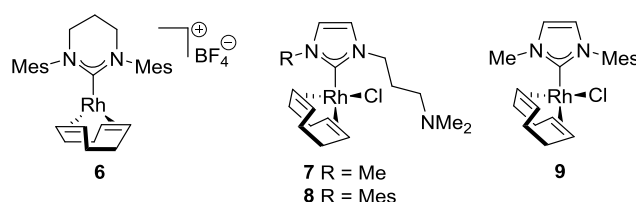
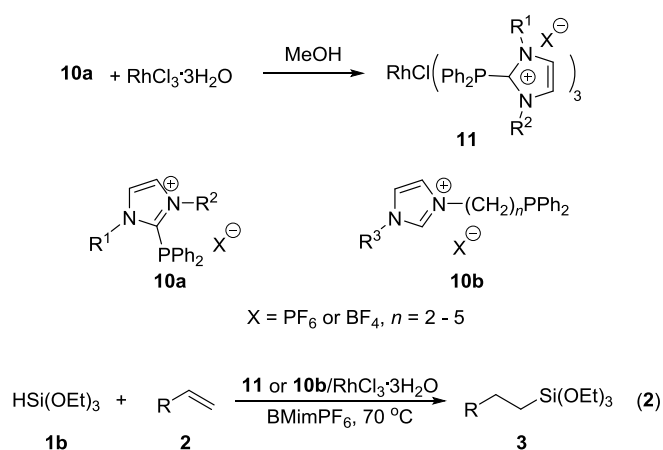


Figure 3.1. Rh-NHC complexes employed in hydrosilylation^{186b, 198, 199}

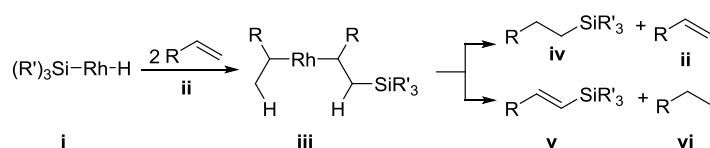
The use of ionic liquids and in some cases supercritical fluids has boosted the activity of Rh-NHC and phosphine functionalised Rh-NHC systems,^{186b, 194b, 197a, 200} enabling hydrosilylation at loadings as low as 0.005 mol%, with TON's of up to 20,000.²⁰⁰ For example, [Rh(cod)(NHC)Cl] (**9**) promoted hydrosilylation of four aliphatic alkenes with HSi(OEt)₃ (**1b**) at 0.02 mol% catalyst loading, but reactions needed to be conducted at 70 °C in ionic liquid such as 1-butyl-3-methylimidazolium hexafluorophosphate (BMimPF₆).^{186b} Modifications to this system have included the use of phosphines functionalised with imidazolium salts such as those shown in Scheme 3.1. The 2-phosphine imidazolium salts **10a** were prepared and reacted with RhCl₃·3H₂O to give complexes of the type depicted by **11**. Catalytic activity of **11** was very high in the hydrosilylation of alkenes by HSi(OEt)₃ (**1b**) in ionic liquid medium as shown (Eq. 2, Scheme 3.1), giving full conversion of aliphatic alkenes at 0.005 mol% catalyst loading of **11a** (R¹ = Me, R² = Et, X = PF₆). The authors postulated that the electron rich heterocycle has a stabilising effect on the Rh-phosphine centre, leading to a highly active catalyst system that could be recycled in ionic liquid.⁴⁶ In a sequential study, the same group used imidazolium functionalised phosphines of the type **10b**, providing ambivalent P,C-donor ligands, in combination with RhCl₃·3H₂O to perform the same hydrosilylation reactions. Catalytic activity was comparable but overall was lower than with the well-defined system **11**. Presumably, the imidazolyl moiety on **10b** stabilises the Rh-phosphine interaction in solution, providing a suitable scaffold for hydrosilylation to take place.^{43a}



Scheme 3.1. Phosphine-NHC functionalised ligands used in hydrosilylation^{197a, 200}

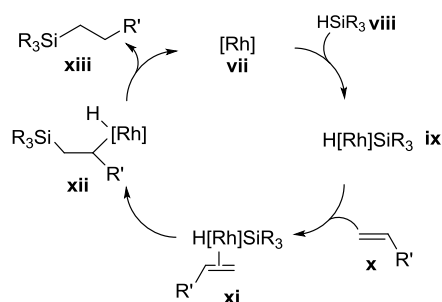
A mechanism for hydrosilylation of alkenes was derived in 1965 by Chalk and Harrod to describe hydrosilylation using Speier's catalyst **4** and comprises a conventional oxidative addition/reductive elimination sequence.²⁰¹ Hence, oxidative

addition of a silane (**1**) to a metal centre (d^8 or d^{10}) is followed by migratory insertion of the alkene into the M-H bond (rate determining step). The resulting metal-silyl-alkyl complex then undergoes reductive elimination by Si-C bond formation, releasing the alkyl silane product (**3**) and a metal-alkene complex, formed in the presence of excess alkene, propagating the cycle.^{192b} Hydrosilylation in the presence of a rhodium catalyst has been documented to proceed *via* different mechanisms. Rhodium complexes are very efficient catalysts in dehydrogenative silylation of multiple bonds, and hence dehydrogenative silylation constitutes the most competitive side reaction for Rh-catalysed systems.^{192b} In the presence of an excess of alkene, the product determining step is a competitive β -H transfer from either the σ -alkyl or σ -silylalkyl fragments of intermediate (**iii**) (Scheme 3.2). In the case of dehydrogenative silylation, β -H transfer from the silylalkyl fragment releases the vinylsilane (**v**) and gives a Rh-alkyl-hydride complex. Reductive elimination will then generate the alkane (**vi**) and the [Rh] complex. Hence, dehydrogenative silylation is favoured by a high alkene : silane ratio.²⁰²



Scheme 3.2 Competitive β -H transfer leading to either alkyl- or vinylsilanes²⁰²

Complexes of Fe, Ni, Co, Pd and Rh have all provided active dehydrogenative silylation catalysts, particularly where alkenes with conjugated substituents are used, such as styrenes.²⁰² Hydrosilylation, catalysed by a rhodium catalyst has been described by modified versions of the Chalk-Harrod mechanism (to account for competitive side reactions such as dehydrogenative silylation) such as that shown in Scheme 3.3.^{192b, 202-203} The process is initiated by oxidative addition of a trisubstituted silane (**viii**) to the Rh complex (**vii**) to give a silyl-Rh(III)-hydride (**ix**). Alkene insertion into the Rh-silyl bond (**x**), followed by C-H reductive elimination then releases the organosilicon product (**xiii**) and regenerates the active species (**vii**), propagating the cycle.^{192b}



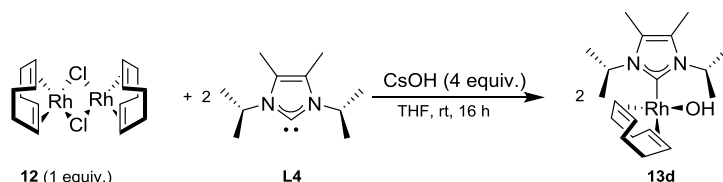
Scheme 3.3. Modified Chalk-Harrod mechanism^{192b}

Following these reports, particularly of Rh-NHC halide complexes being employed in hydrosilylation reactions, we aimed to test the use of Rh-NHC hydroxides. We were encouraged by the reactivity that the Rh(I)-hydroxide motif had shown in catalysing the conjugate addition of arylboronic acids to activated alkenes (Chapter 2) and aimed to extend their utility to hydrosilylation.

Historically, rhodium complexes have performed well as promoters of hydrosilylation and in particular, there is a precedent for the use of $[\text{Rh}(\text{cod})(\text{NHC})\text{Cl}]$ complexes in hydrosilylation reactions.^{84, 118, 127} We wanted to examine the effect of having an internal base on the Rh-NHC scaffold, in the form of a hydroxide. It has previously been established by reports from our group that LTM hydroxides react very easily with silanes to form metal siloxides.^{62d} In Chapter 2, steric variations between three NHC ligands (IPr **L1**, ICy **L2** and IDD **L3**) were implicated as being responsible for differences in catalytic activity, yet we did not fully explore this theory. In addition to the Rh-hydroxides reported in Chapter 1, we aimed to synthesise a novel complex, bearing the small 1,3-di(*isopropyl*)-4,5-dimethylimidazol-2-ylidene ($i\text{Pr}^{\text{Me}}$) ligand. We hoped that $i\text{Pr}^{\text{Me}}$ would impart even less steric bulk than ICy, yet still be stable enough that it would provide a very active catalyst.

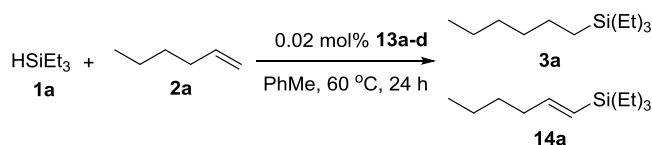
3.2. RESULTS AND DISCUSSION

$[\text{Rh}(\text{cod})(i\text{Pr}^{\text{Me}})(\text{OH})]$ **13d** was prepared from $[\text{Rh}(\text{cod})\text{Cl}]_2$ (**12**) and the free carbene **L4** in the presence of CsOH (Scheme 3.4), according to the established procedure (Chapter 2) and fully characterised.



Scheme 3.4. Preparation of $[\text{Rh}(\text{cod})(\text{IPr}^{\text{Me}})(\text{OH})]$ **3d**

In order to test the series of Rh-complexes **13a-d** in alkene hydrosilylation, the reaction between triethylsilane (**1a**) and 1-hexene (**2a**) was selected as the model reaction (Scheme 3.5). Reaction conditions were optimised using $[\text{Rh}(\text{cod})(\text{ICy})(\text{OH})]$ (**13b**) (see experimental section). Hence, **1a** was reacted with two equivalents of **2a** in toluene at 60 °C in the presence of $[\text{Rh}(\text{cod})(\text{NHC})(\text{OH})]$ (**13a-d**, 0.02 mol%). Gas chromatography-mass spectrometry (GC-MS) and ^1H NMR analysis of the reaction mixture indicated that two products were present: triethyl(hexyl)silane (**3a**) and (*E*)-triethyl(hex-1-enyl)silane (**14a**) (Scheme 3.5). It became clear at this point that competitive dehydrogenative silylation was leading to formation of the vinylsilane **14a**. Selectivity was to become a key issue in these reactions since dehydrogenative silylation often competes with hydrosilylation when catalysed by Rh complexes.¹⁸⁷



Scheme 3.5. Hydrosilylation of terminal alkenes

Table 3.1. Reaction between **1a** and **2a**, catalysed by $[\text{Rh}(\text{cod})(\text{NHC})(\text{OH})]$ (**13a-d**)^a

Entry	Catalyst	NHC	Conversion (%) ^b	3a (%) ^b	14a (%) ^b
1	13a	IPr L1	85	86	14
2	13b	ICy L2	94	83	17
3	13c	IDD L3	93	84	16
4	13d	<i>i</i> Pr ^{Me} L4	93	86	14

^aReaction conditions: HSiEt_3 (**1a**) (0.3 mmol), 1-hexene (**2a**) (0.6 mmol), **13a-d** (0.02 mol%), toluene (1 mL), 60 °C, 24 h. ^bProduct yields calculated from GC-MS (conversion relative to concentration of **1a**) and confirmed by ^1H NMR.

At 60 °C, all four catalysts **13a-d** showed high activity (Table 3.1), with conversions of 85% for **13a** and 93 – 94% for **13b-d**, with similar selectivity towards the alkylsilane **3a** (83 – 86%). In order to obtain a clear comparison between the four catalysts, the reaction was repeated under milder conditions. Reaction profiles for each entry at room temperature showed considerable differences in performance (Figure 3.1).

Paying particular attention to the first 8 h, activity increased in the following order: **13a** < **13c** < **13b** < **13d**. Complex **13d** displayed the highest catalytic activity, boasting full conversion after 8 h. Noteworthy is that while Rh-IDD hydroxide **13c** was slow to initiate, over time the reaction progress surpassed that of Rh-ICy hydroxide **13b**. The selectivity towards alkylsilane **3a** decreased for all entries at lower temperature (71-75%) except that of Rh-*i*Pr^{Me} hydroxide **13d** which showed only 7% vinylsilane production (Table 3.2, Entry 4).

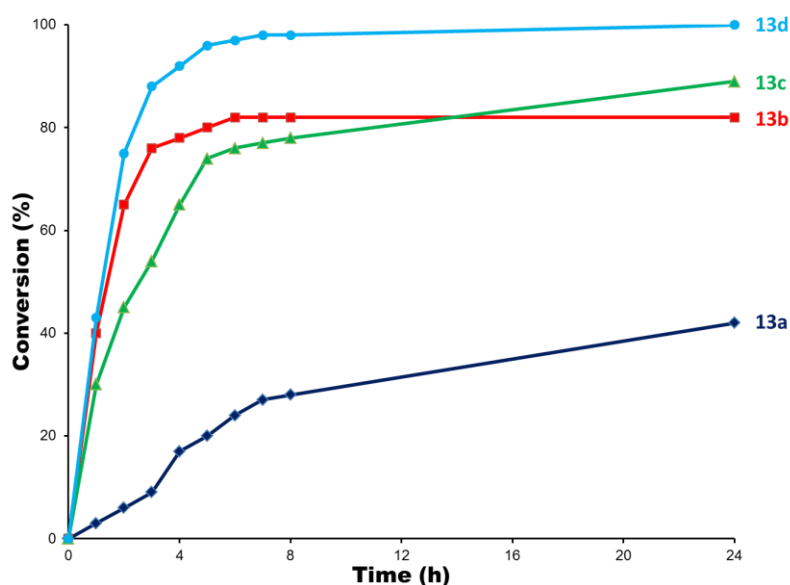


Figure 3.2. Catalytic activity of [Rh(cod)(NHC)(OH)] (**13a-d**) in the hydrosilylation of 1-hexene (**2a**) by HSiEt₃ (**2a**). Reaction conditions shown in Table 3.2

Table 3.2. Hydrosilylation of 1-hexene (**2a**) by HSiEt₃ (**1a**) using **13a-d** at room temperature.^a

Entry	Catalyst	NHC	Conversion (%) ^b	3a (%) ^b	14a (%) ^b
1	13a	IPr L1	42	72	28
2	13b	ICy L2	82	75	25
3	13c	IDD L3	89	71	29
4	13d	<i>i</i> Pr ^{Me} L4	>99	93	7

^aReaction conditions: HSiEt₃ **1a** (0.3 mmol), 1-hexene **2a** (0.6 mmol), **13a-d** (1.0 mol%), toluene (1 mL), rt, 24 h. ^bProduct yields calculated from GC-MS (conversion relative to concentration of HSiEt₃) and confirmed by ¹H NMR.

In order to rationalise the variation in catalyst activity between complexes **13a-d**, the steric and electronic characteristics of the NHC ligands involved (**L1-L4**) were investigated. To compare the steric demand of each ligand, X-ray structures of complexes **13a-d** were obtained from single crystals, grown by slow evaporation of saturated hexane solutions (**13c** and **13d** shown in Figure 3.3, **13a** and **13b** reported in

Chapter 2). The % V_{Bur} was calculated for each ligand (**L1-L4**) using the SambVca software⁹⁸ (Table 3.4).

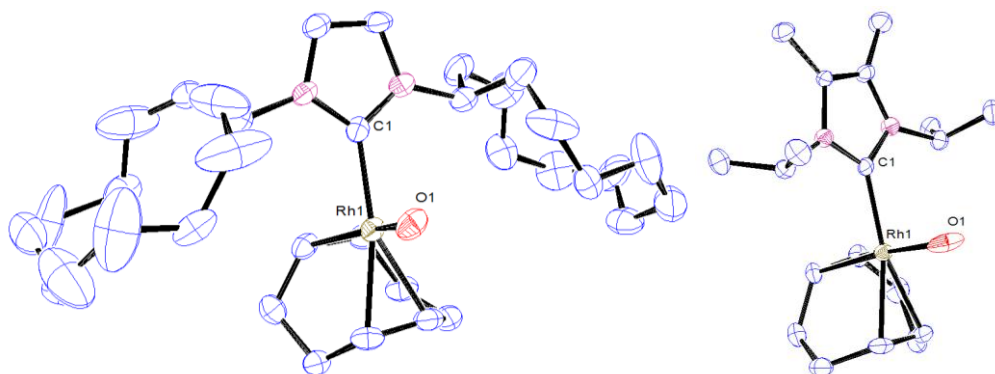


Figure 3.3. Thermal ellipsoid representations of [Rh(cod)(IDD)(OH)] (**13c**) and [Rh(cod)(*i*Pr^{Me})(OH)] (**13d**), showing 50% thermal ellipsoid probability. H atoms have been omitted for clarity. Selected bond lengths (Å) and bond angles (°): **13c** Rh(1)-O(1): 2.024 (6), Rh(1)-C(1): 2.054 (8), C(1)-Rh(1)-O(1): 89.4 (3); **13d** Rh(1)-O(1): 2.074 (3), Rh(1)-C(1): 2.044 (3), C(1)-Rh(1)-O(1): 90.53 (13).

Table 3.3. % V_{Bur} , TEP and selected bond lengths for complexes **13a-d**

Entry	NHC	% V_{Bur} ^a	TEP (cm ⁻¹)	Rh-C ^{NHC} (Å)	Rh-OH (Å)
1	IPr L1	35.1	2051.5 ^c	2.046(6)	2.030(4)
2	ICy L2	27.1	2049.6 ^b	2.022(3)	2.036(2)
3	IDD L3	47.9	2049.0 ^b	2.054(8)	2.024(6)
4	<i>i</i> Pr ^{Me} L4	28.0	2049.6 ^d	2.044(3)	2.074(3)

% V_{Bur} : ^aCalculated using SambVca software (sphere radius = 3.5, distance from centre of sphere = 2.00, mesh spacing = 0.5, hydrogens omitted); ⁹⁸ TEP: calculated from ν_{co} ([Ir(CO)₂Cl(NHC)] in DCM.

^bCalculations by Nolan *et al.* 2010.¹⁷⁶ ^cCalculations by Nolan *et al.* 2008.^{94a}

^dDFT calculations from [Ni(CO)₃(NHC)].^{93b}

As expected, the IDD ligand **L3** displays the highest % V_{Bur} (47.9%), followed by IPr **L1** (35.1%). To our surprise, *i*Pr^{Me} **L4** displayed a higher % V_{Bur} (28.0%) than ICy **L2** (27.1%). The difference is only marginal and probably within experimental error, however we were surprised by the bulk that was displayed by *i*Pr^{Me}. There are two reasons for this: firstly, the methyl groups on the backbone of the NHC will exert a steric repulsion on the *i*Pr substituents, pushing them towards the metal, thereby increasing the bulk of *i*Pr^{Me} within the metal sphere. Secondly, the high degree of flexibility of the cyclohexyl rings on ICy means that they are able to adopt positions that impose minimal steric interference within the metal sphere, and hence a small % V_{Bur} . It should be noted that these measurements are calculated for solid state structures and do not describe behaviour in solution but do nevertheless give us an indication of the steric

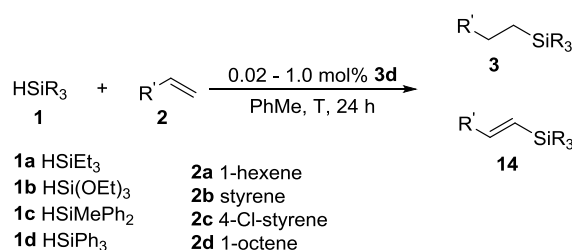
environment at each metal centre. A comparison of the bond lengths in the solid state was measured from the X-ray structures (Figure 3.3) and showed that the Rh-carbene bond of Rh-ICy hydroxide **13b** (Table 3.3, Entry 2) is considerably shorter (2.022(3) Å) than the other entries. The Rh-OH bond, on the other hand is longest on the Rh-*i*Pr^{Me} complex **13d** ((2.074(3) Å, Table 3.3, Entry 4).

To provide a comparison of the electronic character of each ligand, TEP values have been included in Table 3.3.^{93b, 94a, 176} The TEP values indicate that the four NHC ligands vary only slightly in electronic character. There is no difference in σ -donation between ICy **L2** (2049.6 cm⁻¹) and *i*Pr^{Me} **L4** (2049.6 cm⁻¹), while IPr **L1** shows the lowest σ -donation (2051.5 cm⁻¹) and IDD **L3** shows the highest electronic contribution (2049.0 cm⁻¹). Our group has previously reported that in a series of cycloalkyl-substituted NHCs, the size of cycloalkyl *N*-substituents had very little effect on the electronics of the ligand and that differences in performance are more likely to result from steric contributions.¹⁷⁶

In the reaction between 1-hexene (**2a**) and HSiEt₃ (**1a**) at room temperature, Rh-ICy hydroxide **13b** showed considerably lower activity than Rh-*i*Pr^{Me} hydroxide **13d** (Results in Table 3.2, with reaction profiles in Figure 3.2). Catalysts **13b** and **13d** show comparable activity initially, but over time, the reaction with **13b** slows down and finally plateaus after just six hours. This may be as a result of decomposition of the complex, leading to catalyst death, whereas **13d** appears to be more robust. Rh-IDD hydroxide **13c** was slow to initiate hydrosilylation at room temperature, but demonstrated high activity after 24 h. This would indicate that high stability and inherent flexibility of the ligand may be important in enabling a variable steric environment. Our group has shown that the cyclododecyl rings are able to flex in solution, providing fluctuating sterics and enabling lower energy barriers for the interconversion between different conformations.¹⁷⁶ It is interesting that the steric data gathered on **13c** in the solid state (Table 3.3, Entry 3) indicated a sterically congested coordination sphere with a high % *V*_{Bur} (47.9%) for the IDD ligand, yet **13c** showed great potential as a hydrosilylation catalyst, promoting high yield, particularly at elevated temperature (93% conversion for reaction between **1a** and **2a** (Table 3.1, Entry 3); and 94% for the reaction between **1a** and styrene (**2b**) (see experimental section) at 0.02 mol%, 60 °C). Based on these results and those reported separately by our group,¹⁷⁶ it is evident that the high flexibility of the cyclododecyl rings means that

structural data collected in the solid state does not necessarily reflect behaviour in solution or at elevated temperatures and by no means reflects the catalytic capabilities of a complex bearing the IDD ligand.

Having identified Rh- i Pr^{Me} hydroxide **13d** as the most efficient catalyst, we investigated the scope and limitations (Scheme 3.6, Table 3.4) for the hydrosilylation of terminal alkenes, to demonstrate the versatility of the method and investigate the effect of varying the alkene and the silane on catalyst activity and selectivity. In each case, reactions were performed under optimised conditions at 60 °C with 0.02 mol% catalyst loading. For comparison, each reaction was repeated at room temperature with 1.0 mol% catalyst loading. Reactions with triethylsilane (**1a**) showed high conversions, particularly at room temperature in the presence of 1.0 mol% of **13d**. Reactions with aliphatic alkenes (Table 3.4, Entries 1 and 7) gave better selectivity towards the desired alkyl silanes under mild conditions (1.00 mol%, room temperature). Triethoxysilane (**1b**) was a very efficient hydrosilylation reagent, giving full conversion to the alkylsilane (**3**) selectively in each case, with the exception of chlorostyrene **2c** (Table 3.4, Entries 9-16). Methyl(diphenyl)silane (**1c**) also showed high conversions at room temperature with 1.00 mol% catalyst loading, delivering the hydrosilylated products (**3**) with pleasing selectivity, particularly when coupled to the aliphatic alkenes (Table 3.4, Entries 17 and 23). Triphenylsilane (**1d**) proved to be a relatively unreactive substrate, giving low yield when coupled with **2a** and predominant selectivity towards the dehydrogenated product **14b** when coupled with styrene **2b** (Table 3.4, Entries 25-28).



Scheme 3.6. Scope of hydrosilylation of terminal alkenes using Rh hydroxide

Table 3.4. Reaction between silanes **1** and terminal alkenes **2**^a

Entry	Product	13d (mol%)	T (°C)	Conv ^b (%)	3 (%) ^b	14 (%) ^{b,c}
1		1.00	rt	>99	93	7
2		0.02	60	93	86	14
3		0.50	rt	95	50	50
4		0.02	60	94	67	33
5		1.00	rt	65	32	68
6		0.05	60	91	21	79
7		1.00	rt	92	61	29 ^d
8		0.02	60	76	76	16 ^e
9		0.50	rt ^f	>99	>99	-
10		0.02	60 ^f	>99	>99	-
11		0.50	rt ^f	>99	>99	-
12		0.02	60	99	>99	-
13		1.00	rt	>99	92	8
14		0.02	60	99	93	7
15		0.50	rt	>99	>99	-
16		0.02	60	94	>99	-
17		1.00	rt	97	>99	-
18		0.02	60	67	99	<1
19		1.00	rt	>99	88	12
20		0.02	60	95	60	40
21		1.00	rt	>99	73	27
22		0.02	60	38	57	43
23		1.00	rt	96	>99	-
24		0.02	60	64	>99	-
25		1.00	rt	30	97	3
26		0.05	60	32	>99	-
27		0.50	rt	>99	35	65
28		0.02	60	>99	35	65

^aReaction conditions: HSiR₃ **1** (0.3 mmol), alkene **2** (0.6 mmol), **13d**, toluene (1 mL), 24 h (unless stated otherwise). ^bProduct yields calculated from GC-MS (conversion relative to concentration of HSiR₃) and confirmed by ¹H NMR. ^cStereochemistry determined as (*E*) for each entry by ¹H NMR unless stated otherwise. Reaction also produces 2-(triethylsilyl)-1-octene ^d(10%) and ^e(7%). ^fReaction time = 18 h.

Clearly, there is strong competition between hydrosilylation and dehydrogenative silylation in the reactions described (Table 3.4) and selectivity appears to be substrate specific. The alkylsilanes (**1a**, **c** and **d**) are more susceptible to dehydrogenative

silylation than the silyl ether **1b**, while the conjugation in the styrene systems (**2b** and **2c**) makes them good substrates for dehydrogenative silylation. Selectivity towards dehydrogenative silylation ranges from almost non-existent when HSi(OEt)₃ (**1b**) is used (Table 3.4, Entries 9-16) to being the dominant process when styrenes are coupled to triethyl- (**1a**) or triphenylsilane (**1c**) (Table 3.4, Entries 5,6 and 27,28). The selectivity in the reaction with methyl(diphenyl)silane **1c** was interesting. When reacted with the aliphatic alkenes (**2a** and **2c**), the reaction selectively produced the hydrosilylation product (**3**) (Table 3.4, Entries 17 – 18, 23 – 24). However, when coupled to one of the styrenes (**2b** and **2c**), competitive dehydrogenative silylation ranged from 12% to 43% (Table 3.4, Entries 19 – 22).

Intrigued by the competition between hydrosilylation and dehydrogenative silylation, we investigated the selective preparation of vinylsilanes by dehydrogenative silylation of alkenes using **13d**, under similar conditions. The ability to prepare vinylsilanes directly from alkenes is a valuable process, particularly if stereocontrol is achieved, since hydrosilylation of alkynes is often accompanied by side reactions and can lead to isomers of the olefinic product.²⁰⁴ During reaction optimisation it was evident that increasing the alkene concentration favoured the dehydrogenative process. In particular, when the styrene (**2b**) concentration was increased in the reaction with **1a**, the selectivity could be increased from 40% (Table 3.5, Entry 1) to 95% (Entry 4).

Table 3.5. Reaction between HSiEt₃ (**1a**) and varied concentrations of styrene (**2b**)^a

Entry	2b (equiv.) ^b	Conversion ^c (%)	3b ^c (%)	14b ^c (%)
1	1	93	60	40
2	4	>99	19	82
3	7	>99	11	89
4	10	>99	5	95

^aReaction conditions: **1a** (0.3 mmol), **2b**^b(molar equivalence relative to **1a**), **13b** 1.0 mol%, toluene (1 mL), 60 °C, 2.5 h. ^cConversion and product ratio calculated by GC-MS and confirmed by ¹H NMR.

Under similar conditions as before, silanes **1a-d** were reacted with alkenes **2a-d** (10 equiv.) at 60 °C (Table 3.6). In eight of the fourteen entries, we observed preferential dehydrogenative silylation towards vinylsilane **14** as the major products (Table 3.6, Entries 1 – 4, 10, 11, 13 and 14), with seven of the entries showing a substantial shift in selectivity (Entries 1 – 4, 10, 11 and 13). Triethoxysilane (**1b**) only

underwent dehydrogenative silylation in the presence of **2c** (10 equiv., Table 3.6, Entry 7) with no dehydrogenative silylation for the other entries (Entries 5,6 and 8). ^1H NMR analyses of products indicated the exclusive formation of the (*E*)-vinylsilane products (undetermined for **14n**, Table 3.6, Entry 14).

Table 3.6. Reaction between silanes and terminal alkenes (10 equiv.)^a

Entry	Product	Conv (%) ^b	3 (%) ^b	14 (%) ^{b,c}
1		99	43	57
2		>99	5	95
3		>99	8	92
4		92	35	60 ^d
5		>99	>99	-
6		>99	>99	-
7		>99	65	35
8		>99	>99	-
9		>99	85	15
10		96	38	62
11		93	38	62
12		>99	83	17
13		99	12	88
14		>99	8	92 ^e

^aReaction conditions: HSiR_3 **1** (0.3 mmol), alkene **2** (3.0 mmol), **13d** (0.05 mol%), toluene (1 mL), 60 °C, 24 h. ^bProduct yields calculated from GC-MS (conversion relative to concentration of HSiR_3) and confirmed by ^1H NMR analysis. ^cStereochemistry determined by ^1H NMR. ^dReaction also produces branched product **15a** (5%). ^eStereochemistry unclear.

3.3. CONCLUSIONS

In summary we have investigated the catalytic potential of a series of four [Rh(cod)(NHC)(OH)] complexes in the hydrosilylation of terminal alkenes. The Rh(I)-hydroxide motif proved to be an efficient catalytic system in hydrosilylation reactions with the alkyl-substituted NHCs proving to be better ligands than their aryl-substituted counterpart (IPr). Following the reaction profile for the reaction between HSiEt₃ (**1a**) and 1-hexene (**2a**), we identified Rh-IPr^{Me} hydroxide **13d** as the most active and robust catalyst. A scope of limitations was developed for the hydrosilylation reaction, catalysed by **13d**. Reactions between terminal alkenes and silanes could be performed for a variety of substrates, with catalytic activity rivalling some of the most active catalysts reported.^{186b, 197a, 200, 205} However, selectivity proved to be a key issue, with dehydrogenative silylation competing with hydrosilylation to give vinylsilane products. Selectivity was very substrate specific, with dehydrogenative silylation ranging from non-existent when triethoxysilane (**1b**) was used, to being the dominant process when triphenylsilane (**1d**) was coupled to styrene (**2b**).

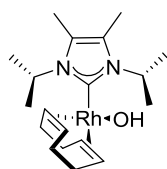
We were able to exploit this competitive side reaction by simply increasing the quantity of alkene in relation to the silane. Hence, vinylsilanes were prepared from alkenes by dehydrogenative silylation in the presence of **13d** (0.05 mol%). In several cases we observed a substantial shift in selectivity from hydrosilylation to dehydrogenative silylation, showing good regio- and stereocontrol at low catalyst loading, comparable to the most active catalysts reported in the literature.^{202, 206, 207}

3.4. EXPERIMENTAL DETAILS

3.4.1. General considerations

Synthesis of Rh-IPr^{Me} hydroxide was performed inside an MBraun Glovebox under inert conditions. All reagents were supplied by Aldrich and used without further purification and solvents were distilled and dried as required. NMR data was obtained using either a Bruker 400 MHz or 300 MHz spectrometer in the specified deuterated solvent. All chemical shifts are given in ppm and coupling constants in Hz. Signals on the ¹³C{¹H} NMR spectra are singlets unless otherwise stated. Spectra were referenced to residual protonated solvent signals (for ¹H) or solvent signals (for ¹³C): (C₆D₆: ¹H δ 7.16 ppm, ¹³C δ 128.0 ppm; CDCl₃: ¹H δ 7.26 ppm). Elemental analyses were performed at the London Metropolitan University. Gas chromatography (GC) analyses were performed on an Agilent 7890A apparatus equipped with a flame ionisation detector and a (5%-Phenyl)-methylpolysiloxane column (30 m, 320 μm, film: 0.25 μm). Flow rate 1 mL min⁻¹ constant flow, inlet temperature 260 °C, column temperature 50 °C, 20 °C min⁻¹ increase to 70 °C (held for 1 min), 50 °C min⁻¹ increase to 300 °C (held for 1 min), total time 7.6 min. GC-MS measurements were performed on a Trace GC Ultra gas chromatograph equipped with a DSQ II mass selective detector and a RXI[®]-1ms column (30 m, 0.25 mm, film: 0.25 μm). [Rh(cod)(NHC)(OH)] complexes **13a-d** were prepared in the manner reported in Chapter 2. CCDC-867621 (**13c**) and CCDC-867622 (**13d**). Crystallographic data can be obtained free of charge from The Cambridge Crystallographic Data Centre *via* www.ccdc.cam.ac.uk/data_request/cif.

3.4.2. Synthesis and Characterisation



[Rh(cod)(IPr)(OH)] (**13d**)

A 25 mL Schlenk tube was charged with [Rh(cod)Cl]₂ (**12**) (100 mg, 0.2 mmol), IPr^{Me} **L4** (73 mg, 0.4 mmol) and CsOH (122 mg, 0.8 mmol) in THF (5 mL). The resultant mixture was stirred overnight then filtered on celite and concentrated *in vacuo*. The resultant solid was washed with hexane (3 x 10 mL) and dried *in vacuo* to give

[Rh(cod)(*i*Pr^{Me})(OH)] (**13d**) (132.5 mg 80.0 %) as a yellow solid; ¹H NMR (300 MHz, C₆D₆): δ 6.46 (quint, 2H, ³J_{HH} = 7.1, NCH), 5.32 – 5.18 (m, 2H, cod-CH), 3.16 – 3.05 (m, 2H, cod-CH), 2.65 – 2.36 (m, 4H, cod-CH₂), 2.14 – 1.99 (m, 2H, cod-CH₂), 1.96 – 1.80 (m, 2H, cod-CH₂), 1.60 (s, 6H, NC(CH₃)), 1.32 (d, 6H, ³J_{HH} = 7.0, CH(CH₃)₂), 1.29 (d, 6H, ³J_{HH} = 7.0, CH(CH₃)₂); ¹³C{¹H} NMR (75 MHz, C₆D₆): δ 184.9 (d, ¹J_{RhC} = 56, Rh-NHC), 124.6 (NC(CH₃)), 95.9 (d, ¹J_{RhC} = 8, cod-CH), 71.7 (d, ¹J_{RhC} = 14, cod-CH), 53.8 (CH(CH₃)₂), 34.0 (cod-CH₂), 29.2 (cod-CH₂), 22.4 (CH₃), 22.3 (CH₃), 9.8 (CH₃); **Anal. Calcd.** for C₁₉H₃₃N₂ORh (MW 408.38): C, 55.88, H, 8.14, N, 6.86. Found: C, 55.76; H, 8.24; N, 6.88.

3.4.3. Catalysis

3.4.4. General method for catalytic hydrosilylation

[Rh(cod)(NHC)(OH)] (**13a-d**) was dissolved in toluene (1 mL) and removed from the glove-box. HSiR₃ **1a-d** and alkene **2a-d** were added and the reaction mixture was stirred at the stated temperature for 24 h. Conversion to products was determined by GC and GC-MS (conversion relative to concentration of HSiR₃) and confirmed by ¹H NMR after separation from starting materials by flash chromatography on silica gel with hexane as eluent. Stereochemistry of vinylsilanes was determined by ¹H NMR. ¹H NMR and MS were compared to literature values.

3.4.5. Optimisation studies

Table 3.7 Solvent optimisation for reaction: HSiEt₃ (**1a**) and styrene (**2b**)^a

Entry	Solvent	T = 5 h			T = 24 h		
		Conversion	3b	14b	Conversion	3b	14b
1	Benzene	80	51	49	90	56	44
2	Dioxane	60	61	39	80	65	35
3	MeOH	7	32	68	8	40	60
4	THF	62	50	50	88	56	44
5	Toluene	70	53	47	92	58	42

^aReaction Conditions: **1a** (0.3 mmol), **2b** (0.3 mmol), [Rh(cod)(ICy)(OH)] (**13b**) (1.0 mol%), rt, solvent (1 mL). Conversions and relative product yields as %; calculated from GC-MS (relative to concentration of **1a**) and confirmed by ¹H NMR.

Table 3.8 Temperature optimisation for reaction: HSiEt₃ (**1a**) and styrene (**2b**)^a

Entry	Temp (°C)	T = 2.5 h			T = 5 h		
		Conversion	3b	14b	Conversion	3b	14b
1	rt	32	53	47	70	55	45
2	60	93	60	40	93	65	35
3	80	93	65	35	94	67	33

^aReaction Conditions: **1a** (0.3 mmol), **2b** (0.3 mmol), [Rh(cod)(ICy)(OH)] (**13b**) (1.0 mol%), t, Toluene (1mL). Conversions and relative product yields as %; calculated from GC-MS (relative to concentration of **1a**) and confirmed by ¹H NMR.

Table 3.9 Reaction of HSiEt₃ (**1a**) with different concentrations of Styrene (**2b**)^a

Entry	Styrene (equiv.)	T = 2.5 h			T = 5 h		
		Conversion	3b	14b	Conversion	3b	14b
1	1	93	60	40	93	65	35
2	4	>99	19	82	>99	18	82
3	7	>99	11	89	>99	11	89
4	10	>99	5	95	>99	5	95

^aReaction Conditions: **1a** (0.3 mmol), **2b** (molar equivalence relative to **1a**), [Rh(cod)(ICy)(OH)] (**13b**) (1.0 mol%), 60 °C, Toluene (1mL). Conversions and relative product yields as %; calculated from GC-MS (relative to concentration of **1a**) and confirmed by ¹H NMR.

Table 3.10 Catalyst loading optimisation for reaction: HSiEt₃ (**1a**) and styrene (**2b**)^a

Entry	[Rh] 3b (mol%)	T = 1 h			T = 2.5 h			T = 5 h		
		Conversion	3b	14b	Conversion	3b	14b	Conversion	3b	14b
1	1.000	77	54	44	88	51	49	96	53	47
2	0.500	68	63	37	82	57	43	90	50	50
3	0.100	32	70	30	47	69	31	86	65	35
4	0.005	17	80	20	32	77	23	74	71	29
5	0.001	1	50	50	4	50	50	12	60	40

^aReaction Conditions: **1a** (0.3 mmol), **2b** (0.6 mmol), [Rh(cod)(ICy)(OH)] (**13b**) (mol% relative to **1a**), 60 °C, Toluene (1mL). Conversions and relative product yields as %; calculated from GC-MS (relative to concentration of **1a**) and confirmed by ¹H NMR.

Table 3.11 Reaction of HSiEt₃ (**1a**) with different concentrations of 1-hexene (**2a**)^a

Entry	1-hexene 2a (eq.)	T = 1 h			T = 2.5 h			T = 5 h		
		Conversion	3a	14a	Conversion	3a	14a	Conversion	3a	14a
1	1	35	54	46	54	52	48	55	47	53
2	2	53	85	15	88	94	6	>99	99	1
3	3	92	82	18	97	85	15	>99	84	16
4	5	>99	60	40	>99	77	23	>99	70	30

^aReaction Conditions: **1a** (0.3 mmol), **2a** (molar equivalence relative to **1a**), [Rh(cod)(ICy)(OH)] (**13b**) (1.0 mol%), 60 °C, Toluene (1mL). Conversions and relative product yields as %; calculated from GC-MS (relative to concentration of **1a**) and confirmed by ¹H NMR.

Table 3.12 Catalyst loading optimisation for reaction: HSiEt₃ (**1a**) and 1-hexene (**2a**)^a

Entry	[13b] (mol%)	T = 4 h			T = 24 h		
		Conversion	3a	14a	Conversion	3a	14a
1	1.00	99	99	1	>99	99	1
2	0.50	98	95	5	>99	98	2
3	0.10	90	88	12	93	94	6
4	0.05	90	85	15	92	88	12

^aReaction Conditions: **1a** (0.3 mmol), **2a** (0.6 mmol), [Rh(cod)(ICy)(OH)] (**13b**) (mol% relative to **1a**), 60 °C, Toluene (1mL). Conversions and relative product yields as %; calculated from GC-MS (relative to concentration of **1a**) and confirmed by ¹H NMR.

Table 3.13 Catalyst comparison for reaction: HSiEt₃ (**1a**) and 1-hexene (**2a**) at rt^a

Entry	[Rh(cod)(NHC)(OH)] NHC =		Conversion to Products (3a + 14a) (%) / Time (h)								
	1	2	1	2	3	4	5	6	7	8	24
1	13a	IPr L1	3	6	9	17	20	24	27	28	42
2	13b	ICy L2	40	65	76	78	80	82	82	82	82
3	13c	IDD L3	30	45	54	65	74	76	77	78	89
4	13d	ⁱ Pr ^{Me} L4	43	75	88	92	96	97	98	98	>99

^aReaction Conditions: **1a** (0.3 mmol), **2a** (0.6 mmol), [Rh(cod)(NHC)(OH)] (**13a-d**) (1.0 mol%), rt, Toluene (1mL). Conversions and relative product yields as %; calculated from GC-MS (relative to concentration of **1a**) and confirmed by ¹H NMR.

3.4.6. Characterisation data

triethyl(hexyl)silane **3a** ¹H NMR (300 MHz, CDCl₃) δ 1.37 – 1.20 (m, 8H), 0.89 – 0.85 (m, 12H), 0.58 – 0.40 (m, 8H); GC-MS *m/z* = 171 (M-C₂H₅, 100), 163, 143, 115.²⁰⁸

(*E*)-triethyl(hex-1-en-1-yl)silane **14a**: ¹H NMR (300 MHz, CDCl₃, representative signals) δ 6.08 (dt, 1H, ³*J*_{HH} = 18.7, 6.3), 5.59 (dt, 1H, ³*J*_{HH} = 18.7, 1.5), 2.04 – 1.94 (m, 2H); GC-MS *m/z* = 198 (M⁺), 169 (M-C₂H₅, 100), 141, 113.²⁰⁹

triethyl(phenethyl)silane **3b**: ¹H NMR (400MHz, C₆D₆, representative signals) δ 2.74 (t, ³*J*_{HH} = 8.0, 2H), 1.02 (t, 2H, ³*J*_{HH} = 8.0), 0.83 (q, 9H, ³*J*_{HH} = 8.0), 0.66 (q, 6H, ³*J*_{HH} = 8.0); GC-MS *m/z* = 191 (M-C₂H₅, 100), 163, 135.^{194b}

(*E*)-triethyl(styryl)silane **14b**: ¹H NMR (400MHz, C₆D₆) δ 7.20 (d, ³*J*_{HH} = 19.0, 1H), 6.60 (d, 1H, ³*J*_{HH} = 19.0), 1.19 (t, 9H, ³*J*_{HH} = 7.9), 1.11 (t, 6H, ³*J*_{HH} = 7.9); GC-MS *m/z* = 218 (M⁺), 189 (M-C₂H₅, 100), 161, 131.²⁰⁹

(4-chlorophenethyl)triethylsilane **3c**: ¹H NMR (300 MHz, CDCl₃, representative signals) δ 2.43 – 2.30 (m, 2H), 0.99 (t, 2H, ³*J*_{HH} = 7.6); GC-MS *m/z* 225 (M-C₂H₅), 197, 169, 141, 115, 87 (100).²¹⁰

(*E*)-(4-chlorostyryl)triethylsilane **14c**: $^1\text{H NMR}$ (300 MHz, CDCl_3 , representative signals) δ 6.61 (d, $^3J_{\text{HH}} = 19.3$, 1H), 6.17 (d, 1H, $^3J_{\text{HH}} = 19.3$); GC-MS m/z 252 (M^+), 223 (M- C_2H_5 , 100), 195, 167, 131.²¹¹

triethyl(octyl)silane **3d**: $^1\text{H NMR}$ (300 MHz, CDCl_3) δ 1.40 – 1.19 (m, 12H), 0.98 – 0.84 (m, 12H), 0.60 – 0.44 (m, 8H); GC-MS m/z 200 (M- C_2H_5), 199 (100), 171, 115, 87.

(*E*)-triethyl(oct-1-en-1-yl)silane **14d**: $^1\text{H NMR}$ (400MHz, CDCl_3 , representative signals) δ 6.13 (dt, 1H, $^3J_{\text{HH}} = 18.7$, 6.3), 5.63 (dt, 1H, $^3J_{\text{HH}} = 18.7$, 1.5) 2.17 -2.08 (m, 2H); GC-MS m/z 226 (M^+), 207, 197 (M- C_2H_5 , 100), 169.²¹²

triethoxy(hexyl)silane **3e**: $^1\text{H NMR}$ (300 MHz, CDCl_3) δ 3.81 (q, $^3J_{\text{HH}} = 7.0$, 6H), 1.67 – 1.47 (m, 17H), 0.94 – 0.82 (m, 3H), 0.70 – 0.58 (m, 2H); GC-MS m/z 248 (M^+), 203 (M- OC_2H_5 , 100), 163, 149, 139, 119.^{186b}

triethoxy(phenethyl)silane **3f**: $^1\text{H NMR}$ (300 MHz, CDCl_3) δ 7.34 – 7.13 (m, 5H), 3.83 (q, 6H, $^3J_{\text{HH}} = 7.0$), 2.79 – 2.70 (m, 2H), 1.24 (t, 9H, $^3J_{\text{HH}} = 7.0$), 1.04 – 0.96 (m, 2H); GC-MS m/z 268 (M^+), 240, 223, 195, 163 (100).²⁰⁰

(4-chlorophenethyl)triethoxysilane **3g**: $^1\text{H NMR}$ (300 MHz, CDCl_3 , representative signals) δ 3.82 (q, $^3J_{\text{HH}} = 7.4$, 6H), 2.75 – 2.65 (m, 2H), 0.99 – 0.91 (m, 2H); GC-MS m/z 287 (M- CH_3), 259 (100), 181.²¹³

(*E*)-(4-chlorostyryl)triethoxysilane **14e**: $^1\text{H NMR}$ (300 MHz, CDCl_3 , representative signals) δ 6.15 (d, 1H, $^3J_{\text{HH}} = 19.3$); GC-MS m/z 285 (M- CH_3), 259, 207, 183, 181(100).²¹⁴

triethoxy(octyl)silane **3h**: $^1\text{H NMR}$ (300 MHz, CDCl_3) δ 3.91 (q, 6H, $J = 7.0$), 1.58 – 1.26 (m, 21H), 0.97 (t, 3H, $^3J_{\text{HH}} = 6.7$), 0.78 – 0.67 (m, 2H); GC-MS m/z 276 (M^+), 231, 207, 187, 163 (100), 149, 135, 119.²¹⁵

hexyl(methyl)diphenylsilane **3i**: $^1\text{H NMR}$ (300 MHz, CDCl_3) δ 7.60 – 7.48 (m, 4H), 7.43 – 7.28 (m, 6H), 1.44 – 1.20 (m, 8H), 1.12 – 1.04 (m, 2H), 0.81 – 0.93 (m, 3H), 0.56 (s, 3H); GC-MS m/z 281 (M^+), 267 (M- CH_3), 225, 204, 197 (100), 183, 165, 121, 105.²¹⁶

(*E*)-hex-1-en-1-yl(methyl)diphenylsilane **14f**: $^1\text{H NMR}$ (300 MHz, CDCl_3 , representative signals) δ 6.21 (dt, 1H, $^3J_{\text{HH}} = 18.5$, 6.2), 5.99 (dt, 1H, $^3J_{\text{HH}} = 18.5$, 1.3), 0.95 (t, 3H, $^3J_{\text{HH}} = 7.2$), 0.65 (s, 3H); GC-MS m/z 280 (M^+), 265, 223, 197 (100), 183, 145, 121, 105.²¹⁷

methyl(phenethyl)diphenylsilane **3j**: $^1\text{H NMR}$ (300 MHz, CDCl_3 , representative signals) δ 2.72 – 2.64 (m, 2H), 1.47 – 1.40 (m, 2H), 0.56 (s, 3H); GC-MS m/z 287 (M- CH_3), 224, 197 (100), 183, 165, 146, 121, 105.²¹⁶⁻²¹⁷

(*E*)-methyl(diphenyl(styryl)silane **14g**: $^1\text{H NMR}$ (300 MHz, CDCl_3 , representative signals) δ 6.96 (d, $^3J_{\text{HH}} = 19.0$, 1H), 6.75 (d, 1H, $^3J_{\text{HH}} = 19.0$), 0.71 (s, 3H); GC-MS m/z 300 (M^+), 285, 222, 207 (100), 197, 183, 165, 155, 145, 129, 121, 105.²¹⁸

(4-chlorophenethyl)(methyl)diphenylsilane **3k**: $^1\text{H NMR}$ (300 MHz, CDCl_3 , representative signals) δ 2.72 – 2.63 (m, 2H), 1.46 – 1.37 (m, 2H), 0.55 (s, 3H); GC-MS m/z 321 (M- CH_3), 281, 258, 243, 207, 197 (100).²¹⁶

(*E*)-(4-chlorostyryl)(methyl)diphenylsilane **14h**: $^1\text{H NMR}$ (300 MHz, CDCl_3) δ 7.58 (d, 2H, $^3J_{\text{HH}} = 7.5$), 7.47 (d, 2H, $^3J_{\text{HH}} = 7.6$), 7.43 – 7.26 (m, 10H), 6.97 (d, 1H, $^3J_{\text{HH}} = 19.1$), 6.76 (d, 1H, $^3J_{\text{HH}} = 19.1$), 0.72 (s, 3H); GC-MS m/z 334 (M^+), 319, 256, 241 (100), 222, 207, 183, 179, 165, 155, 121, 105.

methyl(octyl)diphenylsilane **3l**: $^1\text{H NMR}$ (300 MHz, CDCl_3) δ 7.46 – 7.33 (m, 10H), 1.49 – 1.21 (m, 12H), 1.15 – 1.07 (m, 2H), 0.91 (t, 3H, $^3J_{\text{HH}} = 7.0$), 0.58 (s, 3H); GC-MS m/z 295 (M- CH_3), 232, 197 (100), 183, 165, 121, 105.²¹⁶

(*E*)-methyl(oct-1-en-1-yl)diphenylsilane **14i**: $^1\text{H NMR}$ (300 MHz, CDCl_3 , representative signals) δ 6.21 (dt, 1H, $^3J_{\text{HH}} = 18.6$, 6.2), 5.99 (dt, 1H, $^3J_{\text{HH}} = 18.5$, 1.4), 0.65 (s, 3H); GC-MS m/z 308 (M^+), 293, 281, 223, 197 (100), 183, 145, 121, 105.

hexyltriphenylsilane **3m**: $^1\text{H NMR}$ (300 MHz, CDCl_3 , representative signals) δ 0.89 (t, 2H, $^3J_{\text{HH}} = 7.4$); GC-MS m/z 315 (M- C_2H_5), 282, 267, 259 (100), 181.

(*E*)-hex-1-en-1-yltriphenylsilane **14j**: $^1\text{H NMR}$ (300 MHz, CDCl_3 , representative signals) δ 6.28 – 6.34 (m, 2H), 1.02 (t, 2H, $^3J_{\text{HH}} = 7.2$); GC-MS m/z 342 (M^+), 260, 182 (100).²⁰⁹

phenethyltriphenylsilane **3n**: $^1\text{H NMR}$ (300 MHz, CDCl_3 , representative signals) δ 2.82 – 2.72 (m, 2H), 1.80 – 1.69 (m, 2H); GC-MS m/z 287 (M-C₆H₅), 281, 259 (100), 207, 181.

triphenyl(styryl)silane **14k**: $^1\text{H NMR}$ (300 MHz, CDCl_3) δ 7.55 – 7.43 (m, 6H), 7.41 – 7.18 (m, 14H), 7.18 – 7.13 (m, 2H); GC-MS m/z 285 (M-C₆H₅), 259, 207, 181 (100), 105.²⁰⁹

triethyl(oct-1-en-2-yl)silane **15a**: $^1\text{H NMR}$ (300 MHz, CDCl_3) δ 5.47 – 5.42 (m, 2H), 1.92 – 2.0 (m, 2H); GC-MS m/z 226 (M⁺), 197, 169, 115 (100), 87.²¹²

4. WELL-DEFINED IRIDIUM(I) HYDROXIDES AND THEIR ACTIVITY IN BOND ACTIVATION

4.1. INTRODUCTION

Following the successful preparation of Rh(I)-hydroxides (described in Chapters 2 and 3) we aimed to extend the scope of metal hydroxides to include iridium. The relatively high cost of rhodium and iridium encourages innovative preparations and it is imperative to develop successively more active generations of metal complexes. NHC ligands have proven highly beneficial in enhancing iridium-based catalysis and many Ir-NHC complexes have been prepared in various forms, finding success in myriad applications such as (de)hydrogenation, transfer hydrogenation, hydrosilylation, oxidation, H/D exchange, alkylation and hydroamination, among others.^{84, 119} Ir-NHC complexes are also known to undergo intramolecular C-H bond activations to generate new motifs and have been studied extensively in this regard.^{144, 147a, 147c, 147d, 219} Ir-hydroxide complexes are relatively scarce. Monomeric Ir(I)- and Ir(III)-hydroxide complexes have been prepared predominantly *via* ligand metathesis with inorganic bases or by oxidative addition of water.^{14, 15b, c, 19} Several hydroxide complexes were discussed in Chapter 1 and in particular we focused on the following complexes: [IrCp^{*}(OH)Ph(PMe₃)] (**1**),⁴⁵ [Rh(PPh₃)₂(μ-OH)]₂ (**2**)⁴⁷ and [Ru(dpme)₂(H)(OH)] (**3**).⁵³ The authors of these reports tested the reactivity of complexes **1** – **3** towards a number of organic substrates. In each case, the metal hydroxide was able to deprotonate a range of C-H, O-H and N-H bonds to deliver new species of all three metals.

The first metal hydroxides to be reported by our group were the Au(I) and Cu(I) hydroxides, both of which were isolated with the use of the strongly σ-donating IPr ligand. Both of these metal hydroxides were very efficient bond activation reagents, able to coordinate a large array of substrates by deprotonation of suitably acidic C-H, N-H, O-H, Si-H and P-H bonds.⁶²

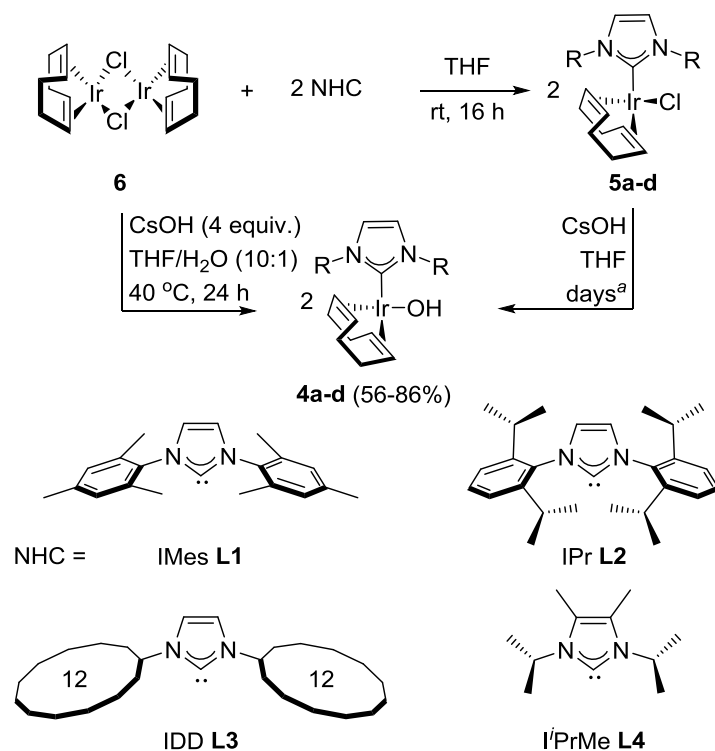
To the best of our knowledge, only a single NHC-bearing Ir(I)-hydroxide complex has been reported in the literature to date: [Ir(cod)(IMes)(OH)] (**4a**) (IMes = 1,3-(2,4,6-trimethylphenyl)imidazol-2-ylidene) was isolated serendipitously by Marciniak and co-workers *via* the reaction between [Ir(cod)(IMes)Cl] (**5a**) and KO^tBu, presumably in the

presence of adventitious water.¹⁷⁷ Although the authors report a crystal structure for **4a** there is no proof of bulk purity and hence, this cannot be seen as a general synthetic approach. Furthermore, the reactivity of this motif has not been explored. In order to approach this important problem, we set out to systematically prepare a series of [Ir(cod)(NHC)(OH)] complexes and probe their reactivity with key reagents. Firstly, a straightforward, reliable and scalable synthetic method was sought. Once a general procedure was established, we endeavoured to fully explore the potential of these complexes as synthons for organometallic chemistry and to establish their value in the development of new catalytic processes and useful materials.

4.2. RESULTS AND DISCUSSION

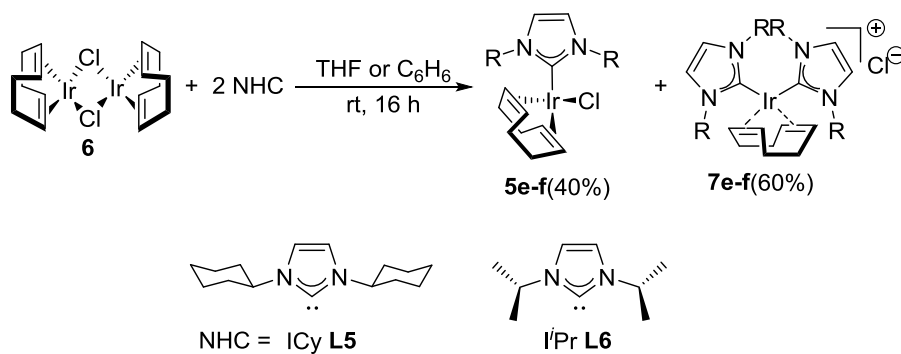
4.2.1. Iridium(I) hydroxide synthesis

[Ir(cod)(NHC)Cl] complexes **5a-d** were prepared from [Ir(cod)Cl]₂ (**6**) and the corresponding free carbene **L1-4** following a simple reported procedure (Scheme 4.1).^{81d, 101b, 106, 220} Subsequent substitution of the chloride moieties on **5a-d** using CsOH at room temperature produced the desired complexes **4a-d**. However, the yields were low even after long reaction times, particularly when aryl-substituted NHC ligands were used. For example, in the case of **4b**, bearing IPr, only 75% conversion was achieved under vigorous stirring for 10 days in the presence of eight equivalents of CsOH. Similarly, in an attempted one-pot preparation (as described in Chapter 2) of [Ir(cod)(NHC)(OH)] from **6** using free NHC and CsOH in THF, attachment of the NHC ligand was swift but chloride substitution was still very slow, as determined by ¹H NMR spectroscopy. We considered that the insolubility of CsOH in THF might be responsible for the low reactivity. Gratifyingly, when **6** was stirred with free NHC and CsOH in THF/H₂O (10:1) under inert atmosphere at 40 °C for only 24 h, [Ir(cod)(NHC)(OH)] (**4a-d**, NHC = IMes **L1**, IPr **L2**, IDD **L3**, IⁱPr^{Me} **L4**) were afforded in moderate to high yields (Scheme 4.1). However, this method was unsuccessful when ICy **L5** and 1,3-diisopropylimidazol-2-ylidene (IⁱPr **L6**), were used, leading instead to a mixture of products.



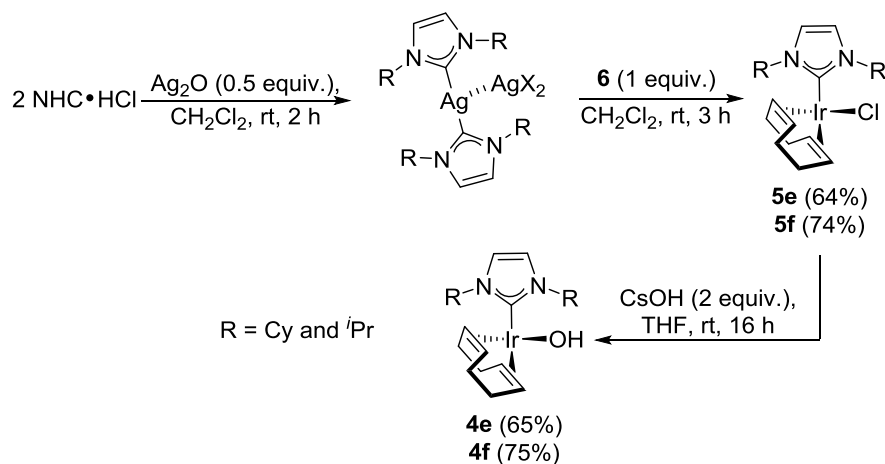
Scheme 4.1. Preparation of [Ir(cod)(NHC)Cl] (**5a-d**) and [Ir(cod)(NHC)(OH)] (**4a-d**) complexes from free NHCs. ^a CsOH: up to 8 equiv. and time: up to 10 days for IPr.

When the reactions were performed with ICy **L5** or *i*Pr **L6** in the absence of CsOH, two products were isolated by silica gel chromatography in each case: [Ir(cod)(NHC)Cl] (**5e-f**) as yellow solids, and [Ir(cod)(NHC)₂]⁺Cl⁻ (**7e-f**) as red solids in a 40:60 ratio, respectively (Scheme 4.2). The formation of *bis*-NHC complexes was not altogether surprising since there is a precedent for their preparation in the literature,^{10a, 11} yet we were surprised that *i*Pr^{Me} showed no propensity towards dicoordination and that **5d** could be prepared following the one-pot procedure. Once isolated, **5e-f** underwent reaction with CsOH under mild reaction conditions to provide the corresponding hydroxides **4e-f**.



Scheme 4.2. Preparation of [Ir(cod)(NHC)Cl] (**5e-f**)

To avoid undesired dicoordination and increase the overall yield, we followed an alternative, silver transmetalation route to prepare [Ir(cod)(NHC)Cl] complexes **5e-f** (Scheme 4.3).^{101b, 102-103, 220} Ag₂O was stirred with the imidazolium salts, ICy-HCl and I^tPr-HCl in CH₂Cl₂ under air to provide the corresponding silver NHC salts, which were then reacted with **6**. This method provided easy access to **5e** and **5f** in moderate to good yields (64% and 74% respectively), avoiding free carbenes and hence the need for rigorously air-free conditions.



Scheme 4.3. Preparation of [Ir(cod)(NHC)(OH)] bearing small NHC ligands

Complexes **4a-f** were fully characterised by ¹H and ¹³C{¹H} NMR spectroscopy as well as elemental analysis. ¹H NMR analysis showed the hydroxyl moiety to resonate as a sharp singlet between 1.66 and 2.47 ppm in C₆D₆. When a drop of degassed D₂O was added to a THF-*d*₈ solution of **4f**, H-D exchange was observed at the hydroxyl moiety and only the corresponding ¹H NMR signal (2.01 ppm) disappeared, thus confirming the assignment. Furthermore, the presence of a hydroxide functionality was confirmed by FTIR (ATR) spectroscopic analysis of **4f** which showed the diagnostic hydroxide stretch as a weak band at δ 3612.7 cm⁻¹. Single crystals of **4c-f** were grown by slow evaporation of saturated alkane solutions; X-ray analysis confirmed the structures, which adopt square planar geometries around the metal with the NHC and OH ligands *cis* to each other (Figure 4.1, the X-ray structure for **4a** is known¹⁹⁶).

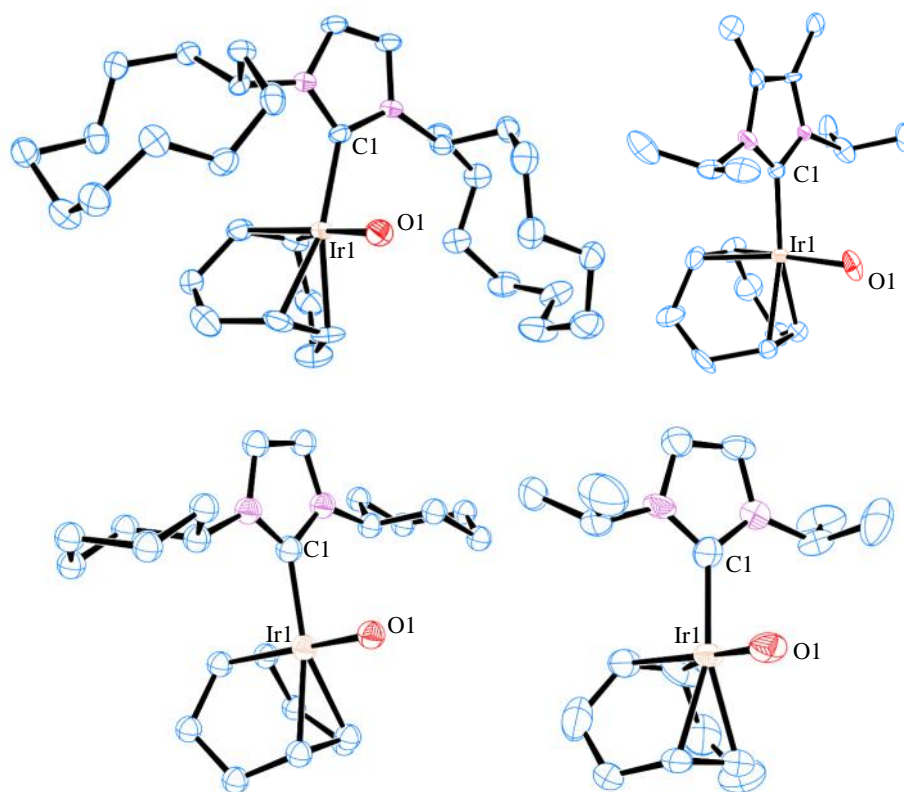


Figure 4.1. Thermal ellipsoid representations of [Ir(cod)(NHC)(OH)] (**4c-f**) (NHC = IDD **4c**, $i\text{Pr}^{\text{Me}}$ **4d**, ICy **4e**, $i\text{Pr}$ **4f**); showing 50% thermal ellipsoid probability. H atoms are omitted for clarity.

Table 4.1. Selected bond lengths (Å) and bond angles (°) for **4c-f**

Entry	Complex	Ir(1)-C(1)	Ir(1)-O(1)	C(1)-Ir(1)-O(1)
1	4c	2.061(6)	2.035(4)	90.27(18)
2	4d	2.058(10)	2.041(8)	92.0(4)
3	4e	2.034(12)	2.015(8)	86.8(4)
4	4f	2.046(9)	2.020(6)	90.1(3)

Table 4.1 provides selected bond lengths and angles for each of **4c-f**. The differences in Ir-carbene bond lengths are minimal when the error is taken into account, as are the Ir-OH bond lengths. TEP values for each of the NHCs, obtained from the literature gives an indication of the electron donation from each ligand, and again the differences are marginal ($2049.6 - 2051.5 \text{ cm}^{-1}$),^{93b, 94a, 176} indicating a similar level of electron donation from each ligand to the Ir centre. In Chapter 3, we reported that differences in reactivity between complexes of rhodium, bearing different NHCs are more likely to be the result of differences in steric rather than electronic

characteristics.^{13b, 25a} Since NHC ligands occupy space within the metal sphere, differences in steric bulk have a direct impact on the ability of the complex to react with other substrates. To quantify the steric bulk of the NHC ligands, percent buried volumes ($\%V_{bur}$) were calculated from the X-ray structures of **4c-f** using the SambVca software.⁹⁸ Steric contour maps were also generated to give a visual distribution of the total $\%V_{bur}$ over four quadrants as viewed along the z-axis (Ir(1)-C(1)) and are shown in Figure 4.2.

It is evident from these calculations (Figure 4.2) that the high degree of flexibility associated with cycloalkyl-substituted NHC ligands enables them to adopt conformations that exert a minimum amount of steric demand on the metal centre. For example, IDD in **4c** has a total $\%V_{bur}$ of only 33.4%, with the steric bulk concentrated into two quadrants, while NHC ligands in **4d-f** show low $\%V_{bur}$ with a more even distribution of bulk around the metal centre. iPr^{Me} shows greater bulk than ICy and iPr , which explains why it does not form *bis*-NHC complexes in the same way as ICy and iPr do. One might expect the cyclohexyl rings on ICy to impart greater bulk than the *isopropyl* groups on iPr^{Me} . However, the flexibility of the cyclohexyl rings means that they may adopt an arrangement that exerts a minimal amount of steric pressure on the metal centre, occupying equal space to an *isopropyl* group within the metal sphere.²²⁰ Hence, the difference in steric bulk between ICy and iPr^{Me} is likely the result of steric repulsion between the backbone substituents and the *N*-substituents. Our group²²¹ and Grubbs²²² have shown experimentally that substitution on the backbone of aryl-substituted NHC ligands has a noticeable effect on electronics and sterics. Grubbs indicated that backbone substitution imposes rotational barriers on the *N*-substituents, which increases the stability of corresponding Ru-complexes by minimising decomposition. Cavallo and co-workers have supported this hypothesis with theoretical calculations, indicating that backbone substitution could significantly alter the conformational behaviour of aryl-substituted NHC ligands²²³ and thus disfavour the first step of Ru-catalyst decomposition *via* C-H insertion on the aryl rings.²²⁴

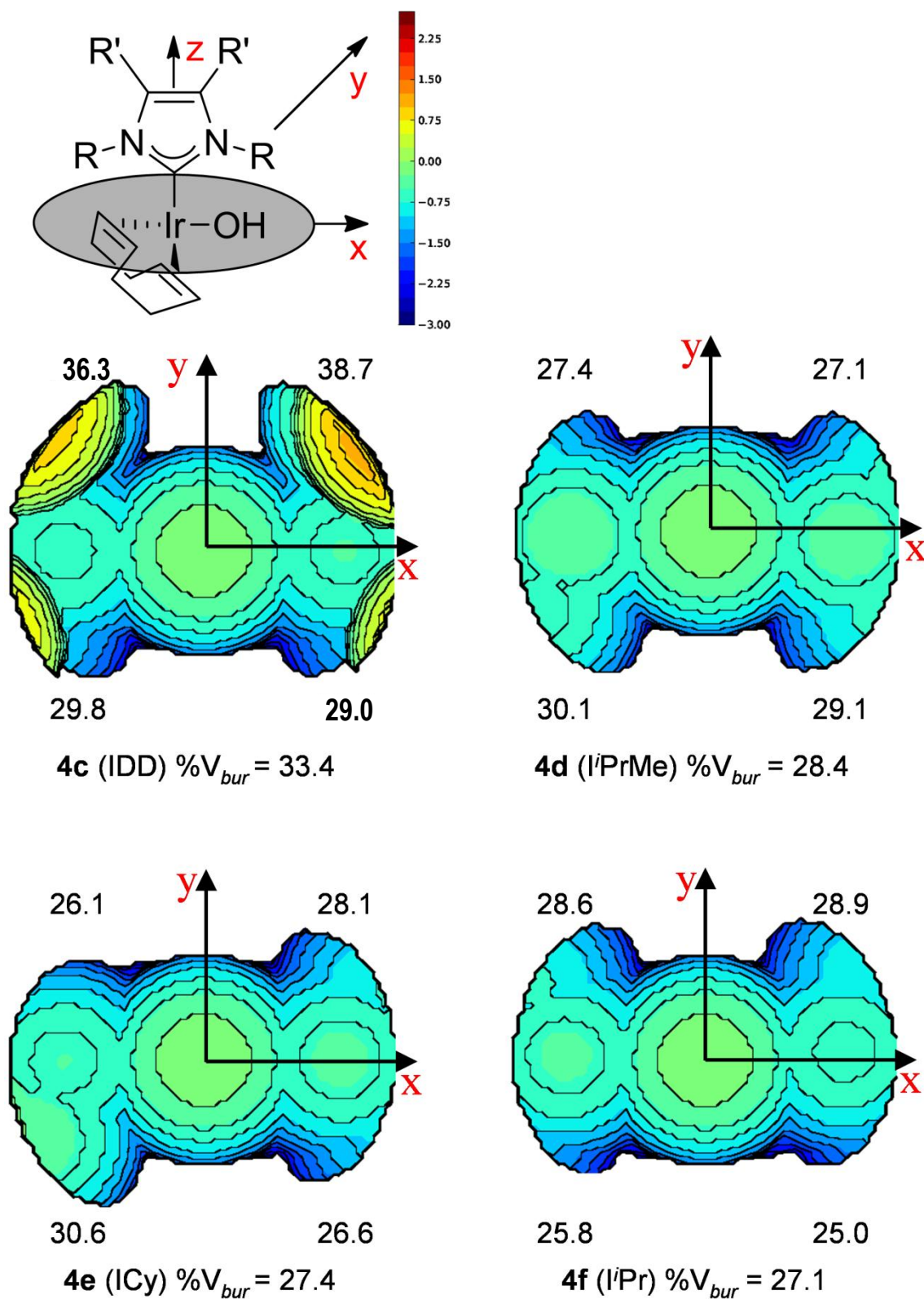
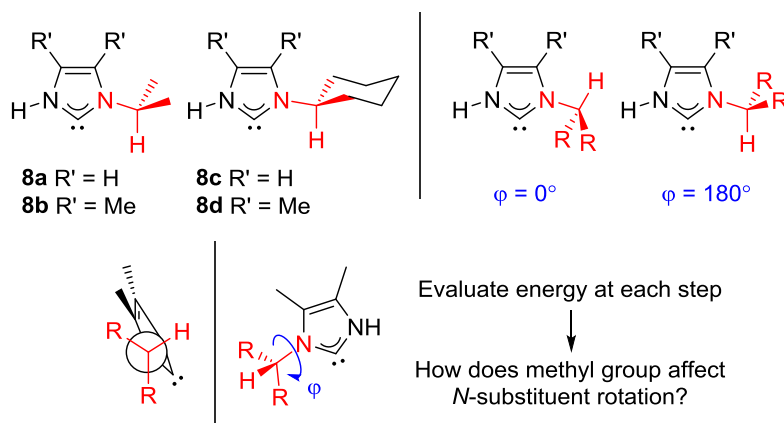


Figure 4.2. Steric contour maps for complexes **4c-f** showing % V_{bur} for each NHC. Calculated using SambVca software (sphere radius = 3.5, distance from centre of sphere = 2.00, mesh spacing = 0.1, hydrogens omitted).⁹⁸

In an effort to better understand the effect of backbone substitution on the spatial arrangement of isopropyl and cyclohexyl *N*-substituents, Dr David Nelson modelled simplified NHCs **8a-d** using Gaussian 09.²²⁵ **8a-d** were constructed ($\varphi = 0^\circ$) and geometries were optimised (B3LYP/6-31+G*) with the cyclohexyl rings in the chair conformation and the imidazolium ring in the equatorial position. Dihedral angle φ was stepped in 10° increments using a relaxed PES scan. The (electronic) energy was evaluated at each step (Scheme 4.4, Figure 4.3).



Scheme 4.4. Theoretical NHC compounds **8a-d** modelled using DFT calculations

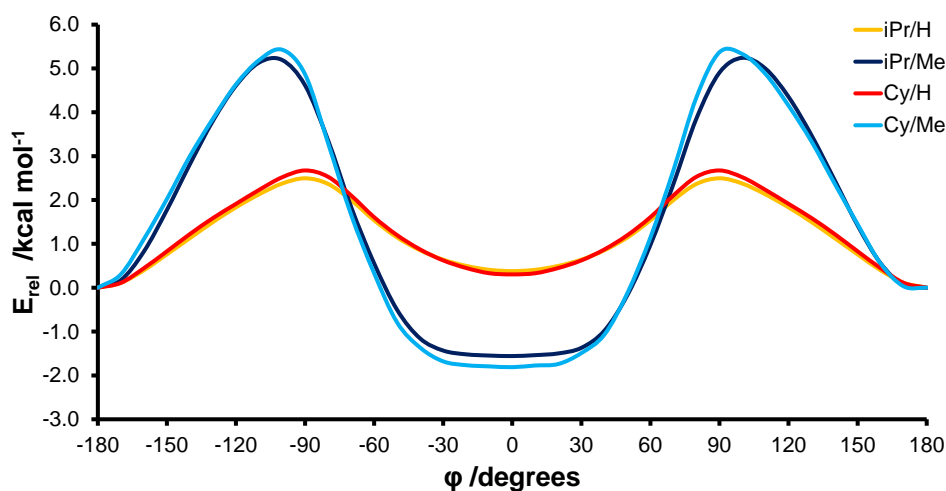


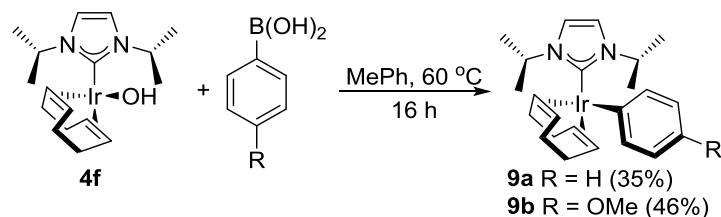
Figure 4.3. Plot of energy (B3LYP/6-31+G*) vs. angle φ in theoretical compounds **8a** (^{*i*}Pr/H), **8b** (^{*i*}Pr/Me), **8c** (Cy/H) and **8d** (Cy/Me); all energies are relative to $E(\varphi = 180^\circ)$.

Figure 4.3 illustrates that the relative energies at $\varphi = 0^\circ$ (alkyl groups pointing towards where the metal centre would be) and $\varphi = 180^\circ$ (alkyl groups pointing away from the metal centre), and the barriers between those two conformations, vary greatly depending on the backbone substitution pattern. However, isopropyl- and cyclohexyl-substituted compounds behave in the same manner, so the backbone substitution only appears to interact with functionality close to the nitrogen atom. Compounds without

backbone substitution (**8a,c**) prefer $\varphi = 180^\circ$ (by *ca.* 2-fold), while when $R' = \text{Me}$ (**8b,d**), $\varphi = 0^\circ$ is preferred (by *ca.* 20 fold). It should be noted, however, that these compounds are models due to the vastly increased computational cost of considering full complexes, and do not contain the metal centre; the inclusion of a (square planar) iridium centre would likely alter the energies of the rotation. However, we feel that this can go some way to explain why $\text{I}^i\text{Pr}^{\text{Me}}$ **L4** behaves as if it is considerably more bulky than ICy **L5** or I^iPr **L6** and forms only monocoordinated complexes of Ir, while ICy and I^iPr favour dicoordination.

4.2.2. Reactivity

Having developed a synthetic route for Ir(I)-hydroxides, their reactivity with a range of functional groups was explored. $[\text{Ir}(\text{cod})(\text{I}^i\text{Pr})(\text{OH})]$ (**4f**) was used as a model complex since previous experience with the isoelectronic Rh(I)-hydroxides dictated that the complexes bearing the smallest NHC ligands were the most active²²⁶ and the highly diagnostic ^1H NMR spectrum of **4f** made it simple to follow the reaction progress. First, nucleophilic attack of (or transmetalation with) arylboronic acids was investigated, since coupling with boronic acids provides convenient access to M-Ar compounds, which are important intermediates for C-C coupling reactions such as conjugate additions.¹⁵ The reaction between phenylboronic acid and Rh-ICy hydroxide gives quantitative conversion to the Rh(I)-phenyl complex almost instantly at room temperature (Chapter 2).²²⁷ However, the reaction between arylboronic acids and **4f** was much slower, requiring heating at 60°C for 16 h to give **9a-b**, which were isolated as red solids in only 35 and 46% yield (Scheme 4.5). X-ray analysis of single crystals of **9b** (Figure 4.4) confirmed the identity of the square planar complex with the aryl group *cis* to the NHC ligand, and slightly twisted from the Ir(1)-carbene plane, analogous to the Rh(I)-phenyl complex.²²⁷ In the conjugate addition study (Chapter 2) we reported that the high activity displayed by Rh-ICy hydroxide was largely due to the ease with which it underwent transmetalation with arylboronic acids, yet this is clearly not the case for iridium(I)-hydroxide.



Scheme 4.5. Transmetalation with arylboronic acids.

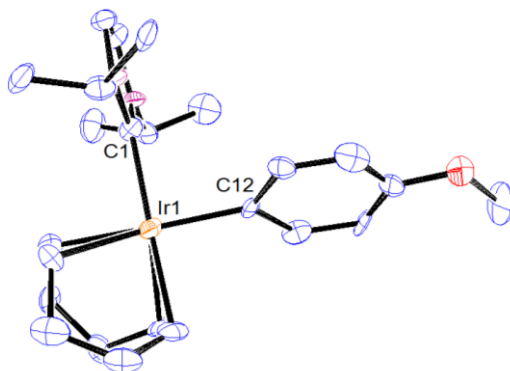


Figure 4.4. Thermal ellipsoid representation of $[\text{Ir}(\text{cod})(\text{IPr})(p\text{-MeOC}_6\text{H}_4)]$ (**9b**), showing 50% thermal ellipsoid probability. H atoms are omitted for clarity. Selected bond lengths (\AA) and bond angles ($^\circ$): Ir(1)-C(1): 2.057(10), Ir(1)-C(12): 2.065(8), C(1)-Ir(1)-C(12): 89.5(4).

Next we probed the activation of silicon compounds, an important step in the preparation of organosilicons and hydrosilylation reactions.^{186-187, 226} Reaction of **4f** with $\text{PhSi}(\text{OMe})_3$ liberated MeOH to give Ir(I)-siloxide **10** (Scheme 4.6, Figure 4.5). Metal siloxide complexes have been investigated extensively due to their immobilisation capabilities on silicate surfaces.^{14a} However, reports of siloxide complexes of LTMs are relatively scarce in comparison to those of early TMs.²²⁸ Monomeric Ir(I)-siloxides were first reported in 2002, by Marciniec.²²⁹ The same group reported the preparation of $[\text{Ir}(\text{cod})(\text{IMes})(\text{OSiMe}_3)]$ in 2008 from the corresponding Ir-(μ -siloxide) dimer¹⁷⁷ and they have shown extensive catalytic potential for Ir-siloxides in silicon-related catalysis.^{202, 230} The isolation of an Ir-Si complex from the reaction with HSiR_3 was not possible, since the formation of an Si-O bond is highly favourable²³¹ and reaction between **4f** and HSiPh_3 again resulted in formation of an Ir(I)-siloxide **11**. X-ray analysis of single crystals confirmed the structure of **11** (Figure 4.5). The Ir(1)-O(1)-Si(1) bond angle for **10** ($137.7(2)^\circ$) is more acute than for **11** ($155.2(5)^\circ$). In agreement with this observation, Marciniec has reported that steric strain has a powerful influence on the Ir-siloxide bond angle and the angle increases with steric bulk of the siloxide substituents.²²⁸ The unexpected formation of **11** was interesting since it represents the preparation of an Ir(I)-siloxide complex *via* deprotonation of a very bulky silane and release of H_2 . It is important to mention that during preparation of **11**, H_2 was released

as a side product. If the reaction vessel was not vented to the atmosphere then an intractable mixture of hydride complexes was obtained as well as **11**, indicating the instability of **4f** to the presence of hydrogen.

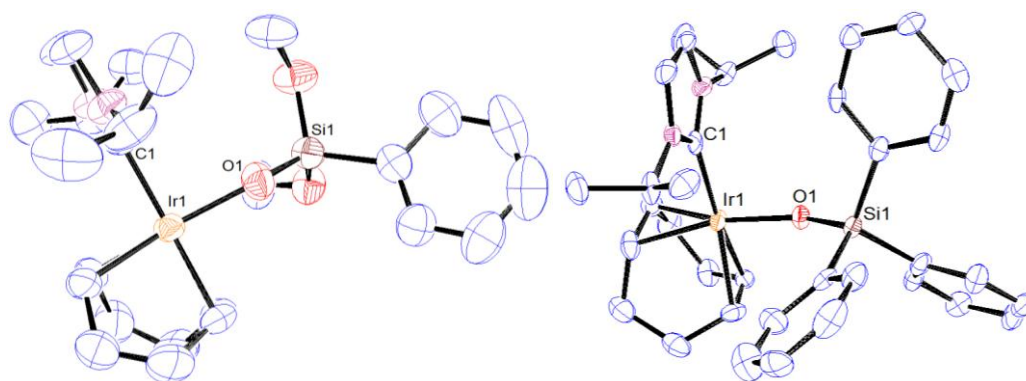
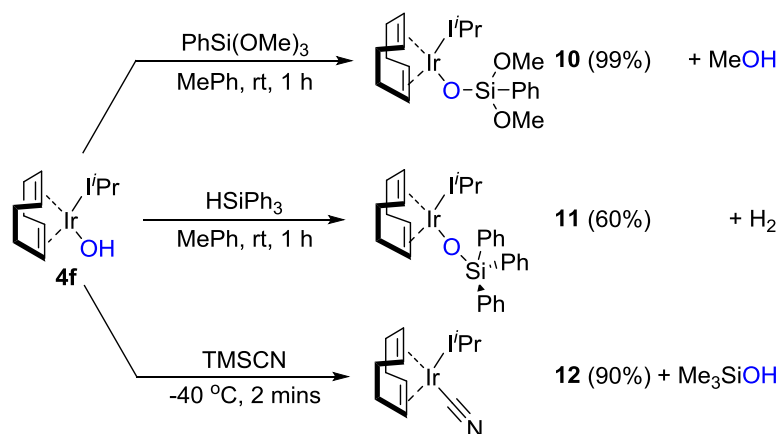


Figure 4.5. Thermal ellipsoid representations of $[\text{Ir}(\text{cod})(\text{I}^t\text{Pr})(\text{OSi}(\text{OMe})_2\text{Ph})]$ (**10**) and $[\text{Ir}(\text{cod})(\text{I}^t\text{Pr})(\text{OSiPh}_3)]$ (**11**) showing 50% thermal ellipsoid probability. H atoms are omitted for clarity. Selected bond lengths (\AA) and bond angles ($^\circ$): **10**: Ir(1)-C(1): 2.047(5), Ir(1)-O(1): 2.041(4), Ir(1)-O(1)-Si(1): 137.7(2); **11**: Ir(1)-C(1): 2.056(11), Ir(1)-O(1): 2.034(7), Ir(1)-O(1)-Si(1): 155.2(5).

In order to identify a different kind of reaction with silicon substrates we examined the reaction between **4f** and trimethylsilylcyanide (TMSCN) in the hope of preparing an Ir(I)-CN complex. Ir-CN adducts have been prepared previously by oxidative addition of HCN to give hydrido-cyano complexes,²³² while Eisenberg has prepared Ir(I)-CN complexes using $(\text{N}(\text{PPh}_3)_2\text{CN})$, and demonstrated their usefulness in the oxidative addition of H_2 and the reduction of CO_2 with alkyl silanes.²³³ Cyclometalated Ir-CN complexes, prepared *via* chloride substitution on the metal using NaCN or KCN, have featured extensively in light-emitting electrochemical cells and oxygen sensor applications.²³⁴ Gratifyingly, **4f** reacted instantaneously with TMSCN at $-40\text{ }^\circ\text{C}$ to give **12** in 90% yield (Scheme 4.6 and Figure 4.6).^{62a, 62d}

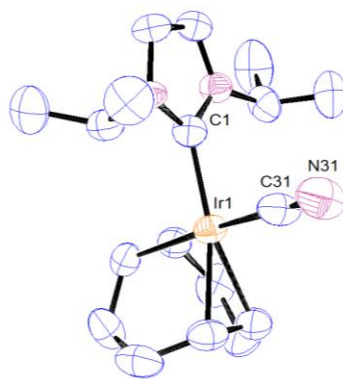
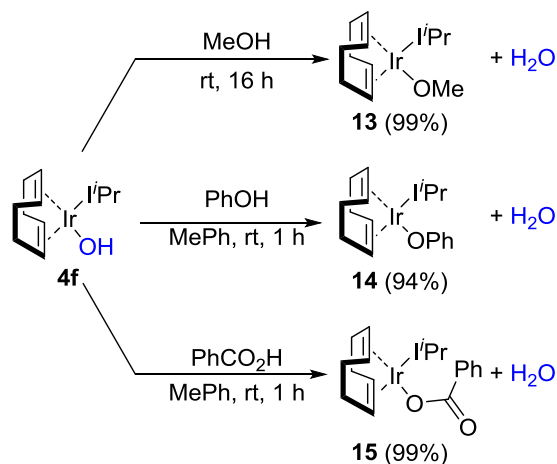


Figure 4.6. Thermal ellipsoid representation of [Ir(cod)(iPr)(CN)] **12** showing 50% thermal ellipsoid probability. H atoms have been omitted for clarity. Selected bond lengths (Å) and bond angles (°): Ir1-C1 2.044(7), Ir1 C31 2.012(9), N31 C31 1.141(12)

Next, we turned our attention to C-H, N-H and O-H bond activation. The attraction of an Ir(I)-hydroxide synthon is that reactivity should be confined to the hydroxyl moiety, which can act as an internal base that is capable of removing suitably acidic protons, to afford new iridium complexes without increasing the oxidation state of the metal. Furthermore, these bond activations should release only water as a by-product, enabling atom efficient transformations with simple purifications. Indeed, **4f** deprotonated MeOH at room temperature to give the Ir(I)-methoxide **13** in almost quantitative yield (Scheme 4.7). Similarly, **4f** reacted with phenol to give the Ir(I)-phenoxide **14** but was unable to react with *tert*-butanol. There are two possible reasons for this inactivity. Firstly, an Ir(I)-O^tBu might be highly sterically strained owing to the steric bulk of the butyl group. Secondly, the p*K*_a of ^tBuOH is higher than that of H₂O (32.0 vs 31.4 in DMSO from Bordwell's p*K*_a tables),²³⁵ hence, the proton may not be acidic enough to be activated by the Ir-OH. Similarly, reaction with benzoic acid furnished Ir-benzoate complex **15**. Single crystal X-ray analysis of **15** confirmed the square planar geometry, with the phenyl ring of the benzoate perpendicular to the NHC plane (Figure 4.7).

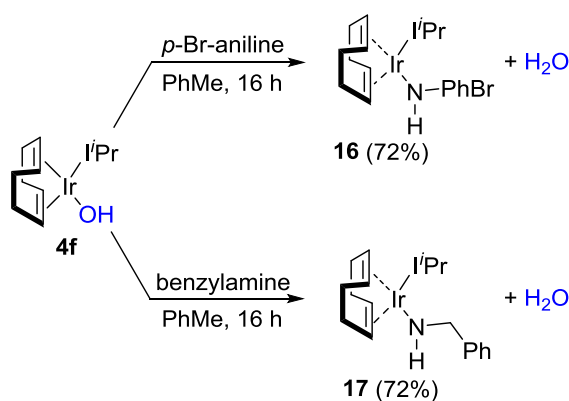
Several Ir-OR complexes have been reported in the literature, particularly *via* metathesis reactions.^{19, 236} Bergman prepared an Ir(III)-ethoxide complex by treating [IrCp^{*}(PPh₃)Cl₂] with NaOEt in EtOH to give [IrCp^{*}H(OEt)(PPh₃)] and CO₂ could be inserted into the Ir-OEt to generate an Ir(III)-carbonate complex.^{14a, 237} Both Ir-alkoxides and Ir-carboxylates have been prepared *via* oxidative addition of alcohols or carboxylic acids, respectively.²³⁸ However, Ir(I)-NHC-carboxylate complexes are to the best of our knowledge, limited to a single example, made by salt metathesis with

AgO_2CCF_3 .²²⁰ The simple deprotonation method shown here provides a straightforward route to Ir(I)-alkoxides and Ir(I)-carboxylates.



Scheme 4.7. Deprotonation of methanol, phenol and benzoic acid by Ir(I)-hydroxide **4f**

The activation of amines was achieved by reacting **4f** with *p*-bromoaniline, affording the Ir(I)-anilide **16**, and with benzylamine to give the Ir(I)-benzamide **17** (Scheme 4.8). Amido complexes of iridium have been prepared in the literature by salt metathesis^{51b} or oxidative addition of amines.²³⁹ The scope of reactivity that these amido complexes are capable of is vast and exciting.^{19, 240} The field has been accelerated by the ability to prepare terminal amido-complexes *via* the activation of anilines and ammonia, and several researchers have made tremendous strides in this regard.²⁴¹



Scheme 4.8. N-H bond activation by **4f** with bromoaniline and benzylamine

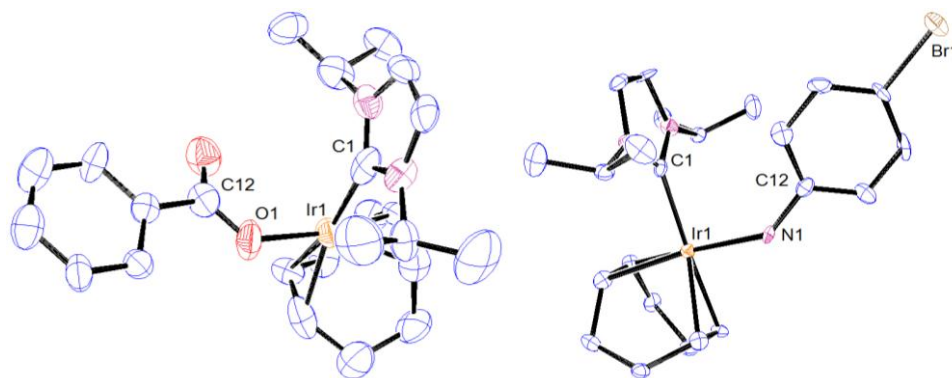
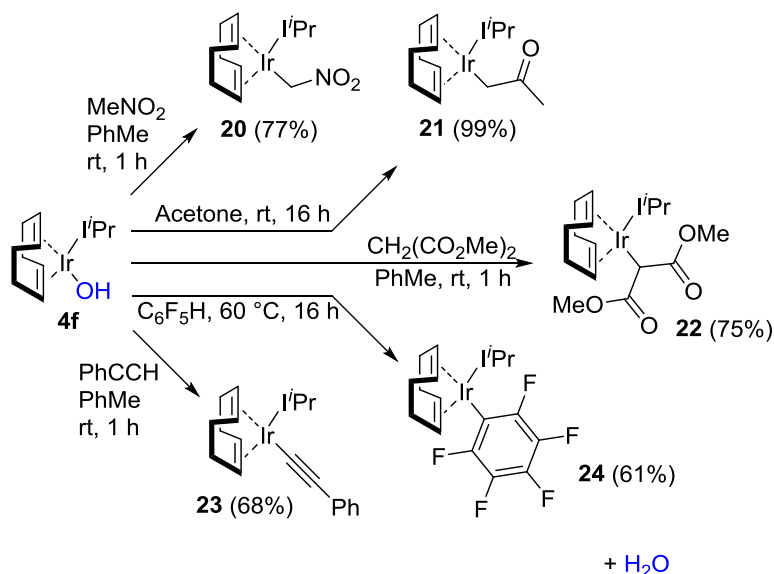


Figure 4.7. Thermal ellipsoid representation of [Ir(cod)(IⁱPr)(OC(O)Ph)] (**15**) and [Ir(cod)(IⁱPr)(NH(C₆H₄Br))] (**16**) showing 50% thermal ellipsoid probability. H atoms have been omitted for clarity. Selected bond lengths (Å) and bond angles (°): **15**: Ir(1)-C(1): 2.08(2), Ir(1)-O(1): 2.068(15), C(1)-Ir(1)-O(1): 90.6(7), Ir(1)-O(1)-C(12): 124.4(14); **16**: Ir(1)-C(1): 2.053(8), Ir(1)-N(1): 2.057(7), N(1)-C(12): 1.395(9), C(1)-Ir(1)-N(1): 94.3(3), Ir(1)-N(1)-C(12): 140.3(5).

Some of the most important bond activations in synthetic chemistry are those involving C-H bonds. The discovery of catalysts capable of selective activation and functionalisation of C-H bonds under mild conditions with low generation of waste is an area of high importance.²⁴² In addition to the reports of metal hydroxides by Alper⁴⁷ and Bergman and their co-workers,^{45, 51a, 53} which were discussed in Chapter 1, Burger and Bergman reported the preparation of [Ir(Cp^{*})Me(OTf)(PMe₃)] (**18**), which is capable of deprotonating a range of organic substrates, generating methane as a by-product and furnishing the corresponding Ir-alkyl products.²⁴³ Somewhat similarly, Murata *et al.* have deprotonated phenylacetylene, acetone and nitromethane using [Ir(Cp^{*})((*S,S*)-TsCYDN)] (**19**) ((*S,S*)-TsCYDN = (*1S,2S*)-*N*-(*p*-toluenesulfonyl)-1,2-cyclohexanediamine), whereby the activated proton is transferred to the amide ligand, yielding an amine, while the remainder of the fragment coordinates to the metal centre.²⁴⁴ Oro *et al.* reported the deprotonation of terminal alkynes with Ir(I)-OMe complexes, generating methanol as the by-product and yielding Ir(I)-acetylides,²⁴⁵ which have been implicated as intermediates in the coupling of terminal alkynes with trialkylsilyl halides²⁴⁶ and the dimerisation of alkynes;²⁴⁷ Ir(I)-acetylides are also useful intermediates *en route* to phosphorescent allenylidene complexes.²⁴⁸

We tested the activity of **4f** in the deprotonation of a number of alkyl complexes bearing *sp*, *sp*² and *sp*³ hybridised centres. Gratifyingly, activation of nitromethane by **4f** was incredibly swift. Yellow Ir(I)-hydroxide **4f** turned an intense red colour immediately upon contact with the substrate. ¹H NMR analysis of the product indicated full conversion to nitromethylene complex **20** (Scheme 4.9), and single crystal X-ray

analysis (Figure 4.8) showed the sp^3 -methylene ($\text{Ir}(1)\text{-C}(12)\text{-N}(13) = 114.5^\circ$) to be slightly twisted from the Ir-NHC bond axis.



Scheme 4.9. C-H bond activations using **4f**.

In addition, **4f** was able to deprotonate acetone and dimethyl malonate to give the alkyl complexes **21** and **22** respectively (Scheme 4.9). Multinuclear NMR and single crystal X-ray analyses for **21** (Figure 4.8) and **22** (Figure 4.9) explicitly confirmed the formal C-H activation in each case to give Ir(I)-alkyl bonds and not co-ordination *via* an oxygen atom. Activation of a C-H bond on an sp -hybridised carbon centre was accomplished *via* reaction of **4f** with phenylacetylene to give a terminal acetylide complex **23** (Scheme 4.9). Single crystal X-ray analysis confirmed the linear triple bond of the acetylide fragment ($\text{C}(12)\text{-C}(13) 1.216(12)$, Figure 4.9).

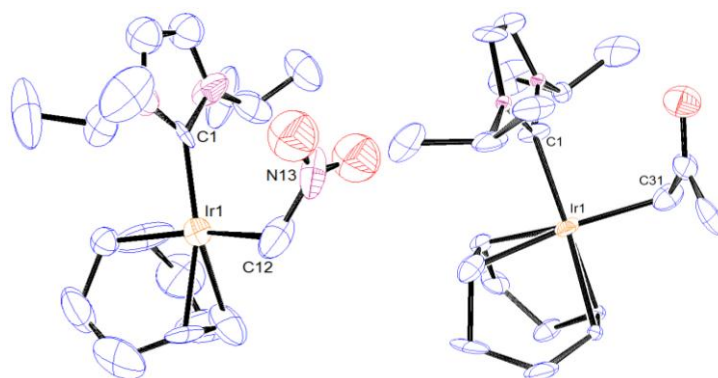


Figure 4.8 Thermal ellipsoid representations of $[\text{Ir}(\text{cod})(i\text{Pr})(\text{CH}_2\text{NO}_2)]$ (**20**), $[\text{Ir}(\text{cod})(i\text{Pr})(\text{CH}_2\text{COCH}_3)]$ (**21**) showing 50% thermal ellipsoid probability. H atoms have been omitted for clarity. Selected bond lengths (\AA) and bond angles ($^\circ$): **20**: $\text{Ir}(1)\text{-C}(1)$: 2.056(10), $\text{Ir}(1)\text{-C}(12)$: 2.116(12), $\text{C}(1)\text{-Ir}(1)\text{-C}(12)$: 95.2(5), $\text{Ir}(1)\text{-C}(12)\text{-N}(13)$: 114.5(10); **21**: $\text{Ir}(1)\text{-C}(1)$: 2.048(14), $\text{Ir}(1)\text{-C}(31)$: 2.134(18)

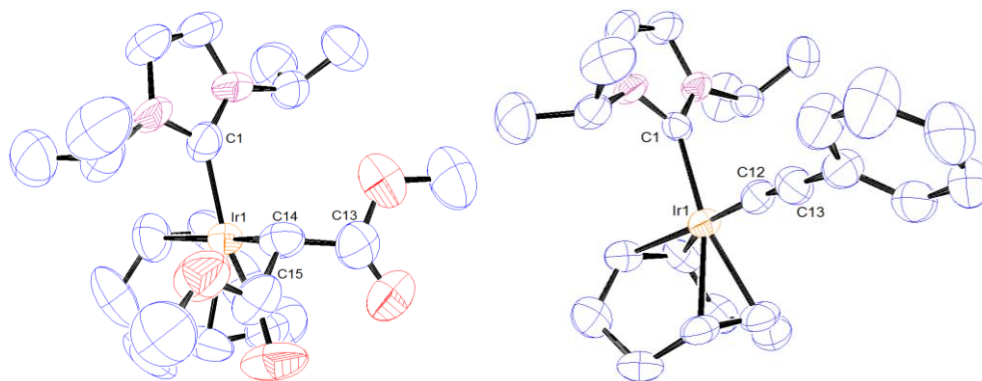


Figure 4.9. Thermal ellipsoid representations of [Ir(cod)(I'Pr)(CH(COOMe)₂)] (**22**) and [Ir(cod)(I'Pr)(CCPh)] (**23**) showing 50% thermal ellipsoid probability. H atoms have been omitted for clarity. Selected bond lengths (Å) and bond angles (°): **22**: Ir(1)-C(1): 2.025(9), Ir(1)-C(14): 2.169(9), C(1)-Ir(1)-C(14): 87.7(4), Ir(1)-C(14)-C(13): 109.3(6); **23**: Ir(1)-C(1): 2.043(7), Ir(1)-C(12): 2.007(8), C(12)-C(13): 1.216(12).

C-H activations of sp^2 carbon centres were also investigated *via* reactions with fluorinated arenes. If the Ir(I)-hydroxide is viewed as a Brønsted base^{62a, 62d} then C-H activation of fluorinated arenes provides an indication of the acidity of protons that can be activated by **4f**. Indeed we were able to activate pentafluorobenzene at 60 °C (**24**, Scheme 4.9) but unable to activate 1,3,5-trifluorobenzene. Guo and co-workers have calculated pK_a (± 1.1 units) for a range of aromatic compounds, including fluoroarenes.²⁴⁹ Eisenstein and Perutz have calculated C-H and M-C bond strengths for a range of fluoroarenes, and explored the effects of the metal centre and ligand sphere on the strength of the M-C bond.²⁵⁰ The *ortho*-fluorines were found to have the largest effect on the C-H bond strengths, followed by the *para*-fluorines, while the C-H bond was effectively insensitive to the *meta*-fluorines. Therefore, although pK_a may not be the only factor, it does provide a good indication of the substrates that the metal hydroxide will react with. Figure 4.10 shows the substrates that **4f** was able to deprotonate, arranged according to pK_a as taken from Bordwell's pK_a tables.^{235a, 235c, 235d} Inability to react with 1,3,5-trifluorobenzene or *tert*-butanol indicates that the Ir(I)-hydroxide can activate C-H bonds with a pK_a approaching that of H₂O (31.4 in DMSO)^{235a, 235c, 235d} but not higher.

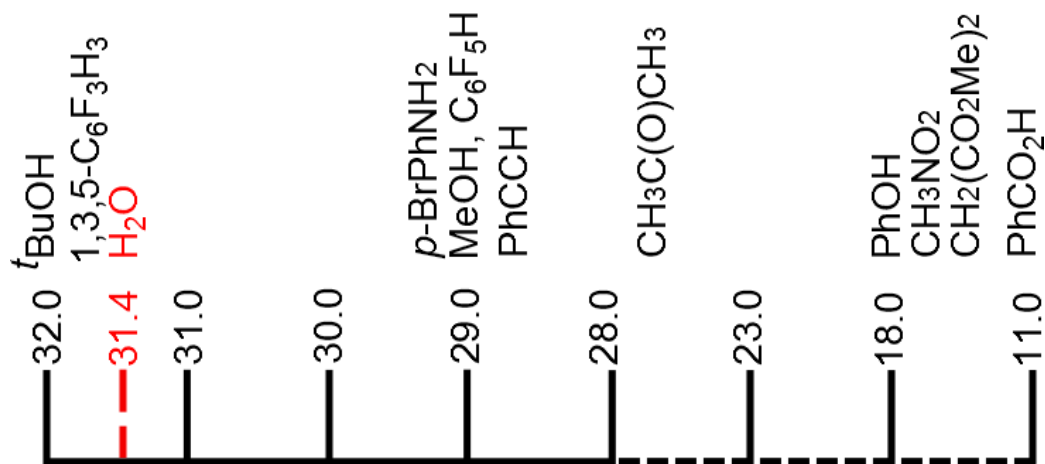


Figure 4.10 Organic substrates that Ir(I)-hydroxide **4f** is able to deprotonate, arranged according to pK_a and compared to H₂O. Values are taken from Bordwell's pK_a tables and calculated from DMSO solutions.^{235a, 235c, 235d}

4.3. CONCLUSIONS

We were able to extend the methodology for preparation of metal hydroxides to include convenient and straightforward methods for the preparation of [Ir(cod)(NHC)(OH)] complexes. We have reported, with full characterisation, six analogous Ir(I)-hydroxide complexes, five of which are novel. We have investigated the structural and steric characteristics of each complex with the use of single crystal X-ray analysis and computational methods. In particular, % V_{bur} and DFT studies helped us to explain the steric differences between alkyl-substituted NHC ligands and the effect that they have on the Ir-centre. These data, together with the experimental results, have indicated the ability of backbone substitution to alter the steric bulk of 1,3-bis(alkyl) NHC ligands by hindering rotation of the *N*-substituents.

We have probed the reactivity of Ir(I)-hydroxides, using [Ir(cod)(*i*Pr)(OH)] (**4f**) as a model substrate. Herein, we have reported transmetalation with boronic acids, which proved to be less facile than with the Rh(I)-hydroxide examined in Chapter 2. Reactivity of the Ir(I)-hydroxide towards various silicon substrates was examined and we have reported a novel route to Ir(I)-siloxide complexes under very mild conditions. We have also investigated bond activation by deprotonation of various O-H, N-H, and C-H moieties under mild conditions with water as the sole by-product. Hence, deprotonation of alcohols allowed isolation of Ir(I)-alkoxides from methanol and phenol, while deprotonation of benzoic acid led to an Ir(I)-carboxylate. The method also

provided access to Ir(I)-amides by deprotonation of anilines and amines. Several Ir(I)-alkyl complexes bearing various sp -, sp^2 - and sp^3 -hybridised centres were prepared by deprotonation of substrates such as acetone and nitromethane. These deprotonation procedures were typically very straightforward, without the need for solvent and occurring instantaneously, accompanied by very dramatic colour changes.

This Ir(I)-hydroxide motif has provided rapid access to a wide range of important complexes that were previously only accessible *via* specialised routes. When considering these facile bond activation processes in the context of the extensive literature on metal catalysed C-H, O-H and N-H bond activation, it is important to make the distinction between deprotonation and oxidative addition. The processes described herein are explicitly deprotonation reactions, generating only the desired Ir-C, Ir-O or Ir-N bond and H₂O without oxidation of the metal centre.

4.4. EXPERIMENTAL DETAILS

4.4.1. General considerations

All manipulations and reactions were performed inside an Argon-filled MBraun Glovebox unless stated otherwise. All reagents were supplied by Aldrich and used without further purification. Solvents were distilled and dried as required. NMR data was obtained using either a Bruker 400 MHz or 300 MHz spectrometer at 303 K in the specified deuterated solvent. All chemical shifts are given in ppm and coupling constants in Hz. Signals on the $^{13}\text{C}\{^1\text{H}\}$ NMR spectra are singlets unless otherwise stated. Spectra were referenced to residual protonated solvent signals (for ^1H) or solvent signals (for ^{13}C): (C_6D_6 : ^1H δ 7.16 ppm, ^{13}C δ 128.06 ppm; CD_2Cl_2 : ^1H δ 5.32 ppm, ^{13}C δ 53.82 ppm; THF- d_8 : ^1H δ 1.72, 3.58 ppm, ^{13}C 67.57, 25.35 ppm). Infrared spectra (ν) were recorded on a Shimadzu Fourier transform IR Affinity-1 Infrared spectrophotometer using a MIRacleTM single reflection horizontal ATR (diamond). Samples were placed directly on the crystal (ATR) in the solid state. Only characteristic peaks have been quoted. Elemental analyses were performed at the London Metropolitan University. CCDC-915472 (**4c**), CCDC-915473 (**4d**), CCDC-915474 (**4e**), CCDC-915475 (**4f**), CCDC-915476 (**9b**), CCDC-915477 (**10**), CCDC-915478 (**11**), CCDC-915479 (**12**), CCDC-915480 (**15**), CCDC-915481 (**16**), CCDC-915482 (**20**), CCDC-915483 (**21**), CCDC-915484 (**22**), CCDC-915485 (**23**), Crystallographic data can be obtained free of charge from The Cambridge Crystallographic Data Centre via www.ccdc.cam.ac.uk/data_request/cif.

4.4.2. Synthesis and characterisation data

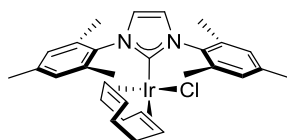
Preparation of known compounds: [Ir(cod)(NHC)Cl] 5a-f via free NHC

A round bottom flask was charged with $[\text{Ir}(\text{cod})\text{Cl}]_2$ (**6**), free NHC **2** and THF. The resultant mixture was stirred at rt overnight. When complete, the reaction mixture was reduced *in vacuo* to a solid and washed with *n*-pentane to give $[\text{Ir}(\text{cod})(\text{NHC})\text{Cl}]$ (**5a-d**). ^1H NMR data matched reported characterisation data.^{94a, 147d, 176} In the case of **5e** and **5f**, instead of washing with pentane, the crude product mixture was removed from the glove box and purified by column chromatography (silica gel chromatography, elution with EtOAc/pentane (4:1) to elute $[\text{Ir}(\text{cod})(\text{NHC})\text{Cl}]$ (**5e** or **5f**), followed by

elution with CH_2Cl_2 to recover $[\text{Ir}(\text{cod})(\text{NHC})_2]^+\text{Cl}^-$ (**7e** or **7f**). ^1H NMR data matched reported characterisation data for **5e**, **5f** and **7e**.^{101b, 251}

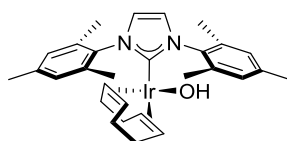
Preparation of $[\text{Ir}(\text{cod})(\text{NHC})\text{Cl}]$ **5e** and **5f** using Ag_2O

Following modified versions of literature procedures,^{101b, 102-103, 220} the $\text{NHC}\cdot\text{HCl}$ salts $\text{ICy}\cdot\text{HCl}$ and $\text{I}^i\text{Pr}\cdot\text{HCl}$ were stirred with Ag_2O (5 equiv.) in CH_2Cl_2 (5 mL) in the dark for 2 h at rt in air. Upon completion, the reaction mixture was filtered through celite and the filtrate was concentrated *in vacuo*. The resultant brown solid was washed with *n*-pentane (3 x 5 mL) to give the $[\text{AgCl}(\text{NHC})]_2$ compound as a white solid. The Ag-complex was stirred with $[\text{Ir}(\text{cod})\text{Cl}]_2$ (**6**) (0.5 equiv.) at rt in CH_2Cl_2 (5 mL) for 3 h, after which time the mixture was filtered through celite and concentrated *in vacuo* to a solid. The crude product was purified by column chromatography (silica gel chromatography, elution with EtOAc/n -pentane (4:1)) to give $[\text{Ir}(\text{cod})(\text{ICy})\text{Cl}]$ (**5e**) as a yellow solid (60%); and $[\text{Ir}(\text{cod})(\text{I}^i\text{Pr})\text{Cl}]$ (**5f**) as a yellow solid (74%). ^1H NMR data matched reported characterisation data.^{101b}



$[\text{Ir}(\text{cod})(\text{IMes})\text{Cl}]$ **5a**

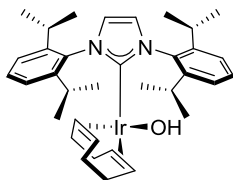
The procedure given above for the preparation of $[\text{Ir}(\text{cod})(\text{NHC})\text{Cl}]$ complexes was followed to give $[\text{Ir}(\text{cod})(\text{IMes})\text{Cl}]$ (**5a**) as a yellow solid. ^1H NMR (400 MHz, C_6D_6): δ 6.80 (s, 2H, ArH), 6.79 (s, 2H, ArH), 6.11 (s, 2H, N-(CH)₂-N), 4.73 – 4.66 (m, 2H, cod-CH), 3.21 – 3.13 (m, 2H, cod-CH), 2.58 (s, 6H, Ar-CH₃), 2.11 (s, 6H, Ar-CH₃), 2.04 (s, 6H, Ar-CH₃), 1.90 – 1.70 (m, 4H, cod-CH₂), 1.42 – 1.28 (m, 4H, cod-CH₂); $^{13}\text{C}\{^1\text{H}\}$ NMR (100 MHz, C_6D_6): δ 182.0 (Ir-C_{carbene}), 138.6 (ArC), 137.9 (ArC), 136.7 (ArC), 134.4 (ArCH), 130.1 (ArCH), 122.1 (N-(CH)₂-N), 83.4 (cod-CH), 50.8 (cod-CH), 34.1 (cod-CH₂), 29.4 (cod-CH₂), 21.1 (Ar-CH₃), 20.2 (Ar-CH₃), 18.3 (Ar-CH₃).⁴



$[\text{Ir}(\text{cod})(\text{IMes})(\text{OH})]$ **4a**

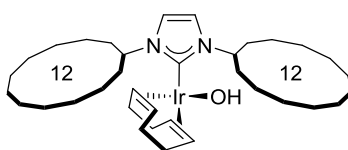
A 25 mL Schlenk flask was charged with $[\text{Ir}(\text{cod})\text{Cl}]_2$ (**6**) (50.0 mg, 0.07 mmol), **IMes 2a** (45.3 mg, 0.15 mmol) and CsOH (45.0 mg, 0.30 mmol.) in THF (5 mL). The

resultant mixture was removed from the glove box and stirred for *ca.* 30 min before degassed H₂O (0.5 mL) was added under Ar on a Schlenk line. The reaction mixture was stirred at 40 °C for 24 h under Ar (progress was monitored by ¹H NMR spectroscopy). Upon completion, the reaction mixture was reduced *in vacuo* to a green solid and returned to the glove box. The crude product was resuspended in THF and the solids were filtered off. The filtrate was reduced *in vacuo* and *n*-pentane was added (3 mL) to form an azeotrope to remove residual solvent. The resultant solid was washed with cold *n*-pentane (3 x 3 mL) and dried *in vacuo* to give [Ir(cod)(IMes)(OH)] (**4a**) (79.6 mg, 86%) as a green solid. ¹H NMR (300 MHz, C₆D₆): δ 6.83 (s, 4H, ArH), 6.16 (s, 2H, N-(CH)₂-N), 3.83 – 3.71 (m, 2H, cod-CH), 2.92 – 2.81 (m, 2H, cod-CH), 2.55 – 2.21 (m, 12H, Ar-CH₃), 2.13 (s, 6H, Ar-CH₃), 2.06 – 1.87 (m, 2H, cod-CH₂), 1.86 – 1.68 (m, 2H, cod-CH₂), 1.68 – 1.53 (m, 2H, cod-CH₂), 1.66 (s, 1H, OH), 1.47 – 1.26 (m, 2H, cod-CH₂); ¹³C{¹H} NMR (75 MHz, C₆D₆): δ 185.8 (Ir-C_{carbene}), 138.3 (ArC), 137.1 (ArC), 129.0 (ArCH)*, 122.3 (N-(CH)₂-N), 78.6 (cod-CH), 45.7 (cod-CH), 34.8 (cod-CH₂), 29.7 (cod-CH₂), 21.1 (Ar-CH₃), 18.8 (Ar-CH₃); ¹H NMR (300 MHz, CD₂Cl₂): δ 7.01 (br, 4H, ArH), 6.97 (s, 2H, N-(CH)₂-N), 3.64 – 3.54 (m, 2H, cod-CH), 2.59 – 2.47 (m, 2H, cod-CH), 2.37 (s, 6H, Ar-CH₃), 2.24 (s, 12H, Ar-CH₃), 1.74 – 1.55 (m, 4H, cod-CH₂), 1.44 (s, 1H, OH), 1.40 – 1.15 (m, 4H, cod-CH₂); ¹³C{¹H} NMR (75 MHz, CD₂Cl₂): δ 184.0 (Ir-C_{carbene}), 138.8 (ArC), 136.8 (ArC), 136.1 (ArC), 129.0 (ArCH), 123.3 (N-(CH)₂-N), 79.6 (cod-CH), 46.5 (cod-CH), 34.3 (cod-CH₂), 29.2 (cod-CH₂), 21.2 (Ar-CH₃), 18.6 (Ar-CH₃); **Anal. Calcd.** for C₂₉H₃₇IrN₂O (MW 621.83): C, 56.01; H, 6.00; N, 4.50. Found: C, 55.83; H, 6.09; N, 4.39. * One ArC signal was undetected in the ¹³C{¹H} NMR spectrum in C₆D₆. These data differ from those reported by Marciniec and co-workers, whose data are consistent with [Ir(cod)(IMes)Cl] (**5a**).¹⁷⁷

[Ir(cod)(IPr)(OH)] **4b**

A 25 mL Schlenk flask was charged with [Ir(cod)Cl]₂ (**6**) (50.0 mg, 0.07 mmol), IPr (58.0 mg, 0.15 mmol) and CsOH (45.0 mg, 0.30 mmol) in THF (5 mL). The resultant mixture was removed from the glove box and stirred for *ca.* 30 mins before degassed H₂O (0.5 mL) was added under Ar on a Schlenk line. The reaction mixture was stirred at 40 °C for 24 h under Ar (progress was monitored by ¹H NMR

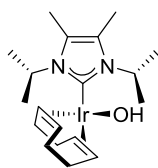
spectroscopy). Upon completion, the reaction mixture was reduced *in vacuo* to a yellow-brown solid and returned to the glove box. The crude product was resuspended in THF and the solids were filtered off. The filtrate was reduced *in vacuo* and *n*-pentane was added (3 mL) to form an azeotrope to remove residual solvent. The resultant solid was washed with cold *n*-pentane (3 x 3 mL) and dried *in vacuo* to give [Ir(cod)(IPr)(OH)] (**4b**) (58.9 mg, 56%) as a yellow-brown solid. $^1\text{H NMR}$ (300 MHz, C_6D_6): δ 7.29 – 7.19 (m, 2H, ArH), 7.15 – 7.04 (m, 4H, ArH), 6.51 (s, 2H, N-(CH) $_2$ -N), 3.85 – 3.76 (m, 2H, cod-CH), 3.49 – 3.15 (m, 4H, CH(CH $_3$) $_2$), 2.79 – 2.59 (m, 2H, cod-CH), 1.94 – 1.70 (m, 4H, cod-CH $_2$), 1.60 (s, 1H, OH), 1.45 (d, 12H, $^3J_{\text{HH}} = 6.7$, CH $_3$), 1.40 – 1.20 (m, 4H, cod-CH $_2$), 1.03 (d, 12H, $^3J_{\text{HH}} = 6.9$, CH $_3$); $^{13}\text{C}\{^1\text{H}\}$ NMR (75 MHz, C_6D_6): δ 186.6 (Ir-C $_{\text{carbene}}$), 146.9 (ArC), 137.0 (ArC), 129.9 (ArCH)*, 123.7 (N-(CH) $_2$ -N), 79.4 (cod-CH), 45.7 (cod-CH), 34.8 (cod-CH $_2$), 29.5 (cod-CH $_2$), 29.1 (CH(CH $_3$) $_2$), 26.4 (CH $_3$), 23.1 (CH $_3$); $^1\text{H NMR}$ (300 MHz, CD_2Cl_2): δ 7.50 (t, 2H, $^3J_{\text{HH}} = 7.7$, ArH), 7.33 (d, 4H, $^3J_{\text{HH}} = 7.7$, ArH), 7.01 (s, 2H, N-(CH) $_2$ -N), 3.85 – 3.70 (m, 2H, cod-CH), 3.01 (sept., 4H, $^3J_{\text{HH}} = 6.8$, (CH(CH $_3$) $_2$), 2.49 – 2.37 (m, 2H, cod-CH), 1.82 – 1.50 (m, 4H, cod-CH $_2$), 1.60 (s, 1H, OH), 1.38 (d, 12H, $^3J_{\text{HH}} = 6.8$, CH $_3$), 1.34 – 1.21 (m, 4H, cod-CH $_2$), 1.11 (d, 12H, $^3J_{\text{HH}} = 6.8$, CH $_3$); $^{13}\text{C}\{^1\text{H}\}$ NMR (75 MHz, CD_2Cl_2): δ 184.2 (Ir-C $_{\text{carbene}}$), 146.5 (ArC), 136.9 (ArC), 129.9 (ArCH), 124.6 (ArCH), 124.0 (N-(CH) $_2$ -N), 81.6 (cod-CH), 46.5 (cod-CH), 34.3 (cod-CH $_2$), 29.3 (CH(CH $_3$) $_2$), 28.9 (cod-CH $_2$), 26.2 (CH $_3$), 22.9 (CH $_3$); **FTIR (ATR)**: $\nu = 3649.32$ (w, OH), 1317.38 (s), 800.46 (s) cm^{-1} . **Anal. Calcd.** for $\text{C}_{35}\text{H}_{49}\text{IrN}_2\text{O}$ (MW 705.99): C, 59.54; H, 7.00; N, 3.97. Found: C, 59.47; H, 7.10; N, 3.88. * One ArC signal was undetected in the $^{13}\text{C}\{^1\text{H}\}$ NMR spectrum in C_6D_6 .



[Ir(cod)(IDD)(OH)] **4c**

A 25 mL Schlenk flask was charged with [Ir(cod)Cl] $_2$ (**6**) (50.0 mg, 0.07 mmol), IDD (60.0 mg, 0.15 mmol) and CsOH (45.0 mg, 0.30 mmol) in THF (5 mL). The resultant mixture was removed from the glove box and stirred for *ca.* 30 mins before degassed H $_2$ O (0.5 mL) was added under Ar on a Schlenk line. The reaction mixture was stirred at 40 °C for 24 h under Ar (progress was monitored by $^1\text{H NMR}$ spectroscopy). Upon completion, the reaction mixture was reduced *in vacuo* to a yellow

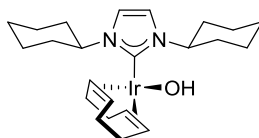
solid and returned to the glove box. The crude product was resuspended in THF and the solids were filtered off. The filtrate was reduced *in vacuo* and *n*-pentane was added (3 mL) to form an azeotrope to remove residual solvent. The resultant solid was washed with cold *n*-pentane (3 x 3 mL) and dried *in vacuo* to give [Ir(cod)(IDD)(OH)] (**4c**) (82.3 mg, 77%) as a yellow solid. The *n*-pentane washings were passed through a micro filter to remove solids and added to hexane (0.5 mL). Single crystals were grown by slow evaporation of the solution for X-ray crystal analysis which indicated the incorporation of an independent H₂O molecule in the lattice. However, CHN and NMR analysis showed that H₂O is not present in the bulk material after purification. ¹H NMR (300 MHz, C₆D₆): δ 6.41 (s, 2H, N-(CH)₂-N), 5.81 – 5.59 (m, 2H, (N-CH(CH₂)₂)), 4.59 – 4.48 (m, 2H, cod-CH), 2.88 – 2.75 (m, 2H, cod-CH), 2.67 – 2.36 (m, 4H, cod-CH), 2.19 (s, 1H, OH), 2.64 – 2.09 (m, 18H, cod-CH₂ + IDD-CH₂), 1.63 – 1.15 (m, 30H, IDD-CH₂); ¹³C{¹H} NMR (75 MHz, C₆D₆): δ 183.3 (Ir-C_{carbene}); 116.9 (N-(CH)₂-N), 81.1 (cod-CH), 56.8 (cod-CH), 44.8 (cod-CH₂), 35.2 (cod-CH₂), 32.4, 31.6, 30.2, 25.1, 24.9, 24.2, 24.1, 23.9, 23.8, 23.6, 23.2, 22.4 (IDD). **Anal. Calcd.** for C₃₅H₆₁IrN₂O (MW 718.09): C, 58.54; H, 8.56; N, 3.90. Found: C, 58.39; H, 8.41; N, 3.86.



[Ir(cod)(^{*i*}Pr^{Me})(OH)] **4d**

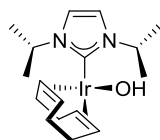
A 25 mL Schlenk flask was charged with [Ir(cod)Cl]₂ (**6**) (50.0 mg, 0.07 mmol), ^{*i*}Pr^{Me} (54.0 mg, 0.15 mmol) and CsOH (45.0 mg, 0.30 mmol.) in THF (5 mL). The resultant mixture was removed from the glove box and stirred for *ca.* 30 mins before degassed H₂O (0.5 mL) was added under Ar on a Schlenk line. The reaction mixture was stirred at 40 °C for 24 h under Ar (progress was monitored by ¹H NMR spectroscopy). Upon completion, the reaction mixture was reduced *in vacuo* to a yellow solid and returned to the glove box. The crude product was resuspended in THF and the solids were filtered off. The filtrate was reduced *in vacuo* and *n*-pentane was added (3 mL) to form an azeotrope to remove residual solvent. The resultant solid was washed with cold *n*-pentane (3 x 3 mL) and dried *in vacuo* to give [Ir(cod)(^{*i*}Pr^{Me})(OH)] (**4d**) (63.0 mg, 85%) as a yellow solid. The *n*-pentane washings were passed through a micro filter to remove solids and added to hexane (0.5 mL) Single crystals were grown by slow evaporation of the solution for X-ray crystal analysis which indicated the

incorporation of an independent H₂O molecule in the lattice. However, CHN and NMR analysis showed that H₂O is not present in the bulk material after purification. ¹H NMR (300 MHz, C₆D₆): δ 6.37 (sept., 2H ³J_{HH} = 5.3, N-CH), 4.79 – 4.63 (m, 2H, cod-CH), 3.00 – 2.83 (m, 2H, cod-CH), 2.62 – 2.31 (m, 4H, cod-CH₂), 2.40 (s, 1H, OH), 2.07 – 1.89 (m, 2H, cod-CH₂), 1.89 – 1.72 (m, 2H, cod-CH₂), 1.61 (s, 6H, CH₃), 1.28 (d, 6H, ³J_{HH} = 7.3, CH(CH₃)₂), 1.25 (d, 6H, ³J_{HH} = 7.1, CH(CH₃)₂); ¹³C{¹H} NMR (75 MHz, C₆D₆): δ 182.2 (Ir-C_{carbene}), 124.2 (NC), 80.9 (cod-CH), 53.5 (N-CH), 44.8 (cod-CH), 35.2 (cod-CH₂), 30.2 (cod-CH₂), 22.3 (CH₃), 22.2 (CH₃), 10.0(CH₃); Anal. Calcd. for C₁₉H₃₃IrN₂O (MW 497.70): C, 45.85, H, 6.68, N, 5.63. Found: C, 45.79; H, 6.57; N, 5.58.

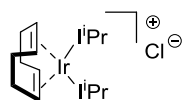


[Ir(cod)(ICy)(OH)] **4e**

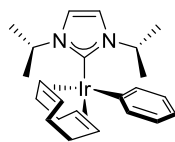
A round bottom flask was charged with [Ir(cod)(ICy)Cl] (**5e**) (100 mg, 0.18 mmol) and CsOH (53.0 mg, 0.35 mmol) in THF (5 mL). The resultant mixture was stirred at rt for 16 h. The reaction progress was monitored periodically by ¹H NMR spectroscopy. Upon completion, the reaction mixture was filtered through celite and the filtrate was reduced *in vacuo*. The resultant solid was washed with cold *n*-pentane (3 x 3 mL) and dried *in vacuo* to give [Ir(cod)(ICy)(OH)] (**4e**) (62.9 mg, 65%) as a yellow solid. ¹H NMR (300 MHz, C₆D₆): δ 6.34 (s, 2H, N(CH₂)₂N), 5.55 (tt, 2H, ³J_{HH} = 11.9, 3.7, N-CH(CH₂)₂), 4.75 – 4.64 (m, 2H, cod-CH), 2.91 – 2.75 (m, 2H, cod-CH), 2.62 – 2.33 (m, 4H, cod-CH₂), 2.44 (s, 1H, OH), 2.32 – 2.19 (m, 2H), 2.05 – 1.76 (m, 6H, cod-CH₂ and ICy-CH₂), 1.73 – 1.17 (m, 10H, ICy-CH₂), 1.17 – 1.04 (m, 2H, ICy-CH₂), 1.03 – 0.80 (m, 4H, ICy-CH₂); ¹³C{¹H} NMR (75 MHz, C₆D₆): δ 182.5 (Ir-C_{carbene}), 116.5 (N(CH₂)₂N), 81.7 (cod-CH), 60.0 (cod-CH), 44.9 (CH(CH₂)₂), 35.3 (cod-CH₂), 34.8 (cod-CH₂), 34.4, 30.3, 26.3, 26.0, 25.7 (ICy-CH₂); **Anal. Calcd.** for C₂₃H₃₇IrN₂O (MW 549.77): C, 50.25; H, 6.78; N, 5.10. Found: C, 50.39; H, 6.82; N, 5.12.

[Ir(cod)(IPr)(OH)] **4f**

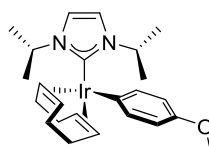
A round bottom flask was charged with [Ir(cod)(IPr)Cl] (**5f**) (250 mg, 0.51 mmol) and CsOH (154.0 mg, 1.02 mmol) in THF (10 mL). The resultant mixture was stirred at rt for 16 h. The reaction progress was monitored periodically by ^1H NMR spectroscopy. Upon completion, the reaction mixture was filtered through celite and the filtrate was reduced *in vacuo*. The resultant solid was washed with cold *n*-pentane (3 x 5 mL) and dried *in vacuo* to give [Ir(cod)(IPr)(OH)] (**4f**) (180.0 mg, 75%) as a yellow solid. ^1H NMR (300 MHz, C_6D_6): δ 6.24 (s, 2H, N(CH) $_2$), 5.87 (sept., 2H, $^3J_{\text{HH}} = 6.8$, CH(CH $_3$) $_2$), 4.77 – 4.62 (m, 2H, cod-CH), 2.89 – 2.76 (m, 2H, cod-CH), 2.59 – 2.29 (m, 4H, cod-CH $_2$), 2.47 (s, 1H, OH), 2.03 – 1.87 (m, 2H, cod-CH $_2$), 1.87 – 1.83 (m, 2H, cod-CH $_2$), 1.15 (d, 6H, $^3J_{\text{HH}} = 6.7$, CH $_3$), 1.10 (d, $^3J_{\text{HH}} = 6.9$, 6H, CH $_3$); $^{13}\text{C}\{^1\text{H}\}$ NMR (75 MHz, C_6D_6): δ 182.1 (Ir-C $_{\text{carbene}}$), 116.0 (N(CH) $_2$ N), 81.9 (cod-CH), 52.2 (CH(CH $_3$) $_2$), 44.8 (cod-CH), 35.1 (cod-CH $_2$), 30.2 (cod-CH $_2$), 24.2 (CH $_3$), 23.0 (CH $_3$). FTIR (ATR): $\nu = 3612.67$ (w, OH), 1217.08 (s), 877.61 (s) cm^{-1} . Anal. Calcd. for $\text{C}_{17}\text{H}_{29}\text{IrN}_2\text{O}$ (MW 469.64): C, 43.48; H, 6.22; N, 5.96. Found: C, 43.37; H, 6.36; N, 5.97.

[Ir(cod)(IPr) $_2$] $^+\text{Cl}^-$ **7f**

A suspension of NaH (10 mg, 0.4 mmol) in EtOH (2 mL) was added slowly to a suspension of [Ir(cod)Cl] $_2$ (**6**) (40 mg, 0.06 mmol) in EtOH (3 mL) and the resultant mixture was stirred at room temperature for 45 mins. IPr \cdot HCl (56 mg, 0.3 mmol) was added to the mixture and stirring was continued for 5 h. Upon completion, the reaction mixture was filtered through celite and concentrated *in vacuo*.^{101b} The resultant product was washed with *n*-pentane (3 x 6 mL) and dried to give [Ir(cod)(IPr) $_2$] $^+\text{Cl}^-$ (**7f**) (74.7 mg, 98%) as a red solid. ^1H NMR (300 MHz, CD_2Cl_2): δ 7.17 (s, 4H, N(CH) $_2$), 5.01 (sept., 4H $^3J_{\text{HH}} = 6.7$, CH(CH $_3$) $_2$), 3.91 (m, 4H, cod-CH), 2.32 – 2.10 (m, 4H, cod-CH), 1.92 – 1.80 (m, 4H, cod-CH $_2$), 1.52 (d, 12H, $^3J_{\text{HH}} = 6.7$, CH $_3$), 1.23 (d, 12H, $^3J_{\text{HH}} = 6.7$, CH $_3$); $^{13}\text{C}\{^1\text{H}\}$ NMR (75 MHz, C_6D_6): δ 174.3 (Ir-C $_{\text{carbene}}$), 119.0 (N(CH) $_2$), 75.1 (CH(CH $_3$) $_2$), 53.2 (cod), 32.0 (cod), 24.7 (CH $_3$), 23.6 (CH $_3$).

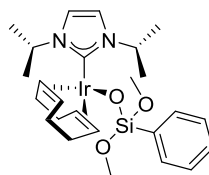
[Ir(cod)(IPr)(Ph)] **9a**

A 25 mL Schlenk flask was charged with [Ir(cod)(IPr)(OH)] (**4f**) (20 mg, 0.043 mmol) and phenylboronic acid (5.2 mg, 0.043 mmol) in PhMe (5 mL). The reaction mixture was removed from the glove box and stirred at 50 °C for 16 h. Upon completion, the reaction mixture was concentrated *in vacuo* and returned to the glove box. The crude product was washed with *n*-pentane (3 x 2 mL) and dried *in vacuo* to give [Ir(cod)(IPr)(Ph)] (**9a**) (7.9 mg, 35%) as a red solid. $^1\text{H NMR}$ (300 MHz, C_6D_6): δ 7.75 – 7.64 (m, 2H, ArH), 7.32 (t, 2H, $^3J_{\text{HH}} = 7.5$, *m*-ArH), 7.01 (tt, 1H, $^3J_{\text{HH}} = 7.3$, 1.4, *p*-ArH), 6.09 (s, 2H, N-(CH)₂-N), 5.61 (sept., 2H, $^3J_{\text{HH}} = 6.6$, CH(CH₃)₂), 4.46 – 4.32 (m, 2H, cod-CH), 3.57 – 3.46 (m, 2H, cod-CH), 2.47 – 2.20 (m, 4H, cod-CH₂), 2.06 – 1.84 (m, 4H, cod-CH₂), 1.08 (d, 6H, $^3J_{\text{HH}} = 6.6$, CH₃), 1.00 (d, 6H, $^3J_{\text{HH}} = 6.7$, CH₃); $^{13}\text{C}\{^1\text{H}\}$ NMR (75 MHz, C_6D_6): δ 184.1 (Ir-C_{carbene}), 173.9 (Ir-ArC), 138.0 (Ar), 127.4 (Ar), 121.4 (Ar), 115.9 (N-CH)₂N), 76.2 (cod-CH), 65.5 (cod-CH), 52.0 (CH(CH₃)₂), 32.5 (cod-CH₂), 32.4 (cod-CH₂), 23.8 (CH₃), 23.7 (CH₃); **Anal. Calcd.** for C₂₃H₃₃IrN₂ (MW 529.74): C, 52.15; H, 6.28; N, 5.29. Found: C, 52.23; H, 6.41; N, 5.05.

[Ir(cod)(IPr)(*p*-MeOC₆H₄)] **9b**

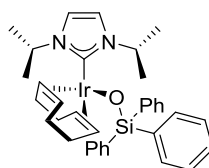
A 25 mL Schlenk flask was charged with [Ir(cod)(IPr)(OH)] (**4f**) (20 mg, 0.043 mmol) and *p*-methoxyphenylboronic acid (6.5 mg, 0.043 mmol) in PhMe (5 mL). The reaction mixture was removed from the glove box and stirred at 50 °C for 16 h. Upon completion, the reaction mixture was concentrated *in vacuo* and returned to the glove box. The crude product was washed with *n*-pentane (3 x 2 mL) and dried *in vacuo* to give [Ir(cod)(IPr)(*p*-MeOC₆H₄)] (**9b**) (11.0 mg, 46%) as a red solid. $^1\text{H NMR}$ (300 MHz, C_6D_6): δ 7.53 (d, 2H, $^3J_{\text{HH}} = 8.4$, ArH), 7.00 (d, 2H, $^3J_{\text{HH}} = 8.4$, ArH), 6.14 (s, 2H, N-(CH)₂), 5.60 (sept., 2H, $^3J_{\text{HH}} = 6.7$, CH(CH₃)₂), 4.56 – 4.71 (m, 2H, cod-CH), 3.49 (s, 3H, OCH₃), 3.52 – 3.45 (m, 2H, cod-CH), 2.46 – 2.27 (m, 4H, cod-CH₂), 2.05 – 1.90 (m, 4H, cod-CH₂), 1.09 (d, 6H, $^3J_{\text{HH}} = 6.8$, CH₃), 0.98 (d, 6H, $^3J_{\text{HH}} = 6.7$, CH₃); $^{13}\text{C}\{^1\text{H}\}$ NMR (75 MHz, C_6D_6): δ 184.9 (Ir-C_{carbene}), 160.7 (Ir-ArC), 156.2 (Ar), 138.6 (Ar),

116.0 (N-(CH)₂), 113.6 (Ar-CO), 75.8 (cod-CH), 64.5 (cod-CH), 54.6 (OCH₃), 52.0 (CH-(CH₃)₂), 32.6 (cod-CH₂), 32.3 (cod-CH₂), 23.8 (CH₃), 23.5 (CH₃). **Anal. Calcd.** for C₂₄H₃₅IrN₂O (MW 559.76): C, 51.50; H, 6.30; N, 5.00. Found: C, 51.37; H, 6.46; N, 4.91.



[Ir(cod)(IⁱPr)(OSi(OMe)₂Ph)] **10**

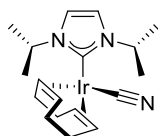
A 10 mL vial was charged with [Ir(cod)(IⁱPr)(OH)] (**4f**) (20 mg, 0.043 mmol) and phenyl trimethoxysilane (8.4 mg, 0.43 mmol) in PhMe (0.5 mL) and the resultant mixture was stirred at rt for 2 h. Upon completion, the reaction mixture was concentrated *in vacuo* and washed with *n*-pentane (3 x 2 mL) before being dried *in vacuo* to give [Ir(cod)(IⁱPr)(OSi(OMe)₂Ph)] (**10**) (27.0 mg, 99%) as a yellow solid. ¹H NMR (400 MHz, C₆D₆): δ 8.02 – 7.94 (m, 2H, ArH), 7.37 – 7.22 (m, 2H, ArH), 6.20 (s, 2H, N-(CH)₂-N), 5.79 (sept., 2H ³J_{HH} = 6.8, CH(CH₃)₂), 4.96 – 4.88 (m, 2H, cod-CH), 3.57 (s, 6H, OCH₃), 2.97 – 2.84 (m, 2H, cod-CH), 2.47 – 2.23 (m, 4H, cod-CH₂), 1.84 – 1.66 (m, 4H, cod-CH₂), 1.20 (d, 6H, ³J_{HH} = 6.7, CH(CH₃)₂), 1.10 (d, 6H, ³J_{HH} = 6.8, CH(CH₃)₂); ¹³C{¹H} NMR (100 MHz, C₆D₆): δ 179.9 (Ir-C_{carbene}), 138.5 (ArC), 135.7 (ArCH), 128.8 (ArCH), 127.6 (ArCH), 116.0 (N-(CH)₂-N), 84.5 (cod-CH), 52.3 (cod-CH), 50.1(OCH₃), 45.2 (CH(CH₃)₂), 34.8 (cod-CH₂), 30.2 (cod-CH₂), 23.8 (CH(CH₃)₂), 23.3 (CH(CH₃)₂). **Anal. Calcd.** for C₂₅H₃₉IrN₂O₃Si (MW 635.89): C, 47.22; H, 6.18; N, 4.41. Found: C, 47.38; H, 6.26; N, 4.48.



[Ir(cod)(IⁱPr)(OSiPh₃)] **11**

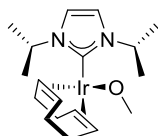
A 10 mL vial was charged with [Ir(cod)(IⁱPr)(OH)] (**4f**) (10 mg, 0.043 mmol) and triphenylsilane (5.2 mg, 0.43 mmol) in PhMe (0.5 mL) and the resultant mixture was stirred at rt for 16 h in a vial with a pierced cap. Upon completion, the reaction mixture was concentrated *in vacuo* and washed with *n*-pentane (3 x 2 mL) before being dried *in vacuo* to give [Ir(cod)(IⁱPr)(OSi(Ph)₃)] (**11**) (8.0 mg, 60%) as a yellow solid. ¹H NMR (400 MHz, C₆D₆): δ 7.93 – 7.77 (m, 6H, ArH), 7.31 – 7.20 (m, 9H, ArH), 6.20 (s, 2H,

N-(CH)₂-N), 5.80 (sept., 2H, ³J_{HH} = 6.7, CH(CH₃)₂), 4.78 – 4.66 (m, 2H, cod-CH), 3.01 – 2.88 (m, 2H, cod-CH), 2.45 – 2.17 (m, 4H, cod-CH₂), 1.84 – 1.56 (m, 4H, cod-CH₂), 1.06 (d, ³J_{HH} = 6.8, 6H, CH₃), 0.89 (d, ³J_{HH} = 6.6, 6H, CH₃); ¹³C{¹H} NMR (75 MHz, C₆D₆): δ 180.1 (Ir-C_{carbene}), 143.2 (ArC), 135.8 (ArCH), 127.5 (ArCH), 116.0 (N-(CH)₂-N), 84.1 (cod-CH), 52.3 (CH(CH₃)₂), 45.0 (cod-CH), 34.7 (cod-CH₂), 29.8 (cod-CH₂), 23.9 (CH₃), 23.2 (CH₃); **Anal. Calcd.** for C₃₅H₄₃IrN₂OSi (MW 728.03): C, 57.74; H, 5.95; N, 3.85. Found: C, 57.66; H, 5.86; N 3.77.



[Ir(cod)(IⁱPr)(CN)] **12**

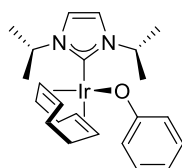
[Ir(cod)(IⁱPr)(OH)] (**4f**) (10mg, 0.02 mmol) and TMSCN (2.50 mg, 0.025 mmol) were weighed into separate 10 mL vials, dissolved in PhMe (0.5 mL) and chilled to -40 °C. The TMSCN solution was added drop wise to the solution of **4f**, which instantly changed colour from yellow to red. After stirring for *ca.* 2 mins, the reaction mixture was reduced *in vacuo* to *ca.* 0.2 mL. Cold *n*-pentane (0.5 mL) was added to the mixture and the resulting precipitate was filtered off, washed with *n*-pentane (3 x 1 mL), and dried *in vacuo* to give [Ir(cod)(IⁱPr)(CN)] (**12**) (9.0 mg, 90%) as a red solid. ¹H NMR (400 MHz, C₆D₆): 6.25 (s, 2H, N-(CH)₂-N), 5.31 (sept., 2H, ³J_{HH} = 6.8, (CH(CH₃)₂), 5.01 – 4.96 (m, 2H, cod-CH), 3.58 – 3.49 (m, 2H, cod-CH), 2.10 – 2.02 (m, 4H, cod-CH₂), 1.76 – 1.69 (m, 4H, cod-CH₂) 1.21 (d, 6H, ³J_{HH} = 6.8, CH₃), 1.00 (d, 6H, ³J_{HH} = 6.7, CH₃); ¹³C{¹H} NMR (100 MHz, C₆D₆): δ 176.7 (Ir-C_{carbene}), 137.5 (CN), 116.7 (N-(CH)₂-N), 76.8 (cod-CH), 70.2 (cod-CH), 52.6 (CH(CH₃)₂), 32.2 (cod-CH₂), 31.7 (cod-CH₂), 23.6 (CH₃), 22.8 (CH₃). **Anal. Calcd.** for C₁₈H₂₈IrN₃ (MW 478.65): C, 45.17; H, 5.90; N, 8.78. Found: C, 45.25; H, 6.05; N, 8.67.



[Ir(cod)(IⁱPr)(OMe)] **13**

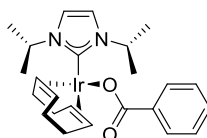
A 10 mL vial was charged with [Ir(cod)(IⁱPr)(OH)] (**4f**) (20 mg, 0.043 mmol) and MeOH (0.5 mL) and the resultant mixture was stirred at rt for 16 h. Upon completion, the reaction mixture was concentrated *in vacuo* and taken up in *n*-pentane (2 mL) and the solid impurities were filtered off. The filtrate was concentrated *in vacuo* to give

[Ir(cod)(IⁱPr)(OMe)] (**13**) (20.4 mg, 99%) as a yellow-brown solid. ¹H NMR (300 MHz, C₆D₆): δ 6.20 (s, 2H, N-(CH)₂-N), 5.85 (sept., 2H, ³J_{HH} = 6.8, CH(CH₃)₂), 5.01 – 4.90 (m, 2H, cod-CH), 4.37 (s, 3H, OCH₃), 2.70 – 2.63 (m, 2H, cod-CH), 2.54 – 2.34 (m, 4H, cod-CH₂), 1.97 – 1.74 (m, 4H, cod-CH₂), 1.14 (d, 6H, ³J_{HH} = 6.7, CH₃), 1.12 (d, 6H, ³J_{HH} = 6.7, CH₃); ¹³C{¹H} NMR (75 MHz, C₆D₆): δ 182.2 (Ir-C_{carbene}), 115.9 (N-(CH)₂-N), 83.7 (cod-CH), 64.0 (OCH₃), 52.2 (CH(CH₃)₂), 44.3 (cod-CH), 34.8 (cod-CH₂), 29.9 (cod-CH₂), 23.7 (CH₃), 23.6 (CH₃); **Anal. Calcd.** for C₁₈H₃₁IrN₂O (MW 483.67): C, 44.70; H, 6.46; N, 5.79. Found: C, 44.62; H, 6.39; N, 5.85.



[Ir(cod)(IⁱPr)(OPh)] **14**

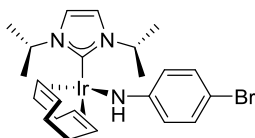
A vial was charged with [Ir(cod)(IⁱPr)(OH)] (**4f**) (20.0 mg, 0.043 mmol) and phenol (4.1 mg, 0.043 mmol) in PhMe (1 mL) and the reaction mixture was stirred at rt for 16 h. Once complete, the mixture was concentrated *in vacuo* and the resultant solid was washed with cold pentane (3 x 1 mL) and dried *in vacuo* to give [Ir(cod)(IⁱPr)(OPh)] (**14**) (22.1 mg, 94%) as a yellow solid. ¹H NMR (300 MHz, C₆D₆): δ 7.24 (t, 2H, ³J_{HH} = 7.8, *m*-ArH), 6.96 (d, 2H, ³J_{HH} = 8.4, *o*-ArH), 6.74 (tt, 1H, ³J_{HH} = 7.2, 1.0, *p*-ArH), 6.13 (s, 2H, N-(CH)₂-N), 5.77 (sept., 2H, ³J_{HH} = 6.8, N-CH(CH₃)₂), 4.92– 4.82 (m, 2H, cod-CH), 2.96 – 2.84 (m, 2H, cod-CH), 2.41 – 2.21 (m, 4H, cod-CH₂), 1.81 – 1.57 (m, 4H, cod-CH₂), 1.12 (d, 6H, ³J_{HH} = 6.7, CH₃), 1.09 (d, 6H, ³J_{HH} = 6.8, CH₃). ¹³C{¹H} NMR (75 MHz, C₆D₆): δ 179.4 (Ir-C_{carbene}), 171.3 (ArC), 129.3 (ArCH), 121.4 (ArCH), 116.1 (N-(CH)₂-N), 115.6 (ArCH), 83.1 (cod-CH), 52.4 (N-CH(CH₃)₂), 45.9 (cod-CH), 34.5 (cod-CH₂), 29.6 (cod-CH₂), 23.7 (CH₃), 23.5 (CH₃). **Anal. Calcd.** for C₂₄H₃₃IrN₂O (MW 545.74): C, 50.62; H, 6.09; N, 5.13. Found: C, 50.55; H, 5.93; N, 5.17.



[Ir(cod)(IⁱPr)(OCOPh)] **15**

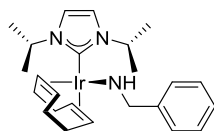
A 10 mL vial was charged with [Ir(cod)(IⁱPr)(OH)] (**4f**) (20 mg, 0.043 mmol) and benzoic acid (5.2 mg, 0.43 mmol) in PhMe (0.5 mL) and the resultant mixture was

stirred at rt for 1 h. Upon completion, the reaction mixture was concentrated *in vacuo* and washed with *n*-pentane (3 x 2 mL) before being dried *in vacuo* to give [Ir(cod)(IⁱPr)(OCOPh)] (**15**) (20.4 mg, 99%) as an orange solid. ¹H NMR (300 MHz, CD₂Cl₂): δ 7.90 – 7.80 (m, 2H, ArH), 7.38 – 7.20 (m, 3H, ArH), 6.90 (s, 2H, N-(CH)₂-N), 5.67 (sept., 2H, ³J_{HH} = 5.8, CH(CH₃)₂), 4.60 – 4.50 (m, 2H, cod-CH), 2.84 – 3.00 (m, 2H, cod-CH), 2.38 – 2.14 (m, 4H, cod-CH₂), 1.75 – 1.55 (m, 4H, cod-CH₂), 1.48 (d, 6H, ³J_{HH} = 6.8, CH₃), 1.37 (d, 6H, ³J_{HH} = 6.7, CH₃); ¹³C{¹H} NMR (75 MHz, CD₂Cl₂): δ 177.7 (Ir-C_{carbene}), 170.8 (ArC), 130.3 (ArCH), 129.7 (ArCH), 127.8 (ArCH), 116.7 (N-(CH)₂-N), 83.1 (cod-CH), 52.8 (CH(CH₃)₂), 48.5 (cod-CH), 34.0 (cod-CH₂), 29.4 (cod-CH₂), 24.0 (CH₃), 23.7 (CH₃). **Anal. Calcd.** for C₂₄H₃₃IrN₂O₂ (MW 483.67): C, 50.24; H, 5.80; N, 4.88. Found: C, 50.34; H, 5.83; N, 4.97. *The C=O ¹³C{¹H} NMR signal was not observed.

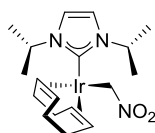


[Ir(cod)(IⁱPr)(NH(-*p*-BrPh))] **16**

A 10 mL vial was charged with [Ir(cod)(IⁱPr)(OH)] (**4f**) (20 mg, 0.043 mmol) and *p*-bromoaniline (7.3 mg, 0.43 mmol) in PhMe (0.5 mL) and the resultant mixture was stirred at rt for 1 h. Upon completion, the reaction mixture was concentrated *in vacuo* and washed with *n*-pentane (3 x 2 mL) before being dried *in vacuo* to give [Ir(cod)(IⁱPr)(NH(-*p*-BrPh))] (**16**) (19.1 mg, 72%) as an orange solid. ¹H NMR (400 MHz, C₆D₆): δ 7.07 (d, 2H, ³J_{HH} = 8.9, ArH), 6.23 (s, 2H, N-(CH)₂-N), 5.66 (d, 2H, ³J_{HH} = 8.9, ArH), 5.57 (sept., 2H, ³J_{HH} = 6.8, CH(CH₃)₂), 5.10 (s, 1H, NH), 4.15 – 4.06 (m, 2H, cod-CH), 2.67 – 2.57 (m, 2H, cod-CH), 2.50 – 2.37 (m, 2H, cod-CH₂), 2.36 – 2.23 (m, 2H, cod-CH₂), 2.03 – 1.89 (m, 2H, cod-CH₂), 1.86 – 1.72 (m, 2H, cod-CH₂), 1.03 (d, 6H, ³J_{HH} = 6.8, CH₃), 0.90 (d, 6H, ³J_{HH} = 6.7, CH₃); ¹³C{¹H} NMR (100 MHz, C₆D₆): δ 179.1 (Ir-C_{carbene}), 159.2 (ArC), 131.4 (ArCH), 118.4 (ArCH), 116.6 (N-(CH)₂-N), 104.4 (ArC), 80.5 (cod-CH), 52.6 (CH(CH₃)₂), 50.3 (cod-CH), 34.5 (cod-CH₂), 30.1 (cod-CH₂), 24.0 (CH₃), 23.0 (CH₃). **Anal. Calcd.** for C₂₃H₃₃BrIrN₃ (MW 623.65): C, 44.30; H, 5.33; N, 6.74. Found: C, 44.20; H, 5.37; N, 6.62.

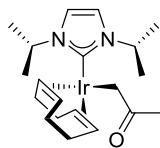
[Ir(cod)(IⁱPr)(NHBn)] **17**

A vial was charged with [Ir(cod)(IⁱPr)(OH)] (**4f**) (20.0 mg, 0.043 mmol) and benzylamine (4.7 mg, 0.043 mmol) in PhMe (1.0 mL) and the reaction mixture was stirred at rt for 16 h. Once complete, the mixture was concentrated *in vacuo*, washed with *n*-pentane (3 x 1 mL) and dried to give [Ir(cod)(IⁱPr)(NHBn)] (**17**) (17.4 mg, 72%) as a yellow solid. ¹H NMR (300 MHz, C₆D₆): δ 7.61 (d, 2H, ³J_{HH} = 7.4, *o*-ArH), 7.28 (t, 2H, ³J_{HH} = 7.5, *m*-ArH), 7.19 – 7.08 (m, 1H, *p*-ArH), 6.17 (s, 2H, N-(CH)₂-N), 5.97 (sept., 2H, ³J_{HH} = 6.7, N-CH(CH₃)₂), 4.50 (d, 2H, ³J_{HH} = 7.8, NH-CH₂), 4.50 – 4.36 (m, 2H, cod-CH), 2.63 (br., 2H, cod-CH), 2.70 – 2.35 (m, 4H, cod-CH₂), 2.28 – 2.10 (m, 2H, cod-CH₂), 2.05 – 1.90 (m, 2H, cod-CH₂), 1.12 (d, 6H, ³J_{HH} = 6.9, CH₃), 1.02 (d, 6H, ³J_{HH} = 6.7, CH₃). ¹³C{¹H} NMR (75 MHz, C₆D₆): δ 182.2 (Ir-C_{carbene}), 149.6 (ArC), 128.1 (*m*-ArCH), 127.4 (*o*-ArCH), 125.9 (*p*-ArCH), 115.8 (N-(CH)₂-N), 76.3 (cod-CH), 59.1 (NH-CH₂), 52.4 (N-CH(CH₃)₂), 45.4 (cod-CH), 35.0 (cod-CH₂), 31.2 (cod-CH₂), 23.6 (CH₃), 23.5 (CH₃). Anal. Calcd. for C₂₄H₃₆IrN₃ (MW 558.78): C, 51.59; H, 6.49; N, 7.52. Found: C, 51.25; H, 6.37; N, 7.38.

[Ir(cod)(IⁱPr)(CH₂NO₂)] **20**

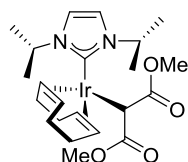
A 10 mL vial was charged with [Ir(cod)(IⁱPr)(OH)] (**4f**) (20 mg, 0.043 mmol). Upon addition of nitromethane (3.0 mg, 0.05 mmol), the yellow solid turned to an intense red colour. ¹H NMR analysis of the compound in C₆D₆ indicated that the reaction was complete. To ensure completion, the reaction mixture was further stirred in PhMe (0.5 mL) at rt for 1 h before being concentrated *in vacuo* and washed with *n*-pentane (3 x 2 mL). The product was dried *in vacuo* to give [Ir(cod)(IⁱPr)(CH₂NO₂)] (**20**) (16.8 mg, 77%) as a red solid. ¹H NMR (400 MHz, C₆D₆): δ 6.23 (s, 2H, N-(CH)₂-N), 5.28 (s, 2H, CH₂), 5.24 (sept., 2H, ³J_{HH} = 6.7, CH(CH₃)₂), 4.11 – 4.00 (m, 2H, cod-CH), 3.32 – 3.22 (m, 2H, cod-CH), 2.19 – 2.02 (m, 4H, cod-CH₂), 1.97 – 1.74 (m, 4H, cod-CH₂), 1.26 (d, 6H, ³J_{HH} = 6.8, CH₃), 1.03 (d, 6H, ³J_{HH} = 6.7, CH₃); ¹³C{¹H} NMR (100 MHz, C₆D₆): δ 181.4 (Ir-C_{carbene}), 116.9 (N-(CH)₂-N), 77.3 (cod-CH), 75.9 (CH₂), 62.0 (cod-CH), 52.3 (CH(CH₃)₂), 32.6 (cod-CH₂), 31.0 (cod-CH₂), 23.9 (CH₃), 23.5

(CH₃). **Anal. Calcd.** for C₁₈H₃₀IrN₃O₂ (MW 512.67): C, 42.17; H, 5.90; N, 8.20. Found: C, 42.11; H, 5.92; N, 8.26.



[Ir(cod)(IⁱPr)(CH₂COCH₃)] **21**

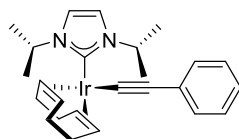
A 10 mL vial was charged with [Ir(cod)(IⁱPr)(OH)] (**4f**) (20 mg, 0.043 mmol) and acetone (0.5 mL). The resultant mixture was stirred at rt for 16 h before being concentrated *in vacuo* and washed with *n*-pentane (3 x 2 mL). The product was dried *in vacuo* to give [Ir(cod)(IⁱPr)(CH₂COCH₃)] (**21**) (21.5 mg, 99%) as a red solid. ¹H NMR (400 MHz, C₆D₆): δ 6.27 (s, 2H, N-(CH)₂-N), 5.19 (sept., 2H, ³J_{HH} = 6.8, CH(CH₃)₂), 4.47 – 4.35 (m, 2H, cod-CH), 3.27 – 3.16 (m, 2H, cod-CH), 2.93 (s, 2H, Ir-CH₂), 2.31 – 2.08 (m, 4H, cod-CH₂), 2.05 (s, 3H, CO-CH₃), 1.90 – 1.87 (m, 2H, cod-CH₂), 1.76 – 1.60 (m, 2H, cod-CH₂), 1.22 (d, 6H, ³J_{HH} = 6.7, CH₃), 1.06 (d, 6H, ³J_{HH} = 6.7, CH₃); ¹³C{¹H} NMR (100 MHz, C₆D₆): δ 209.4 (CO), 183.4 (Ir-C_{carbene}), 116.5 (N-(CH)₂-N), 76.8 (cod-CH), 59.4 (cod-CH), 51.8 (CH(CH₃)₂), 43.9 (CH₂), 32.9 (cod-CH₂), 31.6 (cod-CH₂), 31.2 (CO-CH₃), 23.9 (CH₃), 23.4 (CH₃). **Anal. Calcd.** for C₂₀H₃₃IrN₂O (MW 509.71): C, 47.13; H, 6.53; N, 5.50. Found: C, 46.98; H, 6.69; N, 5.37.



[Ir(cod)(IⁱPr)(CH(CO₂Me)₂)] **22**

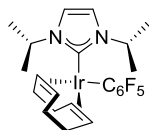
A 10 mL vial was charged with [Ir(cod)(IⁱPr)(OH)] (**4f**) (20 mg, 0.043 mmol). Upon addition of dimethylmalonate (5.6 mg, 0.043 mmol), the yellow solid turned to an intense red colour. The reaction mixture was stirred in PhMe (0.5 mL) for 1 h before being concentrated *in vacuo* and washed with *n*-pentane (3 x 2 mL). The product was dried *in vacuo* to give [Ir(cod)(IⁱPr)(CH(CO₂Me)₂)] (**22**) (18.6 mg, 75%) as a red solid. ¹H NMR (400 MHz, C₆D₆): δ 6.29 (s, 2H, N-(CH)₂-N), 5.31 (sept., 2H, ³J_{HH} = 6.6, CH(CH₃)₂), 4.92 – 4.83 (m, 2H, cod-CH), 4.28 (s, 1H, Ir-CH), 3.45 (s, 6H, CO-CH₃), 3.22 – 3.13 (m, 2H, cod-CH), 2.28 – 2.03 (m, 4H, cod-CH₂), 1.84 – 1.70 (m, 2H, cod-CH₂), 1.67 – 1.55 (m, 2H, cod-CH₂), 1.35 (d, 6H, ³J_{HH} = 6.6, CH₃), 1.09 (d, 6H, ³J_{HH} = 6.8, CH₃); ¹³C{¹H} NMR (100 MHz, C₆D₆): δ 180.7 (Ir-C_{carbene}), 174.2 (CO), 116.7 (N-

(CH)₂-N), 80.7 (cod-CH), 58.9 (OCH₃), 52.2 (CH(CH₃)₂), 49.9 (cod-CH), 41.2 (Ir-C_{carbene}), 32.6 (cod-CH₂), 31.1 (cod-CH₂), 24.7 (CH₃), 23.4 (CH₃). **Anal. Calcd.** for C₂₂H₃₅IrN₂O₄ (MW 583.74): C, 45.27; H, 6.04; N, 4.80. Found: C, 45.19; H, 6.11; N, 4.89.



[Ir(cod)(IⁱPr)(CCPh)] **23**

A 10 mL vial was charged with [Ir(cod)(IⁱPr)(OH)] (**4f**) (20 mg, 0.43 mmol). Upon addition of phenylacetylene (4.4 mg, 0.043 mmol), the yellow solid turned to an intense red colour. The reaction mixture was stirred in PhMe (0.5 mL) for 1 h before being concentrated *in vacuo* and washed with *n*-pentane (3 x 2 mL). The product was dried *in vacuo* to give [Ir(cod)(IⁱPr)(CCPh)] (**23**) (16.0 mg, 68%) as a red solid. ¹H NMR (400 MHz, C₆D₆): δ 7.54 (d, 2H, ³J_{HH} = 7.4, *o*-ArH), 7.07 (t, 2H, ³J_{HH} = 7.7, *m*-ArH), 6.91 (t, 1H, ³J_{HH} = 7.3, *p*-ArH), 6.24 (s, 2H, N-(CH)₂-N), 5.60 (sept., 2H, ³J_{HH} = 6.8, CH(CH₃)₂), 5.16 – 5.05 (m, 2H, cod-CH), 3.58 – 3.47 (m, 2H, cod-CH), 2.38 – 2.21 (m, 4H, cod-CH₂), 2.01 – 1.85 (m, 4H, cod-CH₂), 1.27 (d, 6H, ³J_{HH} = 6.7, CH₃), 1.08 (d, 6H, ³J_{HH} = 7.0, CH₃); ¹³C{¹H} NMR (100 MHz, C₆D₆): δ 180.6 (Ir-C_{carbene}), 131.5 (ArC), 130.0 (ArCH), 125.4 (C≡C), 124.7 (ArCH), 118.9 (C≡C), 116.1(N-(CH)₂-N), 76.6 (cod-CH), 66.2 (cod-CH), 52.3 (CH(CH₃)₂), 32.9 (cod-CH₂), 32.0 (cod-CH₂), 23.7 (CH₃), 22.8 (CH₃). **Anal. Calcd.** for C₂₅H₃₃IrN₂ (MW 553.76): C, 54.22; H, 6.01; N, 5.06. Found: C, 54.20; H, 6.08; N, 4.98.



[Ir(cod)(IⁱPr)(C₆F₅)] **24**

A 10 mL Schlenk flask was charged with [Ir(cod)(IⁱPr)(OH)] (**4f**) (20 mg, 0.043 mmol) and pentafluorobenzene (0.1 mL, 0.9 mmol). The reaction mixture was removed from the glove box to be stirred at 60 °C for 16h. Upon completion, the reaction mixture was concentrated *in vacuo* and returned to the glove box. The crude product was washed with *n*-pentane (3 x 2 mL) and dried *in vacuo* to give [Ir(cod)(IⁱPr)(C₆F₅)] (**24**) (16.1 mg, 61%) as an orange solid. ¹H NMR (400 MHz, C₆D₆): δ 6.08 (s, 2H, N-(CH)₂-N), 5.55 (sept., 2H, ³J_{HH} = 6.7, CH(CH₃)₂), 4.42 – 4.33 (m, 2H, cod-CH), 3.48 – 3.37

(m, 2H, cod-CH), 2.33 – 2.13 (m, 4H, cod-CH₂), 1.86 – 1.69 (m, 4H, cod-CH₂) 1.03 (d, 6H, ³J_{HH} = 6.8, CH₃), 1.02 (d, 6H, ³J_{HH} = 6.6, CH₃); ¹⁹F{¹H} NMR (377 MHz, C₆D₆): δ -117.5 (d, ³J_{FF} = 27, *o*-F), -164.5 (t, ³J_{FF} = 20, *p*-F), -165.2 (t, ³J_{FF} = 23, *m*-F). ¹³C{¹H} NMR (100 MHz, C₆D₆): δ 178.4 (Ir-C_{carbene}), 116.6 (N-(CH)₂-N), 77.0 (cod-CH), 65.6 (cod-CH), 52.1 (CH(CH₃)₂), 32.3 (cod-CH₂), 31.7 (cod-CH₂), 23.9 (CH₃), 23.4 (CH₃);* Signals assigned to the C₆F₅ moiety could not be detected due to multiple F-C coupling interactions. **Anal. Calcd.** for C₂₃H₂₈IrF₅N₂ (MW 619.69): C, 44.58; H, 4.55; N, 4.52. Found: C, 44.58; H, 4.60; N, 4.67.

5. CO₂ FIXATION BY IRIDIUM(I) ALKOXIDE AND AMIDE COMPLEXES

5.1. INTRODUCTION

Green-house gas emissions are constantly increasing, with carbon dioxide being the single largest contributor.²⁵² Emissions have arguably contributed to the global warming crisis faced by mankind and there is continued pressure on world leaders and on the scientific community to develop strategies for the reduction of atmospheric CO₂.²⁵³ Reduction in atmospheric levels can be tackled by three contrasting strategies: (i) decreasing emissions; (ii) storage; and (iii) utilisation of CO₂. The reduction of CO₂ emissions requires a shift from the use of fossil fuels towards renewable resources such as hydrogen. The recovery or sequestering of CO₂ from the atmosphere or from energy conversion processes requires advancements in storage, and finally the recycling of CO₂ for synthetic purposes focuses on CO₂ as an attractive carbon source.²⁵³

The application of carbon dioxide as a C1 source is not only a strategy towards reduction of greenhouse gases but also presents an opportunity for catalytic development and is an area of fundamental attraction. As well as being an attractive and relatively low molecular weight single carbon unit, its origin as a waste product in vast quantities renders it a cost-effective reagent.²⁵³⁻²⁵⁴ However CO₂ activation is still a greatly underdeveloped area of investigation. This is mainly due to its thermodynamic and kinetic stability.²⁵² In fact, its use as a chemical feedstock on an industrial scale is limited to only a few processes, including the synthesis of urea, carbonates, methanol and salicylic acid.^{252-253, 255} Further utilisation of CO₂ is possible only with successful activation of this inert species. Of the CO₂ activation pathways under investigation, including bioconversion, thermal heterogeneous and homogeneous catalysis, electrochemical or photochemical reduction and transition metal activation; all of them share a common process: the coordination of CO₂ to a metal centre.^{252, 256} Coordination to a TM centre lowers the activation barrier associated with subsequent processes and therefore enables conversion of CO₂ into useful products.²⁵²

Transition metals, equipped with the appropriate ligand set, can activate a range of important and useful small molecules. Since the coordination of CO₂ to a metal centre is

a key step in transition metal-catalysed processes utilising it as a feedstock,²⁵² a thorough understanding of the interaction between CO₂ and metal complexes is of fundamental importance.²⁵⁷ Traditionally, it has been regarded as a poor coordinating ligand, however TM complexes are known to bind CO₂ in a variety of fashions, with a large number of coordination modes having been described.^{257d} The different modes of coordination are the result of CO₂ being made up of two Lewis basic sites (oxygen) and a Lewis acidic site (carbon), giving it multiple points for attachment. The linear geometry of the CO₂ moiety usually bends upon coordination, as the LUMO orbitals are occupied, leading to four typical coordination modes in monomeric complexes (A, Figure 5.1).^{257d} CO₂ has the ability to act as a bridging ligand, linking as many as four metals together in a myriad of theoretical binding modes such as those shown (*B, C, Figure 5.1).^{257d}

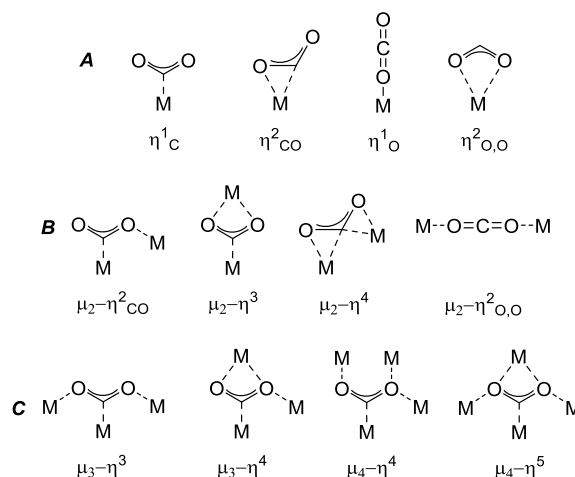
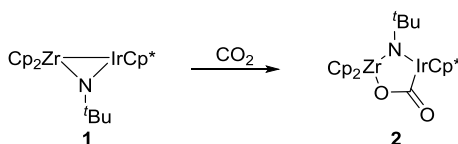


Figure 5.1. Binding modes of CO₂ in **A**: monomeric complexes; and **B, C**: polymetallic complexes^{257d}

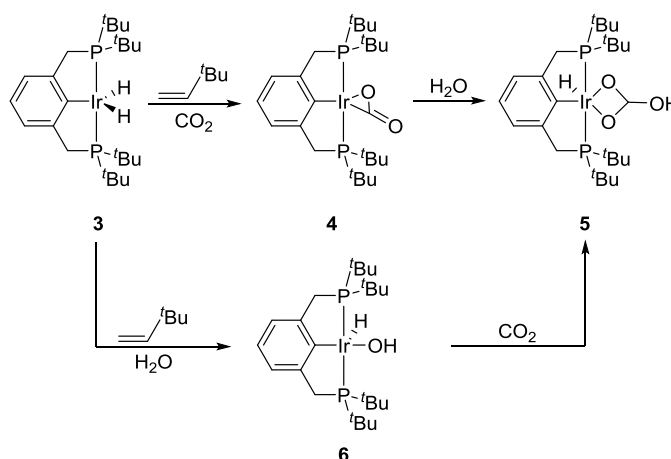
The first crystal structure of an Ir-CO₂ complex was reported in 1995 by Bergman,²⁵⁸ in the form of an [Ir-(μ₂-κ²C,O-CO₂)-Zr] complex **2** by direct insertion of CO₂ into the Ir-Zr bond of **1** (Scheme 5.1).



Scheme 5.1. Preparation of [Ir-(μ₂-κ²C,O-CO₂)-Zr] **2** by Bergman²⁵⁸

Until recently, the only monometallic iridium complexes containing a CO₂ ligand were those reported by Herskovitz in 1977²⁵⁹ and by Morales-Morales in 2003.²⁶⁰ Herskovitz reported that CO₂ reacted with [Ir{(CH₃)₂P(CH₂)₂P(CH₃)₂}]Cl to form

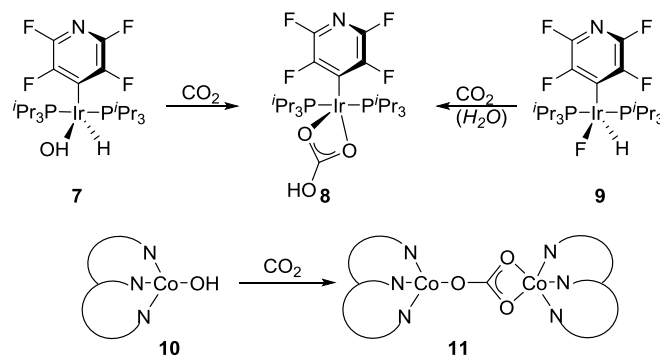
[Ir{(CH₃)₂P(CH₂)₂P(CH₃)₂)₂]Cl·CO₂, assigned as an Ir-η¹-CO₂ complex.²⁵⁹ Morales-Morales reported that reaction between the Ir(III)-dihydride complex **3** and *tert*-butyl ethylether (*t*be) in the presence of CO₂ (Scheme 5.2) gave the η²-CO₂ complex **4**. This structural assignment was based on NMR and IR spectroscopies (which indicated two strong bands at 1756 and 1149 cm⁻¹, assigned to the asymmetric and symmetric stretches respectively). Isolation and full characterisation of **4** was difficult due to the fact that it reacted with adventitious water (present as vapour in the CO₂) to form the hydrogen carbonate adduct **5**. Complex **5** was also prepared *via* CO₂ insertion into the Ir-OH bond of **6**, indicating that the order in which CO₂ and H₂O were added was not important (Scheme 5.2).²⁶⁰



Scheme 5.2. Preparation of Ir-CO₂ complexes by Morales-Morales²⁶⁰

Early reports of CO₂ insertion on metal hydroxides to form metal carbonates were by Vaska²⁶¹ on the reversible insertion of CO₂ on *trans*-[M(CO)(OH)(PPh₃)₂] (M = Rh/Ir) under mild conditions. A Pd(II) hydroxide complex, analogous to **6** was shown to react with CO₂ to selectively form the [(PCP)Pd(II)-(η¹-OCO₂H)] complex.²⁶² Several other LTM hydroxides have been successfully reacted with CO₂ to give metal carbonates, mostly of the type [M₂(μ-κ²O,O:κ²O,O-CO₃)] (M = Cd, Ni, Cu, Co) or [M₂(μ-κ¹O:κ¹O-CO₃)] in the case of Cu.²⁶²⁻²⁶³ Limited examples of group nine metal hydroxides reacting with CO₂ have been reported,^{260, 264} including that of Morales-Morales²⁶⁰ *vide supra*. Braun²⁶⁵ has reported that both the Ir hydrido-hydroxo complex **7** and the Ir hydrido-fluoride **9** (in the presence of adventitious water, Scheme 5.3) react with CO₂ to give the bicarbonate Ir-(κ²O,O-CO₃H) **8**. Singh and co-workers reported the novel dinuclear cobalt complex, [Co₂(L₂)(μ-κ¹O:κ²O,O-CO₃)] **11**, formed from a Co(II)-hydroxide [Co{HB(3-*t*Bu-5-*i*Prpz)₃}(OH)] (**10**) (HB(3-*t*Bu-5-*i*Prpz)₃ = hydro-

tris(3-*tert*-butyl-5-isopropylpyrazol-1-yl)borate) (Scheme 5.3).^{264a} Krogsrud has prepared a similar complex, exhibiting the same binding mode in the form of [Rh₂(μ-κ¹O:κ²O, O-CO₃)(PPh₃)₅]·C₆H₆ (**12**) from [Rh(H)(PPh)₄] or [Rh(H)(PPh)₃] in toluene at 20 °C, under CO₂ over several days.²⁶⁶



Scheme 5.3. Preparation of [Ir(κ²O, O-CO₃H)] **8** by Braun.²⁶⁵ and Co₂(μ-κ¹O:κ²O, O-CO₃) **11** by Singh^{264a}

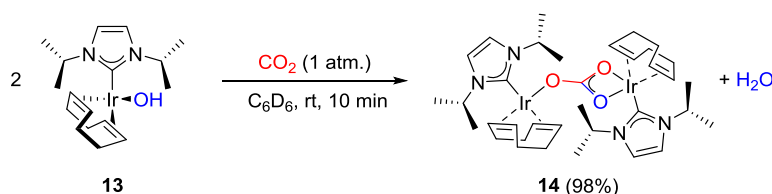
A large majority of the synthetic interest in preparing carbonates from metal hydroxides stems from the biological activity of metalloenzymes in sequestering and hydrolysing CO₂. For example, carbonic anhydrase, arguably the most efficient CO₂-sequestering catalyst known is deprotonated from Zn-OH₂ to give Zn-OH. CO₂ then inserts into the Zn-OH bond to give Zn-OCO₂H which undergoes reversible hydrolysis to extrude HCO₃⁻.²²

In Chapter 4 we reported that [Ir(cod)(*i*Pr)(OH)] (**13**) was a powerful bond activating agent, able to deprotonate a wide range of organic substrates to yield a number of new organoiridium(I) complexes.²⁶⁷ In this investigation we aimed to expand on the reported activity, by utilising **13** and its derivatives to coordinate CO₂. We hoped to prepare new Ir(I)-carbonate and -carbamate complexes so that we may develop an understanding of CO₂ coordination at Ir(I) as a starting point for developing catalytic strategies using CO₂ as a C1-source.

5.2. RESULTS AND DISCUSSION

5.2.1. Reactivity

When a benzene-*d*₆ solution of **13** was exposed to CO₂ (*ca.* 1 atm), a precipitate formed almost immediately. Analysis by ¹H NMR indicated downfield shifts of all signals, compared to the starting material, and disappearance of the signal corresponding to the hydroxyl moiety (δ 2.47 ppm). ¹³C{¹H} NMR analysis of the product was inconclusive since no signal corresponding to a potential carbonate carbon was observed. Analysis by FTIR (ATR) of the solid product indicated that the signal corresponding to the hydroxyl group in the starting material (ν 3612.7 cm⁻¹) had disappeared and had been replaced by two very broad, strong bands at 1616.4 cm⁻¹ and 1415.8 cm⁻¹ which we tentatively assigned to a carbonate moiety. It was only when we obtained an X-ray structure from single crystals grown by slow evaporation of a saturated hexane solution that we were able to fully elucidate the structure of the product. Scheme 5.4 and Figure 5.2 show the product as a dimeric carbonate. One Ir(I) fragment adopts the conventional 16-electron square planar geometry, whilst the second adopts an 18-electron distorted trigonal bipyramidal geometry. The two iridium centres are bound to the same central (essentially planar) carbonate moiety in a μ - $\kappa^1 O$: $\kappa^2 O, O$ fashion and twisted almost 180° away from each other to give $[\{\text{Ir}(\text{cod})(\text{I}^i\text{Pr})\}_2(\mu$ - $\kappa^1 O$: $\kappa^2 O, O$ -CO₃)] (**14**).



Scheme 5.4. Addition of CO₂ to Ir-hydroxide **13** to give $[\{\text{Ir}(\text{cod})(\text{I}^i\text{Pr})\}_2(\mu$ - κ^1 : κ^2 -CO₃)] (**14**)

The chelate nature of the carbonate moiety causes the O-C-O bond angle to decrease from 120° to 116.9(10)°. ²⁶⁶ Notably, the distance between Ir31 and O71 is too long (*ca.* 3.17 Å) for an Ir-O bond and excludes the $[\text{M}_2(\mu$ - $\kappa^2 O, O$: $\kappa^2 O, O$ -CO₃)] conformation often encountered with bridging carbonates. ^{263b} In solution, the magnetic equivalency (at both 187 K and 300 K) of the cod and I^{*i*}Pr ligands on both iridium centres suggests that the 16e⁻ and the 18e⁻ conformations are fluxional and that de-coordination/re-coordination of the carbonyl oxygen may be too fast to be observed on the NMR timescale, hence ¹H NMR analysis showed a symmetrical compound. The μ -

$\kappa^1:\kappa^2$ -CO₃ coordination has been observed in a number of metal systems such as the Co and Rh complexes described earlier.^{264a, 266} The facile insertion of CO₂ into Ir-OH under very mild conditions, has yielded, to our knowledge, a unique [$\{\text{Ir(I)}\}_2$ -(μ - $\kappa^1\text{O}:\kappa^2\text{O},\text{O}-\text{CO}_3$)] complex.

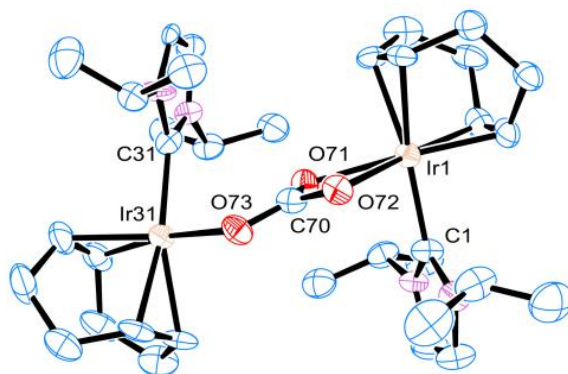
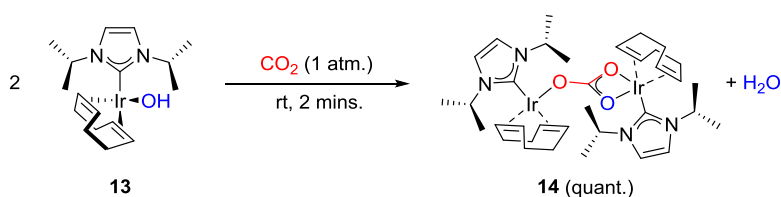


Figure 5.2. Thermal ellipsoid representation of **14** showing 50% thermal ellipsoid probability. H atoms are omitted for clarity. Selected bond lengths (Å) and bond angles (°): Ir1-O71 2.252(7), Ir1-O72 2.273(8), Ir31-O73 2.068(7), O71-C70 1.291(14), O72-C70 1.281(12), O73-C70 1.282(14), O71-Ir1-O72 57.9(3), O71-C70-O72 116.9(10).

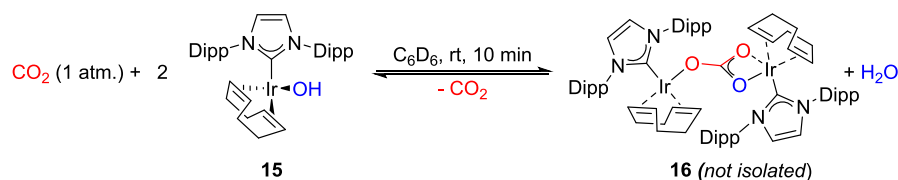
As mentioned, analysis of **14** by $^{13}\text{C}\{^1\text{H}\}$ NMR spectroscopy indicated that the carbonate $^{13}\text{C}\{^1\text{H}\}$ NMR signal was unobservable at natural ^{13}C abundance. To further confirm the solution structure of **14** and incorporation of CO₂, the reaction was repeated using $^{13}\text{CO}_2$, allowing this key signal to be located as a broad resonance at 170.0 ppm (THF-*d*₈). Interestingly, placing a sample of the labelled complex (**14**- ^{13}C) under an atmosphere of CO₂ led to the loss of ^{13}C enrichment at this position. This scrambling has been reported for early transition metal carbamates such as $\text{W}(\text{O}_2\text{CNMe}_2)$ ²⁶⁸ and indicates that the CO₂ insertion and elimination processes are both facile and reversible.

The CO₂ insertion proved to be extremely facile and could be completed in the solid state by simply passing CO₂ over a sample of **13** for *ca.* 2 mins, giving complete conversion to the carbonate **14** (Scheme 5.5). This was confirmed by both FTIR (ATR) and ^1H NMR analysis after three vacuum/purge cycles with argon to remove the CO₂ atmosphere.



Scheme 5.5. Preparation of **14** in the solid state

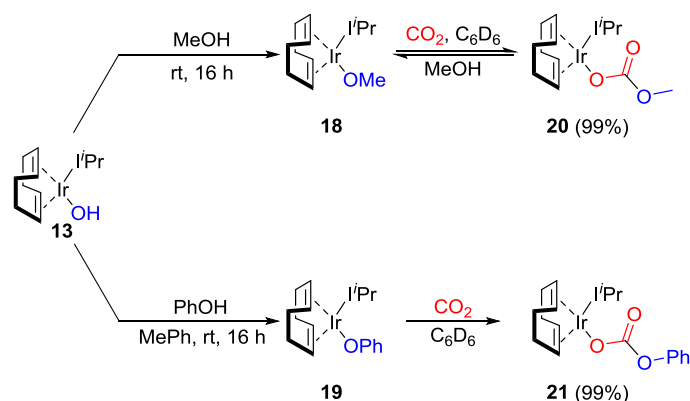
Following the successful preparation of **14**, we examined the reaction with an Ir(I)-hydroxide bearing a more bulky NHC ligand to determine if the procedure was general. Hence [Ir(cod)(IPr)(OH)] (**15**) was reacted with CO₂ in the same way as before (Scheme 5.6). Analysis of the reaction mixture by ¹H and ¹³C{¹H} NMR spectroscopies indicated that a carbonate complex had formed. However, upon release of the CO₂ atmosphere by bubbling Ar through the reaction mixture, the carbonate complex was converted quantitatively back to starting material. Even in the presence of molecular sieves (4 Å) only the starting material could be recovered. It appeared that the increased steric bulk of the IPr ligand had a destabilising effect on the final product and that the equilibrium was dependant on the CO₂ concentration.



Scheme 5.6. reaction between [Ir(cod)(IPr)(OH)] and CO₂

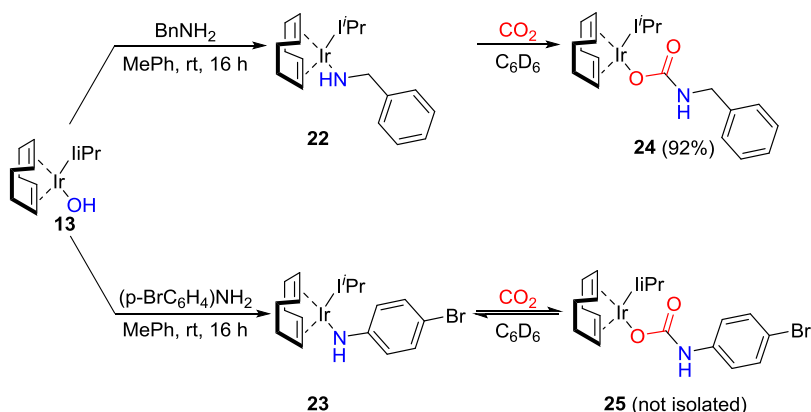
When the reaction was repeated with [Rh(cod)(ICy)(OH)], the product was isolated and identified as a Rh-carbonate complex (**17**) by ¹H and ¹³C{¹H} NMR spectroscopies. However, the product appeared to be unstable and after several days under Ar, the solid had decomposed substantially (by ¹H NMR) and every attempt to analyse the purity of **17** by elemental analysis failed.

The ease with which CO₂ could be inserted into an Ir-OH bond, particularly on the Ir-*i*Pr motif (**13**), led us to examine CO₂ insertion into other Ir(I)-alkoxide bonds in detail. Hence, [Ir(cod)(*i*Pr)(OMe)] (**18**) and [Ir(cod)(*i*Pr)(OPh)] (**19**) (prepared as detailed in Chapter 4),²⁶⁷ were exposed to CO₂. Both complexes rapidly reacted (*ca.* 10 min) to give the corresponding carbonate complexes [Ir(cod)(*i*Pr)(κ¹O-O₂COMe)] (**20**) and [Ir(cod)(*i*Pr)(κ¹O-O₂COPh)] (**21**) respectively (Scheme 5.7), which were isolated as yellow solids quantitatively. When **20** was exposed to methanol, full conversion back to the Ir(I)-methoxide **18** was observed. Presumably methyl hydrogen carbonate was liberated, which is known to spontaneously decompose to yield methanol and CO₂ at temperatures above -36 °C.²⁶⁹



Scheme 5.7. Preparation of monomeric Ir-carbonates by CO₂ insertion.

Amide complexes $[\text{Ir}(\text{cod})(\text{iPr})(\text{NHBN})]$ (**22**) and $[\text{Ir}(\text{cod})(\text{iPr})(\text{NH}(-p\text{-BrC}_6\text{H}_4))]$ (**23**) showed similar reactivity. CO₂ insertion was very fast to give the Ir(I)-carbamate complexes $[\text{Ir}(\text{cod})(\text{iPr})(\kappa^1\text{O-O}_2\text{CNHBN})]$ (**24**) and $[\text{Ir}(\text{cod})(\text{iPr})(\kappa^1\text{O-O}_2\text{CNH}(-p\text{-BrC}_6\text{H}_4))]$ (**25**), respectively (Scheme 5.8). Notably, while both products could be observed and characterised using multinuclear NMR spectroscopies, the former was isolable in quantitative yield, while the latter was only observed under an atmosphere of CO₂. When the CO₂ atmosphere was removed *in vacuo* or Ar was bubbled through the solution, only complex **23** was observed.



Scheme 5.8. CO₂ insertion to prepare Ir(I)-carbamates

Single crystals of **24**, suitable for X-ray analysis were grown from a saturated hexane solution (Figure 5.3). The Ir1-O1 bond is 2.072(6) Å, compared to 2.020(6) Å for Ir(I)-hydroxide **13**.²⁶⁷ The O1-C1 distance is 1.300(10) Å, while O2-C1 is 1.232(10) Å, indicating that the double bond character of the carbonyl is retained. ¹³C{¹H} NMR analysis showed that the quaternary carbamate carbons resonate at 163.2 ppm (**24**) and 159.7 ppm (**25**). This is in agreement with the reported spectra of $[\text{Ir}(\text{CO})(\text{O}_2\text{CNH}(-o\text{-MePh}))(\text{PPh}_3)_2]$, prepared *via* reaction of CO₂ with an amide analogue of Vaska's complex.²⁷⁰ CO₂ insertion into Ir-N bonds may be a crucial step in the conversion of

amines to carbamates or carbamic acids, using CO₂ as a carbon source. This insertion reaction has been reported on several metals, however reports with Ir are scarce.^{257d} The insertion of CO₂ into palladium and platinum amide complexes (bearing PCP pincer ligands) has also been reported, with the carbamate carbon signal resonating at 160.2 ppm (¹³C{¹H} NMR, C₆D₆) for the latter complex.²⁷¹

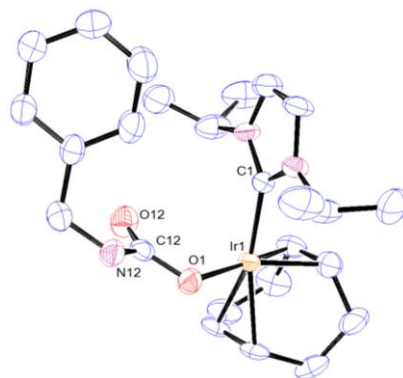
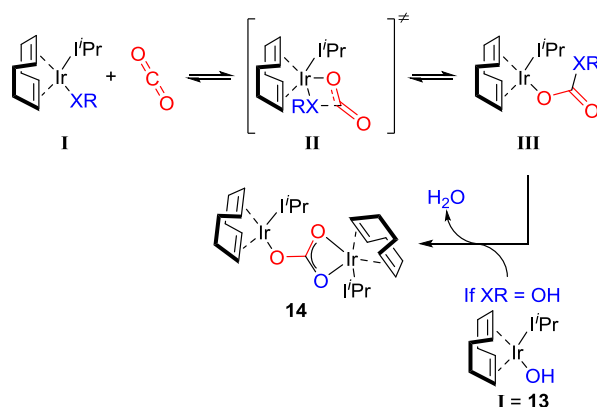


Figure 5.3. Thermal ellipsoid representation of [Ir(cod)(IⁱPr)(κ¹O-O₂CNHBn)] **24** showing 50% thermal ellipsoid probability. Selected bond lengths (Å) and angles (°): Ir1-O1 2.072(6), Ir1-C1 2.058(9), O1-C12 1.300(10), O12-C12 1.232(10), O1-Ir1-C1 91.0(3).

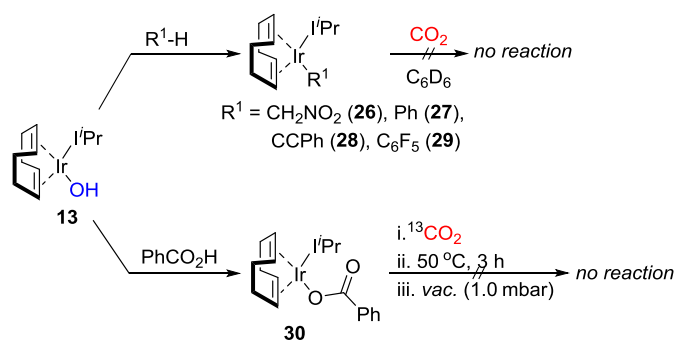
Based on the successful insertion of CO₂ into Ir-N and Ir-O bonds, we proposed that the mechanism might conceivably benefit from a heteroatom on Ir bearing a lone pair. Hence, the proposed mechanism is shown in Scheme 5.9. Nucleophilic attack on the electron-deficient carbon centre of CO₂ by the lone pair of the oxygen or nitrogen (X in compound **I**) would result in transfer of the hydroxide, alkoxide or amide to the carbon atom of the CO₂ moiety, *via* a cyclic transition state **II**. In the case of the starting material being one of the alkoxides or amides, **III** would be the final product, a monomeric carbonate or carbamate respectively. However, if **I** is the Ir(I)-hydroxide (**13**), **III** will be an Ir(I) hydrogen carbonate. The newly formed Ir(I) hydrogen carbonate will have a pK_a of *ca.* 10 (pK_a of NaCO₃H and KCO₃H is 10.3)²⁷² and is therefore open to deprotonation by a second molecule of **13**. This will release a molecule of water and give the bridged carbonate species **14**.



Scheme 5.9. Proposed mechanism for CO₂ insertion into Ir-heteroatom bonds.

To further investigate the scope of this transformation, CO₂ insertion into Ir-C bonds within this scaffold was attempted. There is a precedent for insertion reactions on metal-alkyl complexes, including Rh,²⁷³ Pd²⁷⁴ and Ni,²⁷⁵ hence CO₂ insertion was attempted with various Ir(I)-alkyl complexes bearing *sp*, *sp*² and *sp*³ carbon centres (**26** – **29**, Scheme 5.10, prepared *via* deprotonation reactions from **13**, Chapter 4). Unfortunately all of these complexes proved completely unreactive towards CO₂.

In order to understand whether this inactivity was a result of a lack of thermodynamic favourability or due to a kinetic barrier, we investigated the (de)carboxylation processes involved. Hence, [Ir(cod)(I^{*i*}Pr)(O₂CPh)] (**30**) was prepared from **13** and PhCO₂H (Chapter 4) and dissolved in C₆D₆. Neither heat (50 °C for 3 h) nor vacuum led to any change in the compound structure (as determined by ¹H NMR analysis). The sample was then placed under *ca.* 1 atm. of ¹³CO₂ for 12 h, and ¹³C{¹H} NMR spectroscopic analysis revealed no ¹³C-enrichment on the carbonyl moiety and hence no CO₂ scrambling. These results would suggest that, while both **27** and **30** are stable species, there is a considerable *kinetic* barrier to the (de)carboxylation processes that might link them.²⁷⁶ These results were consistent with our proposed mechanism whereby the CO₂ moiety undergoes nucleophilic attack by an electron-rich heteroatom bound to iridium (Scheme 5.9).



Scheme 5.10. Attempted carboxylation of Ir-C bonds and decarboxylation of Ir-O₂CPh.

5.2.2. Mechanistic studies

Following these results, we were intrigued by how facile the CO₂ insertion reaction was, particularly the reaction with **13** in the solid state. Coupled to this, we sought a better understanding of the reaction mechanism. The nature of the insertion reaction makes it very difficult to isolate potential intermediates and hence, fully elucidate the mechanism. Our approach to the problem was two-fold. We wanted to probe the reaction from a kinetic perspective, using experimental results to calculate the activation parameters. Secondly, we wanted to develop a model of the energy surface to identify potential intermediates and transition states. It was our aim to correlate the experimentally derived activation energies and the theoretically calculated energies to determine the reaction pathway and therefore understand the reaction barriers involved in this reaction. In order to do this, we established collaborations with Dr Paul Webb at Sasol Technologies UK Ltd., to assist us with the kinetic experiments and with Professor Michael Bühl and Hedi Kruger, who investigated the potential energy surface using DFT methods at a PBE0-D3 level of theory.

It is important to know the limitations of theoretical calculations, the accuracy of DFT can be best measured when compared with experimental results obtained by examination of well-defined systems,²⁷⁷ therefore it is important that the two go hand in hand. Investigations of CO₂ insertion into TM-X bonds (where X is an alkoxide or amide) are numerous. However, theoretical investigations of CO₂ insertions of this kind are more limited and direct comparisons between experimental and theoretical findings are rare.^{11, 257d} A good example that draws comparisons between the two approaches has been reported by Lee *et al.*,²⁷⁸ who examined the rapid CO₂ insertion into planar [Ni(II)(pyN₂)(OH)]⁻ (pyN₂ = *N,N'*-(2,6-pyridinedicaboxamidate) to form a Ni-bicarbonate complex.²⁷⁸ The authors reported activation enthalpy ($\Delta H^\ddagger = 3.2(5)$ kcal

mol⁻¹) and entropy ($\Delta S^\ddagger = -20(3)$ cal K⁻¹ mol⁻¹), obtained by monitoring CO₂ fixation by UV/vis spectroscopy. They also performed DFT calculations at the BP86 and B3LYP levels of theory and obtained comparable results for the activation enthalpy (differing by only 1 – 2 kcal mol⁻¹). However, the experimental entropies were consistently lower than the theoretical calculations by *ca.* 14 – 17 cal K⁻¹ mol⁻¹.²⁷⁸ The absolute entropies (and, thus the Gibbs free-energy barriers) are strongly overestimated in computations due to the ideal-gas approximation made in the standard thermodynamic expressions. The activation free energies will suffer from the same over-estimation, particularly in the case of associative, multimolecular transformations, where entropy has a larger contribution to the free energy expression than enthalpy.

Analysis of the Ir(I)-hydroxide **13** by FTIR (ATR) had revealed that the OH stretch was extremely diagnostic ($\nu = 3612.7$ cm⁻¹). Furthermore, the IR spectrum of the product **14** showed no distinct bands in this region. Hence, the hydroxide band of **13** provided a perfect spectroscopic handle with which to monitor reaction progress. An FTIR cell inside a DRIFTS chamber was loaded with **13** (*ca.* 40 mg) and sealed under N₂. A continuous stream of N₂/CO₂ (50:50, 1 atm., 40 mL min⁻¹) was passed over the cell and the reaction progress was monitored by *in situ* FTIR. Figure 5.4 shows a sample stacked plot of the raw FTIR data for the reduced region (ν 3645 – 3577 cm⁻¹) containing the band that corresponds to the OH stretch.

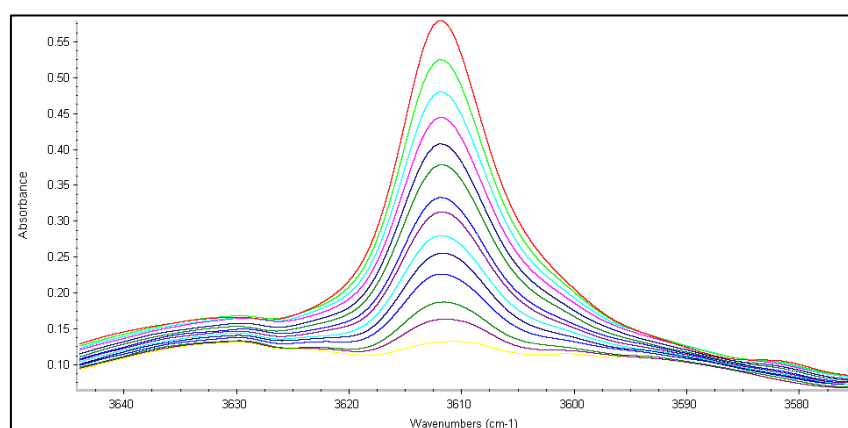


Figure 5.4. Sample raw FTIR data for kinetic experiment (ν 3645 – 3577 cm⁻¹)

Single beam spectra were ratioed against a background of KBr under the same gas atmosphere. The kinetic trace was then determined by measuring the peak height of the OH band as a function of time and the reaction was repeated at five different temperatures between 278 K and 358 K (Figure 5.5). The reaction was studied under pseudo-first order conditions (accounting for a large excess of CO₂) and the kinetic

traces at different temperatures (Figure 5.5) indicated that the reaction was in fact pseudo first order (rate = $k_{\text{obs}}[\mathbf{13}]$).

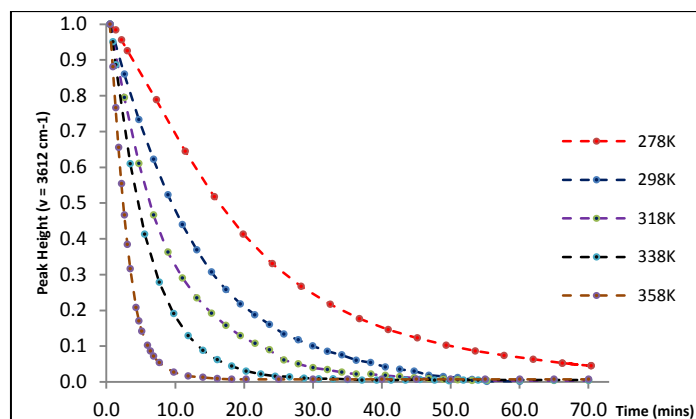


Figure 5.5. Peak height of OH stretch ($\nu = 3612.7 \text{ cm}^{-1}$) vs time at different temperatures

Rate constants were obtained by fitting the kinetic traces to a single exponential using Origin[®] (see experimental section). A linear Eyring plot was obtained with $R^2 = 0.9966$ (Figure 5.6) according to the Eyring equation,

$$k = K \frac{k_B T}{h} e^{\frac{-\Delta G^\ddagger}{RT}} \text{ with } \Delta G^\ddagger = \Delta H^\ddagger - T\Delta S^\ddagger.$$

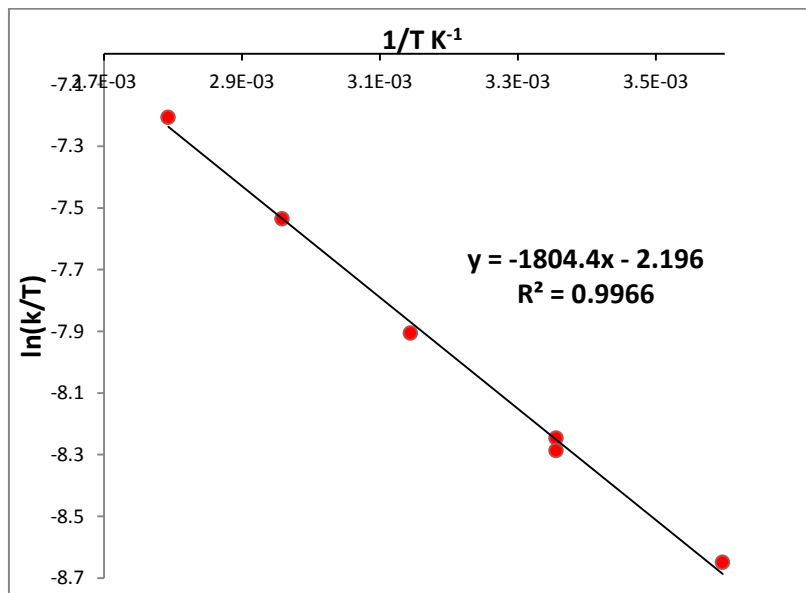


Figure 5.6. Eyring plot ($1/T$ vs $\ln(k/T)$) for reaction between $\mathbf{13}$ and CO₂ in the solid state.

Activation parameters were determined, with error calculated using the least squares method as follows: $\Delta H^\ddagger = 3.6 \pm 0.3 \text{ kcal mol}^{-1}$, $\Delta S^\ddagger = -51.5 \pm 0.9 \text{ cal K}^{-1} \text{ mol}^{-1}$ and ΔG^\ddagger (298 K) = $18.9 \pm 0.4 \text{ kcal mol}^{-1}$. The activation parameters indicate that the insertion of CO₂ is an exergonic process with a small energy barrier to surmount. The

large negative value for entropy is consistent with an associative transition state involving at least two converging molecules.

Following the kinetic experiments, Hedi Kruger and Professor Michael Bühl investigated the potential energy surface using DFT methods at the PBE0-D3 level of theory. Based on our proposed mechanism, the first step in the reaction was considered to be insertion of CO₂ into the Ir-OH bond to yield an iridium hydrogen carbonate intermediate (**32**). An encounter complex was identified as an additional intermediate (**31**) formed by the CO₂ molecule approaching the Ir(I)-OH. Insertion of CO₂ into the Ir-OH bond occurs *via* the four-membered transition state, presenting the first reaction barrier (**TS31-32**, Figure 5.7). Transformation from **31** to **TS31-32** is accompanied by a decrease in inter-atomic distance between the carbon atom and the oxygen atom of the hydroxide moiety (2.62 to 1.54 Å). More importantly, an elongation of the Ir-O bond from 2.02 Å to 2.17 Å was observed. As expected, the geometry of the CO₂ molecule changes from linear to bent with an O-C-O angle of 139.30° as the Ir-OH bond is broken to form the η¹-bicarbonate intermediate (**32**). The insertion of CO₂ to form the bicarbonate intermediate is strongly exothermic such that the enthalpic barrier is insignificant. Hence, the rate limiting step must occur during the encounter with a second molecule of **13** and concomitant elimination of water.

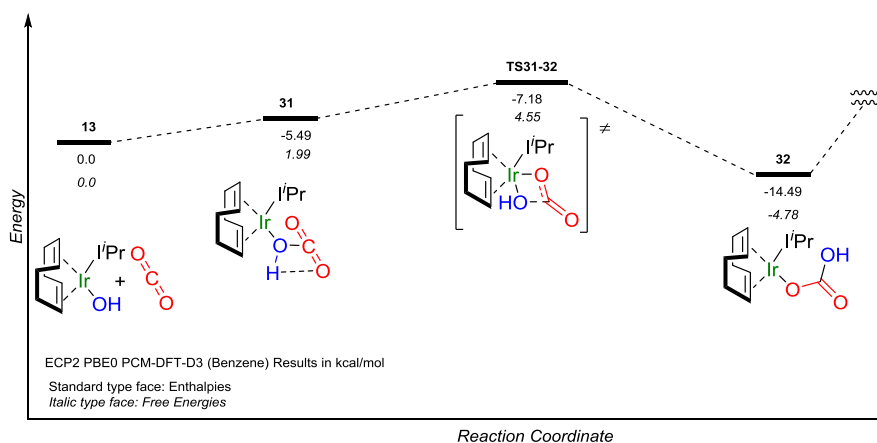


Figure 5.7. Reaction profile (PBE0-D3 level of theory) for CO₂ uptake by **13**

Of the different pathways for dimerisation that were characterised computationally, the most favourable one is shown in Figure 5.8. The encounter between intermediate **32** and a second molecule of **13** leads to formation of a tetrahedral diol intermediate **33**. From intermediate **33**, H₂O elimination occurs *via* an autocatalytic process. An independent water molecule acts as a proton relay, leading to a six

membered transition state (**TS34-14**) and concomitant release of two water molecules to give the final product.

The first enthalpic barrier encountered in the reaction pathway is in the formation of **TS32-33** ($\Delta H^\ddagger = 11.06 \text{ kcal mol}^{-1}$ and $\Delta S^\ddagger = -57.8 \text{ cal K}^{-1} \text{ mol}^{-1}$ at the PBE0-D3 level of theory). The second reaction barrier is the formation of (**TS34-14**), with $\Delta H^\ddagger = 3.47 \text{ kcal mol}^{-1}$ and $\Delta S^\ddagger = -88.5 \text{ cal K}^{-1} \text{ mol}^{-1}$ (both relative to intermediate **32**). At ambient temperature, the first barrier exhibits a $\Delta G^\ddagger = 28.30 \text{ kcal mol}^{-1}$, whilst the second shows a $\Delta G^\ddagger = 29.96 \text{ kcal mol}^{-1}$. The free-energy barrier is largely entropic in nature, in accordance with an associative transition state.

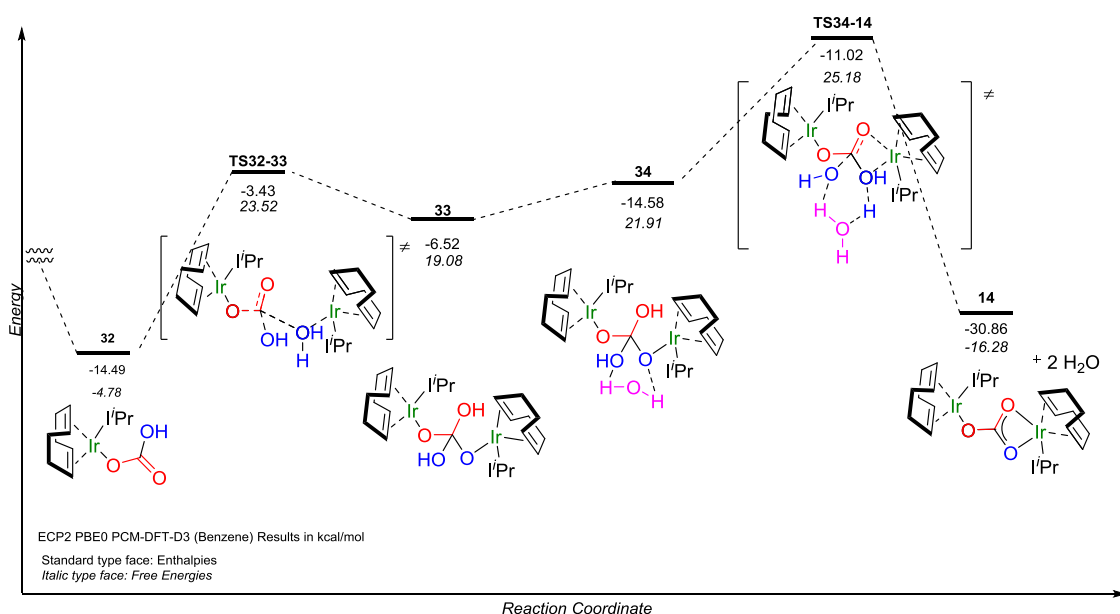


Figure 5.8. Computed (PBE0-D3 level of theory) reaction profile for CO₂ uptake by **13**

The absolute entropies (and, thus the Gibbs free-energy barriers) are strongly overestimated as discussed earlier. Coupled to this is the fact that the kinetic experiments are performed in the solid state and translational entropies in condensed phase tend to be smaller than in the gas phase. Since computed enthalpies are not affected by the overestimation, the near-quantitative accord between measured and calculated ΔH^\ddagger ($3.6 \text{ kcal mol}^{-1}$) gives us confidence that the DFT-derived pathway in Figure 5.7 and 5.8 is reasonable. This implies that a similar mechanism is dominant in the solid state where H₂O would have to diffuse through the solid. It should be noted that **14** is prepared under anhydrous conditions and since the mechanism that is presented depends on the inclusion of autocatalytic water it is reasonable to assume that either the H₂O is present as vapour in the CO₂ and/or that it comes from the reaction

itself. Either way, this will not be the only pathway in operation but rather, it is the most energetically favourable and will become more dominant as the reaction progresses.

In order to understand the apparent equilibrium displayed during the reaction between [Ir(cod)(IPr)(OH)] (**15**) and CO₂ our colleagues calculated the driving force for formation of **16** at the PBE0-D3 level of theory. The driving force for formation of **16** is much lower ($\Delta H = -23.8 \text{ kcal mol}^{-1}$, $\Delta G = -4.0 \text{ kcal mol}^{-1}$) than for the corresponding Ir-IPr product **14** ($\Delta H = -30.9 \text{ kcal mol}^{-1}$, $\Delta G = -15.3 \text{ kcal mol}^{-1}$, Figure 5.9). The small value for ΔG of $-4.0 \text{ kcal mol}^{-1}$ is consistent with the reversible nature of the reaction. The destabilising effect exerted by the added steric bulk appears to manifest in a predicted change in coordination mode from the expected [Ir₂-(μ - $\kappa^1 O$: $\kappa^2 O$, O -CO₃)] to [Ir₂-(μ - $\kappa^1 O$: $\kappa^1 O$ -CO₃)]. Figure 5.9 shows a comparison between the bond lengths of **14** from the obtained crystal structure (italics), calculated bond lengths for **14** (normal type-face) and calculated bond lengths for **16** (bold type-face). From the calculated bond lengths for **16** there appears to be a considerable elongation of the bond between Ir and O² (ca. 2.80 Å). The increase in interatomic distance between these two atoms and decrease in the bond length between Ir and O³ indicates that the μ - κ^1 : κ^1 coordination mode is favoured for this complex. The [{Ir₂-(μ - $\kappa^1 O$: $\kappa^1 O$ -CO₃)] **16** (Figure 5.9) may be unstable and hence, is only observed when under a CO₂ atmosphere.

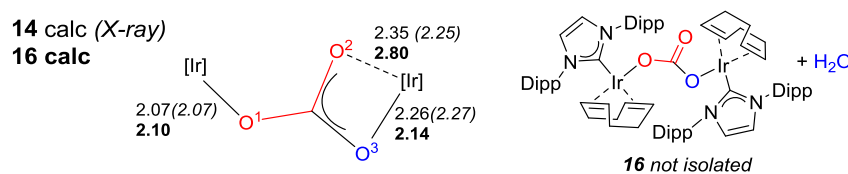


Figure 5.9. Carbonate complexes **14** and **16**. Bond distances shown in Å, **14**: experimental (italics), Calculated (normal type-face), **16** (bold). Calculated at PBE0 level of theory.

5.3. CONCLUSIONS

In summary, we have explored the reactivity of a range of iridium(I) complexes with carbon dioxide, towards the aim of developing new CO₂ fixation strategies. Reaction between Ir(I)-hydroxide and CO₂ led to the isolation of the interesting dimeric 16e⁻/18e⁻ species [Ir₂-(μ - $\kappa^1 O$: $\kappa^2 O$, O -CO₃)] while CO₂ insertion into Ir(I)-alkoxide and Ir(I)-amide bonds led to monomeric Ir(I)-carbonate and Ir(I)-carbamate complexes respectively. The formation of the Ir(I)-carbonate **14** was extremely facile, even in the solid state. The proposed mechanism for CO₂ insertion describes a nucleophilic attack on CO₂ by the lone pair of the bound oxygen or nitrogen atom, resulting in formation of

a new Ir-heteroatom bond. In the case of Ir(I)-hydroxide **13**, a secondary event involves nucleophilic attack by another molecule of Ir(I)-hydroxide to release water and deliver the dimeric carbonate **14**. CO₂ insertion into a variety of Ir(I)-alkyl bonds was unsuccessful, indicating that the mechanism would benefit from the presence of a nucleophilic heteroatom on Ir. To understand the facile nature of the reaction between Ir(I)-hydroxide and CO₂ we performed kinetic investigations in the solid state using FTIR. The derived activation parameters indicated an exergonic reaction with a small energy barrier and an associative transition state. Our collaborators studied the reaction using DFT methods at the PBEO-D3 level of theory based on our proposed mechanism. They found that insertion of CO₂ into the Ir-OH bond was extremely facile with a negligible energy barrier to formation of an iridium hydrogen carbonate intermediate. The rate limiting step involves autocatalytic formation of a six-membered transition state where an independent water molecule acts as a proton relay. In accordance with the experimental values, the entropy for formation of this transition state was high owing to the associative nature of four entities converging. The calculated enthalpy of activation for formation of the transition state ($\Delta H^\ddagger = 3.6 \text{ kcal mol}^{-1}$) is in very good agreement with the experimental value.

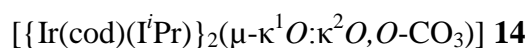
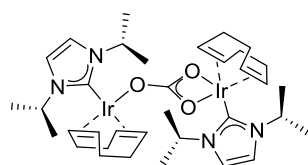
In this study we have shown that iridium complexes may be good candidates for capture of CO₂ and synthetic transformations involving CO₂ as a feedstock. A thorough mechanistic study with comparative theoretical and experimental insights provided valuable information about the nature of CO₂ fixation by Ir(I)-hydroxide.

5.4. EXPERIMENTAL DETAILS

5.4.1. General considerations

All manipulations and reactions were performed on an Ar or CO₂ filled schlenk line unless stated otherwise. All reagents were supplied by Aldrich and used without further purification. Solvents were distilled and dried as required. NMR data was obtained using either a Bruker 300 MHz or 400 MHz spectrometer at 303 K in the specified deuterated solvent. All chemical shifts are given in ppm and coupling constants in Hz. Signals on the ¹³C{¹H} NMR spectra are singlets unless otherwise stated. Spectra were referenced to residual protonated solvent signals (for ¹H) or solvent signals (for ¹³C): (C₆D₆: ¹H δ 7.16 ppm, ¹³C δ 128.06 ppm; THF-*d*₈: ¹H δ 1.72, 3.58 ppm, ¹³C δ 25.31, 67.21 ppm). Infrared spectra (ν) were recorded on a Shimadzu Fourier transform IR Affinity-1 Infrared spectrophotometer using a MIRacle™ single reflection horizontal ATR (diamond). Samples were placed directly on the crystal (ATR) in the solid state. Only characteristic peaks have been quoted. Elemental analyses were performed at the London Metropolitan University. Known compounds were prepared following the procedures reported in the previous chapters. CCDC-956511 (**14**), CCDC-956512 (**24**) contain structural data for new complexes characterised by X-ray single crystal diffraction. Crystallographic data can be obtained free of charge from The Cambridge Crystallographic Data Centre via www.ccdc.cam.ac.uk/data_request/cif.

5.4.2. Synthesis and characterisation data

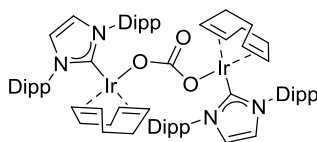


Method A: A J. Young NMR tube was charged with [Ir(cod)(I*Pr)(OH)] **13** (15.0 mg, 0.032 mmol) in C₆D₆ (0.6 mL). The sample was frozen in liquid N₂ and the Ar atmosphere was removed *in vacuo*. The sample was allowed to thaw before CO₂ (*ca.* 1 atm.) was added, a ppt. formed after a few minutes. The reaction mixture was agitated for at least 10 mins before being placed under an Ar atmosphere *via* three vacuum-Ar purge cycles. ¹H NMR analysis revealed full conversion to the product. The product was

dried *in vacuo* to give [$\{\text{Ir}(\text{cod})(\text{I}^i\text{Pr})\}_2(\mu\text{-}\kappa^1\text{O}:\kappa^2\text{O},\text{O}-\text{CO}_3)$] **14** (15.2 mg, 98%) as a yellow solid.

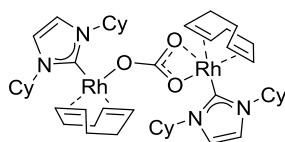
Method B: [$\text{Ir}(\text{cod})(\text{I}^i\text{Pr})(\text{OH})$] **13** (5 mg, 0.011 mmol) was placed in a septum sealed vial and the Ar atmosphere was replaced with CO₂ (1 atm.) by purging the vial for approximately 2 mins. The sample was then placed back under an Ar atmosphere *via* three vacuum-Ar purge cycles before being analysed by IR (ATR) and dissolved in C₆D₆ for analysis by ¹H NMR, which indicated complete conversion to **14**. ¹³C{¹H} NMR analysis was conducted in THF-*d*₈ due to insufficient solubility in C₆D₆.

¹H NMR (500 MHz, C₆D₆): δ 6.30 (s, 4H, N-(CH)₂-N), 5.88 (sept., 4H, ³J_{HH} = 6.7, N-CH(CH₃)₂), 4.60 – 4.53 (m, 4H, cod-CH), 2.76 – 2.65 (m, 4H, cod-CH), 2.41 – 2.30 (m, 4H, cod-CH₂), 2.30 – 2.20 (m, 4H, cod-CH₂), 1.76 – 1.59 (m, 8H, cod-CH₂), 1.47 (d, 12H, ³J_{HH} = 5.3, CH₃), 1.91 (d, 12H, ³J_{HH} = 2.8, CH₃); ¹³C{¹H} NMR (75 MHz, THF-*d*₈): δ 178.8 (Ir-C_{carbene}), 170.0 (CO), 116.9 (N-(CH)₂-N), 82.6 (cod-CH), 53.0 (N-CH(CH₃)₂), 38.8 (cod-CH), 35.3 (cod-CH₂), 30.1 (cod-CH₂), 24.3 (CH₃), 24.1 (CH₃). FTIR (ATR) ν = 1610.6 (s, CO₃), 1411.9 (s, CO₃), 1207.4 (s) cm⁻¹. Anal. Calcd. for C₃₅H₅₆Ir₂N₄O₃ (MW 965.28): C, 43.55; H, 5.85; N, 5.80. Found: C, 43.44; H, 5.86; N, 5.73.



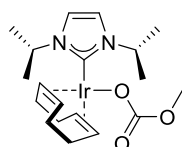
[(Ir(cod)(IPr))₂(CO₃)] **16**

A J-Young type NMR tube was charged with [$\text{Ir}(\text{cod})(\text{IPr})(\text{OH})$] **15** (25 mg, 0.035 mmol) in C₆D₆ (0.6 mL). The sample was frozen in liquid N₂ and the Ar atmosphere was removed *in vacuo*. The sample was allowed to thaw before CO₂ (*ca.* 1 atm.) was added, and the reaction mixture was agitated for at least 10 mins before NMR analysis was conducted. ¹H NMR (300 MHz, C₆D₆): δ 7.29 (t, 5H, ³J_{HH} = 7.6, Ar-H), 7.24 – 7.17 (m, 7H, Ar-H), 6.53 (s, 4H, N-(CH)₂-N), 5.51 – 5.38 (m, 4H, cod-CH), 3.01 – 2.89 (m, 4H, cod-CH), 1.76 – 1.39 (m, 40H, cod-CH₂, CH₃), 1.33 – 1.16 (m, 8H, cod-CH₂), 1.04 (d, 24H, ³J_{HH} = 6.7, CH₃). ¹³C{¹H} NMR (125 MHz, CD₂Cl₂): δ 184.7 (Ir-C_{carbene}), 164.6 (CO₃), 147.1 (ArC), 136.2 (N-ArC), 130.2 (ArCH), 130.0 (ArCH), 124.3 (N-(CH)₂-N), 123.9 (ArCH), 83.7 (cod-CH), 46.7 (cod-CH), 33.3 (CH(CH₃)₂), 29.4 (cod-CH₂), 29.0 (cod-CH₂), 26.8 (CH₃), 22.8 (CH₃).



[{Rh(cod)(ICy)}₂(μ-CO₃)] **17**

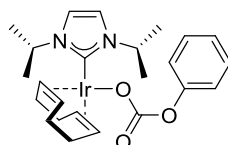
A J-Young NMR tube was charged with [Ir(cod)(ICy)(OH)] (10.0 mg, 0.0217 mmol) in C₆D₆ (0.6 mL). The sample was frozen in liquid N₂ and the Ar atmosphere was removed *in vacuo*. The sample was allowed to thaw before CO₂ (*ca.* 1 atm.) was added. The reaction mixture was agitated for at least 10 mins before NMR analysis was conducted. Once complete, the CO₂ was removed *in vacuo* before the sample was returned to the glove-box. The product was dried to give [{Rh(cod)(ICy)}₂(μ-CO₃)] **17** (11.1 mg, >99%) as a yellow solid. However, the product proved to be unstable in the solid state since ¹H NMR analysis of the same sample after being stored for several days under Ar showed a decomposed product and elemental analysis of the bulk material consistently failed. ¹H NMR (300 MHz, C₆D₆): δ 6.36 (s, 4H, N-(CH)₂-N), 5.56 (tt, 4H, ³J_{HH} = 12.0, 3.8, N-CH(CH₂)₂), 5.54 – 5.46 (m, 4H, cod-CH), 3.46 – 3.29 (m, 4H, cod), 2.75 – 2.60 (m, 4H, ICy-CH₂), 2.51 – 2.26 (m, 8H, cod-CH₂), 2.00 – 0.90 (m, 44H, cod-CH₂, ICy-CH₂). ¹³C{¹H} NMR (75 MHz, THF-*d*₈): δ 182.2 (app. d, Rh-C_{carbene}), 169.3 (¹³CO), 117.2 (N-(CH)₂-N), 97.9 (d, *J* = 7.0, cod-CH), 66.7 (d, *J* = 14.3, cod-CH), 60.5 (N-CH(CH₂)₂), 34.4 (cod-CH₂), 34.3 (ICy-CH₂), 33.7 (ICy-CH₂), 29.5 (cod-CH₂), 26.5 (ICy-CH₂), 26.0 (ICy-CH₂), 25.7 (ICy-CH₂).



[Ir(cod)(*i*Pr)(κ¹O-OCO₂CH₃)] **20**

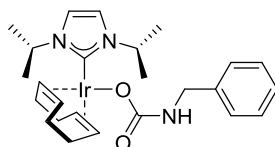
A J. Young NMR tube was charged with [Ir(cod)(*i*Pr)(OMe)] **18** (10.0 mg, 0.021 mmol, prepared following literature procedure²⁶⁷) in C₆D₆ (0.6 mL). The sample was frozen in liquid N₂ and the Ar atmosphere was removed *in vacuo*. The sample was allowed to thaw before CO₂ (*ca.* 1 atm.) was added. The reaction mixture was mixed for at least 10 mins before NMR analysis was conducted. Once complete, the CO₂ atmosphere was removed *in vacuo* before the sample was returned to the glove-box where it was dried *in vacuo* to give [Ir(cod)(*i*Pr)(κ¹O-OCO₂CH₃)] **20** (11 mg, 99%) as a yellow solid. ¹H NMR (300 MHz, C₆D₆): δ 6.22 (s, 2H, N-(CH)₂-N), 5.84 (sept., 2H, ³J_{HH} = 6.6, CH(CH₃)₂), 5.03 – 4.82 (m, 2H, cod-CH), 3.58 (s, 3H, OCH₃), 3.00 – 2.83

(m, 2H, cod-CH), 2.37 – 2.12 (m, 4H, cod-CH₂), 1.71 – 1.51 (m, 4H, cod-CH₂), 1.31 (d, 6H, ³J_{HH} = 6.4, 6H, N-CH(CH₃)₂), 1.12 (d, 6H, ³J_{HH} = 6.8, N-CH(CH₃)₂). ¹³C{¹H} NMR (75 MHz, C₆D₆): δ 178.3 (Ir-C_{carbene}), 160.9 (Ir-OCO), 116.3 (N-(CH)₂-N), 84.3 (N-CH(CH₃)₂), 53.2 (cod-CH), 52.5 (OCH₃), 47.7 (cod-CH), 34.2 (cod-CH₂), 29.4 (cod-CH₂), 23.7 (N-CH(CH₃)₂), 23.6 (N-CH(CH₃)₂). **FTIR (ATR)** ν = 1649.14 (w), 1624.06 (w), 1411.89 (s), 1207.49 (s) cm⁻¹. **Anal. Calcd.** for C₁₉H₃₁IrN₂O₃ (MW 527.68): C, 43.25; H, 5.92; N, 5.31. Found: C, 43.17; H, 6.01; N, 5.40.

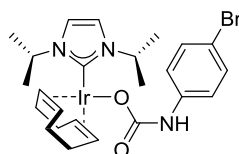


[Ir(cod)(IPr)(κ¹OCO₂Ph)] **21**

A J. Young NMR tube was charged with [Ir(cod)(IPr)(OPh)] **19** (16.9 mg, 0.031 mmol) in C₆D₆ (0.6 mL). The sample was frozen in liquid N₂ and the Ar atmosphere was removed *in vacuo*. The sample was allowed to thaw before CO₂ (*ca.* 1 atm.) was added. The reaction mixture was mixed for at least 10 mins before NMR analysis was conducted. Once complete, the CO₂ atmosphere was removed *in vacuo* before the sample was returned to the glove-box where it was dried *in vacuo* to give [Ir(cod)(IPr)(κ¹OCO₂Ph)] **21** (18.4 mg, >99%) as a yellow solid. ¹H NMR (300 MHz, C₆D₆): δ 7.22 (t, 2H, ³J_{HH} = 7.3, *m*-ArH), 7.09 – 6.94 (m, 2H, *o*-ArH), 6.75 (t, 1H, ³J_{HH} = 7.2, *p*-ArH), 6.14 (s, 2H, N-(CH)₂-N), 5.76 (sept., 2H ³J_{HH} = 6.7, N-CH(CH₃)₂), 4.92–4.82 (m, 2H, cod-CH), 2.95 – 2.83 (m, 2H, cod-CH), 2.39 – 2.18 (m, 4H, cod-CH₂), 1.77 – 1.57 (m, 4H, cod-CH₂), 1.13 (d, 6H, ³J_{HH} = 6.7, CH₃), 1.09 (d, 6H, ³J_{HH} = 6.8, CH₃). ¹³C{¹H} NMR (75 MHz, C₆D₆): δ 179.2 (Ir-C_{carbene}), 129.1 (ArCH), 128.8 (ArCH), 124.8 (ArCH), 116.2 (N-(CH)₂-N), 83.1 (cod-CH), 52.4 (N-CH(CH₃)₂), 46.0 (cod-CH), 34.4 (cod-CH₂), 29.6 (cod-CH₂), 23.7 (CH₃), 23.5 (CH₃). ¹³C{¹H} NMR (75 MHz, THF-*d*₈): δ 179.2 (Ir-C_{carbene}), 176.9 (ArC), 162.9 (br., CO), 128.5 (ArCH), 121.1 (ArCH), 117.2 (N-(CH)₂-N), 114.8 (ArCH), 82.2 (cod-CH), 52.9 (N-CH(CH₃)₂), 46.1 (cod-CH), 34.5 (cod-CH₂), 29.7 (cod-CH₂), 23.7 (CH₃), 23.5 (CH₃). **FTIR (ATR)** ν = 1583.56 (s), 1477.47 (s), 1296.16 (s), 1209.37 (s) cm⁻¹. **Anal. Calcd.** for C₂₄H₃₃IrN₂O₃ (MW 589.75): C, 48.88; H, 5.64; N, 4.75. Found: C, 48.77; H, 5.68; N, 4.79. *ArC and CO ¹³C{¹H} NMR signals were not observed in C₆D₆.

[Ir(cod)(I^{*i*}Pr)(κ¹O₂CNHBn)] **24**

A vial was charged with [Ir(cod)(I^{*i*}Pr)(NHBn)] **22** (17.4 mg, 0.031 mmol) and C₆D₆ (0.6 mL). The sample was frozen in liquid N₂ and the Ar atmosphere was removed *in vacuo*. The sample was allowed to thaw before CO₂ (*ca.* 1 atm.) was added. The reaction mixture was mixed for at least 10 mins before NMR analysis was conducted. Once complete, the CO₂ was removed *in vacuo* before the sample was returned to the glove-box and was dried *in vacuo* to give [Ir(cod)(I^{*i*}Pr)(κ¹O₂CNHBn)] **24** (17.1 mg, 92%) as a yellow solid. ¹H NMR (300 MHz, C₆D₆): δ 7.15 – 7.00 (m, 5H, ArH), 6.29 (s, 2H, N-(CH)₂-N), 5.74 (sept., 2H, ³J_{HH} = 6.7, N-CH(CH₃)₂), 4.95 – 4.82 (m, 2H, cod-CH), 4.49 (t, 1H, ³J_{HH} = 5.8, NH), 4.30 (d, 2H, ³J_{HH} = 5.6, NH-CH₂), 2.98 – 2.86 (m, 2H, cod-CH), 2.41 – 2.19 (m, 4H, cod-CH₂), 1.76 – 1.59 (m, 4H, cod-CH₂), 1.33 (d, 6H, ³J_{HH} = 6.6, CH₃), 1.16 (d, 6H ³J_{HH} = 6.8, CH₃). ¹³C{¹H} NMR (75 MHz, C₆D₆): δ 179.0 (Ir-C_{carbene}), 163.2 (CO), 142.7 (ArC), 128.2 (ArCH, from HSQC and HMBC), 126.4 (ArCH), 116.1 (N-(CH)₂-N), 83.7 (cod-CH), 52.5 (N-CH(CH₃)₂), 47.0 (cod-CH), 46.5 (NH-CH₂), 34.4 (cod-CH₂), 29.5 (cod-CH₂), 23.9 (CH₃), 23.6 (CH₃). ¹H NMR (400 MHz, THF-*d*₈): δ 7.18 – 7.09 (m, 5H, ArH), 7.06 (s, 2H, N-(CH)₂-N), 5.58 (sept., 2H, ³J_{HH} = 6.7, N-CH(CH₃)₂), 4.91 (br., 1H, NH), 4.39 (br., 2H, cod-CH), 4.08 (d, 2H, ³J_{HH} = 6.08, NH-CH₂), 2.70 (br., 2H, cod-CH), 2.27 – 2.07 (m, 4H, cod-CH₂), 1.64 – 1.51 (m, 4H, cod-CH₂), 1.45 (d, 6H, ³J_{HH} = 6.6, CH₃), 1.36 (d, 6H, ³J_{HH} = 6.5, CH₃). ¹³C{¹H} NMR (100 MHz, THF-*d*₈): δ 179.0 (Ir-C_{carbene}), 163.3 (CO), 143.6 (ArC), 128.3 (ArCH), 127.8 (ArCH), 126.4 (ArCH), 116.9 (N-(CH)₂-N), 82.9 (cod-CH), 52.9 (N-CH(CH₃)₂), 46.7 (cod-CH), 46.4 (NH-CH₂), 34.4 (cod-CH₂), 29.6 (cod-CH₂), 23.9 (CH₃), 23.4 (CH₃). **FTIR (ATR)** ν = 2054.19 (s), 1967.39 (s), 1409.96 (s), 1209.37 (s) cm⁻¹. **Anal. Calcd.** for C₂₅H₃₆IrN₃O₂ (MW 602.79): C, 49.81; H, 6.02; N, 6.97. Found: C, 49.80; H, 5.87; N, 7.02. *NMR was run in THF-*d*₈ in order to locate all Ar signals.



[Ir(cod)(IⁱPr)(κ¹O₂CNH-(*p*-BrC₆H₄)] **25**

A J. Young NMR tube was charged with [Ir(cod)(IⁱPr)(NH-(*p*-BrC₆H₄))] **23** (20.0 mg, 0.032 mmol, prepared following literature procedure²⁶⁷) in C₆D₆. The sample was frozen in liquid N₂ and the Ar atmosphere was removed *in vacuo*. The sample was allowed to thaw before CO₂ (*ca.* 1 atm.) was added. The reaction mixture was mixed for at least 10 mins before NMR analysis was conducted. Upon completion it was found that either bubbling Ar through the reaction mixture or concentrating the sample *in vacuo* converted the product back to **23**. ¹H NMR (300 MHz, C₆D₆): δ 7.27 – 7.18 (m, 4H, ArH), 6.24 (s, 2H, N-(CH)₂-N), 5.68 (sept., 2H, ³J_{HH} = 6.7, N-CH(CH₃)₂), 4.96 – 4.86 (m, 2H, cod-CH), 2.98 – 2.4 (m, 2H, cod-CH), 2.38 – 2.16 (m, 4H, cod-CH₂), 1.74 – 1.55 (m, 4H, cod-CH₂), 1.25 (d, 6H, ³J_{HH} = 6.7, CH₃), 1.11 (d, 6H, ³J_{HH} = 6.8, CH₃). ¹³C{¹H} NMR (75 MHz, C₆D₆): δ 178.1 (Ir-C_{carbene}), 159.7 (CO), 142.0 (N-ArC), 131.6 (*m*-ArCH), 119.4 (*o*-ArCH), 116.3 (N-(CH)₂-N), 112.4 (ArCBr), 83.8 (cod-CH), 52.5 (N-CH(CH₃)₂), 47.7 (cod-CH), 34.3 (cod-CH₂), 29.4 (cod-CH₂), 23.7 (CH₃), 23.6 (CH₃).

5.4.1. Kinetic Experiments

Kinetic measurements were performed in the solid state using a low temperature DRIFTS chamber (Harrick). Complex **13** (*ca.* 40 mg) was loaded into the chamber, which was then purged with N₂ (50 mL min⁻¹) for *ca.* 30 minutes. The chamber was then heated or cooled to the desired reaction temperature and isolated using ball valves situated at the inlet and outlet lines. The gas inlet line was then purged with a mixture of N₂ and CO₂ (1:1, 1 atm, 40 mL min⁻¹ combined). During the collection of a data series (Nicolet Nexus FTIR spectrometer, 4 cm⁻¹ resolution, 32 scans per spectrum) the N₂/CO₂ gas stream was passed through the chamber at 40 mL min⁻¹. Single beam spectra were ratioed against a background of KBr under the same gas atmosphere. Kinetic traces were then determined by measurement of the peak height of the OH stretch of Ir-OH as a function of time.

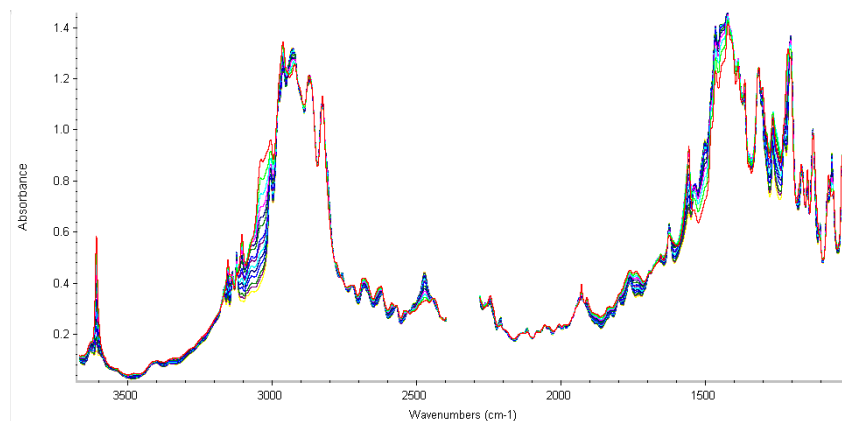


Figure 5.10 Sample raw FTIR data for kinetic experiment (ν 3700 – 1000 cm^{-1})

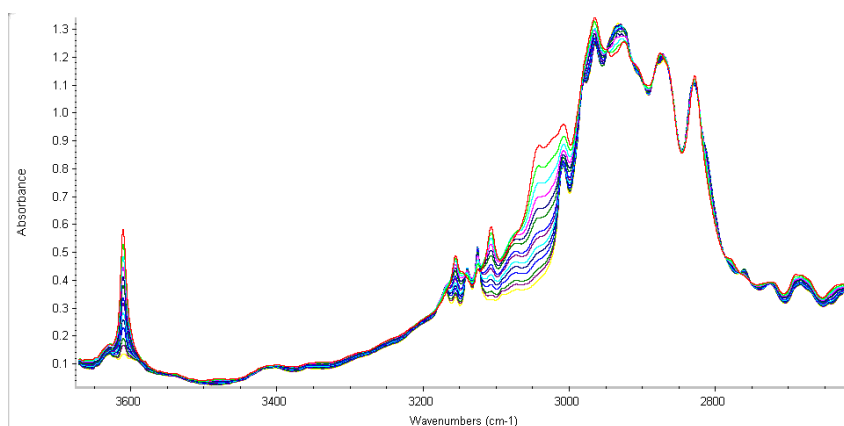


Figure 5.11 Sample raw FTIR data for kinetic experiment (ν 3700 – 2600 cm^{-1})

Table 5.1 Peak Height vs time at 278K

Time (mins)	Peak Height	Normalised time (mins)	Normalised peak Height
2.5260	0.5540	0.5000	1.0000
3.3690	0.5450	1.3430	0.9838
4.2110	0.5300	2.1850	0.9567
5.0530	0.5130	3.0270	0.9260
9.2630	0.4370	7.2370	0.7888
13.4740	0.3570	11.4480	0.6444
17.6840	0.2870	15.6580	0.5181
21.8950	0.2290	19.8690	0.4134
26.1060	0.1830	24.0800	0.3303
30.3170	0.1480	28.2910	0.2671
34.5280	0.1200	32.5020	0.2166
38.7380	0.0980	36.7120	0.1769
42.9490	0.0810	40.9230	0.1462
47.1590	0.0680	45.1330	0.1227
51.3690	0.0570	49.3430	0.1029
55.5790	0.0480	53.5530	0.0866
59.7890	0.0410	57.7630	0.0740
64.0000	0.0350	61.9740	0.0632
68.2100	0.0290	66.1840	0.0523
72.4210	0.0250	70.3950	0.0451
68.2100	0.0290	66.1840	0.0523
72.4210	0.0250	70.3950	0.0451

Table 5.2 Peak Height vs time at 298K (A)

Time (mins)	Peak Height	Normalised time (mins)	Normalised peak Height
2.5260	0.5960	0.5000	1.0000
4.6320	0.5130	2.6060	0.8607
6.7370	0.4370	4.7110	0.7332
8.8420	0.3710	6.8160	0.6225
10.9470	0.3120	8.9210	0.5235
13.0510	0.2620	11.0250	0.4396
15.1550	0.2200	13.1290	0.3691
17.2590	0.1830	15.2330	0.3070
19.3640	0.1540	17.3380	0.2584
21.4680	0.1300	19.4420	0.2181
23.5720	0.1120	21.5460	0.1879
25.6760	0.0960	23.6500	0.1611
27.7800	0.0800	25.7540	0.1342
29.8840	0.0700	27.8580	0.1174
31.9890	0.0600	29.9630	0.1007
34.0930	0.0510	32.0670	0.0856
36.1970	0.0450	34.1710	0.0755
38.3010	0.0360	36.2750	0.0604
40.4050	0.0320	38.3790	0.0537
42.5100	0.0250	40.4840	0.0419
44.6150	0.0210	42.5890	0.0352
46.7200	0.0180	44.6940	0.0302
48.8240	0.0110	46.7980	0.0185
50.9280	0.0090	48.9020	0.0151

53.0320	0.0070	51.0060	0.0117
55.1370	0.0040	53.1110	0.0067
57.2410	0.0010	55.2150	0.0017
57.2410	0.0010	60.0000	0.0017

Table 5.3 Peak Height vs time at 298K (B)

Time (mins)	Peak Height	Normalised time (mins)	Normalised peak Height
2.1050	0.5640	0.5000	1.0000
2.5260	0.5550	0.9210	0.9840
4.6310	0.4950	3.0260	0.8777
6.7350	0.4250	5.1300	0.7535
8.8400	0.3570	7.2350	0.6330
10.9440	0.3020	9.3390	0.5355
13.0480	0.2560	11.4430	0.4539
15.1530	0.2180	13.5480	0.3865
17.2570	0.1860	15.6520	0.3298
19.3610	0.1630	17.7560	0.2890
21.4650	0.1420	19.8600	0.2518
23.5690	0.1250	21.9640	0.2216
25.6730	0.1100	24.0680	0.1950
27.7770	0.0970	26.1720	0.1720
29.8810	0.0870	28.2760	0.1543
31.9860	0.0770	30.3810	0.1365
34.0900	0.0690	32.4850	0.1223
36.1940	0.0610	34.5890	0.1082
38.2980	0.0540	36.6930	0.0957
40.4020	0.0490	38.7970	0.0869
42.5060	0.0430	40.9010	0.0762
44.6110	0.0390	43.0060	0.0691
46.7150	0.0340	45.1100	0.0603
48.8190	0.0300	47.2140	0.0532
50.9240	0.0270	49.3190	0.0479
53.0280	0.0240	51.4230	0.0426
55.1310	0.0210	53.5260	0.0372
57.2350	0.0180	55.6300	0.0319
57.2350	0.0180	60.0000	0.0319
57.2350	0.0180	65.0000	0.0319
57.2350	0.0180	70.0000	0.0319

Table 5.4 Peak Height vs time at 318K

Time (mins)	Peak Height	Normalised time (mins)	Normalised peak Height
2.5270	0.5570	0.5000	1.0000
4.6320	0.4430	2.6050	0.7953
6.7380	0.3400	4.7110	0.6104
8.8430	0.2600	6.8160	0.4668
10.9480	0.2020	8.9210	0.3627
13.0530	0.1620	11.0260	0.2908
15.1580	0.1310	13.1310	0.2352
17.2630	0.1070	15.2360	0.1921
19.3690	0.0880	17.3420	0.1580
21.4740	0.0720	19.4470	0.1293
23.5800	0.0600	21.5530	0.1077
25.6850	0.0500	23.6580	0.0898
27.7900	0.0410	25.7630	0.0610
29.8950	0.0340	27.8680	0.0503
31.9990	0.0280	29.9720	0.0395
34.1030	0.0220	32.0760	0.0341

36.2070	0.0190	34.1800	0.0269
38.3110	0.0150	36.2840	0.0215
40.4150	0.0120	38.3880	0.0215
42.5190	0.0120	40.4920	0.0180
44.6230	0.0100	42.5960	0.0144
46.7270	0.0080	44.7000	0.0108
48.8310	0.0060	46.8040	0.0090
50.9350	0.0050	48.9080	0.0072
53.0390	0.0040	51.0120	0.0054
55.1430	0.0030	53.1160	0.0036
57.2470	0.0020	55.2200	0.0036
57.2470	0.0020	60.0000	0.0036
57.2470	0.0020	65.0000	0.0036
57.2470	0.0020	70.0000	0.0036

Table 5.5 Peak Height vs time at 338K

Time (mins)	Peak Height	Normalised time (mins)	Normalised peak Height
1.6850	0.5660	0.5000	1.0000
2.1060	0.5380	0.9210	0.9505
2.5270	0.5020	1.3420	0.8869
4.6340	0.3450	3.4490	0.6095
6.7390	0.2340	5.5540	0.4134
8.8450	0.1580	7.6600	0.2792
10.9500	0.1080	9.7650	0.1908
13.0550	0.0730	11.8700	0.1290
15.1590	0.0500	13.9740	0.0883
17.2630	0.0350	16.0780	0.0618
19.3670	0.0250	18.1820	0.0442
21.4710	0.0170	20.2860	0.0300
23.5750	0.0123	22.3900	0.0217
25.6790	0.0090	24.4940	0.0159
27.7830	0.0080	26.5980	0.0141
29.8880	0.0060	28.7030	0.0106
31.9920	0.0050	30.8070	0.0088
34.0970	0.0050	32.9120	0.0088
36.2020	0.0040	35.0170	0.0071
38.3070	0.0030	37.1220	0.0053
40.4120	0.0030	39.2270	0.0053
42.5160	0.0030	41.3310	0.0053
44.6210	0.0030	43.4360	0.0053
46.7250	0.0040	45.5400	0.0071
48.8300	0.0030	47.6450	0.0053
50.9340	0.0020	49.7490	0.0035
53.0390	0.0030	51.8540	0.0053
55.1430	0.0030	53.9580	0.0053
55.1430	0.0030	55.0000	0.0053
55.1430	0.0030	60.0000	0.0053
55.1430	0.0030	65.0000	0.0053
55.1430	0.0030	70.0000	0.0053

Table 5.6 Peak Height vs time at 358K

Time (mins)	Peak Height	Normalised time (mins)	Normalised peak Height
1.6850	0.5570	0.5000	1.0000
2.1070	0.4910	0.9220	0.8815
2.5280	0.4270	1.3430	0.7666
2.9490	0.3650	1.7640	0.6553
3.3700	0.3090	2.1850	0.5548

3.7910	0.2600	2.6060	0.4668
4.2120	0.2140	3.0270	0.3842
4.6340	0.1760	3.4490	0.3160
5.4750	0.1160	4.2900	0.2083
5.8960	0.0950	4.7110	0.1706
6.3170	0.0790	5.1320	0.1418
7.1590	0.0570	5.9740	0.1023
7.5800	0.0480	6.3950	0.0862
8.0010	0.0400	6.8160	0.0718
8.8440	0.0300	7.6590	0.0539
10.9500	0.0150	9.7650	0.0269
13.0550	0.0090	11.8700	0.0162
15.1610	0.0070	13.9760	0.0126
17.2670	0.0050	16.0820	0.0090
19.3730	0.0040	18.1880	0.0072
21.4790	0.0040	20.2940	0.0072
21.4790	0.0040	25.0000	0.0072
21.4790	0.0040	30.0000	0.0072
21.4790	0.0040	35.0000	0.0072
21.4790	0.0040	40.0000	0.0072
21.4790	0.0040	45.0000	0.0072
21.4790	0.0040	50.0000	0.0072
21.4790	0.0040	55.0000	0.0072
21.4790	0.0040	60.0000	0.0072
21.4790	0.0040	65.0000	0.0072
21.4790	0.0040	70.0000	0.0072

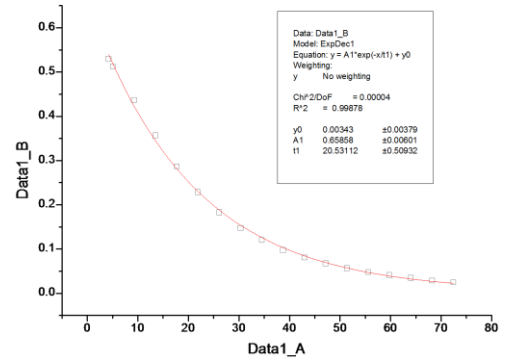


Figure 5.12 Single exponential fit for data collected at 278K

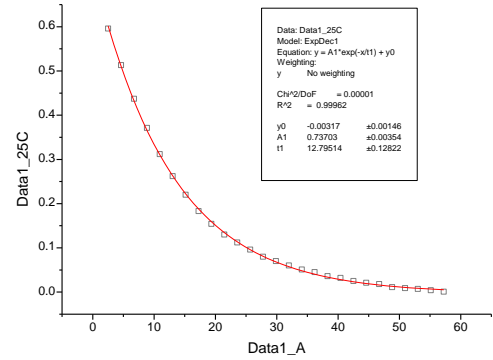


Figure 5.13 Single exponential fit for data collected at 298K

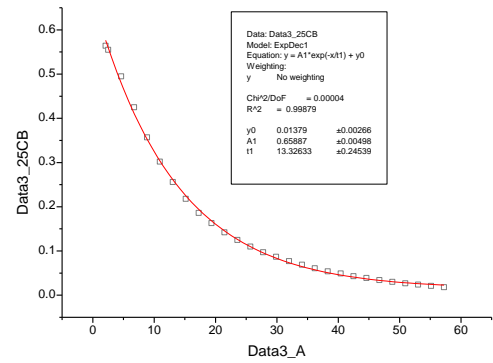


Figure 5.14 Single exponential fit for data collected at 298K

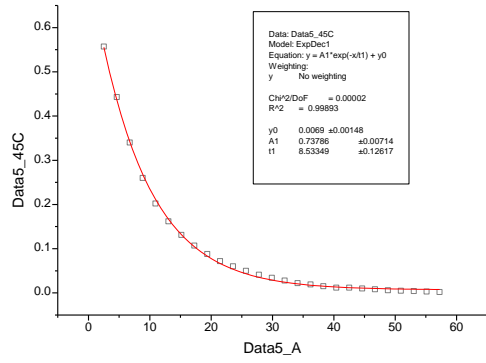


Figure 5.15 Single exponential fit for data collected at 318K

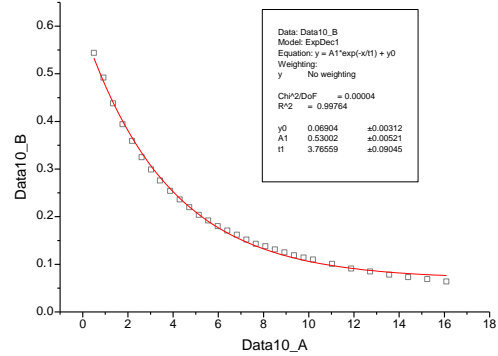


Figure 5.17 Single exponential fit for data collected at 358K

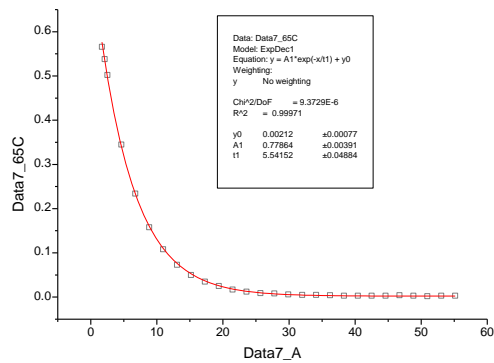


Figure 5.16 Single exponential fit for data collected at 338K

Table 5.7 Values for k, Ln(k) and Ln(k/T) from ORIGIN fitting

T(K)	1/T (K ⁻¹)	t1	k _{obs} (s ⁻¹)	ln(k)	ln(k/T)
278	0.003597	20.53112	0.048707	-3.02194	-8.64956
298	0.003356	12.79514	0.078155	-2.54907	-8.24616
298	0.003356	13.32633	0.075039	-2.58974	-8.28684
318	0.003145	8.53349	0.117185	-2.144	-7.90605
338	0.002959	5.54152	0.180456	-1.71227	-7.53531
358	0.002793	3.76559	0.265563	-1.3259	-7.20644

5.4.2. Calculation of activation parameters

The Activation parameters were determined using the following equations:

Free energy equation:

$$\Delta G^\ddagger = \Delta H^\ddagger - T\Delta S^\ddagger$$

Eyring Equation:

$$k = K \frac{k_b T}{h} e^{-\frac{\Delta G^\ddagger}{RT}}$$

for K = 1:

$$\ln\left(\frac{k}{T}\right) = -\frac{\Delta H^\ddagger}{R} \cdot \frac{1}{T} + \ln\left(\frac{k_b}{h}\right) + \frac{\Delta S^\ddagger}{R}$$

- k = rate constant (k_{obs})
- R = 8.3144 J mol⁻¹ K⁻¹
- K = transmission coefficient; assumed to be 1
- k_B = 1.381 · 10⁻²³ J K⁻¹
- T = absolute temperature (K)
- h = Plank's constant (6.626 10⁻³⁴ J s)
- ΔG[‡] = free energy of activation
- ΔH[‡] = enthalpy of activation
- ΔS[‡] = entropy of activation

Calculation of errors:

$$S_{y/x} = \sqrt{\frac{\sum_i (y_i - \hat{y}_i)^2}{n - 2}}$$

$$S_b = \frac{S_{y/x}}{\sqrt{\sum_i (x_i - \bar{x})^2}}$$

$$S_a = S_{y/x} \sqrt{\frac{\sum_i x_i^2}{n \cdot \sum_i (x_i - \bar{x})^2}}$$

$$S_{\Delta H^\ddagger} = R \cdot S_b$$

$$S_{\Delta S^\ddagger} = R \cdot S_a$$

$$S_{\Delta G^\ddagger} = \sqrt{(S_{\Delta H^\ddagger})^2 + (T \cdot S_{\Delta S^\ddagger})^2}$$

$$\text{Error}_X = t_{95\%} \cdot S_X$$

$$t_{95\% (n=2)} = 4.30$$

$$t_{95\% (n=3)} = 3.18$$

$$t_{95\% (n=4)} = 2.78$$

$$t_{95\% (n=10)} = 2.23$$

$$S_{y/x} = \text{Model STD}$$

$$S_b = \text{slope STD}$$

$$S_a = \text{intercept STD}$$

y_i = experimental values on the y axis

ŷ_i = calculated values on the y axis

n = number of experimental value

$N = n - 2 =$ degrees of freedom

$x_i =$ experimental values on the x axis

$\bar{x} =$ x_i average values

$t =$ t-student parameter with N degrees of freedom (95% confidence level)

$b =$ slope

$a =$ intercept

Table 5.8. Calculated activation parameters

a (intercept)	-2.196032	$\Delta H^\ddagger = 3.6 \pm 0.3 \text{ kcal mol}^{-1}$ $\Delta S^\ddagger = -51.5 \pm 0.9 \text{ cal mol}^{-1} \text{ K}^{-1}$ $\Delta G^\ddagger_{(298\text{K})} = 18.9 \pm 0.4 \text{ kcal mol}^{-1}$
b (slope)	-1804.429	
$S_{y/x}$	0.034831	
S_a	0.170036	
S_b	52.9361	
$t_{95\%}$	2.776445	
K_B (cal/K)	3.298E-24	
h (cal s)	1.584E-34	
R (cal/mol K)	1.986	
Error a	0.472095	
Error b	146.9742	
ΔH^\ddagger (kcal/mol)	3.6	
ΔS^\ddagger (cal/mol K)	-51.5	
$\Delta G^\ddagger_{298\text{K}}$ (kcal/mol)	18.9	
$S\Delta H^\ddagger$ (kcal/mol)	0.11	
$S\Delta S^\ddagger$ (cal/mol K)	0.34	
$S\Delta G^\ddagger_{298\text{K}}$ (kcal/mol)	0.146	
Error ΔH^\ddagger (kcal/mol)	0.3	
Error ΔS^\ddagger (cal/mol K)	0.9	
Error ΔG^\ddagger (kcal/mol)	0.4	

5.4.3. DFT Calculations

Gaussian 09, Revision **D.01**, M. J. Frisch, G. W. Trucks, H. B. Schlegel, G. E. Scuseria, M. A. Robb, J. R. Cheeseman, G. Scalmani, V. Barone, B. Mennucci, G. A. Petersson, H. Nakatsuji, M. Caricato, X. Li, H. P. Hratchian, A. F. Izmaylov, J. Bloino, G. Zheng, J. L. Sonnenberg, M. Hada, M. Ehara, K. Toyota, R. Fukuda, J. Hasegawa, M. Ishida, T. Nakajima, Y. Honda, O. Kitao, H. Nakai, T. Vreven, J. A. Montgomery, Jr., J. E. Peralta, F. Ogliaro, M. Bearpark, J. J. Heyd, E. Brothers, K. N. Kudin, V. N. Staroverov, R. Kobayashi, J. Normand, K. Raghavachari, A. Rendell, J. C. Burant, S. S. Iyengar, J. Tomasi, M. Cossi, N. Rega, J. M. Millam, M. Klene, J. E. Knox, J. B. Cross, V. Bakken, C. Adamo, J. Jaramillo, R. Gomperts, R. E. Stratmann, O. Yazyev, A. J. Austin, R. Cammi, C. Pomelli, J. W. Ochterski, R. L. Martin, K. Morokuma, V. G. Zakrzewski, G. A. Voth, P. Salvador, J. J. Dannenberg, S. Dapprich, A. D. Daniels, Ö. Farkas, J. B. Foresman, J. V. Ortiz, J. Cioslowski, and D. J. Fox, Gaussian, Inc., Wallingford CT, 2009.

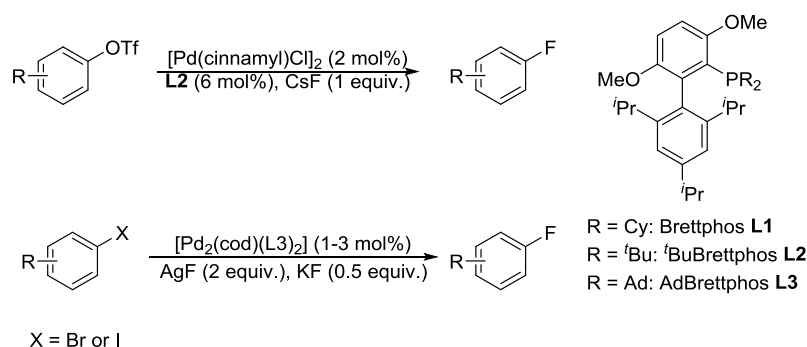
6. FLUORIDE, BIFLUORIDE AND TRIFLUOROMETHYL COMPLEXES OF IRIDIUM(I) AND RHODIUM(I)

6.1. INTRODUCTION

The importance of ancillary ligands on transition metal complexes has been discussed at length. Halides feature prolifically as ancillary ligands in the field of TM catalysis, owing in large part to the stability of metal-halide bonds.²⁷⁹ However, this abundance excludes fluorinated organometallic complexes. Fluorides are known to confer properties to the metal unique among the halides and their coordination can lead to some fascinating reactivity. Nevertheless metal fluorides remain the least understood member of the metal-halide family.^{14b}

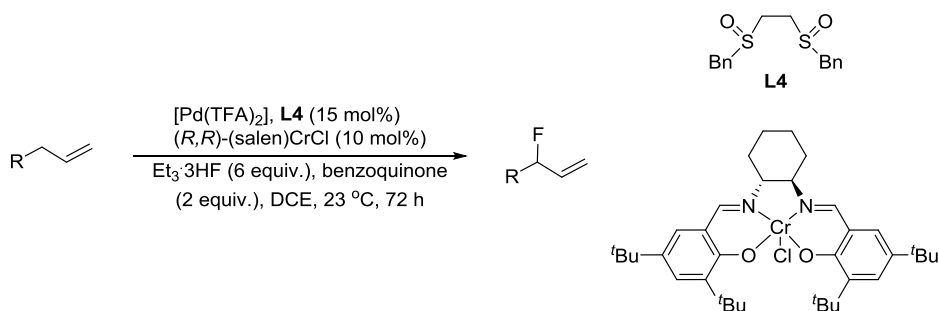
The catalytic preparation of fluorinated organic compounds is an area of great importance for pharmaceutical, agrochemical, and materials industries.^{280,281} Due to fluorine's high electronegativity and small size, it confers unique properties to organic molecules through strong polar interactions.²⁸⁰ For example, roughly 20% of all pharmaceutical compounds contain fluorine groups. The introduction of fluorine on drug targets can make them more bioavailable, lipophilic and metabolically stable as well as increasing the strength of the compound's interactions with target proteins.²⁸⁰ Roughly 30% of all agrochemicals contain fluorine groups, while in materials one of the most important polymers, polytetrafluoroethylene (Teflon), is a perfluorinated substance. Perfluorination of Teflon accounts for its low friction coefficient and hydrophobicity, making it invaluable as a non-stick coating for cook-ware.²⁸¹ Perfluorinated solvents, when mixed with organic solvents or water form immiscible 'fluorous phases' that are useful for catalyst recovery and purification procedures.²⁸² In positron emission tomography (PET) imaging, the non-natural isotope ¹⁸F is the most commonly used positron-emitter.²⁸¹ The utility of fluorinated substances is unquestionable, yet fluorination strategies, particularly for the generation of C-F bonds, are extremely challenging.²⁸¹ The isolation of fluorinated organometallic complexes allows us to study the behaviour of potential catalysts and catalytic intermediates. This knowledge is important in designing new catalytic reactions and improving existing fluorination methods.

To date, fluorination and trifluoromethylation reactions, particularly of aryl and allyl substrates has been dominated by Pd and to a lesser extent, Cu catalysis. The preparation of biologically active and radio-labelled aryl fluorides is an area of high interest and several investigators have made tremendous strides in this area. Buchwald elegantly described an efficient fluorination of aryl triflates,^{61a} and recently aryl bromides and iodides,^{61c} using his palladium/BrettPhos system (Scheme 6.1). The reactions deliver aryl fluorides in high yields and high selectivity with very low generation of protonated arenes, which is considered to be a major side product in these reactions. The Buchwald group also described the trifluoromethylation of (hetero)aryl chlorides, using the same system.^{61b} High yields were obtained and high functional group tolerance was exhibited on a wide range of substrates under mild conditions.



Scheme 6.1. Preparation aryl fluorides by Buchwald and co-workers^{61a,61c,61b}

Doyle and co-workers have reported Pd catalysed nucleophilic fluorination of allylic chlorides^{61e} and their detailed mechanistic studies led to the first catalytic allylic C-H fluorination reaction using a nucleophilic fluoride source ($\text{Et}_3\cdot 3\text{HF}$) using the procedure shown in Scheme 6.2.^{61f}



Scheme 6.2. Allylic fluorination^{61e, 61f}

Efficient fluorination strategies have been described by Hartwig *et al.* using relatively simple $\text{Cu}(\text{OTf})$ complexes and silver fluoride to prepare aryl fluorides from aryl iodides.²⁸³ Hartwig's method is tolerant of a wide range of functional groups and

limited heterocyclic systems and was later extended to include aryl boronate esters, affording high yields, even with sterically hindered substrates.²⁸⁴ A similar $\text{Cu}(\text{CF}_3)$ complex has been employed by the Hartwig group in the trifluoromethylation and perfluoroalkylation of aryl iodides and bromides stoichiometrically.²⁸⁵

The fluoride ion, is the smallest and most weakly polarisable of the halides and, by the Pearson system,¹³ is considered a hard base. Low-valent transition metal centres form weakly polarising cations and hence, are considered as soft acids.^{14b} HSAB theory or the Pearson rule-of-thumb predicts that soft acids will form more stable complexes in solution with soft bases (as discussed for LTM-hydroxides). This theory accounts in large part for the rarity of TM fluorides.^{14b, 33, 279} The expectation of weak TM-fluoride bonds is reinforced by reports that fluoride ligands coordinated to Rh(I) and Ir(I) can be replaced by chloride, bromide or iodide *via* salt metathesis with corresponding sodium salts.²⁸⁶ Another reason for the comparative rarity of metal fluorides is the lack of convenient synthetic routes, using easy to handle reagents. For example, the difficulties associated with using elemental fluorine and hydrogen fluoride (HF) are major deterrents.^{14b}

Stabilisation of M-F bonds and isolation of TM-fluorides has mostly been reported using phosphine, *N*-donor or σ -aryl ancillary ligands.²⁸⁷ Indeed, some of the most extensively investigated fluoride complexes are analogues of Vaska's complex ($[\text{IrCl}(\text{CO})(\text{PPh}_3)_2]$) and related Rh-complexes.^{14b, 288} In contrast, fluoride complexes bearing olefinic ligands remain scarce,^{265a, 289} and even more scarce are those containing NHC ligands. NHCs have featured extensively in the literature as electron-rich donor ligands, and have proven particularly useful in stabilising hard/soft metal-ligand mismatches such as metal hydroxides as discussed in the previous chapters.^{227, 267} Nevertheless, only a small number of LTM-NHC fluorides have been reported, including the Cu(I),²⁹⁰ Au(I),^{290b, 291} Ag(I),^{290b} Ni(II),²⁹² Ru(II),²⁹³ and Ir(III)²⁸⁷ complexes shown in Figure 6.1.

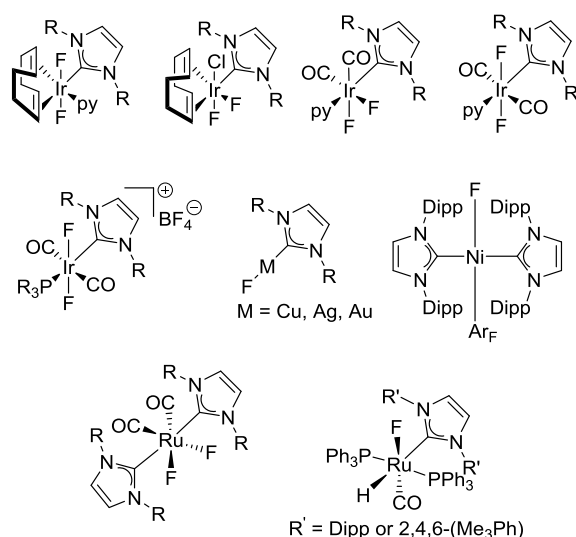
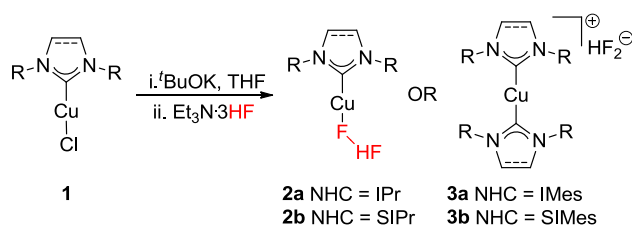


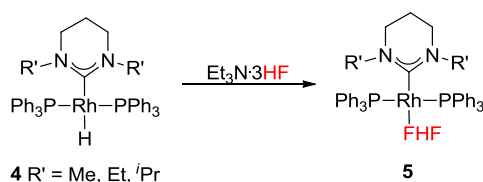
Figure 6.1. Examples of LTM-fluoride complexes bearing NHC supporting ligands^{287, 290-292}

Bifluoride complexes $[M(\text{FHF})]$ are also very interesting, and since the first report by Coulson²⁹⁴ on Pt, several examples of metal bifluorides have been reported, including Mn,²⁹⁵ W,²⁹⁶ Pd,²⁹⁷ Ru,²⁹⁸ Mo,²⁹⁹ Ni,³⁰⁰ and Rh,^{288a, 289, 301} mostly bearing phosphine or amine based supporting ligands. Reports of metal bifluorides bearing NHC ligands are limited to only two examples. Riant and Leyssens^{302,303} reported a method for the preparation of $[\text{Cu}(\text{NHC})(\text{HF}_2)]$ (**1a** and **1b**, NHC = IPr, SIPr) from $\text{Et}_3\text{N}\cdot 3\text{HF}$ and $[\text{Cu}(\text{NHC})(\text{O}^t\text{Bu})]$ (prepared *in situ* from the $[\text{Cu}(\text{NHC})\text{Cl}]$). The same method led to *bis*-NHC complexes **2a** and **2b** when IMes or SIMes were used as NHC, giving $[\text{Cu}(\text{NHC})_2]\text{HF}_2$, Scheme 6.3. Riant and Leyssens demonstrated the catalytic efficiency of the Cu(I)-bifluorides **2** in ketone hydrosilylation³⁰³⁻³⁰⁴ and recently, Weng *et al.* have reported the fluorination of primary and secondary alkyl bromides using an amine based bifluoride Cu complex.³⁰⁵



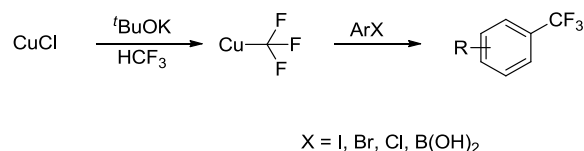
Scheme 6.3. Cu bifluoride complexes³⁰²

Whittlesey and co-workers have reported the preparation of Rh(I)-bifluorides **5** bearing ring expanded six-membered NHC ligands from corresponding Rh(I)-hydrides **4** in yields up to 65% (Scheme 6.4).^{301c, 306} The authors also prepared Rh(I)-fluorides from the Rh(I)-hydrides **4** and perfluoropropene or from the Rh(I)-bifluorides **5** and Me_4NF .^{301c, 306}



Scheme 6.4. Cu and Rh-NHC bifluorides^{301c, 302, 306}

LTM-CF₃ complexes capable of transferring a CF₃ moiety to an organic substrate are extremely important for trifluoromethylation chemistry. To the best of our knowledge, there are no reports of Ir- or Rh-NHC complexes bearing CF₃ groups. In fact reports of [TM(NHC)(CF₃)] complexes are exclusive to Cu.³⁰⁷ In 2011, Grushin and co-workers reported the first successful cupration of fluoroform (HCF₃, Scheme 6.5).^{307b} The ability to use HCF₃ as a CF₃ source was a major breakthrough due to its environmental impact and ready availability. Grushin *et al.* were able to prepare CuCF₃ *via* Cu-O^tBu (formed *in situ* from CuCl, Scheme 6.5) in batch^{307b} and later in continuous stream.³⁰⁸ The Cu-CF₃ proved to be a versatile reagent for synthesising organic CF₃ compounds, but also for the preparation of important Cu-CF₃ and Pd-CF₃ complexes. For example, reaction of Cu-CF₃ with IPr·HCl salt gives the [Cu(CF₃)(IPr)] complex, which has already proven very useful in aryl trifluoromethylation.^{307a} The ‘ligandless’ Cu-CF₃ has been successfully employed in the preparation of aryl- and heteroaryl-CF₃ compounds from a range of aryl halides (I, Br, Cl) with good functional group tolerance under mild conditions (Scheme 6.5).³⁰⁹ Furthermore their method was extended to include the trifluoromethylation of arylboronic acids in air, with full conversion to corresponding trifluoromethyl arenes under very mild conditions, showing substantial improvements to existing protocols.³¹⁰ Grushin’s group has also reported the first nucleophilic trifluoromethylation of carbonyl compounds using CuCF₃ to activate α-haloketones.³¹¹ The same group has also extended this methodology to Pd-CF₃ complexes as discussed in Chapter 1.⁵⁸



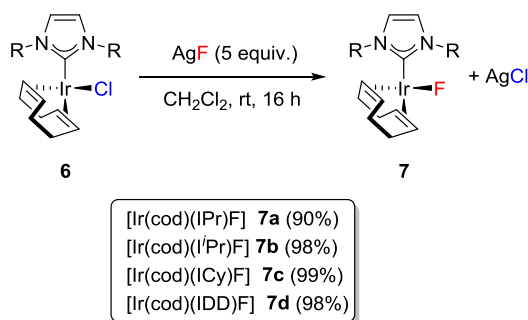
Scheme 6.5 Cupration of fluoroform and transfer of CF₃ group to aryl compounds^{307b, 309-310}

In order to build on the reactivity of Ir(I) and Rh(I), we aimed to establish robust methods for the preparation of fluorinated complexes. Based on previous success in stabilising M-OH bonds on Rh(I) and Ir(I), our strategy was to use the

[M(cod)(NHC)(X)] scaffold (M = Rh, Ir; X = Cl, OH) to gain access to M(I)-F, M(I)-HF₂ and M(I)-CF₃ complexes.

6.2. DISCUSSION

Our first approach was to investigate the preparation of M(I)-F complexes *via* a transmetallation/halide substitution reaction between [Ir(cod)(NHC)Cl] (**6**) and AgF. Gratifyingly, this reaction delivered [Ir(cod)(NHC)F] complexes **7a-d** as yellow solids in excellent yields at room temperature (Scheme 6.6). Multinuclear NMR spectroscopy and elemental analysis were used to unambiguously confirm the identity of the products with the ¹⁹F NMR signals corresponding to the Ir(I)-F moiety resonating between -221 and -227 ppm (see experimental section).



Scheme 6.6. Preparation of Ir(I)-fluoride complexes using AgF

The Ir(I)-F motif was also accessible from the corresponding Ir(I)-hydroxide **8** and AgF in similar yields. It was clear that the three species were intrinsically linked and we were able to convert the Ir(I)-fluoride **7** to either the Ir(I)-hydroxide **8** (*via* reaction with CsOH or KOH), or to the Ir(I)-chloride **6** (*via* reaction with NaCl, Figure 6.2).

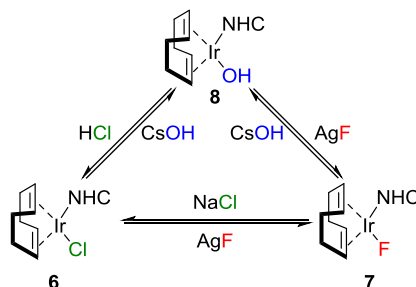
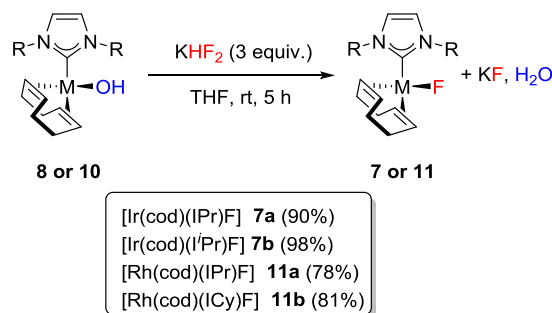


Figure 6.2. Processes that link the Ir fluoride, chloride and hydroxide

However, when we attempted to extend the methodology to rhodium, the reactions were at best very slow (65% conversion after 60 h for [Rh(cod)(IPr)Cl] **9a**). Treating either of the metal chlorides or hydroxides with fluoride salts such as KF or

CsF were also unsuccessful and a new approach was investigated. To our delight, the Rh(I)-hydroxides **10a-b** were able to react with the cheap and readily available KHF_2 , and deliver the desired Rh(I)-fluorides **11a-b** in high yield in just 5 h. This method proved general for both metals (Scheme 6.7) and analysis by ^{19}F NMR indicated that Rh(I)-F signals resonated at a higher field than the analogous Ir(I)-F complexes (δ -253, d, $^1J_{\text{RhF}} = 77$ Hz (**11a**); δ -258, br (**11b**)).



Scheme 6.7. Preparation of Ir(I) and Rh(I) fluorides using KHF_2

X-ray analysis of single crystals of complexes **7a**, **7b**, **11a** and **11b** (Figure 6.3 and 6.4) indicated $16e^-$ complexes, adopting the usual square planar geometry and crystallising as two independent molecules in the unit cell in **7a** and **7b** and three independent molecules in **11b** (selected bond lengths and bond angles in Table 6.1). Compared to the parent complexes, the M(I)-F bonds (1.991 – 2.032 Å for Ir and 2.016 – 2.092 Å for Rh) are shorter than M(I)-Cl bonds (2.334 – 2.382 Å)^{94a, 108, 312} and closer in magnitude to the corresponding M(I)-OH bonds (2.014 – 2.038 Å).^{226-227, 267}

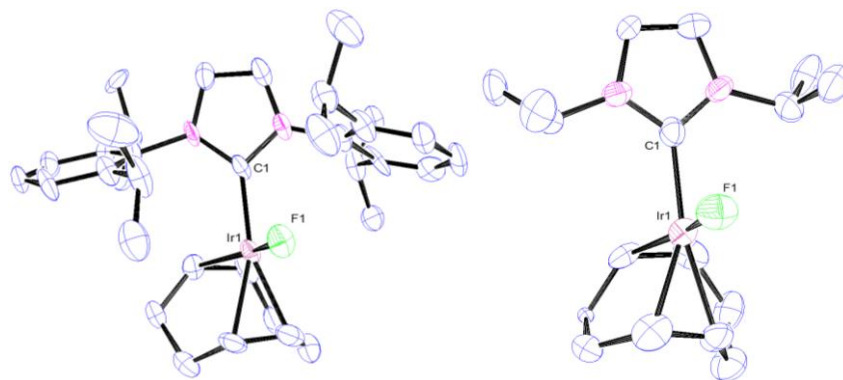


Figure 6.3. Thermal ellipsoid representations of complexes **7a** and **7b**, showing 50% probability. H atoms are omitted for clarity.

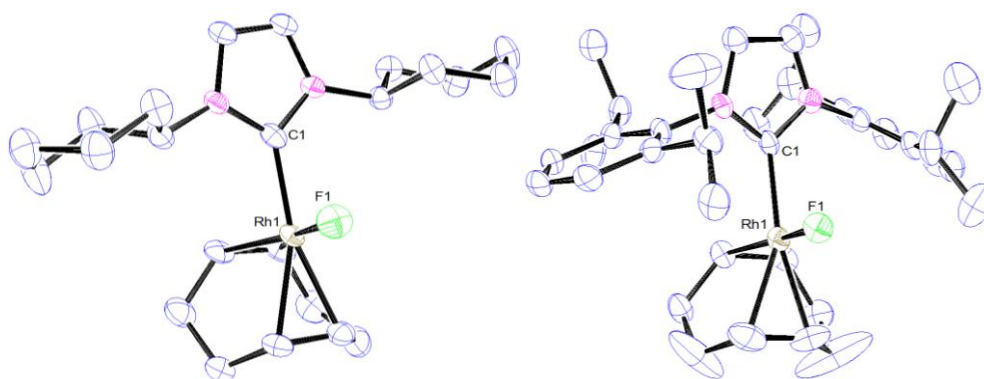


Figure 6.4. Thermal ellipsoid representations of complexes **11a** and **11b** showing 50% probability. H atoms are omitted for clarity.

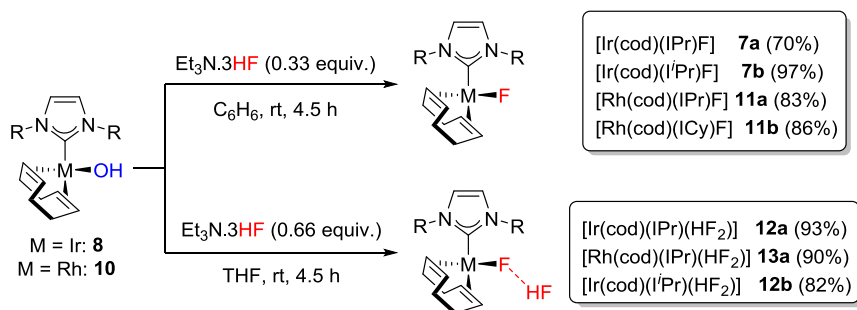
Table 6.1. Selected bond lengths (Å) and bond angles (°) for **7a-b** and **11a-b**

Entry	Complex	M(1)-C(1)	M(1)-F(1)	C(1)-M(1)-F(1)
1	7a	2.014(16), 2.029(17)	2.023(9), 2.002(11)	87.5(5), 88.2(6)
2	7b	2.038(17), 2.035(16)	2.002(10), 2.012(9)	88.4(5), 88.6(5)
3	11a	2.022(3)	2.028(5)	88.20(11)
4	11b	2.044(8), 2.063(8), 2.035(8)	2.028(5), 2.086(6), 2.033(5)	89.1(3), 85.6(3), 88.0(3)

Two independent molecules in the unit cell for **7a** and **7b** and three independent molecules in the unit cell for **11b**

As a third method, we examined the reaction between the Rh(I)- and Ir(I)-hydroxides and $\text{Et}_3\text{N}\cdot 3\text{HF}$, since Leysens *et al*³⁰² reported that the reaction between $[\text{Cu}(\text{NHC})(\text{O}^t\text{Bu})]$ and $\text{Et}_3\text{N}\cdot 3\text{HF}$ could be tailored to deliver either the mono- or the bifluoride complex. In an effort to test these strategies on our complexes, Ir(I)-hydroxide complexes **8a** and **8b** and Rh(I)-hydroxides complexes **10a** and **10b** were reacted with $\text{Et}_3\text{N}\cdot 3\text{HF}$ (0.33 equiv.) in benzene to successfully deliver the Ir(I)-fluorides **7a-b** and the Rh-fluorides **11a-b** (4.5 h, rt; Scheme 6.8). Changing the solvent to THF and increasing the relative volume of $\text{Et}_3\text{N}\cdot 3\text{HF}$ (0.66 equiv.) allowed $[\text{Ir}(\text{cod})(\text{IPr})(\text{OH})]$ (**8a**) and $[\text{Rh}(\text{cod})(\text{IPr})(\text{OH})]$ (**10a**) to afford the expected bifluoride species, $[\text{Ir}(\text{cod})(\text{IPr})(\text{HF}_2)]$ (**12a**) and $[\text{Rh}(\text{cod})(\text{IPr})(\text{HF}_2)]$ (**13a**), as bright yellow solids in each case (Scheme 6.8). The NMR analysis of these new complexes showed subtle differences to the analogous fluoride complexes (**7a** and **11a**). At room temperature the ^1H NMR spectra for each compound contained a low-field broad doublet (δ 11.4, $^1J_{\text{FH}} = 395.0$ Hz (**12a**); δ 12.3, $^1J_{\text{FH}} = 350.0$ (**13a**)). Upon cooling (200K, CD_2Cl_2) the signals partially resolved into doublets of doublets in each case with a spin-spin coupling of 395

and 40 Hz for **12a** and 350 and 25 Hz for **13a** (see experimental). These ^1H NMR signals were assigned to the acidic proton of the bifluoride moiety; bearing a strong bond to one fluoride and a second, weaker bond to another fluoride.



Scheme 6.8. Reaction of Rh(I) and Ir(I) hydroxides with $\text{Et}_3\text{N}\cdot 3\text{HF}$

This assignment was confirmed by the identification of two fluoride groups by ^{19}F NMR of **12a** and **13a**. In each case, a ^{19}F NMR signal was observed in the same region as that on **7a** and **11a**, corresponding to the metal-bound (proximal) fluoride. In addition, a doublet resonated further downfield with a spin-spin coupling constant of 395 Hz on **12a** and 350 Hz on **13a**. These signals were assigned to the distal fluoride, showing a strong bond to the acidic proton. At 200 K, all ^{19}F NMR signals resolved into distinct doublets of doublets, e.g. for **12a**: ^{19}F NMR δ -178 (dd, $^1J_{\text{HF}} = 395$, $^2J_{\text{FF}} = 120$, Ir-F \cdots HF), -239 (dd, $^2J_{\text{FF}} = 120$, $^1J_{\text{HF}} = 40$, Ir-F \cdots HF, see experimental section). Based on these results, we identified the structures of **12a** and **13a** as $[\text{Ir}(\text{cod})(\text{IPr})(\text{FHF})]$ and $[\text{Rh}(\text{cod})(\text{IPr})(\text{FHF})]$ respectively (Scheme 6.8) with the HF_2 moieties comprising a strong bond between the metal and the proximal fluoride, and a relatively weak hydrogen bond to the HF moiety (i.e. $[\text{M}]-\text{F}\cdots\text{HF}$ as opposed to $[\text{M}]\cdots\text{F}-\text{HF}$), in agreement with literature reports.^{298a, 301a, 301b, 302, 306}

X-ray crystallographic analysis of single crystals of **12a** and **13a** (Figure 6.5) showed square planar complexes, adopting the same geometry as the mono-fluorides and co-crystallising in each case as two independent molecules in the unit cell. The X-ray structure for **12a** shows a significantly elongated M-F bond compared to the monofluoride **7a**, (2.054 – 2.064 (**12a**) compared to 1.991 – 2.032 Å (**7a**), Table 6.2). This weakening of the M-F bond is a consequence of the hydrogen bond to HF.^{298a} There is considerable uncertainty involved in accurately locating the acidic proton. Hence, when discussing the relative bond strengths and symmetry within the bifluoride moiety, it is more useful to discuss the inter-atomic distance between the two fluorines. The F–F separation for **12a** is in the range of 2.352 – 2.387 Å and 2.316 – 2.331 Å for

complex **13a** (Table 6.2). These values are considerably less than the sum of the van der Waals radii for two F atoms (2.94 \AA)³¹³ and are indicative of strong hydrogen bonds between the proton and the two fluorides, in agreement with reports for other metal bifluorides including Mo and Rh.^{296, 297c, 298a, 298c, 299-301, 301c, 302, 306} However, compared to true ionic bifluoride salts ($2.24 - 2.28 \text{ \AA}$),^{299, 314} the larger interatomic separations indicate weaker hydrogen bonds (relative to $[\text{HF}_2]^-$); as a result of the strong interaction between the Ir(I)/Rh(I) metal and the proximal fluoride.

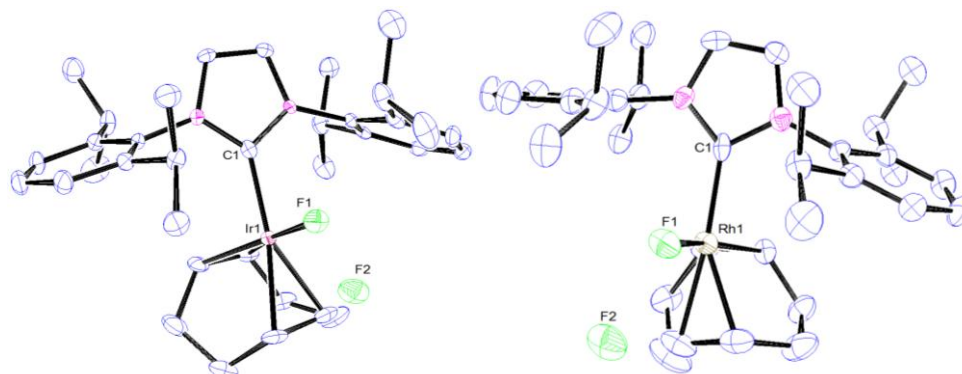


Figure 6.5. Thermal ellipsoid representations of **12a** and **13a** showing 50% thermal ellipsoid probability. H atoms are omitted for clarity.

Table 2. Selected bond lengths (\AA) and bond angles ($^\circ$) for **12a** and **12b**^a

Entry	Complex	Ir(1)-C(1)	Ir(1)-F(1)	C(1)-Ir(1)-F(1)
1	12a	2.033(4), 2.049(4)	2.057(3), 2.062(2)	88.92(13), 92.59(12)
2	13a	2.047(5), 2.035(6)	2.089(3), 2.069(3)	93.09(16), 89.14(18)

^aTwo independent molecules in the unit cell for 12a and 12b

The unsymmetrical nature of the HF_2 ligand was further supported by IR analyses of **12a** and **13a**. FTIR (ATR) analyses of **12a** and **13a** showed two broad absorptions each (**12a**: $\nu = 2623$ and 1807 cm^{-1} ; **13a**: $\nu = 2530$ and 1890 cm^{-1}) corresponding to the H-F modes of the bifluoride (These broad bands are absent from IR spectra of the mono-fluorides **7a** and **11a**).^{297b, 299, 306} Compared to the IR bands expected for free HF ($\nu = 3896$ and 3895 cm^{-1} in an Ar matrix),³¹⁵ it is clear that there is weakened hydrogen bonding within the HF moiety as a result of the H-bond to the proximal fluoride, causing a shift to lower wavelength. Compared to symmetrical inorganic bifluoride salts, for example Cs^+ , K^+ or $\text{Na}^+ \text{HF}_2^-$ ($1372 - 1284 \text{ cm}^{-1}$),³¹⁶ the IR bands exhibited for **12a** and **13a** are considerably higher in wavelength, indicating that the HF_2 moiety in these complexes is highly unsymmetrical, with a stronger hydrogen bond to one fluorine atom than the other.

In addition to **12a** and **13a**, an alkyl-substituted NHC complex of Ir(I)-(HF₂) was prepared in the form of [Ir(cod)(I^{*t*}Pr)(HF₂)] (**12b**) (Scheme 6.8). The less sterically encumbered (**12b**) exhibited different structural characteristics to **12a** and **13a**, both in the solid state and in solution. For example, at room temperature the ¹H NMR signal corresponding to the acidic proton resonates as a broad unresolved peak, as do both signals in the ¹⁹F NMR spectrum (see experimental section). Upon cooling to 200 K, the signals resolved into doublets of doublets in the same way as **12a** and **13a**.

From the X-ray structure of **12b** (Figure 6.6) it is clear that while the Ir-F bond is comparable to **12a** (2.064(5), [2.082(4)] Å) the F-F separation (2.457(6), [2.587(6)] Å) is considerably higher, even when compared to the values for most metal bifluorides reported to date. This observation is most likely indicative of weaker interactions between the proton and the fluoride groups.^{289, 296-299, 301-302, 306, 317} The Ir(1)-F(1)-F(2) angle is *ca.* 116.33° – 117.98°, much lower than that for **12a** (*ca.* 122.13° – 132.36°), although the angle between metal and bifluoride tends to vary substantially for different compounds in the literature, (109° on Cu to 156° on W).^{296, 302} On closer inspection of the X-ray structures of **12a** and **13a** it is clear that F(1) and the *isopropyl* proton on each side of the IPr ligand are in very close proximity to each other. For **12a** this distance lies in the range of 2.3316 – 2.4949 Å and for **13a** the contact is in the range of 2.3150 – 2.4348 Å. This is considerably less than the sum of the van der Waals radii for H and F (2.67 Å)³¹³ The same close proximity of the bifluoride and the NHC substituents is not possible on **12b** and the added flexibility may account for the fluxional behaviour in solution that was associated with complex **12b** (this short contact is not observed in **7a**).

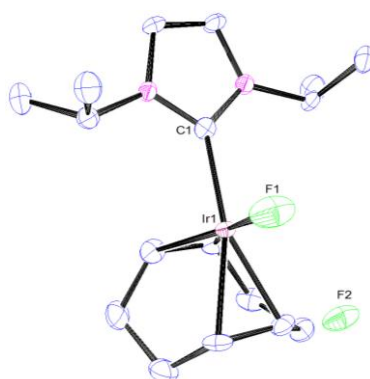


Figure 6.6. Thermal ellipsoid representation of **12b** showing 50% thermal ellipsoid probability. H atoms are omitted for clarity. Selected bond lengths (Å) and bond angles (°): Ir(1)-C(1) 2.045(6), [2.053(6)]; Ir(1)-F(1) 2.064(5), [2.082(4)]; C(1)-Ir(1)-F(1) 91.0(2), [87.5(2)].

Next we studied the relationship between the fluoride and bifluoride complexes. The ease with which the bifluoride can be generated from the monofluoride and the lability of the HF molecule is especially important for catalytic fluorination and fluorination/ring-opening processes,³¹⁸ where catalysts, particularly metal fluorides, are coupled with an HF source. In order to examine the persistence of the bifluoride moiety in the presence of a base, both the Rh(I)- and Ir(I)-bifluorides (**12a** and **13a**) were reacted with a stoichiometric amount of KOH. In both cases, full conversion to the corresponding monofluorides (**7a** and **11a**) was seen within 2 h. Interestingly, the addition of a second equivalent of KOH yielded the corresponding metal hydroxide **8a** or **10a**; whilst addition of Et₃N·3HF (0.33 equiv.) to **7a** or **11a** regenerated the metal bifluorides (**12a** and **13a**). Hence, the three species are inherently linked (Figure 6.7) and in the presence of an excess of Et₃N·3HF, a metal fluoride will more than likely deliver the metal bifluoride.

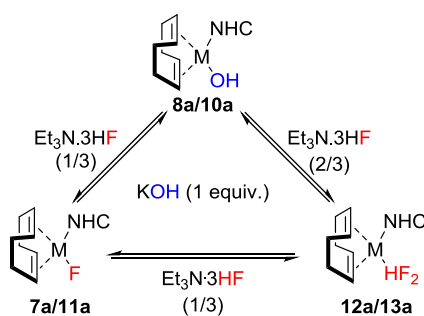
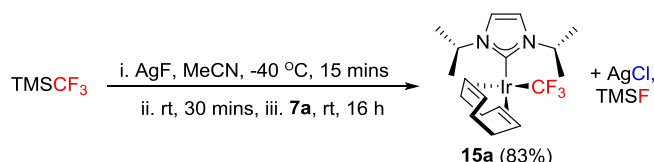


Figure 6.7. Processes linking M(I)-OH, M(I)-F and M(I)-(HF₂) (M = Rh and Ir)

Having established reliable routes to mono- and bifluoride complexes of Ir(I) and Rh(I) as well as studied the processes that link them, our final goal was to access the first examples of Ir(I)(NHC)-CF₃ and Rh(I)(NHC)-CF₃ complexes. Our initial attempts were conducted using Ruppert-Prakash's reagent, trifluoromethyl(trimethyl)silane (TMSCF₃). Unfortunately all attempts to transfer the CF₃ from Si to Ir or Rh failed. The only complex that reacted with TMSCF₃ was [Ir(cod)(IⁱPr)(OH)] (**8a**). The reaction delivered [Ir(cod)(IⁱPr)(OSiMe₃)] (**14**) (96%), with HCF₃ as a side product. The ease with which this substrate reacts with silanes to form Ir(I)-siloxide complexes has been discussed in Chapter 4.²⁶⁷ No reaction was observed between TMSCF₃ and any of the other Ir(I)- or Rh(I)-hydroxides (**8** or **10**), or the chlorides (**6** or **9**). The fluoride complexes (**7** and **11**) were completely unreactive to TMSCF₃ and the reaction between the bifluorides (**12** and **13**) and TMSCF₃ only led to inseparable mixtures of products. It was clear that TMSCF₃ was not an ideal CF₃ source and that a new approach was

necessary. Roper has reported the preparation of Ir(I)-CF₃ complexes from [Ir(CO)₂(PPh₃)₂H] using Hg(CF₃)₂ and similar strategies have been employed on other metals using Hg- or Cd(CF₃)₂.³¹⁹ In an attempt to avoid such toxic reagents, we considered that Ag might be a more convenient approach. Hence, AgCF₃ was prepared *in situ* from AgF and TMSCF₃ at -40 °C³²⁰ and reacted with [Ir(cod)(IⁱPr)Cl] (**6a**) to give [Ir(cod)(IⁱPr)(CF₃)] (**15a**) as a bright red solid (Scheme 6.9).



Scheme 6.9. Preparation of [Ir(cod)(IⁱPr)(CF₃)] (**15a**)

All attempts at isolating the Ir(IPr)-CF₃ **15b** and Rh(IPr)-CF₃ **16a** using this procedure failed as the products appeared to be unstable. In order to rationalise these results we studied the structure of the isolated compound **15a**. Hence, single crystals of **15a** were grown and analysed by X-ray diffraction (Figure 6.8). In the solid state it was clear that two of the fluorine atoms were in very close proximity to a methine proton on each side of the NHC ligand (*ca.* 2.451 Å). This distance is considerably less than the sum of the Van der Waals radii of H and F (2.67 Å)³¹³ and may indicate an interaction between the two groups. Therefore, it is possible that the *isopropyl* groups of the IⁱPr ligand are interacting with the CF₃, stabilising the complex. Furthermore, this interaction is evident in the ¹³C{¹H} NMR of **15a** where a spin-spin coupling interaction causes one of the ¹³C{¹H} methyl signals to split into a quartet (δ 22.8 ppm, *J*_{FC} = 1 Hz). Since the methyl group is separated from the fluorine atoms by six bonds, the interaction must be a "through-space" coupling.³²¹ The proximity of the *isopropyl* groups to the CF₃ moiety indicated that there were considerable steric constraints to take into account. Thus, the presence of bulky NHC ligand substituents such as *diisopropyl(phenyl)* on IPr would hinder the coordination of a CF₃ group to the metal centre, rendering [M(cod)(IPr)(CF₃)] unstable.

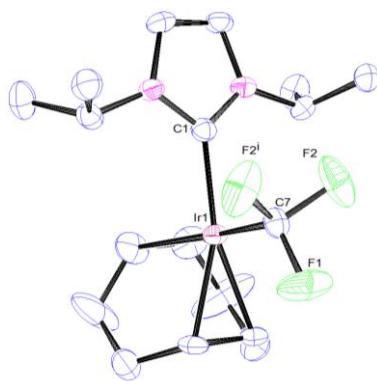
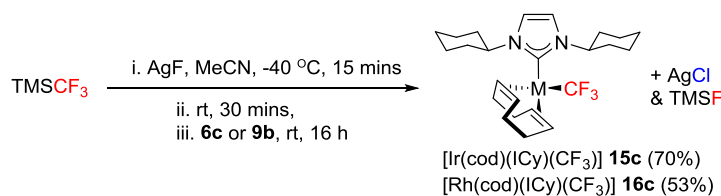


Figure 6.8. Thermal ellipsoid representation of **15a** showing 50% thermal ellipsoid probability.

H atoms are omitted for clarity. Selected bond lengths (Å) and bond angles (°): Ir(1)-C(1) 2.065(8); Ir(1)-C(7) 2.086(8); C(7)-F(1) 1.357(10); C(7)-F(2) 1.359(7); C(1)-Ir(1)-C(7) 88.3(3).

To test this hypothesis, we investigated the reaction between $[M(\text{cod})(\text{ICy})\text{Cl}]$ (**6c** and **9b**) and AgCF_3 , which delivered $[M(\text{cod})(\text{ICy})(\text{CF}_3)]$ (**15c** and **16c**, Scheme 6.10). The same structural features were evident in the $^{13}\text{C}\{^1\text{H}\}$ NMR spectrum of **15c**, showing a spin-spin coupling interaction between a methylene on the cyclohexyl ring and the fluoride groups of the CF_3 . Furthermore, an X-ray crystal structure of **16c** (Figure 6.9) indicated a similar close proximity between the fluorides and a proton on each of the cyclohexyl rings (2.505 – 2.520 Å). Hence, this method was somewhat limited by the steric bulk of the NHC ligands and proved more successful for Ir than Rh, with **16c** being isolated in only 53% yield. However, interesting structural investigations have given us further insight into the stability of this scaffold and the viability of the method.



Scheme 6.10. Preparation of Ir(I)- CF_3 and Rh(I)- CF_3 complexes

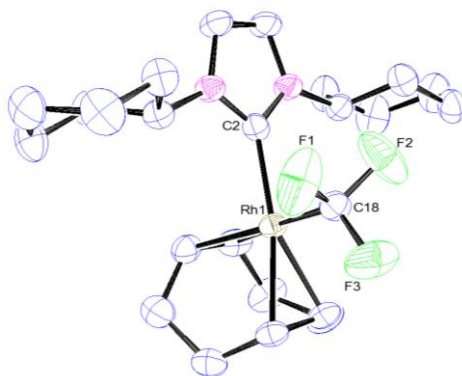


Figure 6.9 Thermal ellipsoid representation of **16c** showing 50% thermal ellipsoid probability. H atoms are omitted for clarity. Selected bond lengths (Å) and bond angles (°): Rh(1)-C(2) 2.042(5); Rh(1)-C(18) 2.067(5); C(18)-F(1) 1.366(6); C(18)-F(2) 11.331(8); C(18)-F(3) 1.354(6); C(8)-Rh(1)-C(29) 87.3(2).

6.3. CONCLUSIONS

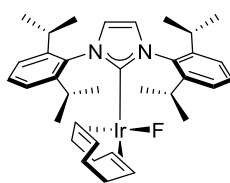
We have successfully utilised three methods for accessing Ir(I)-NHC fluoride compounds *via* AgF, KHF₂ and Et₃N·3HF, with the two latter methods proving equally effective on rhodium. Synthesis of the first examples of Ir(I) bifluorides was achieved in high yields. Access to Ir(I) and Rh(I) mono- and bifluorides allowed us to examine the link between the two species. Knowledge of the relationship between the metal fluorides and metal bifluorides could prove paramount in developing new fluorination strategies since the bifluoride can be quantitatively generated from the monofluoride in solution and *vice versa*. A new methodology was also established to access the first examples of Ir(I)-NHC and Rh(I)-NHC trifluoromethyl complexes. Consequently, we have assembled a toolbox for the preparation of fluorinated Ir(I) and Rh(I) complexes to take advantage of the reactivity of already successful Ir(I)-NHC and Rh(I)-NHC scaffolds. These complexes may prove important in the pursuit of fluorination strategies and may well provide active catalytic species or intermediates.

6.4. EXPERIMENTAL DETAILS

6.4.1. General considerations

All manipulations and reactions were performed inside an Argon-filled Innovative Technologies glovebox or on an Argon-supplied Schlenk line unless stated otherwise. All reagents were supplied by Aldrich and used without further purification. Solvents were distilled and dried as required. NMR data was obtained using either a Bruker 300, 400 or 500 MHz spectrometer at 303 K (unless stated otherwise) in the specified deuterated solvent. All chemical shifts are given in ppm and coupling constants in Hz. Signals on the $^{13}\text{C}\{^1\text{H}\}$ NMR spectra are singlets unless otherwise stated. Spectra were referenced to residual protonated solvent signals (for ^1H) or solvent signals (for ^{13}C): (C_6D_6 : ^1H δ 7.16 ppm, ^{13}C δ 128.06 ppm, CD_2Cl_2 ^1H δ 5.32 ppm, ^{13}C δ 53.84 ppm). Infrared spectra (ν) were recorded on a Shimadzu Fourier transform IR Affinity-1 Infrared spectrometer using a MIRacleTM single reflection horizontal ATR (diamond). Samples were placed directly on the crystal (ATR) in the solid state. Only characteristic peaks have been quoted. Elemental analyses were performed at the London Metropolitan University. CCDC- 1000750 (**7a**), 1000751 (**7b**), 1000754 (**11a**), 1001352 (**11b**), 1000753 (**12a**), 1000755 (**12b**), 1000754 (**13a**), 1000756 (**15a**), 1000757 (**16c**), contain structural data for complexes characterized by X-ray diffraction. Crystallographic data can be obtained free of charge from The Cambridge Crystallographic Data Centre via www.ccdc.cam.ac.uk/data_request/cif.

6.4.2. Synthesis and Characterisation data



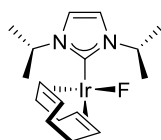
[Ir(cod)(IPr)(F)] **7a**

Method A: A vial was charged with [Ir(cod)(IPr)(Cl)] (**6a**) (50 mg, 0.071 mmol) and AgF (43.8 mg, 0.35 mmol) in CH_2Cl_2 (1 mL) and the reaction mixture was stirred at rt in the dark for 16 h. Once complete, pentane (1 mL) was added to the mixture and left to stand for 10 mins. The reaction mixture was filtered through celite and concentrated *in vacuo* to give a yellow solid. The solid was washed with cold pentane (3 x 1 mL), taken up in a mixture of THF (0.2 mL) and pentane (1 mL) and filtered through a PTFE

syringe filter (0.2 μm) to remove residual Ag compounds. The product was dried *in vacuo* to give $[\text{Ir}(\text{cod})(\text{IPr})(\text{F})]$ (**7a**) (45 mg, 90%) as a yellow solid.

Method B: A vial was charged with $[\text{Ir}(\text{cod})(\text{IPr})(\text{OH})]$ (**8a**) (20 mg, 0.028 mmol) and KHF_2 (6.6 mg, 0.085 mmol) in THF (1 mL) and the reaction mixture was stirred at rt for 5 h. Once complete, the reaction mixture was filtered through celite and concentrated *in vacuo* to give a yellow solid. The solid was washed with cold pentane (3 x 1 mL) and dried *in vacuo* to give $[\text{Ir}(\text{cod})(\text{IPr})(\text{F})]$ (**7a**) (20 mg, 99%) as a yellow solid.

Method C: A Schlenk tube was charged with $[\text{Ir}(\text{cod})(\text{IPr})(\text{OH})]$ (**8a**) (50 mg, 0.071 mmol) in benzene (1 mL). $\text{NEt}_3 \cdot 3\text{HF}$ (4.0 μL , 0.024 mmol) was added under Ar and the reaction mixture was stirred at rt for 4.5 h. The product was reduced *in vacuo* and azeotroped with hexane (2 x 2 mL) to give a yellow solid. The solid was washed with hexane (2 x 1 mL) and dried *in vacuo* to give $[\text{Ir}(\text{cod})(\text{IPr})(\text{F})]$ (**7a**) (35 mg, 70%) as a yellow solid. **^1H NMR** (500 MHz, CD_2Cl_2): δ 7.51 (t, 2H, $^3J_{\text{HH}} = 7.7$, *p*-ArH), 7.34 (d, 4H, $^3J_{\text{HH}} = 7.7$, *m*-ArH), 7.02 (s, 2H, N-(CH)₂-N), 4.02 – 3.92 (m, 2H, cod-CH), 2.95 (sept., 4H, $^3J_{\text{HH}} = 6.8$, CH(CH₃)₂), 2.64 – 2.58 (m, 2H, cod-CH), 1.73 – 1.64 (m, 2H, cod-CH₂), 1.59 – 1.49 (m, 2H, cod-CH₂), 1.37 (d, 12H, $^3J_{\text{HH}} = 6.7$, CH₃), 1.28 – 1.18 (m, 4H, cod-CH₂), 1.10 (d, 12H, $^3J_{\text{HH}} = 6.8$, CH₃). **^{19}F NMR** (282 MHz, C_6D_6): δ -221 (br.). **$^{13}\text{C}\{^1\text{H}\}$ NMR** (125 MHz, CD_2Cl_2): δ 183.6 (Ir-C_{carbene}), 146.9 (ArC), 136.3 (ArC), 129.9 (ArCH), 124.4 (ArCH), 123.9 (N-(CH)₂-N), 83.3 (d, $^2J_{\text{FC}} = 4$, cod-CH), 45.0 (d, $^2J_{\text{FC}} = 4$, cod-CH), 34.2 (cod-CH₂), 29.1 (CH(CH₃)₂), 28.4 (cod-CH₂), 26.3 (CH₃), 22.8 (CH₃). **FTIR (ATR)** $\nu = 800.46$ (s), 756.10 (s) cm^{-1} . **Anal. Calcd.** for $\text{C}_{35}\text{H}_{48}\text{FIrN}_2$ (MW 707.98): C, 59.38; H, 6.83; N, 3.96. Found: C, 59.38; H, 6.97; N, 4.01.



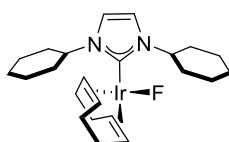
$[\text{Ir}(\text{cod})(\text{IPr})(\text{F})]$ **7b**

Method A: A vial was charged with $[\text{Ir}(\text{cod})(\text{IPr})(\text{Cl})]$ (**6b**) (50.0 mg, 0.102 mmol) and AgF (65.0 mg, 0.512 mmol) in CH_2Cl_2 (1 mL) and the reaction mixture was stirred at rt in the dark for 16 h. Once complete, pentane (1 mL) was added to the mixture and left to stand for 10 mins. The reaction mixture was filtered through celite

and concentrated *in vacuo* to give a yellow solid. The solid was washed with cold pentane (3 x 1 mL), taken up in a mixture of THF (0.2 mL) and pentane (1 mL) and filtered through a PTFE syringe filter (0.2 μm) to remove residual Ag compounds. The product was dried *in vacuo* to give $[\text{Ir}(\text{cod})(\text{I}^i\text{Pr})(\text{F})]$ (**7b**) (47 mg, 98%) as a yellow solid.

Method B: A vial was charged with $[\text{Ir}(\text{cod})(\text{I}^i\text{Pr})(\text{OH})]$ (**8b**) (20 mg, 0.043 mmol) and KHF_2 (10.0 mg, 0.13 mmol) in THF (1 mL) and the reaction mixture was stirred at rt for 5 h. Once complete, the reaction mixture was filtered through celite and concentrated *in vacuo* to give a yellow solid. The solid was washed with cold pentane (3 x 1 mL) and dried *in vacuo* to give $[\text{Ir}(\text{cod})(\text{I}^i\text{Pr})(\text{F})]$ (**7b**) (15 mg, 74%) as a yellow solid.

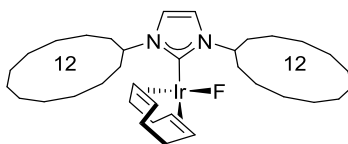
Method C: A Schlenk tube was charged with $[\text{Ir}(\text{cod})(\text{I}^i\text{Pr})(\text{OH})]$ (**8b**) (100 mg, 0.213 mmol) in benzene (1 mL). $\text{NEt}_3 \cdot 3\text{HF}$ (12 μL , 0.07 mmol) was added under Ar and the reaction mixture was stirred at rt for 4.5 h. The product was reduced *in vacuo* and azeotroped with hexane (2 x 2 mL) to give a yellow solid. The solid was washed with pentane (3 x 1 mL) and dried to give $[\text{Ir}(\text{cod})(\text{I}^i\text{Pr})(\text{F})]$ (**7b**) (97.9 mg, 97%) as a yellow solid. $^1\text{H NMR}$ (300 MHz, C_6D_6): δ 6.28 (s, 2H, N-(CH)₂-N), 5.80 (sept., 2H, $^3J_{\text{HH}} = 6.8$, N-CH(CH₃)₂), 5.10 – 4.97 (m, 2H, cod-CH), 2.96 – 2.87 (m, 2H, cod-CH), 2.45 – 2.22 (m, 4H, cod-CH₂), 1.80 – 1.58 (m, 4H, cod-CH₂), 1.21 (app. d, 6H, $^3J_{\text{HH}} = 6.4$ CH₃), 1.11 (app. d, 6H, $^3J_{\text{HH}} = 6.8$, CH₃). $^{19}\text{F NMR}$ (282 MHz, C_6D_6): δ -227 (br). $^{13}\text{C}\{^1\text{H}\}$ NMR (75 MHz, C_6D_6): δ 180.7 (Ir-C_{carbene}), 116.2 (N-(CH)₂-N), 84.4 (cod-CH), 52.5 (cod-CH), 43.8 (N-CH(CH₃)₂), 34.9 (cod-CH₂), 29.5 (cod-CH₂), 24.3 (CH₃), 23.0 (CH₃). **FTIR (ATR)** $\nu = 1413.82$ (s), 1211.30 (s), 881.47 (w) cm^{-1} . **Anal. Calcd.** for $\text{C}_{17}\text{H}_{28}\text{FIrN}_2$ (MW 471.63): C, 43.29; H, 5.98; N, 5.94. Found: C, 43.23; H, 6.05; N, 6.05.



$[\text{Ir}(\text{cod})(\text{ICy})(\text{F})]$ **7c**

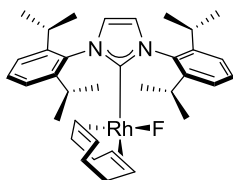
A vial was charged with $[\text{Ir}(\text{cod})(\text{ICy})(\text{Cl})]$ (**6c**) (50 mg, 0.088 mmol) and AgF (56 mg, 0.44 mmol) in CH_2Cl_2 (1 mL) and the reaction mixture was stirred at rt in the dark for 16 h. Once complete, pentane (1 mL) was added to the mixture and left to stand

for 10 mins. The reaction mixture was filtered through celite and concentrated *in vacuo* to give a yellow solid. The solid was washed with cold pentane (3 x 1 mL), taken up in a mixture of THF (0.2 mL) and pentane (1 mL) and filtered through a PTFE syringe filter (0.2 μm) to remove residual Ag compounds. The product was dried *in vacuo* to give [Ir(cod)(ICy)(F)] (**7c**) (44 mg, 90%) as a yellow solid. $^1\text{H NMR}$ (300 MHz, C_6D_6): δ 6.35 (s, 2H, N-(CH)₂-N), 5.46 (tt, 2H, $^3J_{\text{HH}} = 11.7, 3.6$ N-CH(ICy)), 5.02 – 4.92 (m, 2H, cod-CH), 3.00 – 2.89 (m, 2H, cod-CH), 2.51 – 2.23 (m, 6H, cod-CH₂, ICy-CH₂), 1.94 – 1.81 (m, 2H, ICy-CH₂), 1.81 – 1.02 (m, 18H, ICy-CH₂), 1.02 – 0.80 (m, 2H, ICy-CH₂). $^{19}\text{F}\{^1\text{H}\}$ NMR (282 MHz, C_6D_6): δ -227 (s). $^{13}\text{C}\{^1\text{H}\}$ NMR (75 MHz, C_6D_6): δ 181.2 (Ir-C_{carbene}), 116.6 (N-(CH)₂-N), 84.1 (cod-CH), 60.3 (cod-CH), 43.8 (N-CH(CH₃)₂), 35.1 (cod-CH₂), 34.4 (ICy-CH₂), 29.7 (cod-CH₂), 26.3, 25.7, 22.7, 14.3 (ICy-CH₂). **Anal. Calcd.** for C₂₃H₃₆FIrN₂ (MW 551.77): C, 50.07; H, 6.58; N, 5.08. Found: C, 49.96; H, 6.65; N, 5.12.



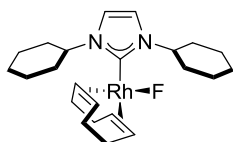
[Ir(cod)(IDD)(F)] **7d**

A vial was charged with [Ir(cod)(IDD)(Cl)] (**6d**) (50.0 mg, 0.068 mmol) and AgF (43.0 mg, 0.34 mmol) in CH_2Cl_2 (1 mL) and the reaction mixture was stirred at rt in the dark for 16 h. Once complete, pentane (1 mL) was added to the mixture and left to stand for 10 mins. The reaction mixture was filtered through celite and concentrated *in vacuo* to give a yellow solid. The solid was washed with cold pentane (3 x 1 mL), taken up in a mixture of THF (0.2 mL) and pentane (1 mL) and filtered through a PTFE syringe filter (0.2 μm) to remove residual Ag compounds. The product was dried *in vacuo* to give [Ir(cod)(IDD)(F)] (**7d**) (48 mg, 98%) as a yellow solid. $^1\text{H NMR}$ (400 MHz, C_6D_6): δ 6.43 (s, 2H, N-(CH)₂-N), 5.78 – 5.68 (m, 2H, N-CH(IDD)), 5.04 – 4.96 (m, 2H, cod-CH), 2.97 – 2.90 (m, 2H, cod-CH), 2.60 – 2.39 (m, 4H, cod-CH₂), 2.17 – 2.03 (m, 2H, IDD-CH₂), 2.00 – 1.84 (m, 4H, cod-CH₂), 1.83 – 1.61 (m, 12H, IDD-CH₂), 1.52 – 1.17 (m, 30H, IDD-CH₂). $^{19}\text{F}\{^1\text{H}\}$ NMR (470 MHz, C_6D_6): δ -219.7 (s). $^{13}\text{C}\{^1\text{H}\}$ NMR (100 MHz, C_6D_6): δ 182.0 (Ir-C_{carbene}), 117.0 (N-(CH)₂-N), 84.3 (cod-CH), 56.8 (cod-CH), 43.3 (N-CH(CH₃)₂), 35.1 (cod-CH₂), 32.5, 31.7, 29.5, 25.3, 25.1, 24.1, 23.8, 23.7, 23.5, 23.4, 23.3, 22.4. **Anal. Calcd.** for C₃₅H₆₀FIrN₂ (MW 720.09): C, 58.38; H, 8.40; N, 3.89. Found: C, 58.44; H, 8.48; N, 3.91.

[Rh(cod)(IPr)(F)] **11a**

Method A: A Schlenk tube was charged with [Rh(cod)(IPr)(OH)] (**10a**) (50 mg, 0.081 mmol) in benzene (1 mL). NEt₃·3HF (4.5 μL, 0.027 mmol) was added under Ar and the reaction mixture was stirred at rt for 3.5 h. The product was reduced *in vacuo* and azeotroped with hexane (2 x 2 mL) to give a yellow solid. The solid was washed with hexane (2 x 1 mL) and dried to give [Rh(cod)(IPr)(F)] (**11a**) (41.5 mg, 83%) as a yellow solid.

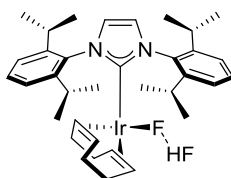
Method B: A vial was charged with [Rh(cod)(IPr)(OH)] (**10a**) (20 mg, 0.032 mmol) and KHF₂ (8.0 mg, 0.098 mmol) in THF (1 mL) and the reaction mixture was stirred at rt for 5 h. Once complete, the reaction mixture was filtered through celite and concentrated *in vacuo* to give a yellow solid. The solid was washed with cold pentane (3 x 1 mL) and dried *in vacuo* to give [Rh(cod)(IPr)(F)] (**11a**) (15.5 mg, 78%) as a yellow solid. ¹H NMR (300 MHz, C₆D₆): δ 7.33 (t, 2H, ³J_{HH} = 7.6, *p*-ArH), 7.25 (d, 4H, ³J_{HH} = 7.6, *m*-ArH), 6.57 (s, 2H, N-(CH)₂-N), 4.96 – 4.75 (m, 2H, cod-CH), 3.39 – 3.08 (m, 4H, CH(CH₃)₂), 3.04 – 2.85 (m, 2H, cod-CH), 1.99 – 1.76 (m, 4H, cod-CH₂), 1.52 (d, 12H, ³J_{HH} = 6.7, CH₃), 1.45 – 1.20 (m, 4H, cod-CH₂), 1.05 (d, 12H, ³J_{HH} = 6.9, CH₃). ¹⁹F{¹H} NMR (282 MHz, C₆D₆): δ -252.8 (d, ¹J_{RhF} = 77). ¹³C{¹H} NMR (75 MHz, C₆D₆): δ 189.1 (d, ¹J_{RhC} = 54, Rh-C_{carbene}), 147.2 (ArC), 136.7 (ArC), 130.1 (ArCH), 124.0 (N-(CH)₂-N), 123.9 (ArCH), 97.0 (d, ¹J_{RhC} = 5, cod-CH), 61.4 (d, ¹J_{RhC} = 15, cod-CH), 33.6 (cod-CH₂), 28.9 (CH(CH₃)₂), 28.2 (cod-CH₂), 26.5 (CH₃), 23.2 (CH₃). IR (ATR) ν = 800.46 (s), 754.17 (s) cm⁻¹. **Anal. Calcd.** for C₃₅H₄₈FRhN₂ (MW 618.67): C, 67.95; H, 7.82; N, 4.53. Found: C, 68.04; H, 7.76; N, 4.39.

[Rh(cod)(ICy)F] **11b**

Method A: A vial was charged with [Rh(cod)(ICy)(OH)] (**10b**) (20 mg, 0.032 mmol) and KHF₂ (8.0 mg, 0.10 mmol) in THF (1 mL) and the reaction mixture was stirred at rt for 5 h. Once complete, the reaction mixture was filtered through celite and

concentrated *in vacuo* to give a yellow solid. The solid was washed with cold pentane (3 x 1 mL) and dried *in vacuo* to give [Rh(cod)(ICy)(F)] (**11b**) (16 mg, 81%) as a yellow solid.

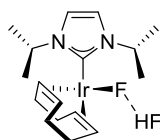
Method B: A Schlenk tube was charged with [Rh(cod)(ICy)OH] (**10b**) (50 mg, 0.11 mmol) in benzene (1 mL). NEt₃·3HF (6.0 μL, 0.036 mmol) was added under Ar and the reaction mixture was stirred at rt for 3.5 h. The product was reduced *in vacuo* and azeotroped with hexane (2 x 2 mL) to give a yellow solid. The solid was washed with pentane (2 x 1 mL) and dried to give [Rh(cod)(ICy)(F)] (**11b**) (43 mg, 86%) as a yellow solid. ¹H NMR (500 MHz, C₆D₆): δ 6.39 (s, 2H, N-(CH)₂-N), 5.69 – 5.56 (m, 2H, NCH), 5.38 – 5.26 (m, 2H, cod-CH), 3.14 – 3.04 (m, 2H, cod-CH), 2.69 – 2.51 (m, 2H, ICy-CH₂), 2.52 – 2.29 (m, 4H, cod-CH₂), 1.96 – 1.80 (m, 4H, cod-CH₂), 1.80 – 1.71 (m, 2H, ICy-CH₂), 1.71 – 1.58 (m, 4H, ICy-CH₂), 1.57 – 1.05 (m, 10H, ICy-CH₂), 1.05 – 0.85 (m, 2H, ICy-CH₂). ¹⁹F{¹H} NMR (470 MHz, C₆D₆): δ -257 (br, Rh-F). ¹³C{¹H} NMR (125 MHz, CD₂Cl₂): δ 181.0 (Ir-C_{carbene}, from HMBC), 117.4 (N-(CH)₂-N), 98.0 (br, cod-CH), 62.3 (br, cod-CH), 60.8 (N-(CH)₂-N), 35.1 (ICy-CH₂), 34.6 (ICy-CH₂), 33.7 (cod-CH₂), 28.7 (cod-CH₂), 26.5 (ICy-CH₂), 26.4 (ICy-CH₂), 25.8 (ICy-CH₂). FTIR (ATR) ν = 705.95 (s), 1990.24 (w, br), 2924.09 (s) cm⁻¹. Anal. Calcd. for C₂₃H₃₆FRhN₂ (MW 462.45): C, 59.74; H, 7.85; N, 6.06. Found: C, 59.58; H, 7.66; N, 6.18.



[Ir(cod)(IPr)(HF₂)] **12a**

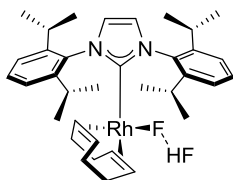
A Schlenk tube was charged with [Ir(cod)(IPr)(OH)] (**8a**) (400 mg, 0.57 mmol) in THF (2 mL). NEt₃·3HF (63 μL, 0.38 mmol) was added under Ar and the reaction mixture was stirred at rt for 4.5 h. The product was reduced *in vacuo* and azeotroped with pentane (3 x 2 mL) to give a yellow solid. The solid was washed with hexane (3 x 2 mL) and dried to give [Ir(cod)(IPr)(HF₂)] (**12a**) (384 mg, 93%) as a yellow solid. ¹H NMR (300 MHz, C₆D₆): δ 11.32 (d, 1H, ¹J_{FH} = 395.0, F-HF), 7.27 (t, 2H, ³J_{HH} = 7.7, *p*-ArH), 7.17 (d, 4H, ³J_{HH} = 7.7, *m*-ArH), 6.49 (s, 2H, N-(CH)₂-N), 4.67 – 4.57 (m, 2H, cod-CH), 3.04 (sept., 4H, ³J_{HH} = 6.8, CH(CH₃)₂), 2.91 – 2.82 (m, 2H, cod-CH), 1.75 – 1.58 (m, 4H, cod-CH₂), 1.50 (d, 12H, ³J_{HH} = 6.7, CH₃), 1.25 – 1.15 (m, 4H, cod-CH₂),

1.02 (d, 12H, $^3J_{HH} = 6.8$, CH₃); $^1\text{H NMR}$ (500 MHz, 200K, CD₂Cl₂): δ 11.73 (app. dd, 1H, $^1J_{FH} = 395.0$, $^1J_{FH} = 40.0$, Ir-F-HF). $^{19}\text{F NMR}$ (282 MHz, C₆D₆): δ -185.2 (br. d, $^1J_{HF} = 395$, Ir-F-HF), -236.2 (br s., Ir-F-HF). $^{19}\text{F NMR}$ (470 MHz, 200K, CD₂Cl₂): δ -177.9 (dd, $^1J_{HF} = 395$, $^2J_{FF} = 120$, Ir-F-HF), -238.9 (dd, $^2J_{FF} = 120$, $^1J_{HF} = 40$, Ir-F-HF). $^{13}\text{C}\{^1\text{H}\}$ NMR (75 MHz, C₆D₆): δ 183.7 (Ir-C_{carbene}), 146.8 (ArC), 136.0 (ArC), 130.3 (ArCH), 124.1 (N-(CH)₂-N), 123.9 (ArCH), 84.7 (d, $^2J_{FC} = 2$, cod-CH), 45.0 (d, $^2J_{FC} = 4$, cod-CH), 34.3 (cod-CH₂), 29.1 (CH(CH₃)₂), 28.4 (cod-CH₂), 26.4 (CH₃), 22.9 (CH₃). **FTIR (ATR)** $\nu = 2623.19$ (s, br, HF₂), 1807.30 (w, HF₂), 1215.15(s) cm⁻¹. **Anal. Calcd.** for C₃₅H₄₉F₂IrN₂ (MW 727.99): C, 57.74; H, 6.78; N, 3.85. Found: C, 57.90; H, 6.83; N, 3.80.

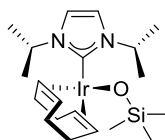


[Ir(cod)(IⁱPr)(HF₂)] **12b**

A Schlenk tube was charged with [Ir(cod)ⁱPr](OH)] (**8b**) (50.0 mg, 0.107 mmol) in THF (1 mL). NEt₃·3HF (11.8 μL , 0.071 mmol) was added under Ar and the reaction mixture was stirred at rt for 4.5 h. The reaction mixture was reduced *in vacuo* and azeotroped with hexane (2 x 2 mL) to give a yellow solid. The solid was washed with pentane (2 x 2 mL) and dried to give [Ir(cod)(IⁱPr)(HF₂)] (**12b**) (43.0 mg, 82%) as a yellow solid. $^1\text{H NMR}$ (500 MHz, C₆D₆): δ 12.22 – 11.32 (br s, 1H, Ir-F-HF), 6.25 (s, 2H, N-(CH)₂-N), 5.68 (sept., 2H, $^3J_{HH} = 6.8$, CH(CH₃)₂), 4.98 – 4.92 (m, 2H, cod-CH), 2.95 – 2.87 (m, 2H, cod-CH), 2.87 – 2.11 (m, 4H, cod-CH₂), 1.61 – 1.49 (m, 4H, cod-CH₂), 1.26 (d, 6H, $^3J_{HH} = 6.6$, CH₃), 1.07 (d, 6H, $^3J_{HH} = 6.8$, CH₃); $^1\text{H NMR}$ (500 MHz, 197.5K, CD₂Cl₂): δ 11.53 (dd, $^1J_{FH} = 403.0$, $^1J_{FH} = 44.8$, Ir-F-HF); $^{19}\text{F NMR}$ (470 MHz, C₆D₆): δ -187.5 (br, Ir-F-HF), -243.5 (br, Ir-F-HF). $^{19}\text{F NMR}$ (470 MHz, 197.5K, CD₂Cl₂): δ -184.3 (dd, $^1J_{HF} = 403$, $^2J_{FF} = 99$, Ir-F-HF), -246.5 (app. dd, $^2J_{FF} = 95$, $^1J_{HF} = 45$, Ir-F-HF). $^{13}\text{C}\{^1\text{H}\}$ NMR (MHz, C₆D₆): δ 178.1 (Ir-C_{carbene}), 116.6 (N-(CH)₂-N), 85.0 (cod-CH), 52.7 (cod-CH), 44.9 (CH(CH₃)₂), 34.5 (cod-CH₂), 29.1 (cod-CH₂), 24.1 (CH₃), 23.1 (CH₃). **FTIR (ATR)** $\nu = 2546.04$ (s, br, HF₂), 1869.02 (s, br HF₂), 1215.15 (s) cm⁻¹. **Anal. Calcd.** for C₁₇H₂₉F₂IrN₂ (MW 491.64): C, 41.53; H, 5.95; N, 5.70. Found: C, 41.62; H, 5.87; N, 5.78.

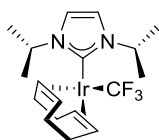
[Rh(cod)(IPr)(HF₂)] **13a**

A Schlenk tube was charged with [Rh(cod)(IPr)(OH)] (**10a**) (400 mg, 0.65 mmol) in THF (2 mL). NEt₃·3HF (72 μL, 0.43 mmol) was added under Ar and the reaction mixture was stirred at rt for 4.5 h. The product was reduced *in vacuo* and azeotroped with hexane (3 x 2 mL) to give a yellow solid. The solid was washed with pentane (3 x 1 mL) and dried to give [Rh(cod)(IPr)(HF₂)] (**13a**) (375 mg, 90%) as a yellow solid. ¹H NMR (400 MHz, C₆D₆): δ 12.4 (d, 1H, ¹J_{FH} = 350.0, Rh-F-HF), 7.31 (t, 2H, ³J_{HH} = 7.7, *p*-ArH), 7.22 (d, 4H, ³J_{HH} = 7.7, *m*-ArH), 6.49 (s, 2H, N-(CH)₂-N), 4.94 – 4.84 (m, 2H, cod-CH), 3.09 – 2.93 (m, 6H, CH(CH₃)₂, cod-CH), 1.83 – 1.68 (m, 4H, cod-CH₂), 1.51 (d, 12H, ³J_{HH} = 6.7, CH₃), 1.45 – 1.25 (m, 4H, cod-CH₂), 1.02 (d, 12H, ³J_{HH} = 6.9, CH₃); ¹H NMR (500 MHz, 200K, CD₂Cl₂): δ 12.89 (app. dd, ¹J_{FH} = 350.0, ¹J_{FH} = 25.0, Rh-F-HF); ¹⁹F{¹H} NMR (470 MHz, C₆D₆): δ -181.5 (br., Rh-F-HF), -255.7 (br, Rh-F-HF). ¹⁹F NMR (470 MHz, 200 K, CD₂Cl₂): δ -173.1 (dd, ¹J_{FH} = 350, ²J_{FF} = 150, Rh-FHF), -253.6 (app. dd, ²J_{FF} = 150, ¹J_{FH} = 50, Rh-F-HF). ¹³C{¹H} NMR (100 MHz, C₆D₆): δ 186.3 (d, ¹J_{RhC} = 52, Rh-C_{carbene}), 147.1 (ArC), 136.3 (ArC), 130.3 (ArCH), 124.4 (N-(CH)₂-N), 124.1 (ArCH), 97.9 (d, ¹J_{RhC} = 8, cod-CH), 62.3 (d, ¹J_{RhC} = 15, cod-CH), 33.3 (cod-CH₂), 29.0 (CH(CH₃)₂), 27.9 (cod-CH₂), 26.5 (CH₃), 23.0 (CH₃). FTIR (ATR) ν = 2530.61 (s, br, HF₂), 1890.24 (s, br, HF₂) 758.02 (s) cm⁻¹. **Anal. Calcd.** for C₃₅H₄₉F₂N₂Rh (MW 638.68): C, 65.82; H, 7.73; N, 4.39. Found: C, 66.0; H, 7.85; N, 4.26.

[Ir(cod)(IPr)(F)] **14**

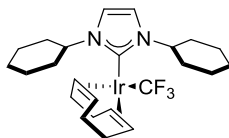
A vial was charged with [Ir(cod)(IPr)(OH)] (**8b**) (82.0 mg, 0.17 mmol) in toluene (1 mL). TMSCF₃ (31 μL, 0.21 mmol) was added and the reaction mixture was stirred at rt for 2 h. Once complete, the mixture was reduced *in vacuo* and azeotroped with hexane (2 x 1 mL) and washed with hexane (2 x 1 mL). The product was dried *in vacuo* to give [Ir(cod)(IPr)(OSiMe₃)] (**14**) (88.4 mg, 96%) as a yellow solid. ¹H NMR (300 MHz, C₆D₆): δ 6.19 (s, 2H, N-(CH)₂-N), 5.76 (sept., 2H, ³J_{HH} = 6.8, N-CH(CH₃)₂), 4.86

– 4.75 (m, 2H, cod-CH), 2.89 – 2.77 (m, 2H, cod-CH), 2.49 – 2.20 (m, 4H, cod-CH₂), 1.86 – 1.66 (m, 4H, cod-CH₂), 1.20 (d, 6H, ³J_{HH} = 6.7, CHCH₃), 1.11 (d, 6H, ³J_{HH} = 6.8, CHCH₃), 0.27 (s, 9H, Si-CH₃). ¹³C{¹H} NMR (75 MHz, C₆D₆): δ 180.6 (Ir-C_{carbene}), 115.9 (N-(CH)₂-N), 83.6 (cod-CH), 51.9 (cod-CH), 44.5 (N-CH(CH₃)₂), 34.8 (cod-CH₂), 29.9 (cod-CH₂), 23.6 (CHCH₃), 5.0 (Si-CH₃). **Anal. Calcd.** for C₂₀H₃₇IrN₂OSi (MW 541.82): C, 44.33; H, 6.88; N, 5.09. Found: C, 44.25; H, 6.70; N, 5.09.

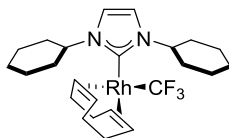


[Ir(cod)(I'Pr)(CF₃)] **15a**

A Schlenk tube was charged with AgF (78.0 mg, 0.61 mmol) and acetonitrile (2 mL), in the dark and cooled under Ar to -40 °C. TMSF₃ (245 μL, 1.64 mmol) was added and after 15 mins the reaction mixture was warmed to rt, where it was stirred for 30 mins. [Ir(cod)(I'Pr)Cl] (**6b**) (200 mg, 0.410 mmol) was added and the reaction mixture was stirred for 16 h. Upon completion, the solvent was removed *in vacuo*, the product dissolved in THF (2 mL) and filtered through a tightly packed celite column to give a red solution. The solvent was removed *in vacuo* and the resultant solid was washed with a cold mixture of pentane/Et₂O (2:1, 3 x 1 mL). The product was dried *in vacuo* to give [Ir(cod)(I'Pr)(CF₃)] (**15a**) (160 mg, 75%) as a red solid. ¹H NMR (500 MHz, C₆D₆): δ 6.21 (s, 2H, N-(CH)₂-N), 5.46 (sept., 2H, ³J_{HH} = 6.8, N-CH(CH₃)₂), 4.91 – 4.86 (m, 2H, cod-CH), 3.64 – 3.58 (m, 2H, cod-CH), 2.26 – 2.08 (m, 4H, cod-CH₂), 1.84 – 1.76 (m, 4H, cod-CH₂), 1.16 (d, 6H, ³J_{HH} = 6.7, CHCH₃), 1.04 (d, 6H, ³J_{HH} = 6.8, CHCH₃). ¹⁹F{¹H} NMR (470 MHz, C₆D₆): δ -25.8 (s). ¹³C{¹H} NMR (125 MHz, C₆D₆): δ 180.2 (q, ³J_{FC} = 5, Ir-C_{carbene}), 146.3 (q, ¹J_{FC} = 346, CF₃), 116.3 (N-(CH)₂-N), 75.2 (app. q, ³J_{FC} = 1, cod-CH), 71.6 (q, ³J_{FC} = 2, cod-CH), 52.5 (cod-CH₂), 31.8 (cod-CH₂), 31.5 (N-CH(CH₃)₂), 23.7 (CH₃), 22.8 (q, ⁶J_{FC} = 1, CH₃). **Anal. Calcd.** for C₁₈H₂₈F₃IrN₂ (MW 521.65): C, 41.45; H, 5.41; N, 5.37. Found: C, 41.31; H, 5.32; N, 5.60. **MS** (+ve EI) for C₁₈H₂₈F₃IrN₂ (MW: 521.65, Exact mass calcd. 522.18); m/z 522.1 (100, M⁺, ¹⁹³Ir), 520.1 (64, M⁺, ¹⁹¹Ir); **HRMS**: 520.18601 (520.1805 for C₁₈H₂₈F₃¹⁹¹IrN₂).

[Ir(cod)(ICy)(CF₃)] **15c**

A Schlenk tube was charged with AgF (14 mg, 0.11 mmol) and MeCN (1 mL) in the dark. TMSCF₃ (44 μL, 0.30 mmol) was added under Ar at -40 °C. After 15 mins the reaction mixture was warmed to rt, where it was stirred for 30 mins. [Ir(cod)(ICy)Cl] (**6c**) (42 mg, 0.074 mmol) was added and the reaction mixture was stirred at rt for 16 h. Upon completion, the solvent was removed *in vacuo*, the product dissolved in THF (2 mL) and filtered through celite to give a red solution. The solvent was removed *in vacuo* and the resultant solid was washed with a cold mixture of pentane/Et₂O (3:1, 3 x 1 mL). The product was dried *in vacuo* to give [Ir(cod)(ICy)(CF₃)] (**15c**) (35 mg, 79%) as a red solid. ¹H NMR (500 MHz, C₆D₆): δ 6.34 (s, 2H, N-(CH)₂-N), 5.19 (tt, 2H, ³J_{HH} = 11.8, ³J_{HH} = 3.6, N-CH(ICy)), 4.94 – 4.81 (m, 2H, cod-CH), 3.72 – 3.61 (m, 2H, cod-CH), 2.33 (br. d, 2H, ³J_{HH} = 12.0, ICy-CH₂), 2.27 – 2.10 (m, 4H, cod-CH₂), 1.91 – 1.73 (m, 6H, cod-CH₂, ICy-CH₂), 1.70 – 1.54 (m, 4H, ICy-CH₂), 1.48 (br. d, 2H, ³J_{HH} = 13.0, ICy-CH₂), 1.44 – 1.30 (m, 4H, ICy-CH₂), 1.23 (qd, 2H, ³J_{HH} = 12.5, ³J_{HH} = 3.5 ICy-CH₂), 1.11 (qd, 2H, ³J_{HH} = 12.0, ³J_{HH} = 3.5 ICy-CH₂), 0.98 – 0.88 (m, 2H, ICy-CH₂). ¹⁹F{¹H} NMR (470 MHz, C₆D₆): δ -26.0 (s). ¹³C{¹H} NMR (125 MHz, C₆D₆): δ 180.4 (q, ³J_{FC} = 5, Ir-C_{carbene}), 146.1 (q, ¹J_{FC} = 347, CF₃), 116.9 (N-(CH)₂-N), 74.9 (cod-CH), 71.6 (q, ³J_{FC} = 2, cod-CH), 60.4 (N-CH(ICy)), 35.2 (ICy-CH₂), 33.6 (q, ⁶J_{FC} = 1, ICy-CH₂), 32.1 (cod-CH₂), 31.6 (cod-CH₂), 26.3 (ICy-CH₂), 25.9 (ICy-CH₂), 25.6 (ICy-CH₂). **Anal. Calcd.** for C₂₄H₃₆F₃IrN₂ (MW 601.77): C, 47.90; H, 6.03; N, 4.66. Found: C, 47.85; H, 5.95; N, 4.75.

[Rh(cod)(ICy)(CF₃)] **16c**

A Schlenk tube was charged with AgF (40 mg, 0.31 mmol) and MeCN (1 mL) in the dark and TMSCF₃ (110 μL, 0.730 mmol) was added under Ar to -40 °C. After 15 mins the reaction mixture was warmed to rt, where it was stirred for 30 mins. [Rh(cod)(ICy)Cl] (**9b**) (100 mg, 0.21 mmol) was added and the reaction mixture was stirred for 16 h. Upon completion, the reaction mixture was filtered on celite and

concentrated *in vacuo*. The resultant solid was dissolved in hexane and filtered on celite. The eluent was concentrated *in vacuo* to give [Rh(cod)(ICy)(CF₃)] (**16c**) (57 mg, 53%) as a yellow solid. ¹H NMR (400 MHz, C₆D₆): δ 6.36 (s, 2H, N-(CH)₂-N), 5.34 (tt, 2H, ³J_{HH} = 12.0, ³J_{HH} = 7.3, N-CH(ICy)), 5.27 – 5.18 (m, 2H, cod-CH), 4.16 – 4.08 (m, 2H, cod-CH), 2.40 (br. d, 2H, ³J_{HH} = 12.2, ICy-CH₂), 2.36 – 2.20 (m, 4H, cod-CH₂), 2.05 – 1.95 (m, 4H, cod-CH₂), 1.84 (br. d, 2H, ³J_{HH} = 12.2, ICy-CH₂), 1.70 – 1.57 (m, 4H, ICy-CH₂), 1.47 – 1.38 (m, 4H, ICy-CH₂), 1.25 (qd, 2H, ³J_{HH} = 12.6, ³J_{HH} = 3.6, ICy-CH₂), 1.14 (qd, 2H, ³J_{HH} = 12.4, ³J_{HH} = 3.8, ICy-CH₂), 1.02 – 0.90 (m, 4H, ICy-CH₂). ¹⁹F{¹H} NMR (376 MHz, C₆D₆): δ -21.7 (d, ²J_{RhF} = 27 Hz. ¹³C{¹H} NMR (125 MHz, C₆D₆): δ 185.6 (m, Rh-C_{carbene}), 117.0 (N-(CH)₂-N), 87.7 (d, ³J_{FC} = 9, cod-CH), 86.0 (d, ³J_{FC} = 7, cod-CH), 60.8 (N-CH(ICy)), 35.2 (ICy-CH₂), 33.8 (ICy-CH₂), 31.3 (cod-CH₂), 31.2 (cod-CH₂), 26.4 (ICy-CH₂), 26.0 (ICy-CH₂), 25.7 (ICy-CH₂). **Anal. Calcd.** for C₂₄H₃₆F₃N₂Rh (MW 512.47): C, 56.25; H, 7.08; N, 5.47. Found: C, 56.37; H, 7.15; N, 5.64. *(CF₃ not observed by ¹³C{¹H} NMR)

7. CONCLUSIONS

The initial aims of this project were to identify and execute robust synthetic methods for the preparation of Rh(I)-hydroxide complexes and to explore their reactivity, with a fundamental focus on their catalytic capabilities. The Rh(I)-NHC hydroxides proved to be very active catalysts in the conjugate addition of arylboronic acids to α,β -unsaturated ketones, challenging the state of the art catalysts which employ very electron deficient ancillary ligands. Rh(I)-hydroxides were also active catalysts in the hydrosilylation of terminal alkenes, boasting high activities. However, selectivity proved to be a key issue, with dehydrogenative silylation being very competitive with hydrosilylation. We were able to exploit this unwanted side reaction, and demonstrated remarkable shifts in selectivity towards dehydrogenative silylation, by optimising the ratio of the starting materials.

When we extended the methodology of metal-NHC hydroxides to include iridium, the focus was on reactivity as opposed to catalysis. Having established general procedures for the preparation of a family of [Ir(cod)(NHC)(OH)] complexes, we tested the reactivity of the motif towards a number of organic substrates. Reactivity was confined to the hydroxyl moiety and the Ir-hydroxide deprotonated a number of Si-H, O-H, N-H and C-H bonds to afford a wide array of new iridium complexes. The bond activation reactions were very straight-forward and atom economical, generating only the desired product and H₂O in each case. Following this study, we examined the reactivity of these new Ir(I)-alkoxides and Ir(I)-amides towards carbon dioxide. CO₂ was found to insert into several Ir-N and Ir-O bonds under very mild conditions. In the case of Ir(I)-NHC hydroxide, insertion of CO₂ led to the unique [$\{\text{Ir(I)}\}_2(\mu\text{-}\kappa^1\text{O}:\kappa^2\text{O},\text{O-CO}_3)$] complex, both in solution and in the solid state. Kinetic and theoretical calculations were performed, confirming the facile nature of the CO₂ insertion reaction *via* an associative transition state, providing valuable mechanistic insight into the CO₂ fixation reaction.

As a final study, we used the Rh-NHC and Ir-NHC scaffolds to prepare fluorinated organometallic complexes. General routes for the preparation of Ir and Rh fluoride, bifluoride and trifluoromethyl complexes have been reported and access to these complexes allowed us to investigate the relationships between these interesting species.

8. REFERENCES

1. (a) R. R. Schrock, *Angew. Chem. Int. Ed.*, 2006, **45**, 3748-3759; (b) R. H. Grubbs, *Angew. Chem. Int. Ed.*, 2006, **45**, 3760-3765; (c) Y. Chauvin, *Angew. Chem. Int. Ed.*, 2006, **45**, 3740-3747.
2. (a) A. Suzuki, *Angew. Chem. Int. Ed.*, 2011, **50**, 6722-6737; (b) E.-i. Negishi, *Angew. Chem. Int. Ed.*, 2011, **50**, 6738-6764.
3. (a) J. Huang, E. D. Stevens, S. P. Nolan and J. L. Petersen, *J. Am. Chem. Soc.*, 1999, **121**, 2674-2678; (b) M. Scholl, S. Ding, C. W. Lee and R. H. Grubbs, *Org. Lett.*, 1999, **1**, 953-956.
4. (a) L. F. Tietze, H. Ila and H. P. Bell, *Chem. Rev.*, 2004, **104**, 3453-3516; (b) T. W. Lyons and M. S. Sanford, *Chem. Rev.*, 2010, **110**, 1147-1169; (c) C. A. Fleckenstein and H. Plenio, *Chem. Soc. Rev.*, 2010, **39**, 694-711; (d) G. C. Fortman and S. P. Nolan, *Chem. Soc. Rev.*, 2011, **40**, 5151-5169.
5. G. A. Somorjai and K. McCrea, *App. Catal. A: General*, 2001, **222**, 3-18.
6. C. A. Busacca, D. R. Fandrick, J. J. Song and C. H. Senanayake, *Adv. Synth. Catal.*, 2011, **353**, 1825-1864.
7. P. Anastas and N. Eghbali, *Chem. Soc. Rev.*, 2010, **39**, 301-312.
8. R. A. Sheldon, *Green Chem.*, 2007, **9**, 1273-1283.
9. C. Marcilly, *J. Catal.*, 2003, **216**, 47-62.
10. F. S. Stone, *J. Catal.*, 2003, **216**, 2-11.
11. R. V. Chaudhari, A. Seayad and S. Jayasree, *Catal. Today*, 2001, **66**, 371-380.
12. H. W. Roesky, S. Singh, K. K. M. Yusuff, J. A. Maguire and N. S. Hosmane, *Chem. Rev.*, 2006, **106**, 3813-3843.
13. R. G. Pearson, *J. Am. Chem. Soc.*, 1963, **85**, 3533-3539.
14. (a) R. G. Bergman, *Polyhedron*, 1995, **14**, 3227-3237; (b) N. M. Doherty and N. W. Hoffmann, *Chem. Rev.*, 1991, **91**, 553-573.
15. T. Hayashi, M. Takahashi, Y. Takaya and M. Ogasawara, *J. Am. Chem. Soc.*, 2002, **124**, 5052-5058.
16. (a) M. A. Bennett and T. Yoshida, *J. Am. Chem. Soc.*, 1978, **100**, 1750-1759; (b) D. P. Arnold and M. A. Bennett, *J. Organomet. Chem.*, 1980, **199**, 119-135; (c) M. A. Bennett and T. Yoshida, *J. Am. Chem. Soc.*, 1973, **95**, 3030-3031; (d) C. M. Jensen and W. C. Trogler, *J. Am. Chem. Soc.*, 1986, **108**, 723-729.
17. (a) C. M. Jensen and W. C. Trogler, *Science*, 1986, **233**, 1069-1071; (b) G. Dong, P. Teo, Z. K. Wickens and R. H. Grubbs, *Science*, 2011, **333**, 1609-1612.
18. T. Yoshida, T. Matsuda, T. Okano, T. Kitani and S. Otsuka, *J. Am. Chem. Soc.*, 1979, **101**, 2027-2038.
19. H. E. Bryndza and W. Tam, *Chem. Rev.*, 1988, **88**, 1163-1188.
20. (a) D. Choudhury and D. J. Cole-Hamilton, *Dalton Trans.*, 1982, 1885-1893; (b) T. Yoshida, Y. Ueda and S. Otsuka, *J. Am. Chem. Soc.*, 1978, **100**, 3941-3942.
21. D. Milstein, *Chem. Commun.*, 1986, 817-818.
22. G. Parkin, *Chem. Rev.*, 2004, **104**, 699-768.
23. W. J. Evans, M. A. Hozbor, S. G. Bott, G. H. Robinson and J. L. Atwood, *Inorg. Chem.*, 1988, **27**, 1990-1993.
24. S. S. Al-Juaid, N. H. Buttrus, C. Eaborn, P. B. Hitchcock, A. T. L. Roberts, J. D. Smith and A. C. Sullivan, *Chem. Commun.*, 1986, 908-909.
25. M. Weidenbruch, M. Herrndorf, A. Schäfer, S. Pohl and W. Saak, *J. Organomet. Chem.*, 1989, **361**, 139-145.
26. B. K. Nicholson and S. K. Whitley, *J. Organomet. Chem.*, 2004, **689**, 515-521.
27. G. Gregorio, G. Pregaglia and R. Ugo, *Inorg. Chim. Acta.*, 1969, **3**, 89-93.
28. C. A. Read and W. R. Roper, *Dalton Trans.*, 1973, 1370-1375.
29. L. Vaska and J. Peone, *Chem. Commun.*, 1971, 418-419.
30. C. A. Miller, T. S. Janik, C. H. Lake, L. M. Toomey, M. R. Churchill and J. D. Atwood, *Organometallics*, 1994, **13**, 5080-5087.

31. (a) J. W. Kang and P. M. Maitlis, *J. Organomet. Chem.*, 1971, **30**, 127-133; (b) A. Nutton and P. M. Maitlis, *Dalton Trans.*, 1981, 2335-2338; (c) A. Nutton, P. M. Bailey and P. M. Maitlis, *Dalton Trans.*, 1981, 1997-2002.
32. L. M. Green and D. W. Meek, *Organometallics*, 1989, **8**, 659-666.
33. M. Gorol, Nadia C. Mösch-Zanetti, Herbert W. Roesky, M. Noltemeyer and H.-G. Schmidt, *Eur. J. Inorg. Chem.*, 2004, **2004**, 2678-2682.
34. (a) A. Mori and T. Kato, *Synlett.*, 2002, **7**, 1167-1169; (b) T. Koike, X. Du, A. Mori and K. Osakada, *Synlett.*, 2002, **02**, 0301-0303.
35. A. Mori, Y. Danda, T. Fujii, K. Hirabayashi and K. Osakada, *J. Am. Chem. Soc.*, 2001, **123**, 10774-10775.
36. T. Fujii, T. Koike, A. Mori and K. Osakada, *Synlett.*, 2002, **02**, 0295-0297.
37. T. Fujii, T. Koike, A. Mori and K. Osakada, *Synlett.*, 2002, **02**, 0298-0300.
38. N. Tokunaga, K. Yoshida and T. Hayashi, *Proc Natl Acad Sci U S A*, 2004, **101**, 5445-5449.
39. (a) R. Itooka, Y. Iguchi and N. Miyaura, *J. Org. Chem.*, 2003, **68**, 6000-6004; (b) J.-G. Boiteau, R. Imbos, A. J. Minnaard and B. L. Feringa, *Org. Lett.*, 2003, **5**, 681-684; (c) J.-G. Boiteau, A. J. Minnaard and B. L. Feringa, *J. Org. Chem.*, 2003, **68**, 9481-9484; (d) F.-X. Chen, A. Kina and T. Hayashi, *Org. Lett.*, 2005, **8**, 341-344; (e) K. Kurihara, N. Sugishita, K. Oshita, D. Piao, Y. Yamamoto and N. Miyaura, *J. Organomet. Chem.*, 2007, **692**, 428-435; (f) K. Okamoto, T. Hayashi and V. H. Rawal, *Org. Lett.*, 2008, **10**, 4387-4389; (g) Y. Ma, C. Song, C. Ma, Z. Sun, Q. Chai and M. B. Andrus, *Angew. Chem. Int. Ed. Engl.*, 2003, **42**, 5871-5874.
40. (a) O. Blum and D. Milstein, *J. Am. Chem. Soc.*, 2002, **124**, 11456-11467; (b) D. Milstein, J. C. Calabrese and I. D. Williams, *J. Am. Chem. Soc.*, 1986, **108**, 6387-6389; (c) R. Dorta, H. Rozenberg, L. J. W. Shimon and D. Milstein, *J. Am. Chem. Soc.*, 2001, **124**, 188-189.
41. D. Morales-Morales, D. W. Lee, Z. Wang and C. M. Jensen, *Organometallics*, 2001, **20**, 1144-1147.
42. C. A. Reed and W. R. Roper, *Dalton Trans.*, 1973, 1014-1020.
43. M. A. Bennett, G. B. Robertson, P. O. Whimp and T. Yoshida, *J. Am. Chem. Soc.*, 1973, **95**, 3028-3030.
44. W. Keim, *J. Organomet. Chem.*, 1968, **14**, 179-184.
45. K. A. Woerpel and R. G. Bergman, *J. Am. Chem. Soc.*, 1993, **115**, 7888-7889.
46. J. C. M. Ritter and R. G. Bergman, *J. Am. Chem. Soc.*, 1997, **119**, 2580-2581.
47. V. V. Grushin, V. F. Kuznetsov, C. Bensimon and H. Alper, *Organometallics*, 1995, **14**, 3927-3932.
48. (a) M. J. Burn, M. G. Fickes, J. F. Hartwig, F. J. Hollander and R. G. Bergman, *J. Am. Chem. Soc.*, 1993, **115**, 5875-5876; (b) J. F. Hartwig, R. G. Bergman and R. A. Andersen, *J. Am. Chem. Soc.*, 1991, **113**, 3404-3418.
49. P. Nun, G. C. Fortman, A. M. Z. Slawin and S. P. Nolan, *Organometallics*, 2011, **30**, 6347-6350.
50. R. F. R. Jazzar, P. H. Bhatia, M. F. Mahon and M. K. Whittlesey, *Organometallics*, 2003, **22**, 670-683.
51. (a) A. W. Kaplan and R. G. Bergman, *Organometallics*, 1997, **16**, 1106-1108; (b) A. W. Kaplan, J. C. M. Ritter and R. G. Bergman, *J. Am. Chem. Soc.*, 1998, **120**, 6828-6829.
52. T. Y. Meyer, K. A. Woerpel, B. M. Novak and R. G. Bergman, *J. Am. Chem. Soc.*, 1994, **116**, 10290-10291.
53. A. W. Kaplan and R. G. Bergman, *Organometallics*, 1998, **17**, 5072-5085.
54. (a) V. V. Grushin and H. Alper, *Organometallics*, 1993, **12**, 1890-1901; (b) A. D. Getty and K. I. Goldberg, *Organometallics*, 2001, **20**, 2545-2551.
55. J. D. Egbert, A. Chartoire, A. M. Z. Slawin and S. P. Nolan, *Organometallics*, 2011, **30**, 4494-4496.
56. B. P. Carrow and J. F. Hartwig, *J. Am. Chem. Soc.*, 2011, **133**, 2116-2119.
57. (a) A. J. Canty, R. T. Honeyman, A. S. Roberts, P. R. Traill, R. Colton, B. W. Skelton and A. H. White, *J. Organomet. Chem.*, 1994, **471**, C8-C10; (b) A. J. Canty, S. D.

- Fritsche, H. Jin, B. W. Skelton and A. H. White, *J. Organomet. Chem.*, 1995, **490**, C18-C19; (c) A. J. Canty, S. D. Fritsche, H. Jin, J. Patel, B. W. Skelton and A. H. White, *Organometallics*, 1997, **16**, 2175-2182.
58. S. Takemoto and V. V. Grushin, *J. Am. Chem. Soc.*, 2013, **135**, 16837-16840.
59. W. Han, Y. Li, H. Tang and H. Liu, *J. Fluorine Chem.*, 2012, **140**, 7-16.
60. A. McCulloch and A. A. Lindley, *Atmos. Environ.*, 2007, **41**, 1560-1566.
61. (a) D. A. Watson, M. Su, G. Teverovskiy, Y. Zhang, J. García-Fortanet, T. Kinzel and S. L. Buchwald, *Science*, 2009, **325**, 1661-1664; (b) E. J. Cho, T. D. Senecal, T. Kinzel, Y. Zhang, D. A. Watson and S. L. Buchwald, *Science*, 2010, **328**, 1679-1681; (c) H. G. Lee, P. J. Milner and S. L. Buchwald, *J. Am. Chem. Soc.*, 2014, **136**, 3792-3795; (d) M. P. Doyle, K. G. High, V. Bagheri, R. J. Pieters, P. J. Lewis and M. M. Pearson, *J. Org. Chem.*, 1990, **55**, 6082-6086; (e) M. H. Katcher and A. G. Doyle, *J. Am. Chem. Soc.*, 2010, **132**, 17402-17404; (f) M.-G. Braun and A. G. Doyle, *J. Am. Chem. Soc.*, 2013, **135**, 12990-12993.
62. (a) S. Gaillard, A. M. Slawin and S. P. Nolan, *Chem. Commun.*, 2010, **46**, 2742-2744; (b) I. I. F. Boogaerts and S. P. Nolan, *J. Am. Chem. Soc.*, 2010, **132**, 8858-8859; (c) A. Gomez-Suarez, R. S. Ramon, A. M. Z. Slawin and S. P. Nolan, *Dalton Trans.*, 2012, **41**, 5461-5463; (d) G. C. Fortman, A. M. Z. Slawin and S. P. Nolan, *Organometallics*, 2010, **29**, 3966-3972; (e) I. I. F. Boogaerts, G. C. Fortman, M. R. L. Furst, C. S. J. Cazin and S. P. Nolan, *Angew. Chem. Int. Ed.*, 2010, **49**, 8674-8677; (f) S. Gaillard, J. Bosson, R. S. Ramón, P. Nun, A. M. Z. Slawin and S. P. Nolan, *Chem. Eur. J.*, 2010, **16**, 13729-13740.
63. S. Gaillard, C. S. J. Cazin and S. P. Nolan, *Acc. Chem. Res.*, 2011, **45**, 778-787.
64. G. C. Fortman, A. Poater, J. W. Levell, S. Gaillard, A. M. Z. Slawin, I. D. W. Samuel, L. Cavallo and S. P. Nolan, *Dalton Trans.*, 2010, **39**, 10382-10390.
65. S. Dupuy, L. Crawford, M. Bühl, A. M. Z. Slawin and S. P. Nolan, *Adv. Synth. Catal.*, 2012, **354**, 2380-2386.
66. S. Dupuy, F. Lazreg, A. M. Z. Slawin, C. S. J. Cazin and S. P. Nolan, *Chem. Commun.*, 2011, **47**, 5455-5457.
67. E. Brulé, S. Gaillard, M.-N. I. Rager, T. Roisnel, V. Guérineau, S. P. Nolan and C. M. Thomas, *Organometallics*, 2011, **30**, 2650-2653.
68. R. S. Ramón, S. Gaillard, A. Poater, L. Cavallo, A. M. Z. Slawin and S. P. Nolan, *Chem. Eur. J.*, 2011, **17**, 1238-1246.
69. A. Gómez-Suárez, Y. Oonishi, S. Meiries and S. P. Nolan, *Organometallics*, 2013, **32**, 1106-1111.
70. Y. Oonishi, A. Gómez-Suárez, A. R. Martin and S. P. Nolan, *Angew. Chem.*, 2013, **125**, 9949-9953.
71. R. H. Crabtree, *J. Organomet. Chem.*, 2005, **690**, 5451-5457.
72. D. Bourissou, O. Guerret, F. P. Gabbañ and G. Bertrand, *Chem. Rev.*, 2000, **100**, 39-92.
73. S. Díez-González, N. Marion and S. P. Nolan, *Chem. Rev.*, 2009, **109**, 3612-3676.
74. S. T. Liddle, I. S. Edworthy and P. L. Arnold, *Chem. Soc. Rev.*, 2007, **36**, 1732-1744.
75. R. S. Bon, F. J. J. de Kanter, M. Lutz, A. L. Spek, M. C. Jahnke, F. E. Hahn, M. B. Groen and R. V. A. Orru, *Organometallics*, 2007, **26**, 3639-3650.
76. H. W. Wanzlick and H. J. Schönherr, *Angew. Chem. Int. Ed.*, 1968, **7**, 141-142.
77. K. Öfele, *J. Organomet. Chem.*, 1968, **12**, P42-P43.
78. (a) M. F. Lappert, *J. Organomet. Chem.*, 1988, **358**, 185-213; (b) D. J. Cardin, B. Cetinkaya and M. F. Lappert, *Chem. Rev.*, 1972, **72**, 545-574.
79. A. J. Arduengo, R. L. Harlow and M. Kline, *J. Am. Chem. Soc.*, 1991, **113**, 361-363.
80. (a) A. J. Arduengo, H. V. R. Dias, R. L. Harlow and M. Kline, *J. Am. Chem. Soc.*, 1992, **114**, 5530-5534; (b) A. J. Arduengo, *Acc. Chem. Res.*, 1999, **32**, 913-921.
81. (a) W. A. Herrmann and C. Köcher, *Angew. Chem. Int. Ed.*, 1997, **36**, 2162-2187; (b) W. A. Herrmann, *Angew. Chem. Int. Ed.*, 2002, **41**, 1290-1309; (c) W. A. Herrmann, M. Elison, J. Fischer, C. Köcher and G. R. J. Artus, *Angew. Chem. Int. Ed.*, 1995, **34**, 2371-2374; (d) W. A. Herrmann, M. Elison, J. Fischer, C. Köcher and G. R. J. Artus, *Chem. Eur. J.*, 1996, **2**, 772-780.

82. (a) J. Henrique Teles, J.-P. Melder, K. Ebel, R. Schneider, E. Gehrler, W. Harder, S. Brode, D. Enders, K. Breuer and G. Raabe, *Helv. Chim. Acta*, 1996, **79**, 61-83; (b) D. Enders, H. Gielen, G. Raabe, J. Runsink and J. H. Teles, *Chem. Ber.*, 1996, **129**, 1483-1488.
83. H. Küçükbay, B. Cetinkaya, S. Guesmi and P. H. Dixneuf, *Organometallics*, 1996, **15**, 2434-2439.
84. S. Díez-González, N. Marion and S. P. Nolan, *Chem. Rev.*, 2009, **109**, 3612-3676.
85. S. Díez-González and S. P. Nolan, *Coord. Chem. Rev.*, 2007, **251**, 874-883.
86. (a) T. Droge and F. Glorius, *Angew. Chem. Int. Ed. Engl.*, 2010, **49**, 6940-6952; (b) P. de Frémont, N. Marion and S. P. Nolan, *Coord. Chem. Rev.*, 2009, **253**, 862-892.
87. T. Weskamp, V. P. W. Böhm and W. A. Herrmann, *J. Organomet. Chem.*, 2000, **600**, 12-22.
88. J. Huang, H.-J. Schanz, E. D. Stevens and S. P. Nolan, *Organometallics*, 1999, **18**, 2370-2375.
89. H. Jacobsen, A. Correa, C. Costabile and L. Cavallo, *J. Organomet. Chem.*, 2006, **691**, 4350-4358.
90. (a) D. M. Khramov, E. L. Rosen, J. A. V. Er, P. D. Vu, V. M. Lynch and C. W. Bielawski, *Tetrahedron*, 2008, **64**, 6853-6862; (b) J. P. Morgan and R. H. Grubbs, *Org. Lett.*, 2000, **2**, 3153-3155; (c) S. T. Nguyen, L. K. Johnson, R. H. Grubbs and J. W. Ziller, *J. Am. Chem. Soc.*, 1992, **114**, 3974-3975.
91. (a) G. C. Fu, S. T. Nguyen and R. H. Grubbs, *J. Am. Chem. Soc.*, 1993, **115**, 9856-9857; (b) S. T. Nguyen, R. H. Grubbs and J. W. Ziller, *J. Am. Chem. Soc.*, 1993, **115**, 9858-9859; (c) N. Stylianides, A. A. Danopoulos, D. Pugh, F. Hancock and A. Zanotti-Gerosa, *Organometallics*, 2007, **26**, 5627-5635.
92. C. A. Tolman, *Chem. Rev.*, 1977, **77**, 313-348.
93. (a) D. J. Nelson and S. P. Nolan, *Chem. Soc. Rev.*, 2013, **42**, 6723-6753; (b) D. G. Gusev, *Organometallics*, 2009, **28**, 6458-6461; (c) D. G. Gusev, *Organometallics*, 2009, **28**, 763-770.
94. (a) R. A. Kelly III, H. Clavier, S. Giudice, N. M. Scott, E. D. Stevens, J. Bordner, I. Samardjiev, C. D. Hoff, L. Cavallo and S. P. Nolan, *Organometallics*, 2008, **27**, 202-210; (b) S. Wolf and H. Plenio, *J. Organomet. Chem.*, 2009, **694**, 1487-1492.
95. A. M. Maj, L. Delaude, A. Demonceau and A. F. Noels, *J. Organomet. Chem.*, 2007, **692**, 3048-3056.
96. L. Cavallo, A. Correa, C. Costabile and H. Jacobsen, *J. Organomet. Chem.*, 2005, **690**, 5407-5413.
97. H. Clavier and S. P. Nolan, *Chem. Commun.*, 2010, **46**, 841-861.
98. A. Poater, B. Cosenza, A. Correa, S. Giudice, F. Ragone, V. Scarano and L. Cavallo, *Eur. J. Inorg. Chem.*, 2009, **13**, 1759-1766.
99. R. Dorta, E. D. Stevens, N. M. Scott, C. Costabile, L. Cavallo, C. D. Hoff and S. P. Nolan, *J. Am. Chem. Soc.*, 2005, **127**, 2485-2495.
100. L. Benhamou, E. Chardon, G. Lavigne, S. Bellemin-Laponnaz and V. César, *Chem. Rev.*, 2011, **111**, 2705-2733.
101. (a) C. Köcher and W. A. Herrmann, *J. Organomet. Chem.*, 1997, **532**, 261-265; (b) G. D. Frey, C. F. Rentzsch, D. von Preysing, T. Scherg, M. Mühlhofer, E. Herdtweck and W. A. Herrmann, *J. Organomet. Chem.*, 2006, **691**, 5725-5738.
102. H. M. J. Wang and I. J. B. Lin, *Organometallics*, 1998, **17**, 972-975.
103. A. R. Chianese, X. Li, M. C. Janzen, J. W. Faller and R. H. Crabtree, *Organometallics*, 2003, **22**, 1663-1667.
104. W. A. Herrmann, L. J. Goößen and M. Spiegler, *J. Organomet. Chem.*, 1997, **547**, 357-366.
105. D. Enders, H. Gielen, G. Raabe, J. Runsink and H. Henrique Teles, *Chem. Ber.*, 1997, **130**, 1253-1260.
106. W. A. Herrmann, J. Schütz, G. D. Frey and E. Herdtweck, *Organometallics*, 2006, **25**, 2437-2448.

107. A. Tudose, A. Demonceau and L. Delaude, *J. Organomet. Chem.*, 2006, **691**, 5356-5365.
108. W. A. Herrmann, C. Köcher, L. J. Goossen and G. R. J. Artus, *Chem. Eur. J.*, 1996, **2**, 1627-1636.
109. R. E. Douthwaite, D. Haüssinger, M. L. H. Green, P. J. Silcock, P. T. Gomes, A. M. Martins and A. A. Danopoulos, *Organometallics*, 1999, **18**, 4584-4590.
110. F. Hanasaka, K.-i. Fujita and R. Yamaguchi, *Organometallics*, 2005, **24**, 3422-3433.
111. (a) J. M. Praetorius and C. M. Crudden, *Dalton Trans.*, 2008, 4079-4094; (b) W. A. Herrmann, G. D. Frey, E. Herdtweck and M. Steinbeck, *Adv. Synth. Catal.*, 2007, **349**, 1677-1691.
112. A. J. Arduengo, S. F. Gamper, J. C. Calabrese and F. Davidson, *J. Am. Chem. Soc.*, 1994, **116**, 4391-4394.
113. E. Çetinkaya, P. B. Hitchcock, H. Küçükbay, M. F. Lappert and S. Al-Juaid, *J. Organomet. Chem.*, 1994, **481**, 89-95.
114. (a) S.-T. Liu, T.-Y. Hsieh, G.-H. Lee and S.-M. Peng, *Organometallics*, 1998, **17**, 993-995; (b) R.-Z. Ku, J.-C. Huang, J.-Y. Cho, F.-M. Kiang, K. R. Reddy, Y.-C. Chen, K.-J. Lee, J.-H. Lee, G.-H. Lee, S.-M. Peng and S.-T. Liu, *Organometallics*, 1999, **18**, 2145-2154.
115. (a) M. R. L. Furst and C. S. J. Cazin, *Chem. Commun.*, 2010, **46**, 6924-6925; (b) C. A. Citadelle, E. L. Nouy, F. Bisaro, A. M. Z. Slawin and C. S. J. Cazin, *Dalton Trans.*, 2010, **39**, 4489-4491.
116. (a) A. Kascatan-Nebioglu, M. J. Panzner, J. C. Garrison, C. A. Tessier and W. J. Youngs, *Organometallics*, 2004, **23**, 1928-1931; (b) C. A. Quezada, J. C. Garrison, M. J. Panzner, C. A. Tessier and W. J. Youngs, *Organometallics*, 2004, **23**, 4846-4848; (c) J. Lemke and N. Metzler-Nolte, *Eur. J. Inorg. Chem.*, 2008, **2008**, 3359-3366.
117. K. Fagnou and M. Lautens, *Chem. Rev.*, 2002, **103**, 169-196.
118. M. F. Lappert and R. K. Maskell, *J. Organomet. Chem.*, 1984, **264**, 217-228.
119. V. Cesar, L. H. Gade and S. Bellemin-Laponnaz, in *N-Heterocyclic Carbenes: From Laboratory Curiosities to Efficient Synthetic Tools*, The Royal Society of Chemistry, 2011, vol. 0, pp. 228-251.
120. M. Sakai, M. Ueda and N. Miyaura, *Angew. Chem. Int. Ed.*, 1998, **37**, 3279-3281.
121. A. Fürstner and H. Krause, *Adv. Synth. Catal.*, 2001, **343**, 343-350.
122. C. Yan, X. Zeng, W. Zhang and M. Luo, *J. Organomet. Chem.*, 2006, **691**, 3391-3396.
123. I. Özdemir, S. Demir and B. Çetinkaya, *J. Mol. Catal. A: Chem.*, 2004, **215**, 45-48.
124. H. Türkmen, S. Denizaltı, I. Özdemir, E. Çetinkaya and B. Çetinkaya, *J. Organomet. Chem.*, 2008, **693**, 425-434.
125. M. Yiğit, I. Özdemir, E. Çetinkaya and B. Çetinkaya, *Transit. Met. Chem.*, 2007, **32**, 536-540.
126. (a) I. Özdemir, S. Demir, B. Çetinkaya and E. Çetinkaya, *J. Organomet. Chem.*, 2005, **690**, 5849-5855; (b) N. Imlinger, M. Mayr, D. Wang, K. Wurst and M. R. Buchmeiser, *Adv. Synth. Catal.*, 2004, **346**, 1836-1843.
127. W. A. Herrmann, L. J. Goossen, C. Köcher and G. R. J. Artus, *Angew. Chem. Int. Ed.*, 1996, **35**, 2805-2807.
128. (a) L. H. Gade, V. César and S. Bellemin-Laponnaz, *Angew. Chem. Int. Ed.*, 2004, **43**, 1014-1017; (b) V. César, S. Bellemin-Laponnaz, H. Wadepohl and L. H. Gade, *Chem. Eur. J.*, 2005, **11**, 2862-2873; (c) N. Schneider, M. Finger, C. Haferkemper, S. Bellemin-Laponnaz, P. Hofmann and L. H. Gade, *Angew. Chem. Int. Ed.*, 2009, **48**, 1609-1613.
129. L. Palacios, M. J. Artigas, V. Polo, F. J. Lahoz, R. Castarlenas, J. J. Pérez-Torrente and L. A. Oro, *ACS Catal.*, 2013, **3**, 2910-2919.
130. R. Franke, D. Selent and A. Börner, *Chem. Rev.*, 2012, **112**, 5675-5732.
131. A. C. Chen, L. Ren, A. Decken and C. M. Crudden, *Organometallics*, 2000, **19**, 3459-3461.
132. a. E. M.-M. Macarena Poyatos, José A. Mata, Mercedes Sanau, and E. Peris, *Eur. J. Inorg. Chem.*, 2003, 1215-1221.

133. M. Bortenschlager, M. Mayr, O. Nuyken and M. R. Buchmeiser, *J. Mol. Catal. A: Chem.*, 2005, **233**, 67-71.
134. M. Bortenschlager, J. Schütz, D. von Preysing, O. Nuyken, W. A. Herrmann and R. Weberskirch, *J. Organomet. Chem.*, 2005, **690**, 6233-6237.
135. J. M. Praetorius, M. W. Kotyk, J. D. Webb, R. Wang and C. M. Crudden, *Organometallics*, 2007, **26**, 1057-1061.
136. S. P. Downing, P. J. Pogorzelec, A. A. Danopoulos and D. J. Cole-Hamilton, *Eur. J. Inorg. Chem.*, 2009, **2009**, 1816-1824.
137. J. F. Young, J. A. Osborn, F. H. Jardine and G. Wilkinson, *Chem. Commun.*, 1965, 131-132.
138. J. A. Osborn, F. H. Jardine, J. F. Young and G. Wilkinson, *J. Chem. Soc. A.*, 1966, 1711-1732.
139. G. A. Grasa, Z. Moore, K. L. Martin, E. D. Stevens, S. P. Nolan, V. Paquet and H. Lebel, *J. Organomet. Chem.*, 2002, **658**, 126-131.
140. H. Lebel, V. Paquet and C. Proulx, *Angew. Chem. Int. Ed.*, 2001, **40**, 2887-2890.
141. D. P. Allen, C. M. Crudden, L. A. Calhoun and R. Wang, *J. Organomet. Chem.*, 2004, **689**, 3203-3209.
142. C. M. Crudden and D. P. Allen, *Coord. Chem. Rev.*, 2004, **248**, 2247-2273.
143. E. Peris and R. H. Crabtree, in *Iridium Complexes in Organic Synthesis*, Wiley-VCH Verlag GmbH & Co. KGaA, 2009, pp. 39-54.
144. N. M. Scott, R. Dorta, E. D. Stevens, A. Correa, L. Cavallo and S. P. Nolan, *J. Am. Chem. Soc.*, 2005, **127**, 3516-3526.
145. (a) N. M. Scott, V. Pons, E. D. Stevens, D. M. Heinekey and S. P. Nolan, *Angew. Chem. Int. Ed.*, 2005, **44**, 2512-2515; (b) N. M. Scott and S. P. Nolan, *Eur. J. Inorg. Chem.*, 2005, **2005**, 1815-1828.
146. J. Huang, E. D. Stevens and S. P. Nolan, *Organometallics*, 2000, **19**, 1194-1197.
147. (a) R. Corberán, M. Sanaú and E. Peris, *Organometallics*, 2006, **25**, 4002-4008; (b) R. Corberán, M. Sanaú and E. Peris, *J. Am. Chem. Soc.*, 2006, **128**, 3974-3979; (c) Y. Tanabe, F. Hanasaka, K.-i. Fujita and R. Yamaguchi, *Organometallics*, 2007, **26**, 4618-4626; (d) F. Hanasaka, Y. Tanabe, K.-i. Fujita and R. Yamaguchi, *Organometallics*, 2006, **25**, 826-831.
148. M. Albrecht, J. R. Miecznikowski, A. Samuel, J. W. Faller and R. H. Crabtree, *Organometallics*, 2002, **21**, 3596-3604.
149. E. Mas-Marzá, M. Sanaú and E. Peris, *Inorg. Chem.*, 2005, **44**, 9961-9967.
150. (a) R. R. Schrock and J. A. Osborn, *J. Am. Chem. Soc.*, 1976, **98**, 2134-2143; (b) R. R. Schrock and J. A. Osborn, *J. Am. Chem. Soc.*, 1976, **98**, 2143-2147; (c) R. R. Schrock and J. A. Osborn, *J. Am. Chem. Soc.*, 1976, **98**, 4450-4455.
151. R. H. Crabtree, H. Felkin and G. E. Morris, *J. Organomet. Chem.*, 1977, **141**, 205-215.
152. R. Crabtree, *Acc. Chem. Res.*, 1979, **12**, 331-337.
153. (a) L. D. Vazquez-Serrano, B. T. Owens and J. M. Buriak, *Chem. Commun.*, 2002, 2518-2519; (b) L. D. Vazquez-Serrano, B. T. Owens and J. M. Buriak, *Inorg. Chim. Acta.*, 2006, **359**, 2786-2797.
154. H. M. Lee, T. Jiang, E. D. Stevens and S. P. Nolan, *Organometallics*, 2001, **20**, 1255-1258.
155. L. S. Bennie, C. J. Fraser, S. Irvine, W. J. Kerr, S. Andersson and G. N. Nilsson, *Chem. Commun.*, 2011, **47**, 11653-11655.
156. M. T. Powell, D.-R. Hou, M. C. Perry, X. Cui and K. Burgess, *J. Am. Chem. Soc.*, 2001, **123**, 8878-8879.
157. R. Noyori and S. Hashiguchi, *Acc. Chem. Res.*, 1997, **30**, 97-102.
158. A. C. Hillier, H. M. Lee, E. D. Stevens and S. P. Nolan, *Organometallics*, 2001, **20**, 4246-4252.
159. J. R. Miecznikowski and R. H. Crabtree, *Polyhedron*, 2004, **23**, 2857-2872.
160. (a) C. F. Rentzsch, E. Tosh, W. A. Herrmann and F. E. Kuehn, *Green Chem.*, 2009, **11**, 1610-1617; (b) I. A. I. Mkhallid, J. H. Barnard, T. B. Marder, J. M. Murphy and J. F. Hartwig, *Chem. Rev.*, 2010, **110**, 890-931.

161. T. Ishiyama, Y. Nobuta, J. F. Hartwig and N. Miyaura, *Chem. Commun.*, 2003, 2924-2925.
162. A. C. Marr, C. L. Pollock and G. C. Saunders, *Organometallics*, 2007, **26**, 3283-3285.
163. F. Hanasaka, K.-i. Fujita and R. Yamaguchi, *Organometallics*, 2004, **23**, 1490-1492.
164. M. Sakai, H. Hayashi and N. Miyaura, *Organometallics*, 1997, **16**, 4229-4231.
165. T. Hayashi and K. Yamasaki, *Chem. Rev.*, 2003, **103**, 2829-2844.
166. Y. Takaya, M. Ogasawara, T. Hayashi, M. Sakai and N. Miyaura, *J. Am. Chem. Soc.*, 1998, **120**, 5579-5580.
167. G. A. Slough, R. Hayashi, J. R. Ashbaugh, S. L. Shamblin and A. M. Aukamp, *Organometallics*, 1994, **13**, 890-898.
168. N. Miyaura, K. Yamada, H. Sugimoto and A. Suzuki, *J. Am. Chem. Soc.*, 1985, **107**, 972-980.
169. K. Siegmann, P. S. Pregosin and L. M. Venanzi, *Organometallics*, 1989, **8**, 2659-2664.
170. (a) T. Korenaga, K. Osaki, R. Maenishi and T. Sakai, *Org. Lett.*, 2009, **11**, 2325-2328; (b) T. Korenaga, R. Maenishi, K. Hayashi and T. Sakai, *Adv. Synth. Catal.*, 2010, **352**, 3247-3254; (c) F. Berhal, O. Esseiva, C.-H. Martin, H. Tone, J.-P. Genet, T. Ayad and V. Ratovelomanana-Vidal, *Org. Lett.*, 2011, **13**, 2806-2809.
171. (a) T. Hayashi, K. Ueyama, N. Tokunaga and K. Yoshida, *J. Am. Chem. Soc.*, 2003, **125**, 11508-11509; (b) C.-C. Liu, D. Janmanchi, C.-C. Chen and H.-L. Wu, *Eur. J. Org. Chem.*, 2012, **2012**, 2503-2507.
172. F. Berhal, Z. Wu, J.-P. Genet, T. Ayad and V. Ratovelomanana-Vidal, *J. Org. Chem.*, 2011, **76**, 6320-6326.
173. (a) K. Lukin, Q. Zhang and M. R. Leanna, *J. Org. Chem.*, 2008, **74**, 929-931; (b) A. Kina, H. Iwamura and T. Hayashi, *J. Am. Chem. Soc.*, 2006, **128**, 3904-3905; (c) W.-C. Yuan, L.-F. Cun, L.-Z. Gong, A.-Q. Mi and Y.-Z. Jiang, *Tetrahedron Lett.*, 2005, **46**, 509-512; (d) W.-C. Yuan, L.-F. Cun, A.-Q. Mi, Y.-Z. Jiang and L.-Z. Gong, *Tetrahedron*, 2009, **65**, 4130-4141.
174. M. S. Jeletic, R. J. Lowry, J. M. Swails, I. Ghiviriga and A. S. Veige, *J. Organomet. Chem.*, 2011, **696**, 3127-3134.
175. I. Peñafiel, I. M. Pastor, M. Yus, M. A. Esteruelas and M. Oliván, *Organometallics*, 2012, **31**, 6154-6161.
176. G. C. Fortman, A. M. Slawin and S. P. Nolan, *Dalton Trans.*, 2010, **39**, 3923-3930.
177. I. Kownacki, M. Kubicki, K. Szubert and B. Marciniak, *J. Organomet. Chem.*, 2008, **693**, 321-328.
178. P. Zhao, C. D. Incarvito and J. F. Hartwig, *J. Am. Chem. Soc.*, 2007, **129**, 1876-1877.
179. S. Sakuma and N. Miyaura, *J. Org. Chem.*, 2001, **66**, 8944-8946.
180. (a) A. A. C. Braga, N. H. Morgon, G. Ujaque and F. Maseras, *J. Am. Chem. Soc.*, 2005, **127**, 9298-9307; (b) A. A. C. Braga, G. Ujaque and F. Maseras, *Organometallics*, 2006, **25**, 3647-3658.
181. A. Kina, Y. Yasuhara, T. Nishimura, H. Iwamura and T. Hayashi, *Chem. Asian J.*, 2006, **1**, 707-711.
182. R. Jana and J. A. Tunge, *Org. Lett.*, 2009, **11**, 971-974.
183. C. S. Cho, S.-i. Motofusa, K. Ohe, S. Uemura and S. C. Shim, *J. Org. Chem.*, 1995, **60**, 883-888.
184. K.-s. Lee and A. H. Hoveyda, *J. Org. Chem.*, 2009, **74**, 4455-4462.
185. B. T. Hahn, F. Tewes, R. Fröhlich and F. Glorius, *Angew. Chem. Int. Ed.*, 2010, **49**, 1143-1146.
186. (a) E. de Wolf, E. A. Speets, B.-J. Deelman and G. van Koten, *Organometallics*, 2001, **20**, 3686-3690; (b) J. Li, J. Peng, Y. Bai, G. Lai and X. Li, *J. Organomet. Chem.*, 2011, **696**, 2116-2121; (c) N. Imlinger, K. Wurst and M. R. Buchmeiser, *Monatsh. Chem.*, 2004, **136**, 47-57; (d) D. Troegel and J. Stohrer, *Coord. Chem. Rev.*, 2011, **255**, 1440-1459.
187. B. Marciniak, in *Advances in Silicon Science*, ed. B. Marciniak, Springer Science+Business Media, Australia, 1st edn., 2009, vol. 1, pp. 3-51.
188. L. H. Sommer and J. E. Lyons, *J. Am. Chem. Soc.*, 1969, **91**, 7061-7067.

189. (a) J. L. Speier, J. A. Webster and G. H. Barnes, *J. Am. Chem. Soc.*, 1957, **79**, 974-979; (b) J. L. Speier and D. E. Hook, *United States Pat.*, US2823218, 1958.
190. B. D. Karstedt, *France Pat.*, FR1548775, 1968.
191. (a) I. E. Markó, S. Stérin, O. Buisine, G. Mignani, P. Branlard, B. Tinant and J. P. Declercq, *Science*, 2002, **298**, 204-206; (b) G. Berthon-Gelloz, O. Buisine, J.-F. Brière, G. Michaud, S. Stérin, G. Mignani, B. Tinant, J.-P. Declercq, D. Chapon and I. E. Markó, *J. Organomet. Chem.*, 2005, **690**, 6156-6168; (c) I. E. Markó, S. Stérin, O. Buisine, G. Berthon, G. Michaud, B. Tinant and J.-P. Declercq, *Adv. Synth. Catal.*, 2004, **346**, 1429-1434; (d) J. J. Hu, F. Li and T. S. A. Hor, *Organometallics*, 2009, **28**, 1212-1220; (e) J. J. Dunsford, K. J. Cavell and B. Kariuki, *J. Organomet. Chem.*, 2011, **696**, 188-194; (f) M. A. Taige, S. Ahrens and T. Strassner, *J. Organomet. Chem.*, 2011, **696**, 2918-2927; (g) J. W. Sprengers, M. J. Mars, M. A. Duin, K. J. Cavell and C. J. Elsevier, *J. Organomet. Chem.*, 2003, **679**, 149-152.
192. (a) T. Hayashi, in *Comprehensive Asymmetric Catalysis* eds. E. N. Jacobson, A. Pfaltz and H. Yamamoto, Springer-Verlag, New York, 4th edn., 1999, vol. 1, pp. 319-333; (b) B. Marciniak, *Silicon Chem.*, 2002, **1**, 155-175.
193. A. M. Tondreau, C. C. H. Atienza, K. J. Weller, S. A. Nye, K. M. Lewis, J. G. P. Delis and P. J. Chirik, *Science*, 2012, **335**, 567-570.
194. (a) I. Ojima, M. Nihonyanagi, T. Kogure, M. Kumagai, S. Horiuchi, K. Nakatsugawa and Y. Nagai, *J. Organomet. Chem.*, 1975, **94**, 449-461; (b) J. Li, J. Peng, G. Zhang, Y. Bai, G. Lai and X. Li, *New J. Chem.*, 2010, **34**, 1330.
195. T. Ganicz, U. Mizerska, M. Moszner, M. O'Brien, R. Perry and W. A. Stańczyk, *App. Catal. A: General*, 2004, **259**, 49-55.
196. B. Marciniak, P. Krzyżanowski, E. Walczuk-Guścióra and W. Duczmal, *J. Mol. Catal. A: Chem.*, 1999, **144**, 263-271.
197. (a) J. Li, J. Peng, D. Wang, Y. Bai, J. Jiang and G. Lai, *J. Organomet. Chem.*, 2011, **696**, 263-268; (b) K. H. Park, S. Y. Kim, S. U. Son and Y. K. Chung, *Eur. J. Org. Chem.*, 2003, **2003**, 4341-4345; (c) J. E. Hill and T. A. Nile, *J. Organomet. Chem.*, 1977, **137**, 293-300.
198. (a) N. Imlinger, K. Wurst and M. R. Buchmeiser, *J. Organomet. Chem.*, 2005, **690**, 4433-4440; (b) N. Imlinger, K. Wurst and M. R. Buchmeiser, *Monatsh. Chem.*, 2005, **136**, 47-57.
199. M. V. Jiménez, J. J. Pérez-Torrente, M. I. Bartolomé, V. Gierz, F. J. Lahoz and L. A. Oro, *Organometallics*, 2007, **27**, 224-234.
200. J. Li, J. Peng, Y. Bai, G. Zhang, G. Lai and X. Li, *J. Organomet. Chem.*, 2010, **695**, 431-436.
201. A. J. Chalk and J. F. Harrod, *J. Am. Chem. Soc.*, 1965, **87**, 16-21.
202. B. Marciniak, *Coord. Chem. Rev.*, 2005, **249**, 2374-2390.
203. (a) B. Marciniak, W. Duczmal, W. Urbaniak and E. Śliwińska, *J. Organomet. Chem.*, 1990, **385**, 319-327; (b) S. B. Duckett and R. N. Perutz, *Organometallics*, 1992, **11**, 90-98; (c) S. Sakaki, M. Sumimoto, M. Fukuhara, M. Sugimoto, H. Fujimoto and S. Matsuzaki, *Organometallics*, 2002, **21**, 3788-3802; (d) P. B. Glaser and T. D. Tilley, *J. Am. Chem. Soc.*, 2003, **125**, 13640-13641; (e) S. Park and M. Brookhart, *Organometallics*, 2010, **29**, 6057-6064.
204. (a) R. Takeuchi and N. Tanouchi, *Chem. Commun.*, 1993, 1319-1320; (b) M. L. Christ, S. Sabo-Etienne and B. Chaudret, *Organometallics*, 1995, **14**, 1082-1084.
205. T. Ganicz, *App. Catal. A: General*, 2004, **259**, 49-55.
206. Y. Jiang, O. Blacque, T. Fox, C. M. Frech and H. Berke, *Chem. Eur. J.*, 2009, **15**, 2121-2128.
207. L. J. Hounjet, R. McDonald, M. J. Ferguson and M. Cowie, *Inorg. Chem.*, 2011, **50**, 5361-5378.
208. A. Millan, M. J. Fernandez, P. Bentz and P. M. Maitlis, *J. Mol. Catal.*, 1984, **26**, 89-104.
209. H. Aneetha, W. Wu and J. G. Verkade, *Organometallics*, 2005, **24**, 2590-2596.
210. M. Rubin, T. Schwier and V. Gevorgyan, *J. Org. Chem.*, 2002, **67**, 1936-1940.

211. Y. Seki, K. Takeshita, K. Kawamoto, S. Murai and N. Sonoda, *Angew. Chem.*, 1980, **92**, 974-974.
212. G. De Bo, G. Berthon-Gelloz, B. Tinant and I. E. Markó, *Organometallics*, 2006, **25**, 1881-1890.
213. L. N. Lewis, *J. Am. Chem. Soc.*, 1990, **112**, 5998-6004.
214. W. Prukała, M. Majchrzak, C. Pietraszuk and B. Marciniak, *J. Mol. Catal. A: Chem.*, 2006, **254**, 58-63.
215. R. Bandari and M. R. Buchmeiser, *Catal. Sci. Technol.*, 2012, **2**, 220-226.
216. W.-G. Zhao and R. Hua, *Eur. J. Org. Chem.*, 2006, 5495-5498.
217. S. Schwieger, R. Herzog, C. Wagner and D. Steinborn, *J. Organomet. Chem.*, 2009, **694**, 3548-3558.
218. A. Hamze, O. Provot, J.-D. Brion and M. Alami, *J. Organomet. Chem.*, 2008, **693**, 2789-2797.
219. (a) A. A. Danopoulos, D. Pugh and J. A. Wright, *Angew. Chem. Int. Ed.*, 2008, **47**, 9765-9767; (b) C. Y. Tang, W. Smith, D. Vidovic, A. L. Thompson, A. B. Chaplin and S. Aldridge, *Organometallics*, 2009, **28**, 3059-3066.
220. S. C. Zinner, C. F. Rentzsch, E. Herdtweck, W. A. Herrmann and F. E. Kuhn, *Dalton Trans.*, 2009, 7055-7062.
221. (a) S. Gaillard, X. Bantreil, A. M. Z. Slawin and S. P. Nolan, *Dalton Trans.*, 2009, 6967-6971; (b) C. A. Urbina-Blanco, X. Bantreil, H. Clavier, A. M. Slawin and S. P. Nolan, *Beilstein J. Org. Chem.*, 2010, **6**, 1120-1126.
222. K. M. Kuhn, J.-B. Bourg, C. K. Chung, S. C. Virgil and R. H. Grubbs, *J. Am. Chem. Soc.*, 2009, **131**, 5313-5320.
223. F. Ragone, A. Poater and L. Cavallo, *J. Am. Chem. Soc.*, 2010, **132**, 4249-4258.
224. A. Poater, N. Bahri-Laleh and L. Cavallo, *Chem. Commun.*, 2011, **47**, 6674-6676.
225. M. J. Frisch, G. W. Trucks, H. B. Schlegel, G. E. Scuseria, M. A. Robb, J. R. Cheeseman, G. Scalmani, V. Barone, B. Mennucci, G. A. Petersson, H. Nakatsuji, M. Caricato, X. Li, H. P. Hratchian, A. F. Izmaylov, J. Bloino, G. Zheng, J. L. Sonnenberg, M. Hada, M. Ehara, K. Toyota, R. Fukuda, J. Hasegawa, M. Ishida, T. Nakajima, Y. Honda, O. Kitao, H. Nakai, T. Vreven, J. A. Montgomery Jr., J. E. Peralta, F. Ogliaro, M. Bearpark, J. J. Heyd, E. Brothers, K. N. Kudin, V. N. Staroverov, R. Kobayashi, J. Normand, K. Raghavachari, A. Rendell, J. C. Burant, S. S. Iyengar, J. Tomasi, M. Cossi, N. Rega, J. M. Millam, M. Klene, J. E. Knox, J. B. Cross, V. Bakken, C. Adamo, J. Jaramillo, R. Gomperts, R. E. Stratmann, O. Yazyev, A. J. Austin, R. Cammi, C. Pomelli, J. W. Ochterski, R. L. Martin, K. Morokuma, V. G. Zakrzewski, G. A. Voth, P. Salvador, J. J. Dannenberg, S. Dapprich, A. D. Daniels, Ö. Farkas, J. B. Foresman, J. V. Ortiz, J. Cioslowski and D. J. Fox, *Gaussian 09*, (2009), Wallingford, CT.
226. B. J. Truscott, A. M. Z. Slawin and S. P. Nolan, *Dalton Trans.*, 2013, **42**, 270-276.
227. B. J. Truscott, G. C. Fortman, A. M. Z. Slawin and S. P. Nolan, *Org. Biomol. Chem.*, 2011, **9**, 7038-7041.
228. B. Marciniak and H. Maciejewski, *Coord. Chem. Rev.*, 2001, **223**, 301-335.
229. I. Kownacki, M. Kubicki and B. Marciniak, *Inorg. Chim. Acta*, 2002, **334**, 301-307.
230. (a) I. Kownacki, B. Marciniak and P. Eilbracht, *Appl. Catal., A*, 2010, **390**, 94-101; (b) I. Kownacki, B. Marciniak, A. Macina, S. Rubinsztajn and D. Lamb, *Appl. Catal., A*, 2007, **317**, 53-57; (c) I. Kownacki, B. Marciniak, K. Szubert and M. Kubicki, *Organometallics*, 2005, **24**, 6179-6183; (d) B. Marciniak, I. Kownacki, M. Kubicki, P. Krzyzanowski, E. Walczuk and P. Blazejewska-Chadyniak, in *Perspectives in Organometallic Chemistry*, eds. C. G. Screttas and B. R. Steele, The Royal Society of Chemistry, 2003, pp. 253-264.
231. Y.-R. Luo, *Comprehensive Handbook of Chemical Bond Energies*, CRC Press, Boca Raton, 2007.
232. (a) H. Singer and G. Wilkinson, *J. Chem. Soc. A.*, 1968, 2516-2520; (b) R. N. Haszeldine, R. J. Lunt and R. V. Parish, *J. Chem. Soc. A.*, 1971, 3711-3715.
233. (a) C. E. Johnson, B. J. Fisher and R. Eisenberg, *J. Am. Chem. Soc.*, 1983, **105**, 7772-7774; (b) C. E. Johnson and R. Eisenberg, *J. Am. Chem. Soc.*, 1985, **107**, 6531-6540; (c)

- C. E. Johnson and R. Eisenberg, *J. Am. Chem. Soc.*, 1985, **107**, 3148-3160; (d) T. C. Eischenschmid and R. Eisenberg, *Organometallics*, 1989, **8**, 1822-1824.
234. (a) H.-F. Chen, C. Wu, M.-C. Kuo, M. E. Thompson and K.-T. Wong, *J. Mater. Chem.*, 2012, **22**, 9556-9561; (b) S. Obara, M. Itabashi, F. Okuda, S. Tamaki, Y. Tanabe, Y. Ishii, K. Nozaki and M.-a. Haga, *Inorg. Chem.*, 2006, **45**, 8907-8921; (c) L. Huynh, Z. Wang, J. Yang, V. Stoeva, A. Lough, I. Manners and M. A. Winnik, *Chem. Mater.*, 2005, **17**, 4765-4773.
235. (a) F. G. Bordwell, *Acc. Chem. Res.*, 1988, **21**, 456-463; (b) R. W. Taft and F. G. Bordwell, *Acc. Chem. Res.*, 1988, **21**, 463-469; (c) F. G. Bordwell, G. E. Drucker and H. E. Fried, *J. Org. Chem.*, 1981, **46**, 632-635; (d) W. N. Olmstead, Z. Margolin and F. G. Bordwell, *J. Org. Chem.*, 1980, **45**, 3295-3299.
236. J. C. M. Ritter and R. G. Bergman, *J. Am. Chem. Soc.*, 1998, **120**, 6826-6827.
237. D. S. Glueck, L. J. N. Winslow and R. G. Bergman, *Organometallics*, 1991, **10**, 1462-1479.
238. F. T. Ladipo, M. Kooti and J. S. Merola, *Inorg. Chem.*, 1993, **32**, 1681-1688.
239. (a) Z. Huang, J. Zhou and J. F. Hartwig, *J. Am. Chem. Soc.*, 2010, **132**, 11458-11460; (b) A. C. Sykes, P. White and M. Brookhart, *Organometallics*, 2006, **25**, 1664-1675.
240. (a) J. R. Fulton, A. W. Holland, D. J. Fox and R. G. Bergman, *Acc. Chem. Res.*, 2001, **35**, 44-56; (b) D. Rais and R. G. Bergman, *Chem. Eur. J.*, 2004, **10**, 3970-3978.
241. (a) J. Zhao, A. S. Goldman and J. F. Hartwig, *Science*, 2005, **307**, 1080-1082; (b) I. Mena, M. A. Casado, P. García-Orduña, V. Polo, F. J. Lahoz, A. Fazal and L. A. Oro, *Angew. Chem. Int. Ed.*, 2011, **50**, 11735-11738; (c) A. L. Casalnuovo, J. C. Calabrese and D. Milstein, *Inorg. Chem.*, 1987, **26**, 971-973; (d) E. Morgan, D. F. MacLean, R. McDonald and L. Turculet, *J. Am. Chem. Soc.*, 2009, **131**, 14234-14236.
242. (a) S. K. Hanson, D. M. Heinekey and K. I. Goldberg, *Organometallics*, 2008, **27**, 1454-1463; (b) S. M. Kloek, D. M. Heinekey and K. I. Goldberg, *Angew. Chem. Int. Ed.*, 2007, **46**, 4736-4738; (c) W. J. Tenn, K. J. H. Young, J. Oxgaard, R. J. Nielsen, W. A. Goddard and R. A. Periana, *Organometallics*, 2006, **25**, 5173-5175; (d) W. J. Tenn, K. J. H. Young, G. Bhalla, J. Oxgaard, W. A. Goddard and R. A. Periana, *J. Am. Chem. Soc.*, 2005, **127**, 14172-14173.
243. P. Burger and R. G. Bergman, *J. Am. Chem. Soc.*, 1993, **115**, 10462-10463.
244. K. Murata, H. Konishi, M. Ito and T. Ikariya, *Organometallics*, 2002, **21**, 253-255.
245. M. J. Fernández, M. A. Esteruelas, M. Covarrubias and L. A. Oro, *J. Organomet. Chem.*, 1990, **381**, 275-279.
246. I. Kownacki, B. Marciniak, B. Dudzic and M. Kubicki, *Organometallics*, 2011, **30**, 2539-2545.
247. R. Ghosh, X. Zhang, P. Achord, T. J. Emge, K. Krogh-Jespersen and A. S. Goldman, *J. Am. Chem. Soc.*, 2007, **129**, 853-866.
248. F. Kessler, B. F. E. Curchod, I. Tavernelli, U. Rothlisberger, R. Scopelliti, D. Di Censo, M. Grätzel, M. K. Nazeeruddin and E. Baranoff, *Angew. Chem. Int. Ed.*, 2012, **51**, 8030-8033.
249. K. Shen, Y. Fu, J.-N. Li, L. Liu and Q.-X. Guo, *Tetrahedron*, 2007, **63**, 1568-1576.
250. E. Clot, C. Mégret, O. Eisenstein and R. N. Perutz, *J. Am. Chem. Soc.*, 2009, **131**, 7817-7827.
251. M. Prinz, L. F. Veiros, M. J. Calhorda, C. C. Romão, E. Herdtweck, F. E. Kühn and W. A. Herrmann, *J. Organomet. Chem.*, 2006, **691**, 4446-4458.
252. X. Yin and J. R. Moss, *Coord. Chem. Rev.*, 1999, **181**, 27-59.
253. W. Wang, S. Wang, X. Ma and J. Gong, *Chem. Soc. Rev.*, 2011, **40**, 3703-3727.
254. A. Behr, *Angew. Chem. Int. Ed.*, 1988, **27**, 661-678.
255. (a) M. Aresta and A. Dibenedetto, *J. Mol. Catal. A: Chem.*, 2002, **182-183**, 399-409; (b) M. Aresta and A. Dibenedetto, *Dalton Trans.*, 2007, 2975-2992.
256. T. Sakakura, J.-C. Choi and H. Yasuda, *Chem. Rev.*, 2007, **107**, 2365-2387.
257. (a) W. Leitner, *Coord. Chem. Rev.*, 1996, **153**, 257-284; (b) D. H. Gibson, *Chem. Rev.*, 1996, **96**, 2063-2096; (c) D. H. Gibson, *Coord. Chem. Rev.*, 1999, **185-186**, 335-355;

- (d) F. J. Fernández-Alvarez, M. Iglesias, L. A. Oro and V. Polo, *Chem. Cat. Chem.*, 2013, **5**, 3481-3494.
258. T. A. Hanna, A. M. Baranger and R. G. Bergman, *J. Am. Chem. Soc.*, 1995, **117**, 11363-11364.
259. T. Herskovitz, *J. Am. Chem. Soc.*, 1977, **99**, 2391-2392.
260. D. W. Lee, C. M. Jensen and D. Morales-Morales, *Organometallics*, 2003, **22**, 4744-4749.
261. B. R. Flynn and L. Vaska, *J. Am. Chem. Soc.*, 1973, **95**, 5081-5083.
262. R. Johansson and O. F. Wendt, *Organometallics*, 2007, **26**, 2426-2430.
263. (a) R. A. Allred, L. H. McAlexander, A. M. Arif and L. M. Berreau, *Inorg. Chem.*, 2002, **41**, 6790-6801; (b) N. Kitajima, S. Hikichi, M. Tanaka and Y. Morooka, *J. Am. Chem. Soc.*, 1993, **115**, 5496-5508; (c) Z.-W. Mao, F. W. Heinemann, G. Liehr and R. v. Eldik, *Dalton Trans.*, 2001, 3652-3662.
264. (a) U. Singh, P. Babbar, P. Tyagi and T. Weyhermüller, *Transit. Met. Chem.*, 2008, **33**, 931-940; (b) R. A. Jewsbury, *Inorg. Chim. Acta.*, 1981, **49**, 141-143; (c) V. D. Bianco, S. Doronzo and N. Gallo, *Inorg. Nucl. Chem. Lett.*, 1979, **15**, 187-189.
265. (a) P. Kläring, A.-K. Jungton, T. Braun and C. Müller, *Eur. J. Inorg. Chem.*, 2012, **2012**, 1430-1436; (b) P. Klaring, S. Pahl, T. Braun and A. Penner, *Dalton Trans.*, 2011, **40**, 6785-6791.
266. S. Krogsrud, S. Komiya, T. Ito, J. A. Ibers and A. Yamamoto, *Inorg. Chem.*, 1976, **15**, 2798-2805.
267. B. J. Truscott, D. J. Nelson, C. Lujan, A. M. Z. Slawin and S. P. Nolan, *Chem. Eur. J.*, 2013, **19**, 7904-7916.
268. M. H. Chisholm and M. Extine, *Chem. Commun.*, 1975, 438-439.
269. G. Gattow and W. Behrendt, *Angew. Chem. Int. Ed.*, 1972, **11**, 534-535.
270. M. Rahim, C. White, A. L. Rheingold and K. J. Ahmed, *Organometallics*, 1993, **12**, 2401-2403.
271. (a) J. M. Seul and S. Park, *Bull. Korean Chem. Soc.*, 2010, **31**, 3745-3748; (b) S. Park, *Bull. Korean Chem. Soc.*, 2001, **22**, 1410-1412.
272. R. N. K. Goldberg, Nand; Lennen, Rebecca M, in *CRC Handbook of Chemistry and Physics*, ed. D. R. Lide, CRC Press, Boca Raton, 84 edn., 2003, pp. 7-13.
273. D. J. Darensbourg, G. Groetsch, P. Wiegrefe and A. L. Rheingold, *Inorg. Chem.*, 1987, **26**, 3827-3830.
274. R. Johansson, M. Jarenmark and O. F. Wendt, *Organometallics*, 2005, **24**, 4500-4502.
275. T. J. Schmeier, N. Hazari, C. D. Incarvito and J. A. Raskatov, *Chem. Commun.*, 2011, **47**, 1824-1826.
276. M. T. Johnson, J. Marthinus Janse van Rensburg, M. Axelsson, M. S. G. Ahlquist and O. F. Wendt, *Chem. Sci.*, 2011, **2**, 2373-2377.
277. T. Fan, X. Chen and Z. Lin, *Chem. Commun.*, 2012, **48**, 10808-10828.
278. (a) D. Huang, O. V. Makhlynets, L. L. Tan, S. C. Lee, E. V. Rybak-Akimova and R. H. Holm, *P. Natl. Acad. Sci. USA*, 2011, **108**, 1222-1227; (b) D. Huang, O. V. Makhlynets, L. L. Tan, S. C. Lee, E. V. Rybak-Akimova and R. H. Holm, *Inorg. Chem.*, 2011, **50**, 10070-10081.
279. K. Fagnou and M. Lautens, *Angew. Chem. Int. Ed.*, 2002, **41**, 26-47.
280. K. Müller, C. Faeh and F. Diederich, *Science*, 2007, **317**, 1881-1886.
281. T. Furuya, A. S. Kamlet and T. Ritter, *Nature*, 2011, **473**, 470-477.
282. D. P. Curran, *Angew. Chem. Int. Ed.*, 1998, **37**, 1174-1196.
283. P. S. Fier and J. F. Hartwig, *J. Am. Chem. Soc.*, 2012, **134**, 10795-10798.
284. P. S. Fier, J. Luo and J. F. Hartwig, *J. Am. Chem. Soc.*, 2013, **135**, 2552-2559.
285. H. Morimoto, T. Tsubogo, N. D. Litvinas and J. F. Hartwig, *Angew. Chem. Int. Ed.*, 2011, **50**, 3793-3798.
286. H. L. M. van Gaal and F. L. A. van den Bekerom, *J. Organomet. Chem.*, 1977, **134**, 237-248.
287. J. Fawcett, D. A. J. Harding, E. G. Hope, K. Singh and G. A. Solan, *Dalton Trans.*, 2010, **39**, 10781-10789.

288. (a) S. A. Macgregor, D. C. Roe, W. J. Marshall, K. M. Bloch, V. I. Bakhmutov and V. V. Grushin, *J. Am. Chem. Soc.*, 2005, **127**, 15304-15321; (b) V. V. Grushin and W. J. Marshall, *J. Am. Chem. Soc.*, 2004, **126**, 3068-3069; (c) V. V. Grushin, *Acc. Chem. Res.*, 2009, **43**, 160-171.
289. J. Vicente, J. Gil-Rubio and D. Bautista, *Inorg. Chem.*, 2001, **40**, 2636-2637.
290. (a) J. R. Herron and Z. T. Ball, *J. Am. Chem. Soc.*, 2008, **130**, 16486-16487; (b) D. S. Laitar, Massachusetts Institute of Technology, 2006; (c) T. Fujihara, T. Xu, K. Semba, J. Terao and Y. Tsuji, *Angew. Chem. Int. Ed.*, 2011, **50**, 523-527.
291. D. S. Laitar, P. Müller, T. G. Gray and J. P. Sadighi, *Organometallics*, 2005, **24**, 4503-4505.
292. (a) T. Schaub, P. Fischer, A. Steffen, T. Braun, U. Radius and A. Mix, *J. Am. Chem. Soc.*, 2008, **130**, 9304-9317; (b) T. Schaub, M. Backes and U. Radius, *J. Am. Chem. Soc.*, 2006, **128**, 15964-15965.
293. (a) S. L. Chatwin, M. G. Davidson, C. Doherty, S. M. Donald, R. F. R. Jazzar, S. A. Macgregor, G. J. McIntyre, M. F. Mahon and M. K. Whittlesey, *Organometallics*, 2005, **25**, 99-110; (b) J. Fawcett, D. A. J. Harding, E. G. Hope, K. Singh and G. A. Solan, *Dalton Trans.*, 2009, 6861-6870; (c) S. P. Reade, D. Nama, M. F. Mahon, P. S. Pregosin and M. K. Whittlesey, *Organometallics*, 2007, **26**, 3484-3491.
294. D. R. Coulson, *J. Am. Chem. Soc.*, 1976, **98**, 3111-3119.
295. U. Bentrup, K. Harms, W. Massa and J. Pebler, *Solid State Sci.*, 2000, **2**, 373-377.
296. V. J. Murphy, D. Rabinovich, T. Hascall, W. T. Klooster, T. F. Koetzle and G. Parkin, *J. Am. Chem. Soc.*, 1998, **120**, 4372-4387.
297. (a) N. D. Ball and M. S. Sanford, *J. Am. Chem. Soc.*, 2009, **131**, 3796-3797; (b) N. A. Jasim and R. N. Perutz, *J. Am. Chem. Soc.*, 2000, **122**, 8685-8693; (c) D. C. Roe, W. J. Marshall, F. Davidson, P. D. Soper and V. V. Grushin, *Organometallics*, 2000, **19**, 4575-4582.
298. (a) N. A. Jasim, R. N. Perutz, S. P. Foxon and P. H. Walton, *Dalton Trans.*, 2001, 1676-1685; (b) M. K. Whittlesey, R. N. Perutz, B. Greener and M. H. Moore, *Chem. Commun.*, 1997, 187-188; (c) M. S. Kirkham, M. F. Mahon and M. K. Whittlesey, *Chem. Commun.*, 2001, 813-814.
299. V. J. Murphy, T. Hascall, J. Y. Chen and G. Parkin, *J. Am. Chem. Soc.*, 1996, **118**, 7428-7429.
300. T. Braun, S. P. Foxon, R. N. Perutz and P. H. Walton, *Angew. Chem. Int. Ed.*, 1999, **38**, 3326-3329.
301. (a) J. Vicente, J. Gil-Rubio, D. Bautista, A. Sironi and N. Masciocchi, *Inorg. Chem.*, 2004, **43**, 5665-5675; (b) W. J. Marshall and V. V. Grushin, *Organometallics*, 2004, **23**, 3343-3347; (c) C. Segarra, E. Mas-Marzá, J. P. Lowe, M. F. Mahon, R. C. Poulten and M. K. Whittlesey, *Organometallics*, 2012, **31**, 8584-8590.
302. T. Vergote, F. Nahra, A. Welle, M. Luhmer, J. Wouters, N. Mager, O. Riant and T. Leyssens, *Chem. Eur. J.*, 2012, **18**, 793-798.
303. T. Vergote, F. Nahra, D. Peeters, O. Riant and T. Leyssens, *J. Organomet. Chem.*, 2013, **730**, 95-103.
304. T. Vergote, F. Nahra, A. Merschaert, O. Riant, D. Peeters and T. Leyssens, *Organometallics*, 2014, **33**, 1953-1963.
305. Y. Liu, C. Chen, H. Li, K.-W. Huang, J. Tan and Z. Weng, *Organometallics*, 2013, **32**, 6587-6592.
306. N. Bramananthan, M. Carmona, J. P. Lowe, M. F. Mahon, R. C. Poulten and M. K. Whittlesey, *Organometallics*, 2014, **33**, 1986-1995.
307. (a) G. G. Dubinina, H. Furutachi and D. A. Vacic, *J. Am. Chem. Soc.*, 2008, **130**, 8600-8601; (b) A. Zanardi, M. A. Novikov, E. Martin, J. Benet-Buchholz and V. V. Grushin, *J. Am. Chem. Soc.*, 2011, **133**, 20901-20913.
308. Z. Mazloomi, A. Bansode, P. Benavente, A. Lishchynskiy, A. Urakawa and V. V. Grushin, *Org. Process Res. Dev.*, 2014.
309. A. Lishchynskiy, M. A. Novikov, E. Martin, E. C. Escudero-Adán, P. Novák and V. V. Grushin, *J. Org. Chem.*, 2013, **78**, 11126-11146.

310. P. Novák, A. Lishchynskiy and V. V. Grushin, *Angew. Chem. Int. Ed.*, 2012, **51**, 7767-7770.
311. P. Novák, A. Lishchynskiy and V. V. Grushin, *J. Am. Chem. Soc.*, 2012, **134**, 16167-16170.
312. M. Ahmed, C. Buch, L. Routaboul, R. Jackstell, H. Klein, A. Spannenberg and M. Beller, *Chem. Eur. J.*, 2007, **13**, 1594-1601.
313. A. Bondi, *J. Phys. Chem.*, 1964, **68**, 441-451.
314. (a) T. R. R. McDonald, *Acta Crystallogr.*, 1960, **13**, 113-124; (b) L. K. Frevel and H. W. Rinn, *Acta Crystallogr.*, 1962, **15**, 286-286; (c) J. M. Williams and L. F. Schneemeyer, *J. Am. Chem. Soc.*, 1973, **95**, 5780-5781.
315. L. Andrews and G. L. Johnson, *J. Phys. Chem.*, 1984, **88**, 425-432.
316. B. S. Ault, *Acc. Chem. Res.*, 1982, **15**, 103-109.
317. (a) I. S. Dubinsky-Davidchik, I. Goldberg, A. Vigalok and A. N. Vedernikov, *Chem. Commun.*, 2013, **49**, 3446-3448; (b) M. C. Pilon and V. V. Grushin, *Organometallics*, 1998, **17**, 1774-1781.
318. (a) J. J. Topczewski, T. J. Tewson and H. M. Nguyen, *J. Am. Chem. Soc.*, 2011, **133**, 19318-19321; (b) J. Zhu, G. C. Tsui and M. Lautens, *Angew. Chem. Int. Ed.*, 2012, 12353-12356; (c) C. Hollingworth and V. Gouverneur, *Chem. Commun.*, 2012, **48**, 2929-2942; (d) J. A. Akana, K. X. Bhattacharyya, P. Müller and J. P. Sadighi, *J. Am. Chem. Soc.*, 2007, **129**, 7736-7737; (e) J. A. Kalow and A. G. Doyle, *Tetrahedron*, 2013, **69**, 5702-5709.
319. P. J. Brothers, A. K. Burrell, G. R. Clark, C. E. F. Rickard and W. R. Roper, *J. Organomet. Chem.*, 1990, **394**, 615-642.
320. Y. Zeng, L. Zhang, Y. Zhao, C. Ni, J. Zhao and J. Hu, *J. Am. Chem. Soc.*, 2013, **135**, 2955-2958.
321. J.-C. Hierso, *Chem. Rev.*, 2014, **114**, 4838-4867.